PWM control optimization of a two-level inverter : Application to electric and hybrid vehicles

Adrien Bourgeade

THÈSE DE DOCTORAT DE

L'ÉCOLE CENTRALE DE NANTES

ÉCOLE DOCTORALE N° 601
Mathématiques et Sciences et Technologies de l'Information et de la Communication
Spécialité : *Génie Électrique*

Par
Adrien BOURGEADE

PWM control optimization of a two-level inverter

Application to electric and hybrid vehicles

Thèse présentée et soutenue à Nantes, le 21 Octobre 2022
Unité de recherche : UMR 6004, Laboratoire des Sciences du Numérique de Nantes (LS2N)

Rapporteurs avant soutenance :

Stefano DI GENNARO	Professor, Universita degli Studi dell'Aquila, Italie
Pierre RIEDINGER	Professeur des universités, Université de Lorraine

Composition du Jury :

Président :	Mohamed DJEMAI	Professeur des universités, INSA Hauts-de-France
Examinateurs :	Xuefang LIN-SHI	Professeure des universités, INSA Lyon
	Olivier BÉTHOUX	Professeur des universités, Sorbonne Université
	Abdelkader BOUARFA	Ingénieur, Renault, Guyancourt
Dir. de thèse :	Malek GHANES	Professeur des universités, Ecole Centrale de Nantes
Co-dir. de thèse :	Maurice FADEL	Professeur des universités, ENSEEIHT-INP, Toulouse

Acknowledgement

Ce travail de thèse est le fruit d'une collaboration entre le Laboratoire des Sciences du Numérique de Nantes (LS2N), l'école Centrale de Nantes (ECN) et le groupe constructeur automobile Renault. Ce travail a été realisé dans le cadre de la Chaire Renault avec l'objectif d'améliorer les véhicules électriques et hybrides. Bien que la thèse soit intégralement rédigée en anglais, j'ai fait le choix d'écrire ma reconnaissance aux gens qui m'ont entouré tout le long de ma thèse dans ma langue maternelle, c'est à dire en Français.

Que serais une thèse de Doctorat sans ses directeurs de thèse? C'est ainsi que c'est à eux que viennent mes premières pensées, à ceux qui m'ont, tout le long de ces trois années accompagné conseillé et soutenus. Je pense donc à Malek Ghanes, directeur de la chaire Renault, qui m'a bien souvent mis sur la voie pour trouver des solutions aux problèmes qui se posaient à moi. Je pense aussi à Maurice Fadel, mon co-directeur de thèse, et même si nous ne nous sommes pas vu beaucoup de fois en présentiel, tes remarques étaient pertinentes et utiles et ont réellement contribués à améliorer mon travail de recherche. Du côté industriel, il y a bien évidemment Abdelkader Bouarfa, éternellement débordé, mais qui a toujours su trouver du temps au bon moment pour me donner une idée décisive ou un conseil que je pourrais qualifier de miraculeux. Et bien sûr, il y a Jean-Pierre Barbot qui, grâce à son sens physique exceptionnelement aiguisé et son amour des mathématiques a pu me recadrer de nombreuses fois, me permettant d'éviter les obstacles et qui m'a ainsi mis sur la voie pour devenir un véritable chercheur.

J'adresse également mes sincères remerciements aux personnes qui ont bien voulu constituer mon jury de thèse et que je n'ai pas encore mentionnés, à savoir Professeur Stefano Di Gennaro du laboratoire DISIM en Italie, Professeur Pierre Riedinger du CRAN à Nancy, Professeur Mohamed Djemai du LAMIH à Valenciennes dont j'ai eu l'honneur que ma thèse soit présidé par lui même, Professeure Xuefang Lin-Shi du laboratoire Ampère à Lyon ainsi que Professeur Olivier Bethoux du Geeps à Gif-sur-Yvette. Ainsi, j'ai eu l'honneur d'avoir mes travaux relus et évalués par un jury de qualité couvrant les thématiques de l'automatique ainsi que de la commande des convertisseurs. Et pour tout ça, je vous en suis humblement reconnaissant.

Il y a aussi tous ceux qui ne sont pas officiellement dans ma thèse qui m'ont indu-

bitablement aidé pendant ces années. Je veux bien sûr parler de Robert Boisliveau, qui m'a considérablement aidé sur le côté expérimental de ma thèse. Je pense aussi à Edouard Nègre qui m'a appris l'existence d'une plateforme expérimentale à L'UTC et qui m'a permis de la récupérer et de la comprendre pour la prendre en main. Je veux aussi remercier Blerim Berisha d'avoir accepté un stage avec moi et de s'être donné corps et âme pour faire fonctionner les stratégies dévellopées sur la plateforme de puissance fournie par Renault.

Je garderais aussi des incroyables souvenirs du laboratoire qui possède une ambiance inégalable à grand renforts de débats dans l'atrium. Pour tous ces moments, je souhaite remercier dans l'ordre alphabétique des prénoms (pour ne froisser personne). Adrien Gauché pour des débats politiques autour de Jancovici et du nucléaire. Bastien Serré qui fait preuve d'une répartie inégalée pour défendre ses idées. Enrique Alvaro Mendoza qui fut mon compagnon de bureau pendant toute une année avec qui discuter de la prononciation des mots m'a bien fait rire. Dr. Guillaume Jeanneau pour sa bienveillance sa gentillesse et nos sorties à vélo. Houssein Al-Attar pour sa résillience et sa joie de vivre à toute épreuve. Dr. Julian Erskine qui derrière sa barbe bien taillée se cache un coeur immense. Lorriane Leclerc pour avoir participé à mon ouverture d'esprit et m'a fait voir de nouveaux horizons. Ludivine Morvan pour son énergie débordante pour sauver des vies "à côté de sa thèse". Dr. Maël Millardais avec qui parler et pratiquer le cyclisme fut un vrai régal. Marceau Méthillon alias René Bichu pour nos délires et son humour décapant. Matthieu Furet pour tous les conseils qu'il m'a prodigué et sa patience. Mehdi Latif alias Hugue et ses jeux de mots qui rivalisent d'inventivité. Nicolas Testard que j'envie pour sa chance légendaire (2,5% !) et qui a toujours le mot pour rire. Rémi Parrot dont le calme, la patience et le stoïcisme m'ont toujours impressionné. Dr. Samuel Buchet capable de remonter des montagnes avec ses bras tel le saumon. Dr. Sebastien Rouquet à qui j'envie sa capacité à se débrouiller dans n'importe quelle situation. Dr. Valentin Le Mesle avec qui les blagues les plus tordues et les chansons les plus bizarres deviennent hilarantes. Vanessa Gonzalès pour son sourire éblouissant. Dr. Yassir Dahmane pour son acceuil chaleureux pour Houssein et moi même au début de la thèse.

Puisqu'il n'y a pas que le Laboratoire dans la vie de doctorant, je remercie tous ceux qui m'ont soutenu et donc, en premier lieu il y a ma famille, à mes parents même si ils n'ont pas toujours vu d'un bon oeil ce Doctorat je sais qu'ils ont toujours été là pour moi. A mon Frère qui est toujours une bonne oreille lors des coups de mous. A mes grands parents, qui même si ils ne comprennent pas très bien l'anglais ni ce que je fais vraiment ne manquent jamais une occasion de me soutenir. Et bien sûr tous les autres membres de

la famille plus ou moins éloignés qui suivent mes déboires!

Un remerciement spécial pour Mathilde Pierre pour m'avoir accompagné (et supporté) pendant plus de la moitié de mon cursus désormais! Être à côté de toi amplifie mon amour de jour en jour, et je sais tous les efforts que tu fais pour tenter de comprendre quelque chose à ce que je fais.

Je voudrais aussi remercier mes amis qui sont un peu éparpillés autour du monde, en commençant par ceux que je vais rejoindre bientôt à Toulouse. Julie Fouan, Thibault Boissin, Jordan Mabboux et Alice Couprie, on ne s'est pas beaucoup vus ces dernières années, mais vous gardez toujours une place de choix dans mon coeur. Thomas Chamelot que j'ai failli rejoindre à Grenoble, qui m'avait tant appris au club de robotique. Tout autour de la France, il y a aussi mes amis de prépa, Paul et Luc Dupont, Alan Clemenceau mais aussi Thibaut Sutre, nos discords et nos discussions quotidiennes sont toujours aussi agréables et ce même 6 ans après, ne changez rien les gars! Je souhaite aussi remercier mes amies de Turquie à savoir: Bircan Balseçen, Busra Nur Derinoz et Beliz Ouïghour pour m'avoir permis de découvrir une culture différente que la mienne, même si, il est vrai que la distance ne facilite pas les échanges. À Paris (le seul de mes amis qui s'est égaré là bas) je remercie chaleureusement Éric Noumri sans qui je ne serais ni Ingénieur ni Docteur aujourd'hui, et parceque ce n'est pas rien: merci! Du côté du plat pays, il y a Inès Bernoux, qui est devenue une amie proche grâce au confinement, ce qui me permet de trouver au moins un avantage au Covid!

Je terminerais ces remerciement avec les activités qui m'ont occupés ces trois dernières années. Ainsi c'est chaleureusement que je remercie Iliassou Baldé, mon filleul de Parrains par milles à qui je souhaite une grande réussite pour devenir un excellent ingénieur en Génie Civil. De même à tous les élèves que j'ai pu suivre à l'ACCOORD je vous souhaite bon vent! A tous les cyclistes du club de la CLISSAA je vous souhaite bonne route même si je n'ai pas été très présent la dernière année.

Et enfin, je veux remercier tous les membres du spéléo-club de Saint-Herblain. M' enfouir dans des trous à vos côtés fut un réel plaisir et un réel soulagement au cours de la thèse! Je suis encore aujourd'hui sidéré qu'il m'ai fallu attendre Nantes pour découvrir ce magnifique sport alors que je suis Périgourdin!

J'oublie sans aucun doute des gens et à ceux-là je vous dit vous aussi merci et bonne lecture à toutes et tous!

Table of Contents

Nomenclature . . . 16

Introduction **25**

Context and motivations . . . 25
A brief DC/AC conversion history . . . 28
Problematic . . . 30
Contributions . . . 31
Manuscript organization . . . 32

1 The inverter command **35**

1.1 Carrier based PWM . . . 36
1.1.1 The different classes of CBPWM . . . 36
1.1.1.1 Hypotheses concerning the control loop . . . 36
1.1.1.2 Synchronous carrier based PWM . . . 38
1.1.1.3 Synchronous triangular and saw-tooth PWM comparison . 39
1.1.2 Zero sequence component injection . . . 41
1.1.3 Third harmonic injection PWM . . . 43
1.1.4 Discontinuous PWM . . . 44
1.1.5 Random PWM . . . 47
1.1.6 Other ZSC injection: The OMIPWM example . . . 49
1.2 Space vector PWM . . . 50
1.2.1 Principle . . . 50
1.2.1.1 SVPWM description . . . 53
1.2.2 Space vector based strategy for common mode voltage reduction . . 54
1.2.2.1 Near-state PWM . . . 55
1.2.2.2 Remote state PWM . . . 57
1.2.2.3 Active zero sequence PWM . . . 60
1.2.3 Optimal SVM . . . 61
1.3 Off-line PWM . . . 63
1.3.1 The angle model . . . 63

1.3.1.1 QWS equations . . . 65
1.3.1.2 HWS equations . . . 65
1.3.1.3 FWS equations . . . 66
1.3.2 WTHD reduction . . . 66
1.3.3 Selective Harmonic Elimination . . . 67
1.3.4 OPP resolution techniques . . . 68
1.4 Closed loop PWM strategies . . . 68
1.4.1 The $\Delta\Sigma$ vector modulation . . . 68
1.4.2 Model predictive control . . . 70
1.4.3 Hysteresis control . . . 71
1.5 Conclusion and thesis bias . . . 73
1.5.1 Conclusion . . . 73
1.5.1.1 Global overview . . . 73
1.5.1.2 Space vector strategies . . . 74
1.5.1.3 CBPWM . . . 74
1.5.1.4 OPP . . . 75
1.5.1.5 Closed loop PWM . . . 75
1.5.1.6 Other PWM purposes . . . 75
1.5.2 Thesis bias . . . 75

2 A new off-line PWM: The Phase symmetry relaxation 79
2.1 Classic OPP problem modeling . . . 79
2.2 **P**hases **S**ymmetry **R**elaxation method . . . 81
2.2.1 Problem modeling . . . 81
2.3 Computation Method . . . 84
2.3.1 Random starting point generation . . . 84
2.3.2 Solution search algorithm . . . 85
2.4 Evaluation criteria . . . 86
2.4.1 Smoothness . . . 86
2.5 Simulation results . . . 89
2.5.1 WTHD comparison . . . 89
2.5.2 Smoothness . . . 92
2.5.3 Switching losses influence . . . 94
2.6 Experimental results . . . 96

2.7 PSR and Space vector modulation . . . 101
2.7.1 The zero sequence component extraction . . . 102
2.8 Conclusion . . . 103

3 Synchronous Carrier Based PWM 105
3.1 The carrier based PWM context . . . 105
3.2 A THIPWM generalization: The Zero Sequence Component Modulation . 107
3.2.1 ZSCM description . . . 107
3.2.2 ZSCM optimization . . . 109
3.2.2.1 ZSCM algorithm . . . 110
3.2.3 ZSCM results . . . 112
3.2.3.1 Five switches per quarter period . . . 112
3.2.3.2 Three switches per quarter period . . . 116
3.2.4 ZSCM convergence to a saw-tooth waveform . . . 121
3.3 STIPWM interest for power electronics . . . 121
3.3.1 WTHD reduction . . . 123
3.3.2 Losses reduction . . . 125
3.4 Results and discussion . . . 127
3.4.1 Experimental Results . . . 127
3.4.2 Discussion . . . 127
3.5 Mathematical description and presentation of the incomplete demonstration 129
3.5.1 Problem description and hypothesis . . . 129
3.5.2 An incomplete demonstration . . . 130
3.5.3 A Mathematical intuition on STIPWM . . . 135
3.6 Conclusion . . . 135

Conclusion 137

A The Inverter structure 143
A.1 The Voltage source Inverter . . . 143
A.2 Commutation cells . . . 144
A.3 VSI structure . . . 144
A.4 VSI fundamental principle and equations . . . 146

B THIPWM proof 148

C Space Vector Modulation time computation **151**

D SVM Equivalence with carrier based PWM **154**

E Fourier Decomposition **158**
E.1 QWS 159
E.2 HWS 159
E.3 FWS 159
E.4 PSR 159

F Weighted Total Harmonic Distortion **161**
F.1 Inductive load 161
F.2 Capacitive load 163

G Symmetry harmonics removing **165**

H Double Fourier Decomposition **167**

I Switches losses **170**
I.1 Switching losses 170
I.2 Conduction losses 172

J Motor model **174**
J.1 RLE model 174

K Dead time consideration **176**

Bibliography **179**

List of Figures

1 Climate change impact of a person using their small urban vehicle within 2030 in urban use [1], [7] . . . 26
2 Climate change impact of a person using their core range or high-end vehicle within 2030 on the WHLVTP [1], [7] . . . 27
3 Climate change impact of a person using bus transportation within 2030 [1], [7] . . . 28

1.1 Synchronous electric motor control. In red, the PhD field of study . . . 36
1.2 dq PWM control . . . 37
1.3 Switching differences between saw-tooth based PWM and triangular based PWM . . . 39
1.4 Synchronous triangle and saw-tooth PWM Fourier comparison . . . 40
1.5 WTHD comparison between Triangular and Saw-tooth PWM . . . 41
1.6 ZSC injection principle . . . 42
1.7 DPWM principle, here is presented an example of DPWM computation with a phase ψ [40]. . . . 45
1.8 DPWM synchronous carrier-based PWM with their zero sequence component 46
1.9 Human hearing sensitivity, the more the curve is high the more these frequencies are difficult to hear [46]. . . . 47
1.10 RFPWM based on a random slope . . . 48
1.11 Pseudo RFPWM . . . 48
1.12 OMIPWM control scheme . . . 49
1.13 Complex representation of the feasibles voltages in a three phases two-level VSI. This representation is linked with Table 1.1 . . . 51
1.14 Vector graphic representation with all the switches represented in a $\alpha\beta$ frame 52
1.15 Three phases SVPWM representation with the synchronous carrier (green) 53
1.16 Definition of sectors for NSPWM, discrete line are the VSI feasible vectors and continuous red line define the NSPWM sectors. . . . 56
1.17 An example of NSPWM sequence for an angle between 30° and 90°(sector 2 of Fig. 1.16) . . . 57

1.18 Duty cycle of DPWM1 and NSPWM are overlapping 58
1.19 Near state PWM feasible zone representation, hatched area is the feasible one 59
1.20 An example of Quarter Wave Symmetry 64
1.21 An example of Half Wave Symmetry 64
1.22 An example of Full Wave Symmetry 64
1.23 $\Delta\Sigma$ vector control 69
1.24 A proposition of PWM MPC 71
1.25 abc Hysteresis PWM command 72
1.26 Hysteresis principle 72
1.27 Map of existing PWMs. blue: vector based strategies, green carrier based strategies, purple, closed loop strategies 73

2.1 Three phases inverter example of PSR strategy 84
2.2 Schematic view of the computation algorithm, N_m is the number of modulation index considered and Σ_{fin} is the final set of solutions found by the algorithm. 87
2.3 Comparison between FWS and PSR method according to WTHD for $N_{qp} = 2$ when minimizing WTHD 90
2.4 Comparison between FWS and PSR method according to WTHD for $N_{qp} = 5$ when minimizing WTHD 91
2.5 Example of smoothness for the first angle of the WTHD, for the FWS solution with $N_{qp} = 5$ 93
2.6 Example of smoothness for the first angle of the WTHD, for the PSR solution with $N_{qp} = 5$ 93
2.7 Efficiency relative gap for (ε_η) for $N_{qp} = 2$ 95
2.8 Efficiency relative gap for (ε_η) for $N_{qp} = 5$ 96
2.9 Schematic representation of the experimental bench. 97
2.10 WTHD value for $N_{qp} = 2$, the points have been computed with a step of 0.02 98
2.11 WTHD value for $N_{qp} = 5$, the points have been computed with a step of 0.02 99
2.12 Fourier spectrum for the FWS and PSR for $N_{qp} = 2$ and $m = 0.57$. 100
2.13 Voltage waveform for the FWS and PSR for $N_{qp} = 2$ and $m = 0.57$. 101

2.14 Off-line PWM control in the particular case of a three phase inverter. Solutions depends also on fundamental frequency for the angular precision. For this third dimension, each table should be understood as a frequency interval and not as a specific frequency. 102
2.15 PSR command as a space vector point of view 103

3.1 Principle of ZSCM, a zero sequence component is generated from the computed optimal Fourier specter (here is represented as an example the SVM equivalent one). 107
3.2 First, Fig. 3.2a represent the ZSC and the reference. On Fig. 3.2b it is the modulating signal (sum of the two last ones). Next Fig. 3.2c is the comparison between the modulated signal and the carrier signal. Finally Fig. 3.2d represent the generated switches. 108
3.3 Generation of ZSCM command 109
3.4 Relative margin, (ε_r eq.(3.9)) for optimal harmonic injection compared with SVPWM and THIPWM $\frac{1}{6}$ applied to WTHD (eq.(F.12)) for $N_{qp} = 5$ 113
3.5 Relative margin, (ε_r eq.(3.9)) for optimal harmonic injection compared with SVPWM and THIPWM $\frac{1}{6}$ applied to switches losses only ($\mathcal{P}_K$ eq.(3.6)) for $N_{qp} = 5$ 114
3.6 Relative margin, (ε_r eq.(3.9)) for optimal harmonic injection compared with SVPWM and THIPWM $\frac{1}{6}$ applied to total losses ($\mathcal{P}_{tot}$ eq.(3.7)) for $N_{qp} = 5$ 114
3.7 Normalized and centered v_0 comparison between harmonic injection and SVPWM for WTHD (eq.(F.12)) considering $N_{qp} = 5$ and $m = 0.5$ 115
3.8 Normalized and centered v_0 comparison between harmonic injection and SVPWM according to $\mathcal{P}_k$ and $\mathcal{P}_{tot}$ losses for $N_{qp} = 5$ and $m = 0.1$ 116
3.9 Relative margin, (ε_r eq.(3.9)) for optimal harmonic injection compared with SVPWM and THIPWM $\frac{1}{6}$ applied to WTHD (eq.(F.13)) for $N_{qp} = 3$ 117
3.10 Relative margin, (ε_r eq.(3.9)) for optimal harmonic injection compared with SVPWM and THIPWM $\frac{1}{6}$ applied to switches losses only ($\mathcal{P}_K$ eq.(3.6)) for $N_{qp} = 3$ 117
3.11 Relative margin, (ε_r eq.(3.9)) for optimal harmonic injection compared with SVPWM and THIPWM $\frac{1}{6}$ applied to total losses ($\mathcal{P}_{tot}$ eq.(3.7)) for $N_{qp} = 3$ 118
3.12 Normalised and centred v_0 comparison between harmonic injection and SVPWM for WTHD considering $N_{qp} = 3$ and $m = 0.5$ 119

3.13 Normalised and centred v_0 comparison between harmonic injection and SVPWM according to $\mathcal{P}_k$ and $\mathcal{P}_{tot}$ losses for $N_{qp} = 3$ and $m = 0.5$ 119
3.14 Here are represented the ZSCM initial computation (blue) for $N_{qp} = 3$ and $m = 0.5$, the equivalent saw-tooth wave form with $n_h = 20$ harmonics considered (red) and the exact saw-tooth waveform (yellow). As shown, the ZSCM converged to a perfect saw-tooth as it is impossible to distinguish the ZSCM and the 20^{th} firsts harmonics saw-tooth. 122
3.15 Zoom on a saw-tooth edge to explicitly see the saw-tooth convergence of ZSCM. 122
3.16 Theoretical WTHD values for $N_{qp} = 3$ 124
3.17 Theoritical WTHD improvement against THIPWM for $N_{qp} = 3$ 124
3.18 Saw-tooth amplitude for $N_{qp} = 3$ 125
3.19 Theoritical $\mathcal{P}_K$ improvement against THIPWM for $N_{qp} = 3$ 126
3.20 Theoritical $\mathcal{P}_{tot}$ improvement against THIPWM for $N_{qp} = 3$ 126
3.21 Experimental results of WTHD for different strategies when $N_{qp} = 3$ 128
3.22 Experimental relative gap for different strategies against THIPWM$\frac{1}{6}$ when $N_{qp} = 3$ 128
3.23 Map of existing PWMs after the PhD thesis. blue: vector based strategies, green carrier based strategies, purple, closed loop strategies 139

A.1 Scheme of a three phase two levels VSI 143
A.2 Two examples of commutation cell. Voltage source to a current load (on the left). Current source to a voltage load (on the right). 144
A.3 Possible switch positions for a three level inverter 145
A.4 Modulating signal and carrier based signal in order to select the switches . 147

C.1 first sector symmetric switches 152

H.1 A plane representation of the switches angles generated by the comparison between a triangular carrier (slope) and a SPWM (sines) 168

I.1 Switches nomenclature of current and voltage. "C" means Collector, "E" Emitter and "G" Grid 171

J.1 Description of the RLE model 175

K.1 Dead-time representation 177

List of Tables

1.1 Voltage and vector representations 50
1.2 Common mode voltage per vector **W** 55
1.3 First part pulse pattern of the RSPWM strategies 58
1.4 First part pulse pattern of the AZSPWM strategies 61

2.1 Optimization problem parameters 80
2.2 PSR Optimization problem parameters 83
2.3 Values of the parameters in order to find the presented results 89
2.4 Simulation mean value of WTHD for different solutions in percentage according to (F.13) 91
2.5 Simulation comparison between FWS and PSR for six specific operating points inside the improvement zone. Percentage of improvement have been computed thanks to (F.13) and (2.15). 92
2.6 Value of smoothness for different solutions in percentage (computed with WTHD) according to (2.14) 94
2.7 Experimental parameters 97
2.8 Experimental mean value of WTHD for FWS and PSR in percentage. This percentage was computed with the same points than Figs. 2.10 and 2.11. . 99
2.9 Experimental comparison between FWS and PSR 99

3.1 WTHD improvement againt THIPWM$\frac{1}{6}$ for different N_{qp}, maximum and mean value 118
3.2 Losses improvement againt THIPWM$\frac{1}{6}$ for different N_{qp}, maximum and mean value 120
3.3 Theoretical improvement mean and max value of WTHD against THIPWM for different N_{qp} values 124
3.4 Theoretical improvement mean and max value of Losses against THIPWM for different N_{qp} values 126

C.1 SVM sequence with extra switching respect for a whole switching period T_d 153

NOMENCLATURE

Acronyms

AC/DC **A**lternative/**D**irect **C**urrent

AZSPWM **A**ctive **Z**ero **S**equence **PWM**

BEV **B**attery **E**lectric **V**ehicles

CBPWM **C**arrier **B**ased **PWM**

CMV **C**ommon **M**ode **V**oltage

DPWM **D**iscontinuous **PWM**

E4T **E**tude **E**conomique, **E**nergétique et **E**nvironnementale pour les **T**echnologies du transport routier Français

EMC **E**lectro**M**agnetic **C**ompatibility

EMF **E**lectro**M**otive **F**orce

EV **Electric V**ehicles

FPGA **F**ield-**P**rogrammable **G**ate **A**rray

FWS **F**ull **W**ave **S**ymmetry

HEV **H**ybrid **Electrical V**ehicles

HWS **H**alf **W**ave **S**ymmetry

ICE **I**nternal **C**ombustion **E**ngine

IGBT **I**nsulated-**G**ate **B**ipolar **T**ransistor

MHEV **M**ild **H**ybrid **E**lectric **V**ehicles

MOSFET **M**etal–**O**xide–**S**emiconductor **F**ield-**E**ffect **T**ransistor

MPC **M**odel **P**redictive **C**ontrol

MTR-RSPWM **M**inimum RMS **T**orque **R**ipple RSPWM

NSPWM **N**ear-**S**tate **PWM**

ObF **Ob**jective **F**unction

OMIPWM **O**pposite **M**edian **I**njection **PWM**

OPP **O**ptimal **P**ulse **P**atterns

PHEV **P**lug-in HEV

PMSM **P**ermanent **M**agnet **S**ynchronous **M**otor

PSO **P**articular **S**warm **O**ptimization

PSR **P**hases **S**ymmetry **R**elaxation

PWM **P**ulse **W**idth **M**odulation

QWS **Q**uarter **W**ave **S**ymmetry

RFPWM **R**andom **F**requency **PWM**

RLE Resistive (**R**) and Inductive (**L**) load with a sinusoidal EMF (**E**)

RMS **R**oot **M**ean **S**quare

RPWM **R**andom **PWM**

RSPWM **R**emote-**S**tate **PWM**

RTI **R**eal **T**ime **I**nterface

SHEPWM **S**elective **H**armonic **E**limination **PWM**

SPWM **S**inusoidal **P**ulse **W**idth **M**odulation

STIPWM **S**aw-**T**ooth **I**njection **PWM**

SVM **S**pace **V**ector **M**odulation

SVPWM Carrier based equivalent of SVM

THD **T**otal **H**armonic **D**istortion

THIPWM **T**hird **H**armonic **I**njection **PWM**

U.C. **U**nder **C**onstraints

VSI **V**oltage **S**ource **I**nverter

WHLVTP **W**orldwide **H**armonised **L**ight **V**ehicles **T**est **P**rocedure

WTHD **W**eighted **T**otal **H**armonic **D**istortion

ZSC **Z**ero **S**equence **C**omponent

ZSCM **Z**ero **S**equence **C**omponent **M**odulation

Optimisation parameters and variables

$\alpha_{i,Z}$	Switching angle number i for the phase Z	
α_i	Switching angle number i for the first phase	
Δt	Dead-time value	
δt_{min}	Minimum time gap between two switching	
$\delta\theta_{min}(\omega)$	Minimum electric angle gap	$\delta\theta_{min}(\omega) = \omega\delta t_{min}$
ϵ_θ	Angle tolerance	
ϵ_V	Voltage tolerance	
$\mathbf{K}$	Penalty coefficient vector	$\mathbf{K} = [K_1, K_2]$
$\mathbf{x}$	Decision variable Matrix $(p \times N_d)$	
$\mathbf{x}_0$	Starting point Matrix $(p \times N_d)$	
$\mathbf{x}_Z$	Decision variable vector $(1 \times N_d)$, $Z \in [\![1; p]\!]$	
$\boldsymbol{\alpha}_{FWS}$	HWS solution vector extended to FWS	
$\boldsymbol{\alpha}_{HWS}$	QWS solution vector extended to HWS	
$\boldsymbol{\alpha}_{PSR}$	FWS solution vector extended to PSR	
$\boldsymbol{\alpha}_{QWS}$	QWS solution vector	
θ	Angle variable (electric angle)	$\theta = \omega t$
c_{n,v_0}	Complex Fourier coefficient of ZSC $n \in \mathbb{N}$	
$f(\theta)$	Designate an objective function which depends of θ	
f_s	Switching frequency defined as:	$f_s = 2N_{qp}f_1$
f_v	Current objective value with constraints penalties	

h	Centered saw-tooth amplitude	$h = h_{max} = -h_{min}$
h_{max}	Saw-tooth maximum value	
h_{min}	Saw-tooth minimum value	
$h_{r,k}$	In a SHEPWM context, it correspond to an harmonic chosen to be eliminated	
l_b	Lower bound for the optimization problem	
N_d	Number of decision variables	
n_h	ZSC number of harmonics for the ZSCM strategy	
n_m	Number of harmonics computed	
N_{qp}	Number of commutation per quarter period	
u_b	Upper bound for the optimization problem	
$x_{Z,k}$	k^{th} element of $\mathbf{x}_Z$, $k \in [1, N_d]$	

Motor parameters

ω	Fundamental electric pulsation desired	$\omega = 2\pi f_1$
E_{DC}	Bus voltage afforded by the battery	
f_1	Fundamental electric frequency desired	
L	Inductance in the RLE model	
p	Number of phases of the load	
R	Resistance in the RLE model	
R_s	Stator resistance in the dq model	

Measures, and analysis

η_λ	Efficiency, $\lambda \in \{RL,\ RLE\}$
$\mathbf{a}_{n,I}, \mathbf{b}_{n,I}$	Current Fourier coefficients for harmonic $n \in \mathbb{N}$
$\mathbf{a}_{n,V}, \mathbf{b}_{n,V}$	Voltage Fourier coefficients for harmonic $n \in \mathbb{N}$
$\mathbf{I}_n$	Harmonic current amplitudes vector $n \in [\![2; \infty]\!]$
$\mathbf{V}_1$	Fundamental desired voltage amplitude vector

$\mathbf{V}_n$	Harmonic voltage amplitudes vector $n \in [\![2; \infty]\!]$	
$\mathbf{V}_{mod}$	Modulation vector	$\mathbf{V}_{mod} = \mathbf{V_1} + v_0$
$\mathbf{V}_{ref}$	Desired voltage vector	$\mathbf{V}_{ref} = [\mathbf{V}_{1,ref}; \mathbf{V}_{2,ref}; \mathbf{V}_{3,ref}]$
$\mathbf{W}_k$	Complex space vector associated to the sector k	$\mathbf{W}_k = \frac{2}{3} E_{DC} e^{i(k-1)\frac{\pi}{3}}$
$\varphi_{Z,n}$	n^{th} harmonic phase shift for $Z \in [\![1; p]\!]$	
A_k	SVM sector number k	
$a_{c,n,W}, b_{c,n,W}$	Command Fourier coefficients vector for $W \in \{QWS,\ HWS,\ FWS,\ PSR\}$ and $n \in \mathbb{N}$	
$A_{k,n}, B_{k,n}$	Real and complex part of a double Fourier decomposition $k \in \mathbb{N}, n \in \mathbb{Z}$	
$a_{n,Z,V}, b_{n,Z,V}$	Voltage Fourier coefficients for $Z \in [\![1; p]\!]$ and harmonics $n \in \mathbb{N}$	
B_k	NSPWM sector number k	
$C_{k,n}$	Complex Fourier coefficient $k \in \mathbb{N}, n \in \mathbb{Z}$	
d_j	Duty cycle of the phase j	
dt_{on}, dt_{off}	Builder additional time to compute lost switching energy	
E_{on}, E_{off}	Diode and IGBT energy losses	
$E_{sw}(i_Z(t))$	Energy lost while switching current $i_Z(t)$	
$i(\theta)$	Current function over the angle θ	
I_C	Collector current	
i_0	Initial current value	
i_{inv}	Current at the output of the DC capacitor	
i_{K_i}	Current through the switch K_i	
$I_{Z,n}$	n^{th} harmonic current amplitude for $Z \in [\![1; p]\!]$	
$i_Z(t)$	Instantaneous current at time t, for $Z \in [\![1; p]\!]$	
m	Modulation index	$m = \frac{V_1}{E_{DC}}$
m_{max}	Maximal feasible modulation index	$m_{max} = \frac{2}{\pi}$

m_{min} Minimal feasible modulation index depending on the strategy considered

$P_{con}(i_Z(t))$ Power lost inside the IGBT and the diode because of $i_Z(t)$ current conduction

r_{CE} Resistance of the IGBT

r_F Resistance of the diode

T_d Space vector period $T_d = \frac{1}{f_s}$

T_j Junction temperature of the switch

$T_{\mathbf{W}_k}$ Conduction time of the complex space vector $\mathbf{W}_k$

V_d, V_q Voltages in the dq model

$V_{CE,0}$ Ignition voltage of the IGBT

V_{CE} Voltage between the collector and the emitter

$V_{F,0}$ Ignition voltage of the diode

V_{GE} Grid to emitter voltage

V_{K_i} Voltage of the switch K_i

V_{med} Median voltage $V_{med} = -\max(\mathbf{V}_{ref}) - \min(\mathbf{V}_{ref})$

$V_{Z,n}$ n^{th} harmonic voltage amplitude for $Z \in [\![1; p]\!]$

V_Z Single voltage amplitude of the leg Z, $Z \in [\![1; p]\!]$

$V_Z(t)$ Single voltage signal of the leg Z, $Z \in [\![1; p]\!]$

Others

$< . >$ Mean value

$< \mathbf{x}, \mathbf{y} >$ Scalar product between vectors $\mathbf{x}$ and $\mathbf{y}$

α_{j,m_i} Angle number j corresponding to m_i

β Variable defined as: $\beta = 3kh$

$\lfloor x \rfloor$ As $x \in \mathbb{R}$ $\lfloor x \rfloor$ is the integer part of x

$\mathbf{\Psi}_k$ Vector defined as $\mathbf{\Psi}_k = [\alpha_{k,m_1}, \cdots, \alpha_{k,m_{imax}}]^t$

$\widehat{\mathbf{\Psi}}_k$ Estimated vector of $\mathbf{\Psi}_k$

$\mathbf{E}(X)$	Expectation of X	
$\mathbf{M_j}$	Vector defined as:	$\mathbf{M_j} = [m_0, m_1, \cdots, m_{imax}]^t$
$\mathbf{W}_i$	Complex voltage i feasible inside the inverter	
$\overline{z}$	As $z \in \mathbb{C}$, $\overline{z}$ is the conjugate of z	
sign	Sign function, $\text{sign}(x) = 1$ if $x > 0$, $\text{sign}(x) = -1$ if $x < 0$, $\text{sign}(x) = 0$ otherwise	
$\widehat{\alpha}_{j,m_i}$	Estimated angle of α_{j,m_i}	
$F_\nu(x,y)$	f_ν Anti-derivative form	$F_\nu(x,y) = \int f_\nu(x,y)dy$
$f_\nu(x,y)$	Function defined as:	$f_\nu(x,y) = e^{i(x\sin(y)-\nu y)}$
m_i	Modulation index of the solution number i	
m_{imax}	Maximum modulation index number	
S_i	Initial command value (high: 1, low: 0)	
S_Z	Command for the leg Z, $Z \in [\![1;p]\!]$	
V, I	Voltage and current	
v_0	Zero sequence component	
V_{CMV}	Common mode voltage generated by the VSI	
w	Variable defined as:	$w = km\pi$
y_c	Synchronous triangular carrier signal	

INTRODUCTION

Context and motivations

By 2020, the market for Electric Vehicles (EV) and Plug-in Hybrid Electrical Vehicles (PHEV) represent up to 10% of all the private cars in France[1]. This observation is not specific to France, this trend is also observed in the United States, China, and throughout Europe [1], [2].

This recent growth in electrified vehicles is not innocent, as many countries are encouraging this market through laws concerning the purchase and use of this kind of vehicle. Indeed, in Paris (the French capital) for example, thermal vehicles could be banned until 2035 and the same type of law is considered in England [3], [4].

In addition to consumers, manufacturers are also strongly encouraged to produce low-carbon vehicles, as each gram of excess CO2 is very expensive for the car builder [5].

All these constraints and incentives have the same objective: quickly and efficiently reduce the number of greenhouse gases released into the atmosphere to limit the global warming predicted by climatologists [6].

Even if EVs do not directly produce gases during their use. The energy produced to manufacture them, and to power them, does. The E4T report [7] shows the ecological advantage of some vehicles over each other and it is clear that plug-in electrified vehicles (Hybrids or Electrics) offer the best energy compromise. Figs. 1, 2 and 3 show that for the whole life cycle of a vehicle, the impact of an electrified vehicle is greatly reduced against Internal Combustion Engines (ICE). Furthermore, this observation is still true for every vehicles class, small ones (Fig. 1), core range vehicles (Fig. 2) and bus transportation (Fig. 3).

However, there is one important nuance to be made. These observations are true in France where electric energy is largely decarbonized thanks to nuclear energy and renewable energies. The observations could be different in other countries, but they are not documented in the E4T study as it was driven by the French government [1], [7].

Thus, the pollution caused by EV and PHEV is essentially due to their construction (extraction of materials and their manufacture Figs. 1, 2 and 3). Indeed, today's batteries

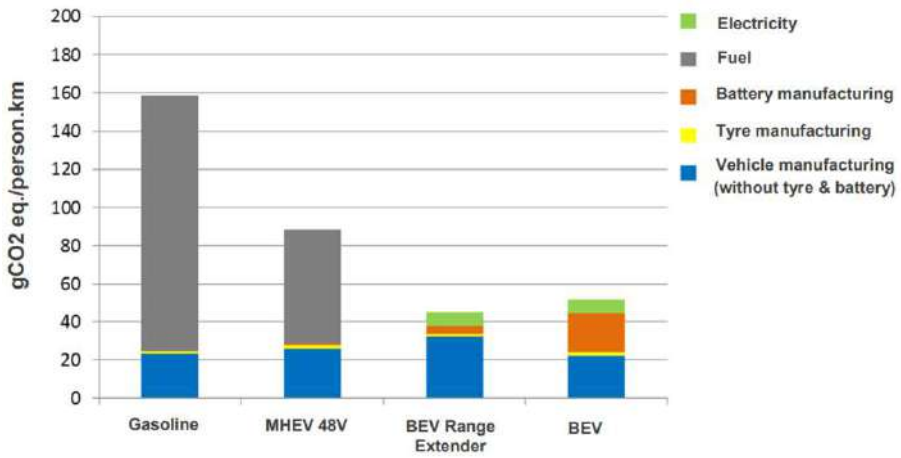

Figure 1 – Climate change impact of a person using their small urban vehicle within 2030 in urban use [1], [7]

are very lithium-intensive and to guarantee greater autonomy to the consumer, very large batteries are produced [1].

Historically, increasing the size of batteries of EVs and PHEVs is the main way to increase the vehicle range. Nevertheless, it is also possible to limit the consumption of electrical energy and thus reduce losses in the vehicle. These losses can be greatly reduced by optimizing some power train elements. The aim is to reduce battery losses, inverter losses, motor losses, transmission losses to the wheels, or any electric intensive part to increase the global vehicle efficiency and thus the vehicle range.

In this manuscript, conducted in the framework of the chair between Renault and École Centrale de Nantes-LS2N, the bet was to be focused on the electric consumption of the entire vehicle. Thus, one part of the global EV/PHEV powertrain is investigated: the control of the two-level three phases inverter.

For reasons of cost and accessibility of EV, the inverter considered by Renault is a three legs voltage inverter with only two levels. This architecture has the advantage of being minimalist as it contains only six power switches (two per leg). However, considering the addition of extra switches, the cost would grow exponentially with the number of vehicles produced. Indeed, to change the hardware structure it is required to perform research and development, change the software and all the dependencies, and finally, the industrialization process will be significantly changed.

All these changes have a non-negligible cost and would be paid by the final customer with more expensive vehicles. Renault's philosophy is not to build expensive cars but

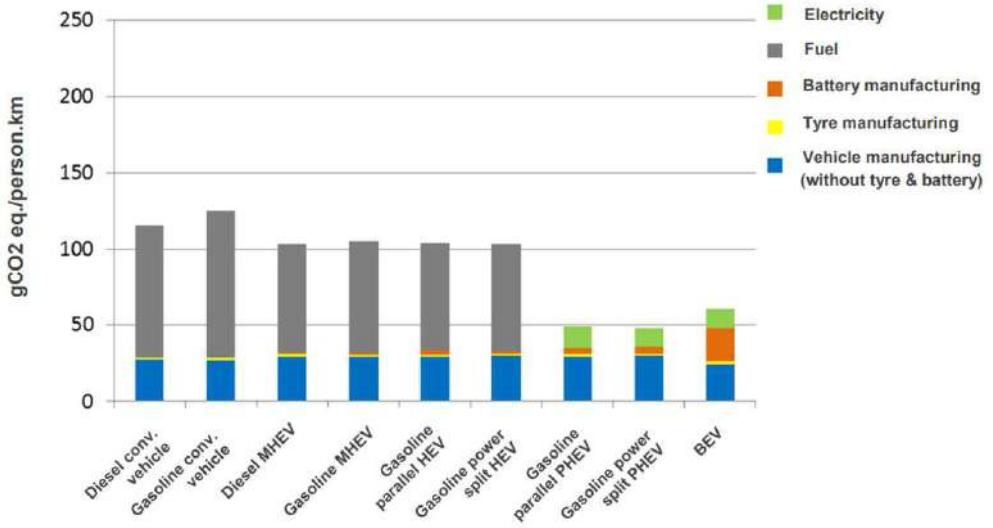

Figure 2 – Climate change impact of a person using their core range or high-end vehicle within 2030 on the WHLVTP [1], [7]

to provide a vehicle to everybody by maintaining high safety and reliability levels. The hardware changes to increase the vehicle range would not be appreciable. This last constraint led Renault to consider software changes in their vehicles instead of hardware ones. More precisely, the global point of view is to modify every software linked with energy consumption to improve their vehicles. Then the charger drive, the inverter drive, the command control drive, etc. are in the scope to be improved [8]–[12].

Thanks to the previous context information, this research work subject is to work on the Pulse Width Modulation (PWM) control of the power inverter, and more precisely on its optimization in the context of EV use. As mentioned, because of the intrinsic structure of the vehicles, the work is limited to the study of two-level inverters. Furthermore, to remove harmonics lower than the electric fundamental one the researches focused on synchronous PWM strategies. Indeed synchronicity force the harmonics generated to be integer multiples of the fundamental one. This assumption can be legitimate as it will necessarily reduce the losses of an inverter, nevertheless, this configuration needs information on the motor angle due to the synchronicity that requires either a mechanical sensor or an observer.

Thanks to the previous exposition of the context, it appears that the ecological, social, and industrial contexts justify the research to improve the two-level inverter. Nevertheless, the inverter studied is not a new device to convert Direct Current (DC) energy to an Alternative Current (AC). Then, a quick overview of DC/AC conversion history is

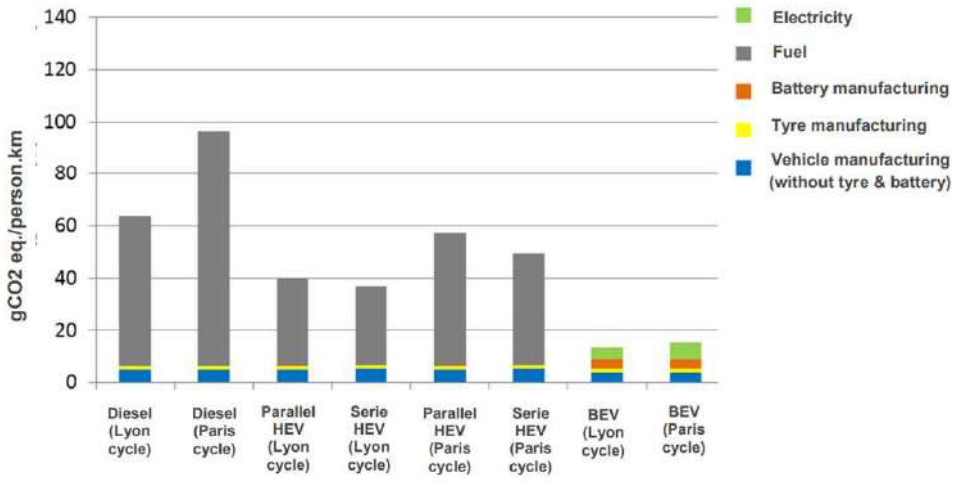

Figure 3 – Climate change impact of a person using bus transportation within 2030 [1], [7]

proposed next to precise the origins and context of actual research on DC/AC conversion.

A brief DC/AC conversion history

The Birth of AC to DC conversion

Since the start of AC usage at the beginning of XXth century, the question of conversion between AC and DC was a problem for engineers.

Indeed, DC power appeared first and was progressively replaced by AC ones because of the development of synchronous electric motors. Despite this replacement, AC and DC devices existed together, and a connection between the DC power and the AC one was required, this way the first AC/DC converters appeared [13].

The first AC/DC converters were done thanks to rotary machines and next by mercury arc rectifiers and finally by solid-state rectifying equipment. This equipment was called rectifiers, the name still used nowadays [1].

The apparition of inverters

The principle of the inverter has been described for the first time in 1925 by David Prince [14], in a research paper called "The inverter". The inverter term is directly linked with the rectifier one presented in the previous paragraph. Indeed inverter works exactly

1. The actual converters are called "static converters" because they do not need rotary devices to perform the conversion

as a rectifier but as a reversed one [15], then an inverter is defined as the inverse of a rectifier. In 1925 the inverter described by Prince is a rotary system, but became progressively, at the same time as the rectifier a "static converter", using power switches.

The command control development of inverters

When the first static DC/AC converters arrived in the industry, it was necessary to control them, a control is done with analogical devices and electronics. Thanks to this command architecture the first control imagined was based on the mean value principle, this is the first PWM control, called "natural PWM" or "Sinusoidal PWM" (SPWM). Nevertheless, with the increase of output amplitude needed, the references overcame the original carrier signal, it is the birth of the so-called "over-modulation". This method was a lot studied, before the appearance of injection methods, with the first Third Harmonic Injection PWM (THIPWM) described for the first time in 1975 by Buja [16] allowing to increase the linear use of inverters. In the following years (1977) the development of Discontinuous PWM (DPWM) appeared to decrease losses instead of increasing the harmonics quality with the Depenbrock works [17] (DPWM1). In addition, the first vectorial PWM methods also appeared approximately ten years after in 1988, as described by Van der Broeck [18]. The Space Vector Modulation (SVM) technique was revealed to be particularly efficient in the case of vectorial motor control. Based on these researches a constant increase of PWM command-control was performed with the appearance of Optimal Pulse Patterns (OPP) and closed-loop PWM as the model predictive control for example. Nevertheless, in parallel with new control structure development, new topologies appeared that are more efficient than the classic three-phase two-level inverter.

The new topologies

As mentioned, "inverter" designates the most basic way to convert DC energy to AC one (three legs and two levels). On the other hand, multilevel converters perform the same transformation but with more switches to perform a better output voltage, redundancy, etc. All these new topologies have their pros and cons, and it would be impossible to provide space for all of them in this manuscript, nevertheless, it is important to know they exist and consist of very efficient alternatives to the classic inverter to perform electric power conversion. Instead, it was decided to propose a short and non-exhaustive list of converters without exploring them in this document [19], [20]:

— Neutral-point clamped converter

— Active neutral-point clamped converter
— Modular Multilevel Converters
— Flying capacitor converter
— Nested neutral-point clamped converter
— Cascaded H-bridge converter
— Cascaded neutral-point clamped converter
— etc.

Those new topologies have many significant advantages as to offer greater flexibility in control, redundancy, better output, and then, better efficiency. Those elements led Franquelo in 2008 to affirm that *"the age of multilevel converter arrives"* [21]. Nevertheless, the inertia of the industry in addition to the development costs, industrial changes, and material costs are reasons explaining why Multilevel converters do not surround us today. Then researches on two-level inverters have to be performed to improve their behavior.

As the historical context is done in addition to the social context and the industrial one, a problem for the research work can be proposed.

Problematic

Electric power conversion, because of its internal structure composed of switches produces a lot of deleterious electrical harmonics for the connected load. For the specific case of an electric motor, copper losses and iron losses would drastically increase. In addition to losses, because of the non-sinusoidal voltage, an unpleasant noise could appear [22] or an important harshness. Furthermore, a bad output quality will be harmful to the battery as this device does not like, high-speed current changes. Current through the inverter will also generate an important electromagnetic field affecting electronics and motor behavior. Efficiency would be also decreased because useless harmonics for the motor and the converter are spoiled energy.

All these sides detrimental effects are due to (or amplified) by the PWM command control of the inverter. Of course, considering a natural PWM control will not forbid the vehicle drive, but, for sure, it will require important hardware modifications, to reduce noise, filter harmonics, and improve the ElectroMagnetic Compatibility (EMC), better battery protection or a bigger one to ensure the predicted autonomy.

If software changes can affect positively one of these constraints or more, this change must be done especially if its equivalent hardware change is expensive or difficult to

archive. As mentioned at the beginning of this manuscript introduction, this software improvement is not only relevant for cost reduction but it is also necessary to increase the performance of EVs and then attract people to buy electrical vehicles in phase with the ecological requirements.

This work is then concerned with the synchronous PWM optimization of a two levels inverter, in an electrical car context. These researches are focused on the three phases, but analog improvements can be found for p-phases inverters.

In addition, the Renault context led to suppose a voltage inverter with an electric motor connected at the output. Nevertheless, all the works presented, are applicable with very few modifications to current inverters and any kind of load requiring an alternative power to work.

The positioning problem is then: "How can we change the PWM control of the inverter to improve its behavior under constraints of synchronicity and for low switching frequencies?".

Contributions

This research work led to some peer-reviewed papers in international conferences and submissions in international journals. As this work is an industrial collaboration between Renault, l'École Centrale de Nantes and the LS2N, the results of the research have been patented by Renault.

The following list is exhaustive about the Ph.D. contributions and publications.

Peer reviewed international journal submitted

— A. Bourgeade, M. Ghanes, M. Fadel, A. Bouarfa, J-P. Barbot and R. Boisliveau, "New PWM inverter control based on optimal pulse pattern computation without phases symmetry constraints," *Control Engineering and practice (CEP)*, 2022 **[submitted]**

— A. Bourgeade, M. Ghanes, M. Fadel, A. Bouarfa, J-P. Barbot and R. Boisliveau, "A new synchronous carrier based PWM control for low switching frequencies: The saw-tooth injection PWM," *IEEE Transaction on power electronics (TPEL)*, 2022 **[submitted]**

Peer reviewed international conferences published

— A. Bourgeade, M. Ghanes, M. Fadel, A. Bouarfa and J-P. Barbot, "Off-line PWM control with three phases relaxed symmetry applied to a two-level inverter," *2021 IEEE Conference on Control Technology and Applications (CCTA)*, 2021, pp. 595-600, doi: 10.1109/CCTA48906.2021.9659137. (**see [23]**)

— A. Bourgeade, M. Ghanes, M. Fadel, A. Bouarfa and J-P. Barbot, "A New PWM Control based on an Optimized Zero Sequence Component injection: Application in a Two-Level Inverter," *IECON 2021 – 47th Annual Conference of the IEEE Industrial Electronics Society*, 2021, pp. 1-6, doi: 10.1109/ IECON 48115. 2021.9589469. (**see [24]**)

Peer reviewed international conferences submitted

— A. Bourgeade, M. Ghanes, M. Fadel, A. Bouarfa and J-P. Barbot, "Open problem: WTHD reduction understanding for a synchronous saw-tooth injection PWM control," *The 22nd World Congress of the International Federation of Automatic Control (IFAC)*, 2023 **[submitted]**

Renault patents linked with the previous work

— A. Bouarfa, A. Bourgeade and M. Ghanes, "Méthode de MLI précalculée basé sur la relaxation angulaire entre phases", *Brevet Renault*, 2021

— A. Bouarfa, A. Bourgeade and M. Ghanes, "Méthode de MLI à porteuse triangulaire par injection de dent de scie", *Brevet Renault*, 2022

Manuscript organization

The following document is organized into three chapters with appendices to help the understanding.

Chapter 1: The First chapter provides a global overview of existing strategies for the two-level inverter. Indeed, many PWM strategies philosophy exists as the carrier-based PWM, the vector-based but also more recent techniques as the OPP but also closed loop ones. All these strategies are explained and their pros and cons are underlined in terms of performance and implementation. At the end of the chapter, a choice is done on the future manuscript development regarding the existing strategies.

Chapter 2: The second chapter is interested in the particular case of OPP strategies it is well known these strategies offer the best results for a given objective. Here, the objective chosen among all the existing ones is the Weighted Total Harmonic Distortion (WTHD), because of its independence to load parameters.

In recent years the OPP tends to always relax the symmetry constraints to improve the output signal quality in terms of WTHD. Nevertheless, the switching angle computation is always done on a single phase and is extrapolated on the remaining ones. The main idea developed in this chapter is to relax this constraint and to compute the switching angles for all the phases independently but with respect to the global output waveform. This consideration, due to the numerous decision variables to deal with led to the introduction of optimization algorithm methods.

These methods were applied to a three phases two-level inverter in simulation and experimentally led to an improvement of the WTHD for low ratio between the fundamental frequency and the switching one. Furthermore, as the Phase Symmetry Relaxation (PSR) proposed could lead to quick changes inside the solution set, a new tool was introduced to quantify the difference in smoothness between PSR strategies and classical ones. This objective led us to conclude that the smoothness quality remains comparable for classical strategies and the PSR.

Chapter 3: The main problem with OPP is the storage of the solutions inside a memory. Then working on more classical strategies seemed to be a good compromise between performance and easy implementation. In this context, carrier-based strategies were explored and more precisely an extension of THIPWM was imagined. This extension is done by computing an infinity of harmonics to inject inside the modulating signal by the zero sequence component instead of a single one as THIPWM does. This strategy is called Zero Sequence Component Modulation (ZSCM).

The first interesting property found of the ZSCM strategy is that it can reproduce any carrier-based strategy as SVPWM or DPWM strategies for example. Then after finding results, an unexpected zero sequence components waveform was found for some specific operating points and objectives which seems to have a shape of a saw-tooth. This Saw-Tooth Injection PWM (STIPWM) was then optimized and studied to understand its properties. Thus, an attempt of demonstration based on double Fourier decomposition was done and some non-conclusive but interesting preliminary results were found to understand deeply STIPWM strategy.

In addition simulation and experimental results were found to compare both ZSCM and STIPWM to classical strategies. The ZSCM was revealed better for every operating point studied. On the other side STIPWM, with its very simple shape is easy to perform and provides very interesting results for some operating points.

Conclusion: As a conclusion, an overview of the work done is performed and perspectives are provided to help anyone who desires to go deeper into the research field of synchronous low frequencies PWM control applied to two-levels inverters.

Furthermore, it is highlighted some very interesting possible developments in multilevel converters or possible applications in other research fields.

Chapter 1

The inverter command

In this chapter, an overview of the most common Pulse Width Modulation (PWM) control used for three phases two-level inverter is proposed, this work is essential, as it will draw a research context and will provide ideas for future developments. In addition, this work will avoids the thesis to do again improvements already existing in the literature.

It is important to mention that, all the strategies presented have specific applications, pros and cons, which would be highlighted. Furthermore, this background cannot be exhaustive, but it provides a general overview of the existing PWM control approaches.

Another objective of this chapter is to motivate the interest in three phases two-level PWM control as it seems to be an old and refined domain as explained in the introduction [21]. This chapter will also position the proposed strategies during the Ph.D against existing approaches.

In this manuscript, it will be often a question of Voltage Source Inverter (VSI), nevertheless, thanks to the fundamental power conversion law [25]–[27], it also exists inverters transforming DC to an AC voltage. But, in practice, a voltage source is more present in the literature as it exists more voltage sources in nature, than current ones. Furthermore, all the reasoning done on voltage is rigorously equivalent to current consideration thanks to Thevenin-Norton consideration [28], [29]. Also, the study is focused on the Renault's electrical vehicles then, for the seek of simplicity, this work is mainly concerned by a DC voltage source with an AC current load.

About the load, in the context of this work, its structure is not important as all the strategies developed are focused on the inverter only. Then, the load is precised when the current information is required.

In the following well known PWM strategies will be explored, the Carrier Based PWM (CBPWM) first [27], next the vectorial ones [30]. Following, the most recent ones, appeared with micro-controllers, the off-line PWM, also called OPP [31] are exposed. Fi-

nally, a short exploration on existing closed loop strategies is performed as the Hysteresis [32] or the $\Delta\Sigma$ ones.

For a reader new to PWM techniques, a short reminder on PWM control command is done in Appendix A. This Appendix does a recall on bases of the PWM control and well known equations. Following sections suppose a good knowledge of PWM bases.

Next section, is directly concerned by some basics CBPWM description, hypotheses and command control assumptions.

1.1 Carrier based PWM

As mentioned in Appendix A the PWM signal can be generated thanks to a comparison between the normalized desired signal and a carrier signal. Nevertheless, it is not the only way to generate command of the power switches inside the inverter. First, a short recall on the command structure will be done, even if in the whole manuscript, this command is considered as a black box.

1.1.1 The different classes of CBPWM

1.1.1.1 Hypotheses concerning the control loop

The reference signal mentioned before have to be provided by the command control loop. An example of a simplified control loop of a Permanent Magnet Synchronous Motor (PMSM) is presented on Fig. 1.1

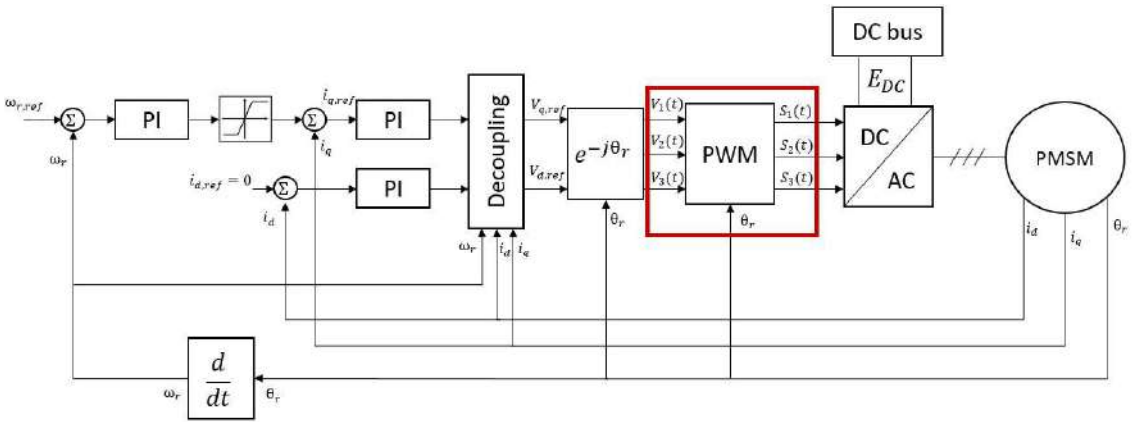

Figure 1.1 – Synchronous electric motor control. In red, the PhD field of study

This control loop can have many forms, with many representation and complexities. A *dq* schematic one can be seen on Fig. 1.2. Nevertheless, all this document is not concerned about the entire control loop, but only on the PWM generation part (Fig. 1.1). Then the regulation part is considered as a black box providing a correct information on desired frequency f_1, voltage amplitude $V_1 = mE_{DC}$ and phase $\varphi_{1,1}$.

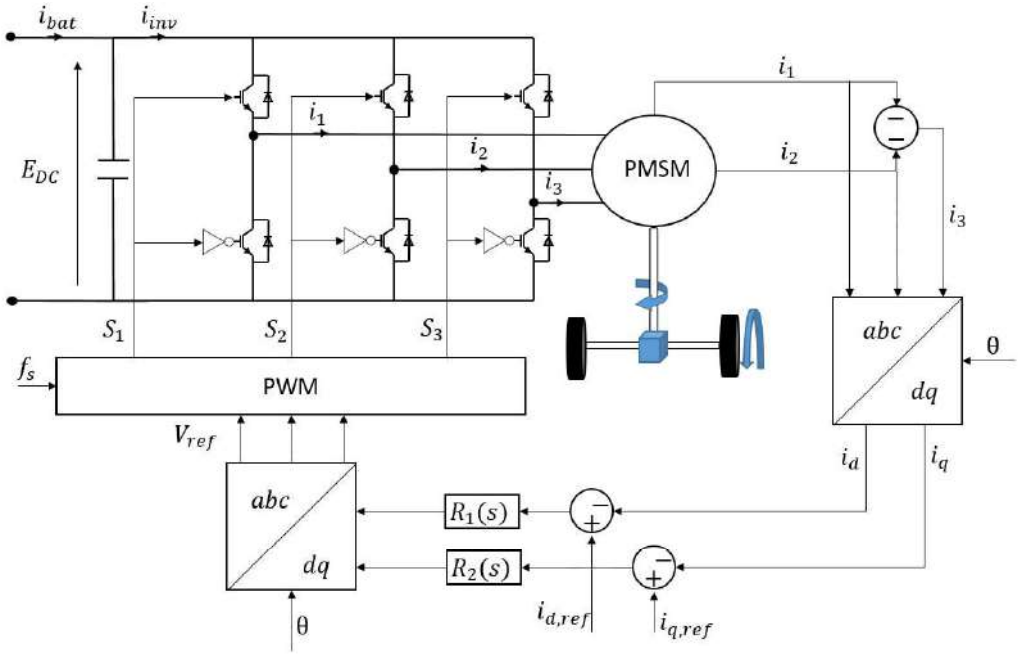

Figure 1.2 – dq PWM control

These informations are enough to control the motor, even if a very large quantity of regulation loop exists.

Indeed, many works treat the global problem of power electronics control in a more global loop without considering the PWM problem [33]–[35]. The purpose of our researches are done in an opposite consideration.

This research paradigm reasonable as the global control loop have not the same purpose than PWM control [1]. The first one is concerned about, speed, torque, observation, etc.. and the second one is concerned about the load harmonics and its impacts [27].

As mentioned before, even if the global control loop is an interesting field of research, this control will be supposed known to focus on the PWM generation and more precisely,

1. Even if they have not the same purpose, it is obvious that PWM directly depends on the global control loop as its computation is based on the closed loop reference.

on synchronous PWM.

Next subsection will do a short drawback on synchronous PWM advantages to justify this bias in our work.

1.1.1.2 Synchronous carrier based PWM

The main advantage of synchronous PWM against asynchronous ones is the absence of harmonics below the fundamental frequency. This is understandable the number of switches is constant per period, and switching angles [2] are preserved. Indeed, even if the desired frequency changes, the synchronous property will ensure the switching angle constancy. [3]

In the opposite, asynchronous PWM will variable switching angles depending on the frequencies [4]. This variation will generate a lot of low frequencies. These frequencies are hard to filter as they are below the fundamental one (i.e. the desired one).

Nevertheless, the main problem of synchronous CBPWM remains that the angle information is needed, in order to meet the synchronicity. To reach this constraint space vector constraints can be privileged as they already require the angle knowledge to generate the PWM (see section 1.2). Nevertheless, space vector PWM are asynchronous as the computation time T_d does not depend on the angle knowledge, and then generate low frequencies harmonics.

Renault company, for the previous reasons, wants to develop synchronous PWM inside the motor command control. To reach this specification, we will introduce several notations. First, synchronicity impose a fixed number of switches per period. This obligation leads to th introduction of N_{qp}, which designates the number of switching per quarter period. This number is linked with the switching frequency defined as $f_s = 2N_{qp}f_1$ and then $4N_{qp}$ switches per period [5].

Under the CBPWM a triangular wave form is implicitly supposed. Nevertheless, the reader have to keep in mind that triangular waveform is not the only possible shape and saw-tooth carrier based PWM also exist in the literature.

Next subsection discuss about the triangular and saw-tooth carrier differences.

2. The switching angle is the switching time reported over a period, in order to ignore the signal frequency for the computation.

3. Even if the switching angles are the same, the switching times are not constant as the frequency changes

4. The switching one and the fundamental one

5. It is important to notice that as f_1 vary the switching frequency f_s is not constant.

1.1.1.3 Synchronous triangular and saw-tooth PWM comparison

In the previous section, we discussed the interest of synchronous PWM against asynchronous one but under a triangular carrier based assumption.

This configuration was studied in the literature and led to less good results as it generates more harmonics than the triangular carrier based PWM [36]. Furthermore as we can see it on Fig. 1.3, triangular CBPWM generates centered pulsations. On the other-side saw-tooth PWM generates right aligned PWM [6].

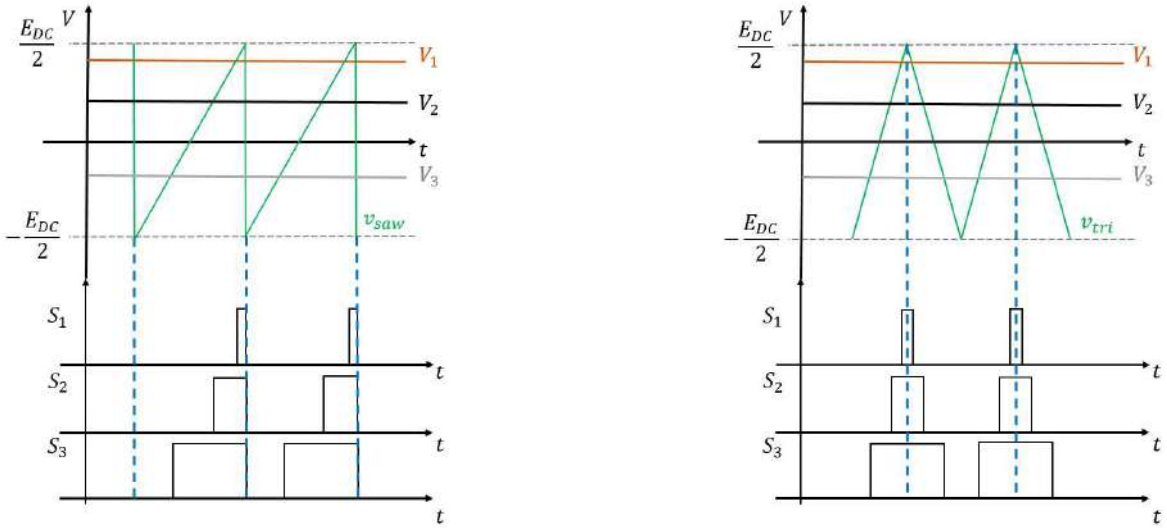

(a) Saw-tooth pattern

(b) Triangular pattern

Figure 1.3 – Switching differences between saw-tooth based PWM and triangular based PWM

The configuration explored Fig. 1.3, leads to better results with triangular CBPWM instead of saw-tooth ones. Indeed, thanks to its intrinsic symmetry, more harmonics are removed, providing better results. As an illustration of this affirmation Figs. 1.4a, 1.4b and 1.5 show that sychronous triangle symmetry afford better results than saw-tooth ones. Fig. 1.5, show a Weighted Total Harmonic Distortion (WTHD) comparison. The WTHD is a Total Harmonic Distortion (THD) modified to provide a better harmonic criteria for inductive loads. Explanations on WTHD and mathematical justifications can be found in Appendix F.

In few words, the WTHD will represent a generic current behavior in a motor. Indeed,

6. A saw-tooth based PWM generating left aligned pulses also exists. Nevertheless, it would lead to significant same results because of the symmetry.

as an electric motor is a low pass filter, the WTHD will filter the voltage in the same way except that WTHD does not depend on specific motor parameters. The WTHD equation is defined thanks to eq. (1.1).

$$V_{WTHD,\%} = \frac{100}{V_1}\sqrt{\sum_{n\geq 2}\frac{V_n^2}{n^2}} \tag{1.1}$$

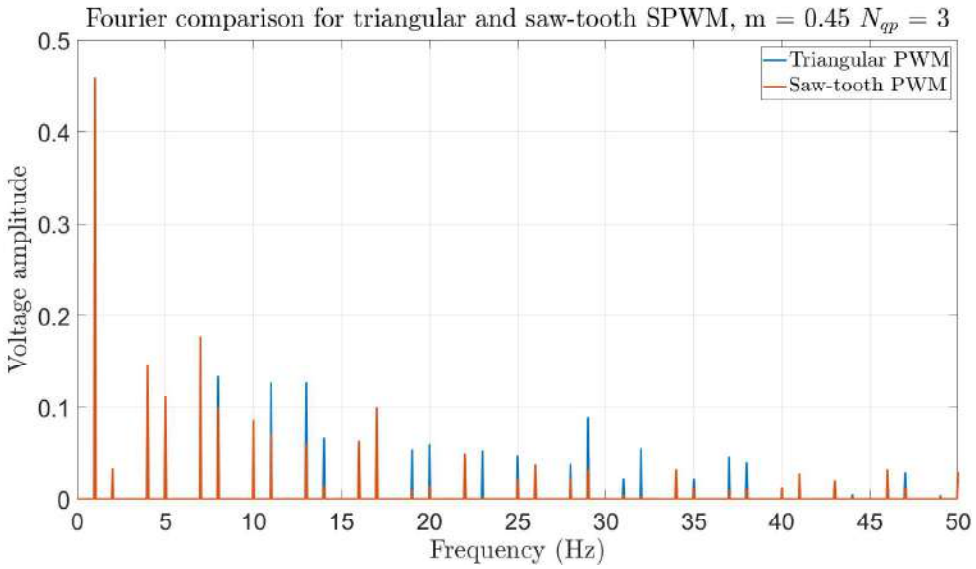

(a) Fourier comparison between Triangular and Saw-tooth PWM

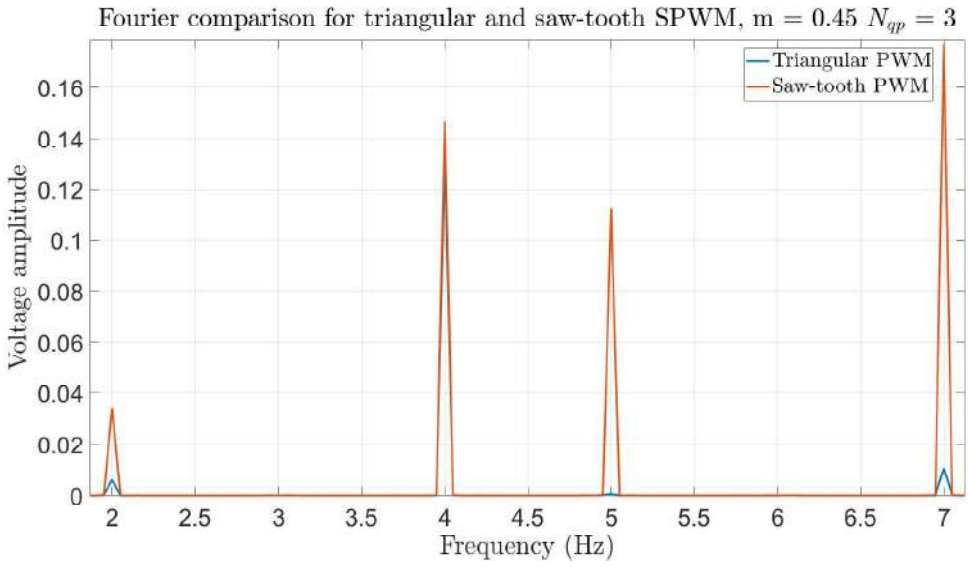

(b) Zoom on first harmonics of Fig. 1.4a, Harmonics 2,5 and 7 are significantly reduced

Figure 1.4 – Synchronous triangle and saw-tooth PWM Fourier comparison

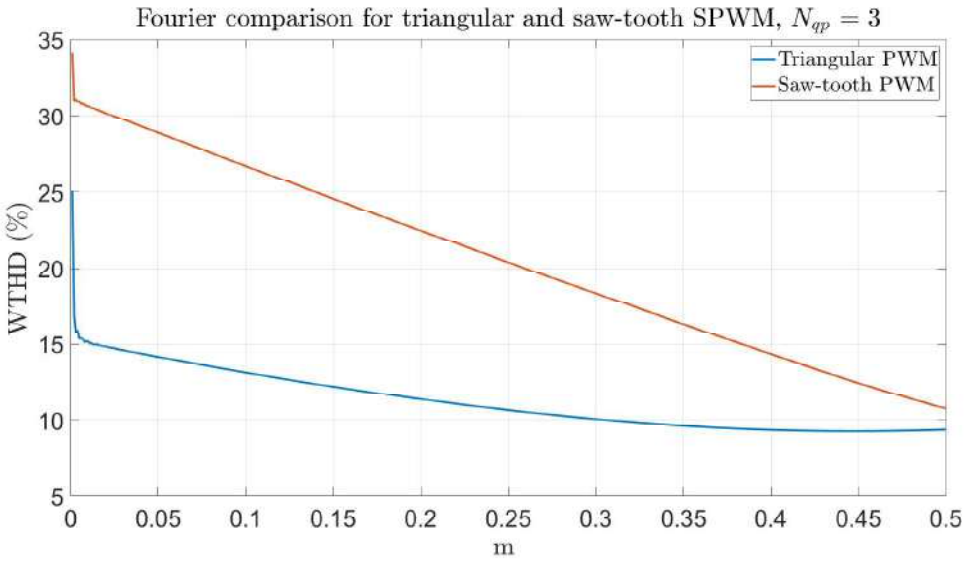

Figure 1.5 – WTHD comparison between Triangular and Saw-tooth PWM

For the seek of simplicity and because triangular carrier based PWM are omnipresent in the literature, CBPWM will designate the synchronous triangular one in the rest of the manuscript.

Next subsection is concerned about one of the usual technique consisting to inject a periodic signal inside the normalized reference one.

1.1.2 Zero sequence component injection

Previously, different kind of CBPWM was presented and especially a comparison between a triangle or a saw-tooth PWM. These methods was compared with the natural PWMto generate the signals. Nevertheless, it is well known that this method is not optimal as only two drived legs are enough to control an inverter [27].

The idea is then to drive only the first two phases of the converter. For that, we introduce the Zero Sequence Component (ZSC) described as: $v_0(t) = \frac{E_{DC}}{3}(S_1(t) + S_2(t) + S_3(t))$. The idea is to inject this signal in the normalized reference one to force the three legs to be controllable.

Because the matrix in eq. (A.1) cannot be inverted, the idea is to impose the ZSC (v_0) voltage instead of the three voltages to obtain better performances. Doing so, and thanks a mean value consideration, eq. (1.2) can be easily obtained.

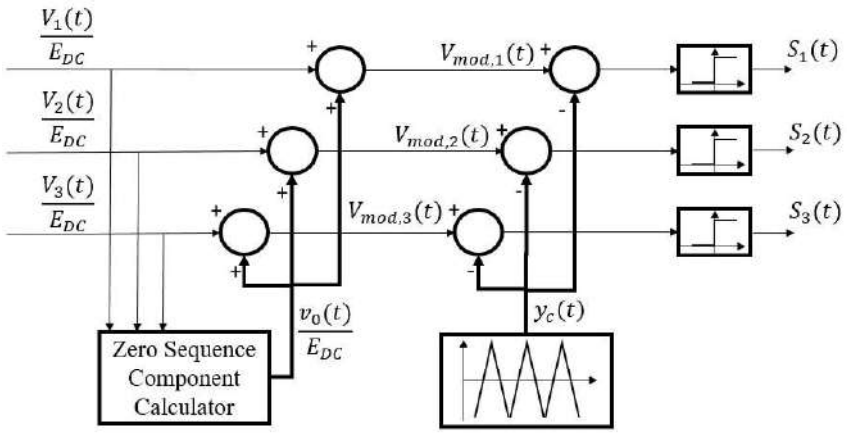

Figure 1.6 – ZSC injection principle

$$\begin{bmatrix} \langle V_1(t) \rangle \\ \langle V_2(t) \rangle \\ v_0(t) \end{bmatrix} = \frac{E_{DC}}{3} \begin{bmatrix} 2 & -1 & -1 \\ -1 & 2 & -1 \\ 1 & 1 & 1 \end{bmatrix} \cdot \begin{bmatrix} d_1(t) \\ d_2(t) \\ d_3(t) \end{bmatrix} \tag{1.2}$$

With $d_1(t)$, $d_2(t)$ and $d_3(t)$ the duty cycles and $\langle \cdot \rangle$ designate a mean value. Duty cycles are defined as the time ratio between the upper state one and the switching period. This definition can be expressed as a sliding average eq. (1.3).

$$d_x(t) = f_s \int_{t-\frac{1}{2f_s}}^{t+\frac{1}{2f_s}} S_x(y)dy \tag{1.3}$$

The duty cycle indicates how long each commutation cell will work. Indeed, doing so, locally the output will be performed properly as explained in the Appendix A.

By inverting the matrix of eq. (1.2), it is possible to compute the duty cycles depending on desired voltage. This inversion can be done as the introduction of the ZSC generates a reversible matrix eq.(1.4).

$$\begin{bmatrix} d_1(t) \\ d_2(t) \\ d_3(t) \end{bmatrix} = \frac{1}{E_{DC}} \begin{bmatrix} 1 & 0 & 1 \\ 0 & 1 & 1 \\ -1 & -1 & 1 \end{bmatrix} \cdot \begin{bmatrix} \langle V_1(t) \rangle \\ \langle V_2(t) \rangle \\ v_0(t) \end{bmatrix} \tag{1.4}$$

Eq. (1.4) indicates that only two voltage knowledge are enough to drive a VSI. In order to exploit this freedom degree, the ZSC, is added to the reference signal as seen on Fig. 1.6.

It is also possible to inject a null ZSC, providing the duty cycle of the SPWM. Nev-

ertheless, SPWM was quickly revealed as sub-optimal by the researchers.

In the middle of the 70' [16], [37] the first zero sequence component strategy appeared, to correct the problems afforded by over-modulation.

This first strategy was a THIPWM technique described by Buja in 1975 [16], [38]. Historically, this strategy was developed to increase the feasibility domain and to avoid the problems afforded by over-modulation techniques which produces a distortion of the output waveform. More precisely, the abrupt dropping of pulses may result in a step change in output voltage, which can cause motor current instability.

Next sub-section is then concerned about the description of THIPWM techniques.

1.1.3 Third harmonic injection PWM

The objective of THIPWM is to find a new modulating signal by injection of a third harmonic in order to increase the feasible domain. Then, the global equation of THIPWM modulating signal is described thanks to (1.5).

$$V_{mod} = m\left(\sin(\theta) + a\sin(3\theta)\right) \tag{1.5}$$

In eq. (1.5), m designates the modulation index and is defined as the percentage of use of the DC bus. Then, $m = \frac{V_1}{E_{DC}}$ where V_1 is the desired amplitude of the output signal.

It is possible to demonstrate that the a coefficient of eq. (1.5) allowing to reach the maximum modulation index by injecting a single third harmonic is equal to $\frac{1}{6}$ [16], [38]. This demonstration is presented in Appendix B.

Thanks to this injection consideration, the maximum modulation index reachable is $m_{max} = \frac{1}{\sqrt{3}}$ and represent a linear modulation increase of approximately 15%.

Even if originally the objective was to increase the linearity zone, an appreciable side effect of this strategy is to improve the harmonic quality of the output voltage. Indeed, the power lost before in the harmonics of the same voltage are now used to reach higher voltages. Then harmonics improvement is a side effect of the increase of the maximum feasible modulating index.

Nevertheless, another THIPWM strategy has been found to be optimal thanks an injection of $\frac{1}{4}$ instead of $\frac{1}{6}$. This method is known to increase the harmonic quality, and more specially the THD, nevertheless THIPWM$\frac{1}{6}$ remains the best to reduce WTHD.

Another point with the THIPWM $\frac{1}{4}$ is, that even if this method seems better about the THD, the linear modulation increase is now of 12% instead of 15% [27], [39]. It is understandable as the THIPWM $\frac{1}{6}$ was designed and proved to afford the greatest linear zone (see Appendix B).

It has been showed that THIPWM method improves the harmonic quality. Nevertheless, it is not the single criterion to qualify a PWM strategy. Next section will focus on the discontinuous PWM, strategies known to reduce the losses inside the inverter.

1.1.4 Discontinuous PWM

Discontinuous PWM also called DPWM are ZSC injection PWM. Their purpose is to minimize the losses inside the inverter by forbid to switch a phase for a certain amount of time. Indeed a lot of losses are due to the joule effect, then DPWM considers a reduction of switching losses and conduction losses. DPWM strategies force a leg to do not switch periodically and the saturated leg also change periodically. To do that, the idea is to force the zero sequence to a specific waveform exactly as harmonic injection seen before (see section 1.1.3). The main difference between THIPWM and DPWM is the final objective. Indeed both of them are concerned about injection of a ZSC inside the normalized reference signal. Nevertheless, THIPWM purpose is to reduce THD or WTHD and DPWM reduce the inveter losses even if the output signal contains more harmonics.

The first DPWM description was done by Depenbrock in 1977 [17] [7]. Depenbrock thoroughly investigated DPWM1 and illustrated its superior voltage linearity range, reduced switching loss, and the superior high modulation range current waveform quality. However, the poor low modulation range performance [8] and implementation complexity have limited the application of this modulator. Nevertheless other researches led to other equivalent implementation and simplifications of the DPWM strategies [40], [41].

Today all the DPWM are well known and some papers compare all the DPWM together [42].

In this manuscript, all the DPWM existing (as far as we know) are all presented on Fig. 1.8. The DPWM computation was done thanks to [40], [41] leading to eqs. (1.6), (1.7), (1.8) and (1.9).

7. Depenbrock did not introduced the "DPWM" name, this name arrived thanks to later works.
8. narrow pulse problems and poor current waveform quality

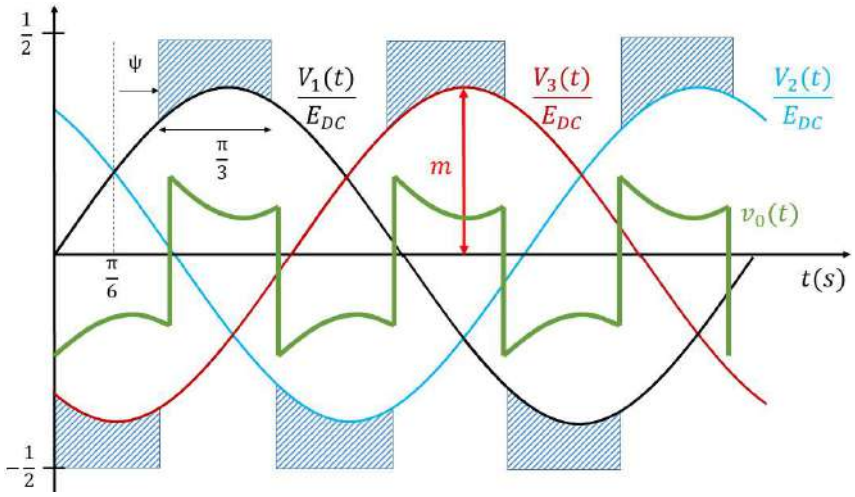

Figure 1.7 – DPWM principle, here is presented an example of DPWM computation with a phase ψ [40].

$$v_0(t) = \frac{1}{2}(1-2\alpha) + (\alpha-1)\max(\mathbf{V}_{ref}) - \alpha \cdot \min(\mathbf{V}_{ref}) \tag{1.6}$$

where

$$\alpha = 1 - \frac{1}{2}\left[1 + \text{sign}\left(\sin\left(3\left(\theta+\delta\right)\right)\right)\right] \tag{1.7}$$

Eqs. (1.6) and (1.7) represent an easy method allowing to implement most of the DPWM strategies by only changing the δ coefficient

The principle by doing it this way is to have the ZSC equal to the opposite of the actual adjacent signal with a phase shift multiple of $\frac{\pi}{6}$ doing so, at some specific instants the modulating signal will be saturated. This principle is more understandable thanks to Fig. 1.7. Even if the variable ψ can have an infinity of value in theory. Only some specific of them are interesting and consist the well known DPWM (0, 1, 2, 3, min and max).

According with eqs. (1.6) and (1.7), the δ parameter can be tuned to generate the desired DPWM:

— DPWM0 , $\delta = \frac{\pi}{6}$ (Fig. 1.8b)
— DPWM1 , $\delta = \frac{2\pi}{6}$ (Fig. 1.8c)
— DPWM2 , $\delta = \frac{3\pi}{6}$ (Fig. 1.8d)
— DPWM3 , $\delta = \frac{4\pi}{6}$ (Fig. 1.8e)

About the DPWMmin and DPWMmax strategies, the point of view is the same, but for an easiest implementation equations are a little bit different, and the ZSC is selected

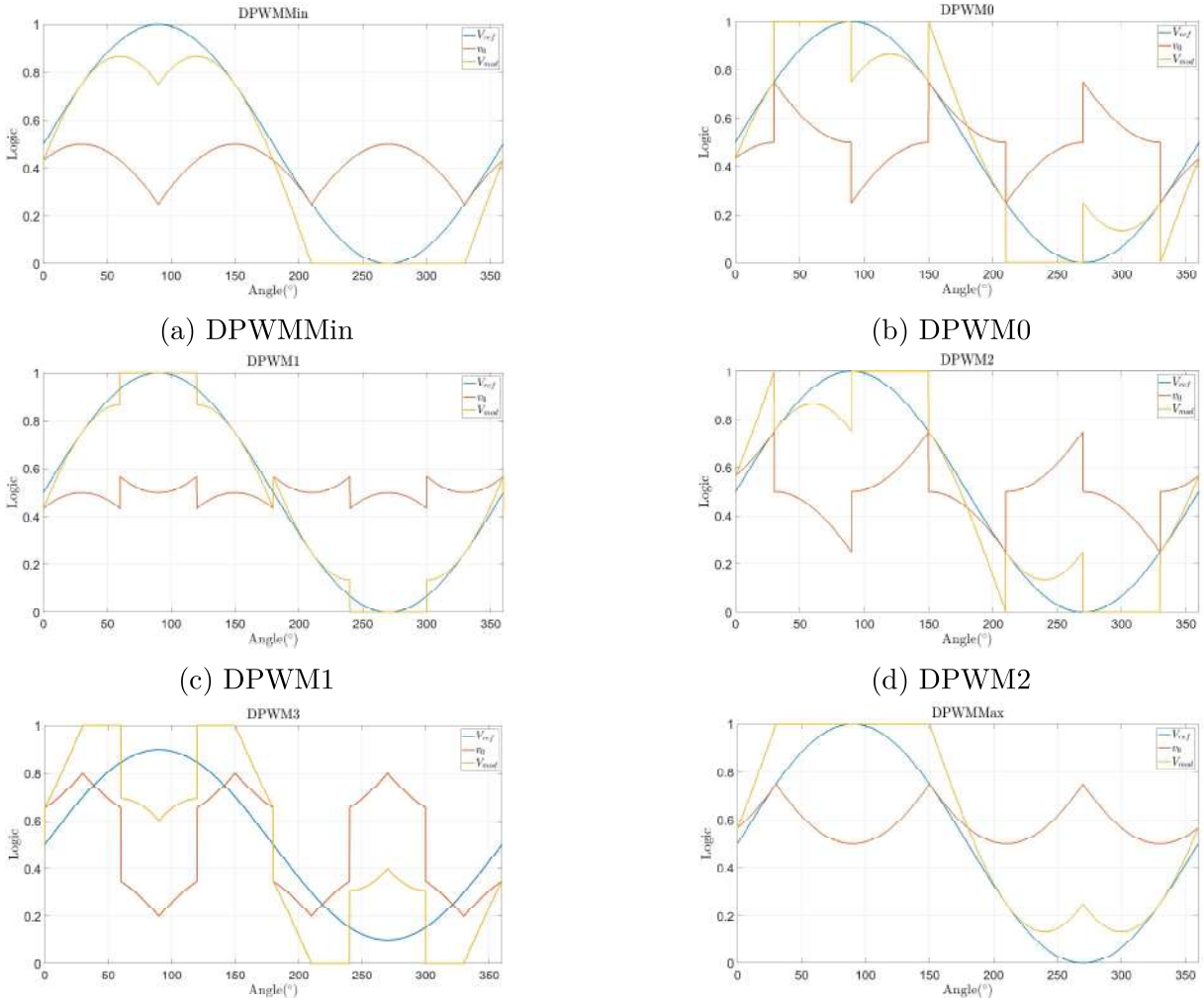

(a) DPWMMin (b) DPWM0

(c) DPWM1 (d) DPWM2

(e) DPWM3 (f) DPWMMax

Figure 1.8 – DPWM synchronous carrier-based PWM with their zero sequence component

equal to the saturation signal (the minimal one for DPWMmin and maximal one for DPWMmax). Giving eq.(1.8) for DPWMmin and eq.(1.9) for DPWMmax.

$$v_{0,DPWMMin} = -\frac{\min(\mathbf{V}_{ref})}{2} \tag{1.8}$$

$$v_{0,DPWMMax} = -\frac{\max(\mathbf{V}_{ref})}{2} \tag{1.9}$$

Thanks to all the previous description, it is possible to represent all the classical DPWM on Fig. 1.8.

We saw that DPWM strategies reduce the losses and THIPWM increase the harmonic

quality. Nevertheless, it exists other objectives as the noise reduction and it is the topic of the next subsection with the random PWM.

1.1.5 Random PWM

It exist, in theory, as many random PWM strategies as we desire. All the Random PWM (RPWM) have the same purpose: reduce the noise feeling of an human and reduce the motor vibrations, also called harshness. Indeed classic PWM works with a fundamental switching frequency (f_s) or with a synchronous frequency ($2N_{qp}f_1$). With these methods, the harmonics generated by the VSI are regular. The idea with a RPWM is to generate an infinity of harmonics with a wide frequency specter in order to reduce the perceived noise [9]. Indeed, the literature mention the feeling of "sand flowing" [22]. This sensation is due to the human ear sensibility, which is neither constant nor linear and a powerful but varying noise will be appreciable against a lower but constant noise. On Fig. 1.9, we can see that 4000Hz frequencies are way more easy to ear than others. To eliminate noise feeling those frequencies have to be avoided or to spread them on a lot of frequencies, which is done with RPWM. In addition with the human noise feeling reduction, mechanical vibrations of the motor will be also significantly reduced [22], [43]–[45].

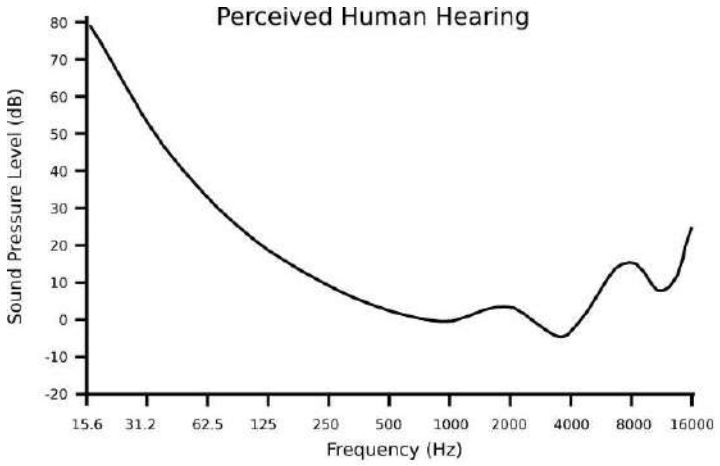

Figure 1.9 – Human hearing sensitivity, the more the curve is high the more these frequencies are difficult to hear [46].

Nevertheless, because RPWM generates a lot of harmonics, it's quality in terms of

9. Let's remark that the noise is reduced only as an illusion, because in reality more harmonics are generated. Nevertheless it is less disagreeable because of the richness of the harmonics.

losses or of WTHD is very poor. Furthermore the fundamental is not always feasible, especially for low switching frequencies. This is why, this method is called a high frequency PWM method. In addition, a lot of securities have to be planned in order to avoid narrow pulses or simultaneous switching.

The most basic idea to generate a PWM is to use a random carrier frequency PWM. The principle is to change randomly the frequency of the carrier [32] compared to the modulating signal. To do so, many techniques exists as selecting the slope randomly inside a range to generate rich harmonics (Fig. 1.10). In order to improve this technique Shi in 2003 [47], proposed a genetic based algorithm, to select the carrier frequency but also to reduce the THD of the signal. This algorithm compute the best frequencies off-line and apply them thanks to a real-time algorithm.

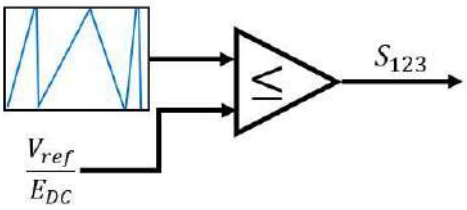

Figure 1.10 – RFPWM based on a random slope

To generate a RPWM, it is also possible to do a pseudo random carrier by selecting $y_c(t)$ or $-y_c(t)$ at the end of each half switching period (Fig. 1.11) [48]. Many other strategies exist as the use of Markov Chains to generate PWM [49].

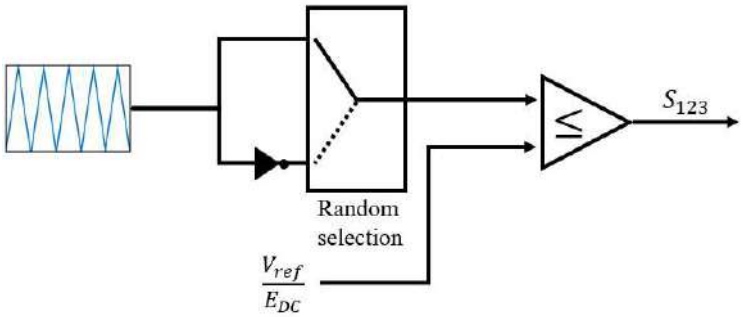

Figure 1.11 – Pseudo RFPWM

Nevertheless, due to their intrinsic random purpose, RPWM are not the privileged strategies to be implemented, even if they benefits great advantages as the noise and harshness reduction but also the diminution of the passive filter's size.

We would finish this section by the presentation of a compromise strategy, which is between the DPWM and THIPWM in terms of performances.

1.1.6 Other ZSC injection: The OMIPWM example

An infinity of ZSC injection strategies can be imagined, but some of them afford interesting effects, this is the case of the Opposite Median Injection PWM (OMIPWM) [50], [51]. This strategy was first imagined to control a four legs three phases two-level inverter but can be easily transposed to a three legs two voltage level application.

The basic principle of this strategy is to add the opposite of the median voltage inside the normalized reference one. Nevertheless, this signal have to be saturated in order to avoid over-modulation (see Fig. 1.12). Doing so, it was showed [50] this strategy afford a compromise between the harmonic quality and the switching losses.

Indeed, this strategy behave exactly as to be half a DPWM and half a continuous one. This behavior is highlighted as the strategy automatically change from a continuous strategy to a discontinuous one while its modulation index increases.

Because of this property, the results provided by the OMIPWM are less good than DPWM for losses reduction but affords a better harmonic quality. About continuous strategies the OMIPWM provide a better losses reduction but a lower harmonic quality. In another words, the OMIPWM is a compromise between harmonic quality and losses reduction.

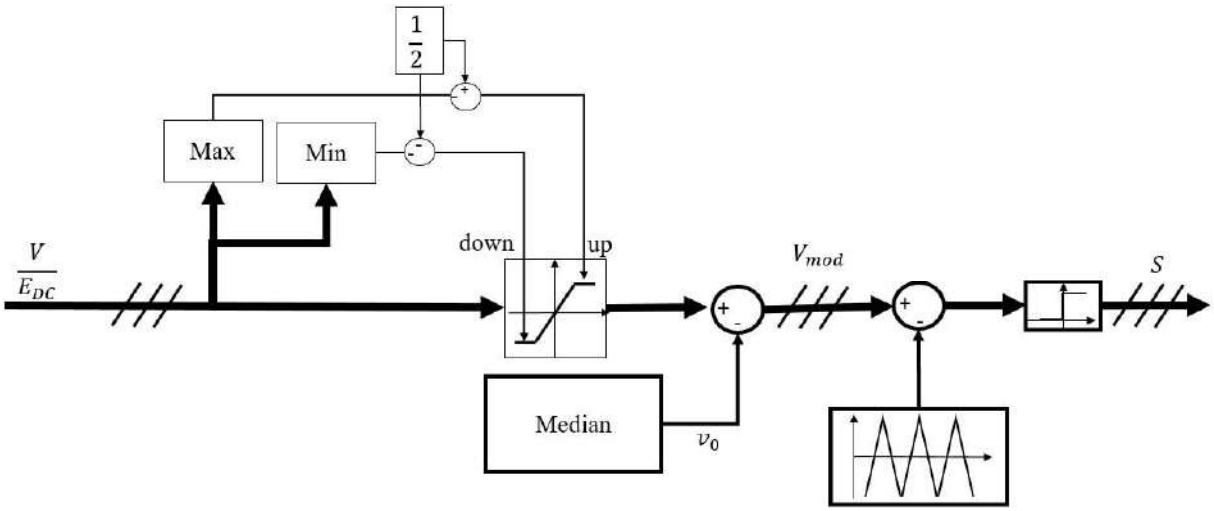

Figure 1.12 – OMIPWM control scheme

With all the strategies presented, we underlined that CBPWM can succeed to improve

many objectives as the losses, the harmonics, noise or some of them together. Nevertheless this PWM generation is not unique and a vector based representation can be useful especially in a motor control command context. Space vector modulation strategies are then the subject of the next section.

1.2 Space vector PWM

In Appendix A, it was shown there are 8 binary possibilities to command the inverter output, nevertheless it is possible to represent this command as a vector where each PWM possible command corresponds to a $\alpha\beta$ frame vector (Table 1.1 and Fig.1.13). This description was first proposed by Van der Broeck in 1988 [18].

S_1	S_2	S_3	V_1	V_2	V_3	$\mathbf{W}_k$	Vector
1	0	0	$\frac{2}{3}E_{DC}$	$-\frac{1}{3}E_{DC}$	$-\frac{1}{3}E_{DC}$	$\frac{2}{3}E_{DC}$	$\mathbf{W}_1$
1	1	0	$\frac{1}{3}E_{DC}$	$\frac{1}{3}E_{DC}$	$-\frac{2}{3}E_{DC}$	$\frac{2}{3}E_{DC}e^{i\frac{\pi}{3}}$	$\mathbf{W}_2$
0	1	0	$-\frac{1}{3}E_{DC}$	$\frac{2}{3}E_{DC}$	$-\frac{1}{3}E_{DC}$	$\frac{2}{3}E_{DC}e^{i\frac{2\pi}{3}}$	$\mathbf{W}_3$
0	1	1	$-\frac{2}{3}E_{DC}$	$\frac{1}{3}E_{DC}$	$\frac{1}{3}E_{DC}$	$\frac{2}{3}E_{DC}e^{i\pi}$	$\mathbf{W}_4$
0	0	1	$-\frac{1}{3}E_{DC}$	$-\frac{1}{3}E_{DC}$	$\frac{2}{3}E_{DC}$	$\frac{2}{3}E_{DC}e^{i\frac{4\pi}{3}}$	$\mathbf{W}_5$
1	0	1	$\frac{1}{3}E_{DC}$	$-\frac{2}{3}E_{DC}$	$\frac{1}{3}E_{DC}$	$\frac{2}{3}E_{DC}e^{i\frac{5\pi}{3}}$	$\mathbf{W}_6$
0	0	0	0	0	0	0	$\mathbf{W}_0$
1	1	1	0	0	0	0	$\mathbf{W}_7$

Table 1.1 – Voltage and vector representations

This vector representation is even more interesting as the desired voltage can also be expressed as a complex time function in the $\alpha\beta$ frame.

This vector representation have the advantage to be represented in two dimensions (Fig. 1.13) and with a single complex vector $\mathbf{W}_k$ in Table 1.1.

1.2.1 Principle

The highly coupled nature of VSI loads such as induction and synchronous machines has led to the use of artificial variables rather than actual (phase) variables for the purpose of simulation as well as for visualization [27], [30].

These currents (phase variables) can be visualized as being components of a single three-dimensional vector (space vector) existing in a three-dimensional orthogonal space. The projection of this vector on the three axes produces the instantaneous values of the

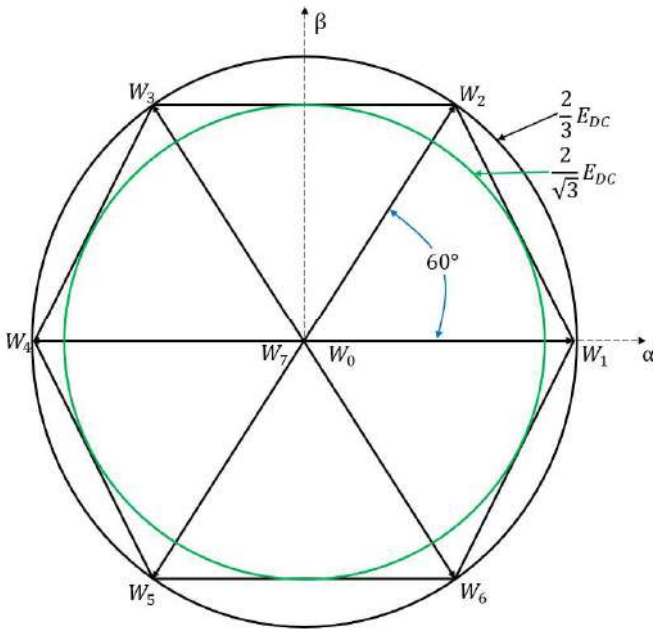

Figure 1.13 – Complex representation of the feasibles voltages in a three phases two-level VSI. This representation is linked with Table 1.1

three stator currents. In most practical cases, the sum of these three currents adds up to zero since most three-phase loads do not have a neutral return path. In this case, the stator current vector is constrained to exist only on a plane defined by:

$$i_1 + i_2 + i_3 = 0 \tag{1.10}$$

The fact that eq. (1.10) defines a particular plane is evident if it is recalled from analytic geometry that the general definition of a plane is $ax + by + cz = d$. Components of the current and voltage vector in the plane are called the d-q components while the component in the axis normal to the plane (in the event that the currents do not sum to zero) is called the ZSC.

The idea is then, to use the ZSC properties under its vectorial representation to perform the desired output voltage and so, to compute the switching states thanks a vector point of view.

To do so, the objective is to compute the switching instants thanks to a vector representation and then to represent either the vector possibilities and the reference voltage in the same frame Fig.1.14.

On Fig.1.14, all the feasible vectors are represented, 6 active vectors and two null.

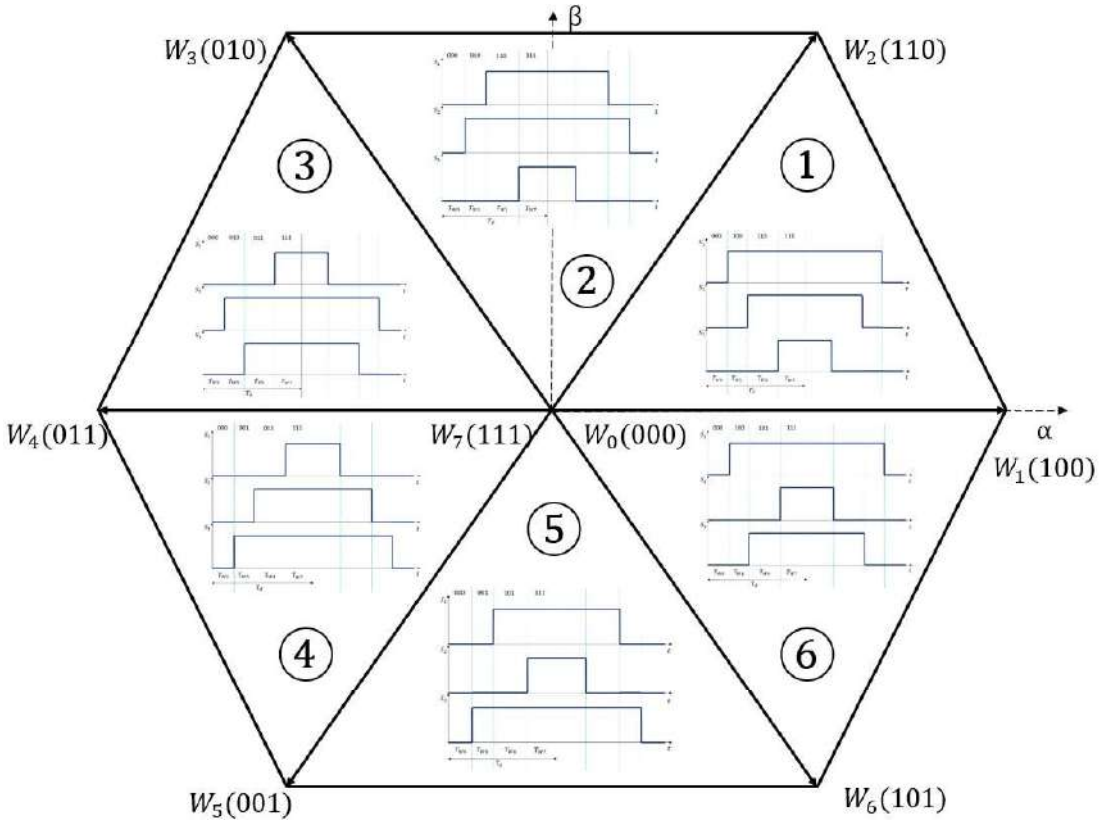

Figure 1.14 – Vector graphic representation with all the switches represented in a $\alpha\beta$ frame

All these vectors cut the space into 6 part called sectors numerated from 1 to 6 (circled numbers on Fig.1.14). Then, to compute the specific switching instants a consideration about vector composition is required. This vector composition is explained in Appendix C but can be also found in Holmes's Book [27].

Nevertheless, this strategy, as for the THIPWM, have the advantage to perform an increase of the feasible space of 15%. Doing so, a reduction of the harmonic impact is also performed in addition with an easy implementation in a motor control context. Nowadays, the Space Vector Modulation (SVM) is the gold standard strategy to control an inverter. Furthermore, it also exists equivalent vector based strategy for inverter with more voltage levels [51].

It is well known that SVM is rigorously equivalent to a carrier based strategy. For the purpose of readability the carrier based equivalent SVM is called the SVPWM. As it is, in fact, the same strategy, the advantages of SVPWM are the same than SVM.

1.2.1.1 SVPWM description

As mentioned before SVPWM is the carrier based equivalent of the SVM. This link is easy to demonstrate by using the property that only two legs are necessary to drive an inverter (see Appendix D). Doing so, a link between a mean value evaluation of the duty cycle leads to consider the ZSC (v_0) to add in the desired voltage is equal to the opposite of the median voltage, then previously eq. (1.4) allows to write the duty cycle equations, and so, the equation of the modulating signal:

$$d_1(t) = \frac{1}{E_{DC}}\left(V_1(t) + v_0(t)\right) \tag{1.11}$$

$$d_2(t) = \frac{1}{E_{DC}}\left(V_2(t) + v_0(t)\right) \tag{1.12}$$

$$d_3(t) = \frac{1}{E_{DC}}\left(V_3(t) + v_0(t)\right) \tag{1.13}$$

$$v_0(t) = \frac{V_{med}(t)}{2} \tag{1.14}$$

A graphic representation of SVPWM's duty cycles can be seen on Fig. 1.15. As mentioned this figure was obtained thanks Eqs. (1.11), (1.12), (1.13) and (1.14).

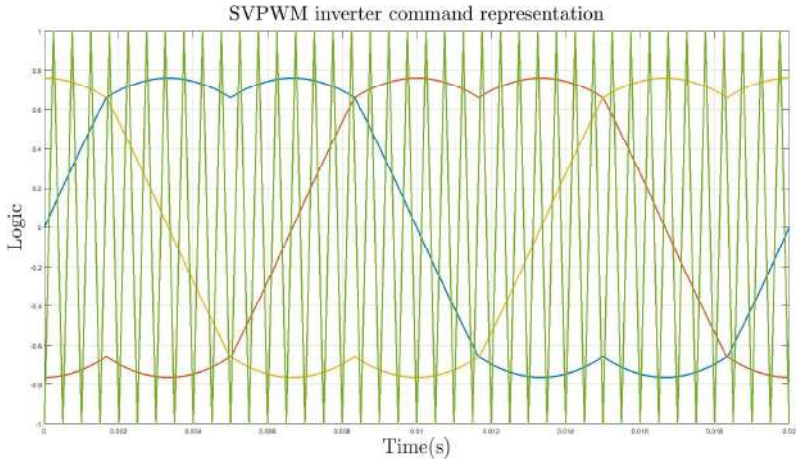

Figure 1.15 – Three phases SVPWM representation with the synchronous carrier (green)

As for the CBPWM, other objectives than harmonic reduction can be considered. In the case of vector based PWM, many works tried to reduce the common mode voltage and then the electromagnetic compatibility issues. These works are presented in the following subsection.

1.2.2 Space vector based strategy for common mode voltage reduction

Space vector modulation does not specifically mean to use the two adjacent vectors ($\mathbf{W}_k$ and $\mathbf{W}_{k+1}$) of the desired voltage and the two null vector ($\mathbf{W}_0$ and $\mathbf{W}_7$) to perform the reference voltage [10].

Literally, space vector modulation, means to perform a Chasles's relation between vectors. Furthermore, previously, it was mentioned that a freedom degree exists to control an inverter, and this freedom degree do not disappear when considering a space vector representation. Then, it is normal to find many space vector based strategies.

In fact, SVM increase the feasible domain and reduce the harmonics, but ignore other problems as the Common Mode Voltage (CMV) reduction problem, directly linked with the EMC.

The CMV mathematical representation is defined by eq. (1.15)

$$V_{CMV} = \frac{1}{3}\left(V_{10} + V_{20} + V_{30}\right) \tag{1.15}$$

V_{10}, V_{20} and V_{30} are defined thanks to eq. (1.16)

$$V_{Z0} = \frac{E_{DC}}{2}\left(2S_k - 1\right) \ \forall Z \in [\![1;3]\!] \tag{1.16}$$

These voltages corresponds to the single voltage of the inverter. In opposition of the single voltage of the load V_k.

Thanks eq.(1.15), the CMV voltage is defined as the potential difference between the star point of the load and the center of the DC-link of the inverter [52].

Since the VSI cannot provide purely sinusoidal voltages and has discrete output voltages generated from the fixed dc-bus voltage E_{DC}, the CMV is always different from zero and may take the values of $\pm\frac{E_{DC}}{6}$ or $\pm\frac{E_{DC}}{2}$, depending on the inverter switch states selected (see Table 1.2). While switch state changes, the CMV changes by $\pm\frac{E_{DC}}{3}$, regardless of the changing states. All conventional CBPWM methods exhibit high CMV despite their other advantages as harmonic or losses reduction [53].

In motor drive applications, CMV may lead to motor bearing failures, electromagnetic interference noise that causes nuisance trip of the inverter drive, or interference with other electronic equipment in the vicinity. In the application field, such problems have increased

10. For more details see Appendix D

S_1	S_2	S_3	$\mathbf{W}$	V_{10}	V_{20}	V_{30}	V_{CMV}
0	0	0	$\mathbf{W}_0$	$-\frac{E_{DC}}{2}$	$-\frac{E_{DC}}{2}$	$-\frac{E_{DC}}{2}$	$-\frac{E_{DC}}{2}$
1	0	0	$\mathbf{W}_1$	$+\frac{E_{DC}}{2}$	$-\frac{E_{DC}}{2}$	$-\frac{E_{DC}}{2}$	$-\frac{E_{DC}}{6}$
1	1	0	$\mathbf{W}_2$	$+\frac{E_{DC}}{2}$	$+\frac{E_{DC}}{2}$	$-\frac{E_{DC}}{2}$	$+\frac{E_{DC}}{6}$
0	1	0	$\mathbf{W}_3$	$-\frac{E_{DC}}{2}$	$+\frac{E_{DC}}{2}$	$-\frac{E_{DC}}{2}$	$-\frac{E_{DC}}{6}$
0	1	1	$\mathbf{W}_4$	$-\frac{E_{DC}}{2}$	$+\frac{E_{DC}}{2}$	$+\frac{E_{DC}}{2}$	$+\frac{E_{DC}}{6}$
0	0	1	$\mathbf{W}_5$	$-\frac{E_{DC}}{2}$	$-\frac{E_{DC}}{2}$	$+\frac{E_{DC}}{2}$	$-\frac{E_{DC}}{6}$
1	0	1	$\mathbf{W}_5$	$+\frac{E_{DC}}{2}$	$-\frac{E_{DC}}{2}$	$+\frac{E_{DC}}{2}$	$+\frac{E_{DC}}{6}$
1	1	1	$\mathbf{W}_7$	$+\frac{E_{DC}}{2}$	$+\frac{E_{DC}}{2}$	$+\frac{E_{DC}}{2}$	$+\frac{E_{DC}}{2}$

Table 1.2 – Common mode voltage per vector $\mathbf{W}$

recently due to increasing PWM frequencies and faster switching times (aimed for higher efficiency, control bandwidth, smaller ripple, filter size, etc.)

The following strategies are some example of vector based CMV reduction PWM and an highlighting is done on their pros and cons. It will be also underline the great impact of null vector sequence in the CMV generation.

1.2.2.1 Near-state PWM

As mentioned, SVM is not the only vector PWM, it exists many other strategies, as for example the Near-state PWM (NSPWM). The conventional SVM method utilizes the two adjacent voltage vectors and the two zero-voltage vectors to program the PWM pulses [18]. The NSPWM method utilizes a group of three-voltage vectors to match the output and reference. These three voltage vectors are selected such that the inverter voltage vector closest to reference voltage vector and its two neighbors (to the right and left) are utilized. Hence, it is named “near state.” [54]

Thanks this new configuration the switching times can be computed for each sector thanks to eqs. (1.17), (1.18) and (1.19) [11].

11. The sector are not defined in the same way than SVM. As an example, first sector is inside: -30° and 30°, next one between 30° and 90° (Fig. 1.16)

$$\frac{T_{\mathbf{W}_{k-1}}}{T_d} = 1 - \sqrt{3}m\sin\left(\theta - \frac{(k-2)\pi}{3}\right) \tag{1.17}$$

$$\frac{T_{\mathbf{W}_k}}{T_d} = -1 + \frac{3}{2}m\left[\cos\left(\theta - \frac{(k-2)\pi}{3}\right) + \sqrt{3}\sin\left(\theta - \frac{(k-2)\pi}{3}\right)\right] \tag{1.18}$$

$$\frac{T_{\mathbf{W}_{k+1}}}{T_d} = 1 - \frac{\sqrt{3}}{2}m\left[\sqrt{3}\cos\left(\theta - \frac{(k-2)\pi}{3}\right) + \sin\left(\theta - \frac{(k-2)\pi}{3}\right)\right] \tag{1.19}$$

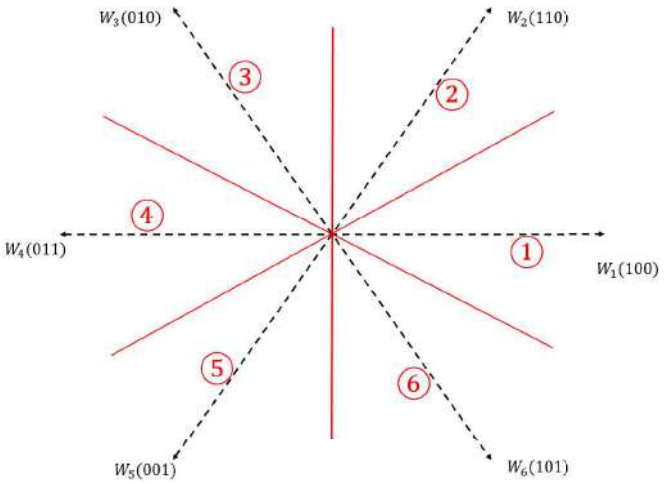

Figure 1.16 – Definition of sectors for NSPWM, discrete line are the VSI feasible vectors and continuous red line define the NSPWM sectors.

Because of the narrow pulse constraint, the only sequence feasible is $[\mathbf{W}_{k+1}; \mathbf{W}_k; \mathbf{W}_{k-1}; \mathbf{W}_k; \mathbf{W}_{k+1}]$ (Fig. 1.17, which is easier to implement than SVM, which needs a vector sequence change for each sector)

The main problem with the NSPWM strategy is its linearity zone, Fig. 1.19. Indeed voltage below $m_{min} = \frac{2}{3\sqrt{3}}$ are not feasible with this strategy. Then it is necessary to use NSPWM in association with other strategies to be operative on an electric motor for example. As for SVM which is rigorously equivalent to SVPWM. NSPWM is equivalent to DPWM1 Fig. 1.18. More generally, every vector based PWM strategy will have its equivalent in carrier based as it was shown by Holmes in 1992 [55], [56].

NSPWM advantage is to reduce losses and to reduce common voltage mode. This last effect reduce the electromagnetic emissions and increase the electromagnetic compatibility [53]. The common-mode voltage reduction is due to the complete lack of null vectors ($\mathbf{W}_0$ and $\mathbf{W}_7$) which generates high variations inside the common-mode voltage (see Table 1.2).

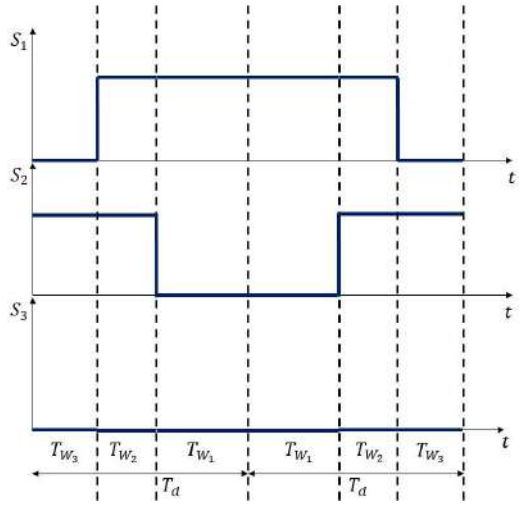

Figure 1.17 – An example of NSPWM sequence for an angle between 30° and 90°(sector 2 of Fig. 1.16)

It especially reduces the leakage current produced by the common-mode voltage of the PWM inverter which is the primary concern of the conducted and radiated electromagnetic interference [57].

Another strategy is not concerned by a vector variation depending on the sector. The following strategy only consider three fixed vectors, and express the desired one thanks to them.

1.2.2.2 Remote state PWM

Remote state PWM (RSPWM) are, as NSPWM, strategies which do not use the null vectors. The main idea here, is to perform the desired voltage but with only few voltages each separated of $\frac{2\pi}{3}$rad. Then, it exists, two strategies using vectors $\mathbf{W}_1$,$\mathbf{W}_3$ and $\mathbf{W}_5$ (RSPWM1 and RSPWM2A). Two other strategies using vectors $\mathbf{W}_2$,$\mathbf{W}_4$ and $\mathbf{W}_6$(RSPWM2B). And finally, it is also possible to do a "mix" between the two strategies (RSPWM3). Nevertheless, all these strategies are different and they are reported on Table 1.3 [52].

The principle is to use two vectors to drive the desired voltage, and to complete the remaining with an association of the three others well balanced vectors. Indeed, as the three vectors are $\frac{2\pi}{3}$ symmetric, their sum is equal to zero.

As the vectors does not changes while the desired voltage changes. The equation doing the link between switching times and vectors is defined thanks to eq. (1.20).

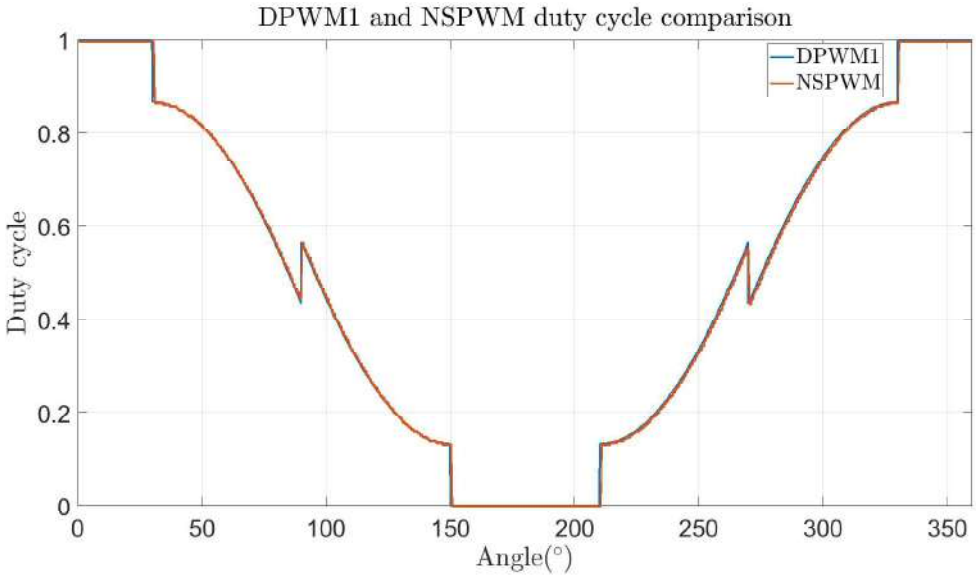

Figure 1.18 – Duty cycle of DPWM1 and NSPWM are overlapping

	A_1	A_2	A_3	A_4	A_5	A_6
RSPWM1	$\mathbf{W}_3\mathbf{W}_1\mathbf{W}_5$	$\mathbf{W}_3\mathbf{W}_1\mathbf{W}_5$	$\mathbf{W}_3\mathbf{W}_1\mathbf{W}_5$	$\mathbf{W}_3\mathbf{W}_1\mathbf{W}_5$	$\mathbf{W}_3\mathbf{W}_1\mathbf{W}_5$	$\mathbf{W}_3\mathbf{W}_1\mathbf{W}_5$
RSPWM2A	$\mathbf{W}_3\mathbf{W}_1\mathbf{W}_5$	$\mathbf{W}_1\mathbf{W}_3\mathbf{W}_5$	$\mathbf{W}_1\mathbf{W}_3\mathbf{W}_5$	$\mathbf{W}_1\mathbf{W}_5\mathbf{W}_3$	$\mathbf{W}_1\mathbf{W}_5\mathbf{W}_3$	$\mathbf{W}_3\mathbf{W}_1\mathbf{W}_5$
RSPWM2B	$\mathbf{W}_4\mathbf{W}_2\mathbf{W}_6$	$\mathbf{W}_4\mathbf{W}_2\mathbf{W}_6$	$\mathbf{W}_2\mathbf{W}_4\mathbf{W}_6$	$\mathbf{W}_2\mathbf{W}_4\mathbf{W}_6$	$\mathbf{W}_2\mathbf{W}_6\mathbf{W}_4$	$\mathbf{W}_2\mathbf{W}_6\mathbf{W}_4$
	B_1	B_2	B_3	B_4	B_5	B_6
RSPWM3	$\mathbf{W}_3\mathbf{W}_1\mathbf{W}_5$	$\mathbf{W}_4\mathbf{W}_2\mathbf{W}_6$	$\mathbf{W}_1\mathbf{W}_3\mathbf{W}_5$	$\mathbf{W}_2\mathbf{W}_4\mathbf{W}_6$	$\mathbf{W}_1\mathbf{W}_5\mathbf{W}_3$	$\mathbf{W}_2\mathbf{W}_6\mathbf{W}_4$

Table 1.3 – First part pulse pattern of the RSPWM strategies

$$\mathbf{W}_{k+1}T_{\mathbf{W}_{k+1}} + \mathbf{W}_{k+3}T_{\mathbf{W}_{k+3}} + \mathbf{W}_{k+5}T_{\mathbf{W}_{k+5}} = \mathbf{V}_{ref}T_d \; k \in \{0,1\} \tag{1.20}$$

This previous equation depends on only 2 unknown parameters. Moreover, in the same way than for SVM, the times are linked together thanks to (1.20).

$$T_{\mathbf{W}_{k+1}} + T_{\mathbf{W}_{k+3}} + T_{\mathbf{W}_{k+5}} = T_d \; k \in \{0,1\} \tag{1.21}$$

Then, thanks the same reasoning than for SVM (see Appendix C) but with these three specific vectors, the conduction time of the vectors can be easily deduced and are equal to eqs. (1.22)-(1.27).

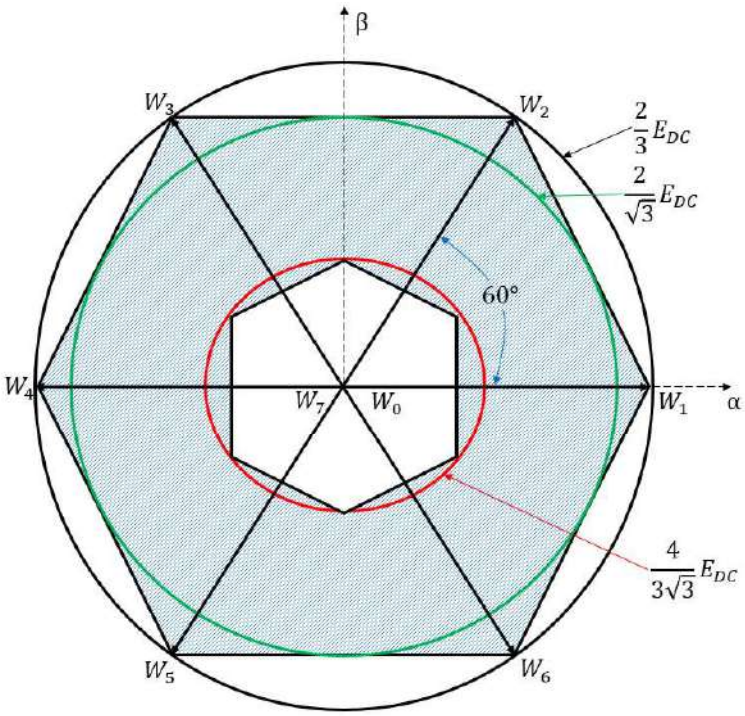

Figure 1.19 – Near state PWM feasible zone representation, hatched area is the feasible one

$$T_{\mathbf{W}_1} = \left(\frac{1}{3} + m\cos(\theta)\right) T_d \tag{1.22}$$

$$T_{\mathbf{W}_2} = \left(\frac{1}{3} + \frac{m}{2}\cos(\theta) + \frac{\sqrt{3}}{2} m\sin(\theta)\right) T_d \tag{1.23}$$

$$T_{\mathbf{W}_3} = \left(\frac{1}{3} - \frac{m}{2}\cos(\theta) + \frac{\sqrt{3}}{2} m\sin(\theta)\right) T_d \tag{1.24}$$

$$T_{\mathbf{W}_4} = \left(\frac{1}{3} - m\cos(\theta)\right) T_d \tag{1.25}$$

$$T_{\mathbf{W}_5} = \left(\frac{1}{3} - \frac{m}{2}\cos(\theta) - \frac{\sqrt{3}}{2} m\sin(\theta)\right) T_d \tag{1.26}$$

$$T_{\mathbf{W}_6} = \left(\frac{1}{3} + \frac{m}{2}\cos(\theta) - \frac{\sqrt{3}}{2} m\sin(\theta)\right) T_d \tag{1.27}$$

To avoid any extra switching, it is fundamental to respect the switching pattern. Indeed, the succession of non adjacent PWM, generate more switches and then more losses for the same output voltage.

As seen on Table 1.2, it is obvious that RSPWM1, RSPWM2A and RSPWM2B does not generate a high CMV. More precisely, the CMV generated is constant and equal to $\pm\frac{E_{DC}}{6}$. This absence of variation is a very appreciable advantage of RSPWM to avoid electromagnetic problems due to the PWM command.

On the other hand the RSPWM3 does not use only three vectors but alternate between RSPWM1 and RSPWM2B. To do so, the same sector definition than the near-state PWM is required (Fig. 1.16). This sector definition is called "B" in Table 1.3. With this equilibrated strategy, the CMV is not constant anymore but is varying periodically between $+\frac{E_{DC}}{6}$ and $-\frac{E_{DC}}{6}$ with a fundamental frequency of T_d. This time, the CMV mean value is equal to zero nevertheless a EMC filter will be required to remove the periodic electromagnetic field generated. It is important to mention that, thanks to its highly previsible shape, this strategy afford a correct controllable CMV.

The last CMV strategy reduction presented in this chapter also remove the null vectors usage (as NSPWM and RSPWM). It is performed by using opposite vectors to simulate the the null sequence and more details are afforded here after.

1.2.2.3 Active zero sequence PWM

The principle of Active Zero Sequence PWM (AZSPWM), were proposed the first time by Oriti in 1997 [58]. The principle is to keep the same formulas than for the SVM, and the same vector succession. Nevertheless the $\mathbf{W}_0$ and $\mathbf{W}_7$ vectors are replaced by two opposite vectors. Doing so, it exist three different AZSPWM [53], [58].

There are only two vectors independent of the two active vectors, indeed for the sector k, the vector $\mathbf{W}_k$ and $\mathbf{W}_{k+1}$ are not independent of vector $\mathbf{W}_{k-3}$ and $\mathbf{W}_{k-2}$. This independence is evident as $\mathbf{W}_k = -\mathbf{W}_{k-3}$ for any sector. Then it remains for a given sector two inactive and free vectors $\mathbf{W}_{k-1}$ and $\mathbf{W}_{k+2}$. Because they are opposite, it is possible to recreate artificially the zero sequence component if they are active the same amount of time.

Thanks to this knowledge, it is possible to deduce the existence of AZSPWM1 and AZSPWM2. Indeed AZSPWM1 uses the vectors by respecting the adjacency of the vectors and AZSPWM2 violates it (see Table 1.4).

The third possible AZSPWM is to extend one of the active vector, and to add at the beginning or at the end of the sequence its opposite vector. This way, according to Table 1.4, for the first sector the sequence is $\mathbf{W}_1\mathbf{W}_1\mathbf{W}_2\mathbf{W}_4$. Then the vector 1 in association with the vector 4 (for this specific sector) will generate the zero sequence component. A

Sector	AZSPWM1	AZSPWM2	AZSPWM3
1	$\mathbf{W_6W_1W_2W_3}$	$\mathbf{W_3W_1W_2W_6}$	$\mathbf{W_1W_2W_4}$
2	$\mathbf{W_4W_3W_2W_1}$	$\mathbf{W_1W_3W_2W_4}$	$\mathbf{W_5W_3W_2}$
3	$\mathbf{W_2W_3W_4W_5}$	$\mathbf{W_5W_3W_4W_2}$	$\mathbf{W_3W_4W_6}$
4	$\mathbf{W_6W_5W_4W_3}$	$\mathbf{W_3W_5W_4W_6}$	$\mathbf{W_1W_5W_4}$
5	$\mathbf{W_4W_5W_6W_1}$	$\mathbf{W_1W_5W_6W_4}$	$\mathbf{W_5W_6W_2}$
6	$\mathbf{W_2W_1W_6W_5}$	$\mathbf{W_5W_1W_6W_2}$	$\mathbf{W_3W_1W_6}$

Table 1.4 – First part pulse pattern of the AZSPWM strategies

pros about AZSPWM is they all have a linearity domain equal to the SVM one even if some operating points are not reachable.

Nevertheless, AZSPWM2 and AZSPWM3 as all the RSPWM allow to have switching of two commutation cells simultaneously and in practice, it is almost impossible to switch two inverter legs simultaneously [12]. Furthermore the significant overvoltage in the motor will damage it. Then Only SVM, NSPWM, and AZSPWM1 are allowed to be implemented in a real motor application.

Furthermore, about the harmonic distortion, all the CMV reduction PWM have a very bad harmonic quality, except NSPWM which is near than SVM.

All these previous strategies are easy to implement as the conduction is computed thanks analytic formulas. Nevertheless, some researches, based on optimization algorithms, found other interesting results by a relaxation of this hypothesis. Some optimal vector based PWM are presented in the next subsection.

1.2.3 Optimal SVM

With the development of computers, a lot of PWM optimization are now possibles, which was impossible in the past. The main problem of optimization is that it often leads to a specific good strategy to meet one objective. Minimizing THD will provide different result than WTHD minimization. The minimization of torque ripple for a specific motor A will provide different results than for the specific motor B. Then it is hopeless to review all the optimization ever studied in the literature. Nevertheless, the optimization methods or the paradigms are possible to explore and we will draw an overview of some of this strategies in this section.

12. Due to unidentical electronic and power hardware in each phase and also the existence of inverter deadtime

As we showed it, it exists a lot of space vector modulation techniques existing. Furthermore, all these strategies have their pros and cons (minimizing WTHD, THD, removing CMV etc...). From this point of view, Gendrin in 2017 [59] decided to propose an algorithm which select depending on the operating point considered, to apply the "best" [13] vector based PWM strategy.

Sun works in 1996 [60] has proposed a new SVM method with a null vector proportion variation. Indeed inside a classic SVM the time $T_{\mathbf{W}_0}$ and $T_{\mathbf{W}_7}$ are supposed to be equal. Thanks to this proportion changes, the idea of Sun was to optimize the current variations inside an inductive load and more specially the THD and then, an objective near the WTHD (see Appendix F).

Not only the classical SVM was tried to be optimized and some works as Baik one in 2020 [52]. Proposed a new vector based method in order to improve the performances of Remote state PWM and proposed a Minimum RMS Torque Ripple RSPWM (MTR-RSPWM). The idea is to compute some several zones inside each sectors, and for each zone, to select the best RSPWM to use. Thanks to this consideration and computation, Baik succeed to minimize the torque ripple of the considered motor.

We will finish this paragraph with the mention of a multilevel inverter strategies. As the McGrath works in 2003 [61] where the objective was to minimize the number of switches per period, as it exist many equivalent sequences with each a different number of switches. Nevertheless this specific problematic is not present in a three phases two level inverter as there is way less freedom degree to perform a SVM.

The presentation of all these methods draw an overview of all the existing space vector based modulation methods without doing the affirmation to be exhaustive. Nevertheless these strategies sample provide an idea of the different levers to be used to improve space vector methods.

CBPWM and vector based methods affords good results and are easy to implement, but their intrinsic structure restrict switching angle possibilities. Then, it is possible to imagine other strategies which would select precisely the switching angles to improve a desired objective function. These strategies appeared with micro-controllers and are called off-line PWM or optimal pulse patterns. Next section is concerned on these strategies.

13. According to the objective function desired

1.3 Off-line PWM

CBPWM exists since middle of the XX$^{\text{th}}$ century to control power electronic devices such as inverters [62]. Many works tried to improve the PWM by injecting harmonics in the modulated signal [27], [32], [51], [63], [64], or by vector modulation methods [56], [65].

More recently, with the technical progress, the micro-controllers and memory storage improvement. A new PWM class appeared, the off-line ones [66], [67]. This new class is based on the storage of switching angles. One of the main advantages of OPP, is that their working zone is extended to the modulation index $m_{\max} = \frac{2}{\pi}$, [27]. This extension is significant in comparison with classical symmetries (as SVM or THIPWM$\frac{1}{6}$ for example) limited to $m_{\max} = \frac{1}{\sqrt{3}}$.

Many works tried to minimize the impact of harmonics (THD or WTHD [47], [66], [68]–[72]. Indeed it is very simple to compute harmonic distortion, and furthermore, WTHD is a good way to evaluate current behaviour in an inductive load [67], [73] (see Appendix F). The weights on harmonics of the WTHD will behave like in an inductive load with the advantage that it do not depends on any physical parameter. This independence to parameters, is the main reason why WTHD is a classical objective function in inverter PWM issues.

Other works are dedicated to Selective Harmonic Elimination (SHEPWM). The principle is to select the harmonics to eliminates and then try to reduce them, [70], [74]–[80]. This objective is the second most classic objective function. SHEPWM can be summarized as a particular case of WTHD in the case of low harmonic reduction, and then in the case of a VSI connected to an inductive load. In addition SHEPWM obliges to choose among all the harmonics which one to eliminate. This choice is quite complex and depend on the considered load and objective.

All the off-line PWM presented before are based on the same modelisation, with the set of precise switching angles. This computation and this modelisation is the topic of the next subsection.

1.3.1 The angle model

In Birth's article of 2019 [66], it appears that, choosing the angles position inside a same period, with respect to synchronism, affords better results than SVM or carrier based PWM. Indeed choosing precisely switching angles [14] in order to perform the desired

14. Here after, "angles" designates a switching angles for the seek of simplicity.

voltage or current is known as the best method to solve the optimization tracking problem. Solving this problem is difficult due to the large amount of different solutions. Here after is a Fourier description of the classical angle model depending on different symmetries.

It exists three main types of symmetries (Quarter Wave Symmetry (QWS) Fig. 1.20, Half Wave Symmetry (HWS) Fig. 1.21 and Full wave symmetry (FWS) Fig. 1.22) [66].

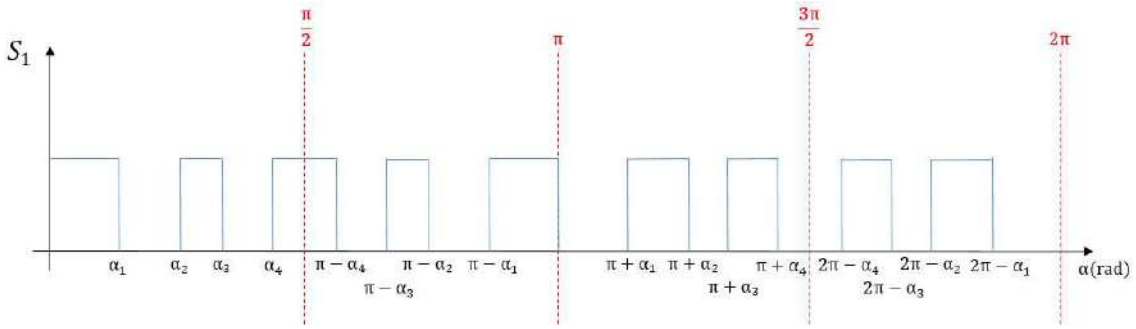

Figure 1.20 – An example of Quarter Wave Symmetry

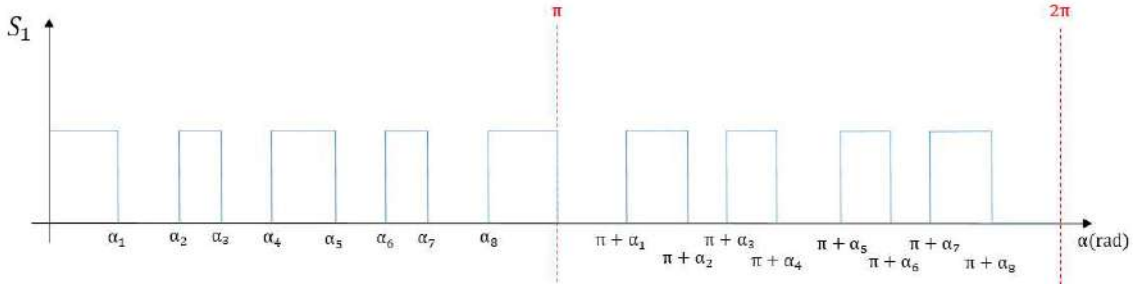

Figure 1.21 – An example of Half Wave Symmetry

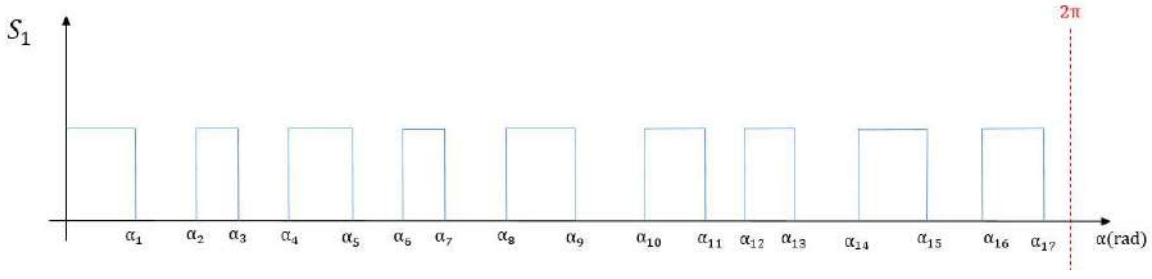

Figure 1.22 – An example of Full Wave Symmetry

As seen on Fig. 1.20, the principle of the QWS is to select angles of the first quarter period, and then deduce all the others angles of the signal thanks to the known symmetry.

The advantage of this solution, resides in the low number of angles to compute. This number is half in comparison with HWS (Fig. 1.21) and fourth less than FWS (Fig. 1.22). With the angle knowledge, computation of Fourier coefficients of the formal control (0 or 1), driving the switches is performed, for each symmetry. Then, Fourier decomposition provides a precise expected behaviour description of the inverter with only the angle knowledge.

In a real application, and due to the switching of the switches, it is impossible to realize a pure sine wave. However, by imposing the angles on each phase it is possible to minimize the harmonic distortion thanks to the knowledge of Fourier description Appendix E [27], [63], [66].

1.3.1.1 QWS equations

For the QWS strategy the command S_1 is described thanks to the symmetries by $a_{c,0,QWS} = \frac{1}{2}$ and $a_{c,n,QWS} = 0 \; \forall n \in [\![1; \infty]\!]$ and $b_{c,n,QWS}$ is defined by eq. (1.28). Harmonics multiples of two are systematically removed due to the $(1 + (-1)^{n+1})$ term. Thanks eq. (E.2) (see Appendix E), eq. (1.28) can be computed.

The S_i value is the initial value of the command S_1. For example in Figs. 1.20, 1.21 and 1.22, $S_i = 1$. Indeed, for t = 0, the S_1 signal is equal to 1 (High state). Then, a $S_i = 0$, correspond to a low state and is then the opposite signal introducing a minus in the equations. This initial value dependency is represented in the equation with the $(-1)^{S_i}$ term.

$$b_{c,n,QWS} = \frac{1}{n\pi}(-1)^{S_i}\left(1 + (-1)^{n+1}\right)\left(2\sum_{j=1}^{N_{qp}}(-1)^{j+1}\cos(n\alpha_j) - 1\right) \tag{1.28}$$

1.3.1.2 HWS equations

For the HWS strategy, $a_{c,0,HWS} = \frac{1}{2}$, $a_{c,n,HWS}$ is defined by eq. (1.29) and $b_{c,n,HWS}$ by eq. (1.30). As for the QWS the $(1 + (-1)^{n+1})$ term will remove all the harmonics multiples of two. Thanks eq. (E.3) (see Appendix E), eq. (1.29) and (1.30) can be computed.

$$a_{c,n,HWS} = \frac{1}{n\pi}(-1)^{S_i+1}\left(1 + (-1)^{n+1}\right)\left(\sum_{j=1}^{2N_{qp}}(-1)^{j+1}\sin(n\alpha_j)\right) \tag{1.29}$$

$$b_{c,n,HWS} = \frac{1}{n\pi}(-1)^{S_i}\left(1+(-1)^{n+1}\right)\left(\sum_{j=1}^{2N_{qp}}(-1)^{j+1}\cos(n\alpha_j)-1\right) \tag{1.30}$$

1.3.1.3 FWS equations

For the FWS strategy, $a_{c,0,FWS}$, $a_{c,n,FWS}$ and $b_{c,n,FWS}$ are respectively defined by eqs. (1.31)-(1.33). Here the harmonics multiples of two, are not systematically removed due to the full period symmetry. Thanks eq. (E.4) (see Appendix E), eqs. (1.31), (1.32) and (1.33) can be computed.

$$a_{c,0,FWS} = \frac{1}{\pi}(-1)^{S_i+1}\left(\sum_{j=1}^{4N_{qp}+1}(-1)^{j+1}\alpha_j + 2\pi\right) \tag{1.31}$$

$$a_{c,n,FWS} = \frac{1}{n\pi}(-1)^{S_i+1}\left(\sum_{j=1}^{4N_{qp}+1}(-1)^{j+1}\sin(n\alpha_j)\right) \tag{1.32}$$

$$b_{c,n,FWS} = \frac{1}{n\pi}(-1)^{S_i}\left(\sum_{j=1}^{4N_{qp}+1}(-1)^{j+1}\cos(n\alpha_j)-1\right) \tag{1.33}$$

1.3.2 WTHD reduction

It said previously, it exist many ways to obtain the best OPP strategies. Furthermore defining the "best" is not an easy task. Indeed, it is possible to reduce, the inverter losses, the torque ripple, or the current harmonics.

These objectives are sometimes not that much easy to quantify and they highly depend on the considered load. Nevertheless, in the case of a VSI connected to a motor, it is possible to generalize the computation of the quality of the current in a motor. Indeed, all the interesting parameters to minimize in a motor depends on the current quality.

As the motor is inductive, it behaves exactly as a low pass filter. Then the THD objective is not that much relevant to estimate the quality of a PWM strategy. A much more interesting one is the WTHD. This parameter is exactly as the THD but with a weight for each harmonic. Then the WTHD is written thanks to eq.(1.34).

$$V_{\text{WTHD},\%} = \frac{100}{mE_{DC}}\sqrt{\sum_{n\geq 2}\frac{V_n^2}{n^2}} \tag{1.34}$$

The proof that the WTHD show the harmonic quality of the current through a motor is afforded in the appendix of this present document (see Appendix F). Nevertheless, we

are aware this objective is just an objective among others, but a choice have to be done and WTHD seems to be the more global one.

1.3.3 Selective Harmonic Elimination

Since the WTHD try to globally reduce the harmonics of the current, SHEPWM select some harmonics important to remove and try to reduce or eliminate them. Since the WTHD try to reduce all the first harmonics indifferently, the SHEPWM seems to be a particular case of WTHD where the weight on several harmonics are higher than the others.

Furthermore, the SHEPWM are very well known strategies in the literature as they exist since 1964 with Turnbull research work [74]. The SHEPWM paradigm is with the WTHD the main evaluation criteria of off-line PWM, as they are generalists and does not depends on the load. The advantage of SHEPWM against WTHD is to select the harmonics to remove, doing so, with the fundamental reference constraint it is possible to have a full constrained problem (N_{qp} equations with N_{qp} switching angles for the QWS eq. (1.35)).

$$\begin{aligned} \frac{\pi}{4}(-1)^{S_i}m + \frac{1}{2} &= \sum_{j=1}^{N_{qp}}(-1)^{j+1}\cos(\alpha_j) \\ \frac{1}{2} &= \sum_{j=1}^{N_{qp}}(-1)^{j+1}\cos(h_{r,1}\alpha_j) \\ &\vdots \\ \frac{1}{2} &= \sum_{j=1}^{N_{qp}}(-1)^{j+1}\cos(h_{r,N_{qp}}\alpha_j) \end{aligned} \tag{1.35}$$

In eq. (1.35), $h_{r,k}$ correspond to the number of the harmonic we desire to remove.

Doing so, many techniques exists to solve this kind of problem described by eq. (1.35) [68], [70], [74]–[79].

This objective is the second most classic objective function in the literature. The main problem of SHEPWM is, it obliges to choose among all the harmonics which one to eliminate which is not the case in the WTHD consideration. Furthermore as mentioned previously the harmonic choice is quite complex and depend on the considered load and

objective as the current influence is not the same for all the harmonics.

1.3.4 OPP resolution techniques

The OPP described before with the different objectives as the WTHD or the SHE was widely studied in the literature and especially the best way to find solutions was explored. The literature around OPP is really rich and many strategies to find the best solutions were explored.

— Deterministic solver [51], [68], [81], [82]
— Meta-heuristics (Particular Swarm Optimization (PSO), ant colony, deep-learning) [69], [72], [83]–[85]
— Local deterministic search (as fmincon) [31], [66], [67], [70], [71], [78], [79], [86]–[89]

All these researches led to very good results, and with many applications. Nevertheless, all are based on the same paradigm of symmetry inside a phase and between phases. Indeed, the three phases have the same reference, it seems logic to consider symmetries will remove several harmonics [15] and then afford the best results. Furthermore, symmetry inside a single phase allow to eliminate even harmonics as shown in Appendix E with eqs. (E.2) and (E.3). Nevertheless, some recent works showed that a symmetry relaxation inside a single phase lead to better results [66], [87].

With all the previous strategies presented, no feedback is ever used. Nevertheless, it exists techniques which use a feedback of the output to work, and some of these techniques are exposed here after.

1.4 Closed loop PWM strategies

Previous strategies studied, are called open loop strategies, as the PWM is a slave of the global control loop. Nevertheless, it was also studied in the literature some other PWM strategies called closed loop. Where the global control still exist, but, the inverter, to select the correct state to use, will refer to its own output.

1.4.1 The $\Delta\Sigma$ vector modulation

All the vector based methods presented before are open-loop methods as there is no feedback from the output of the inverter. Nevertheless, it exists closed loop methods

15. More precisely harmonics multiple of the number of phases considered

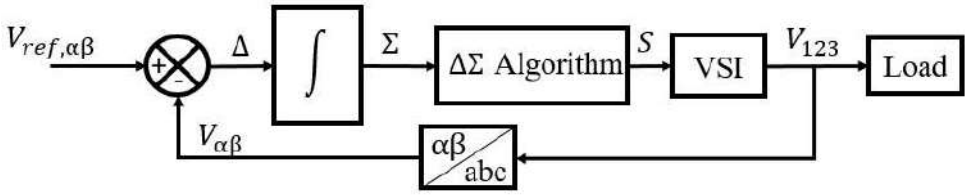

Figure 1.23 – $\Delta\Sigma$ vector control

vector based and the $\Delta\Sigma$ Modulation is one of them.

The $\Delta\Sigma$ method was First described by Friedrich in 1987 [90] for a mono-phased VSI before a generalization to three phases by his colleague Vilain in 1995 [91]. The general principle of the technique is showed with Fig. 1.23.

The principle is, thanks to the actual knowledge of the desired voltage, the algorithm will select the vector allowing to respect the voltage. To do so, when the voltage error Σ is greater than a specific value S, then the algorithm have to change the active vector $\mathbf{W}_k$ to another one. First, we define Σ as the integral of the error Δ. On the other hand, we define $\mathbf{\Delta}_{\mathbf{W}_k}$ as the difference between the desired voltage vector and the vector $\mathbf{W}_k$.

$$\mathbf{\Sigma} = \begin{pmatrix} \sigma_\alpha \\ \sigma_\beta \end{pmatrix} \tag{1.36}$$

$$\mathbf{\Delta}_{\mathbf{W}_k} = \begin{pmatrix} \delta_{\mathbf{W}_k,\alpha} \\ \delta_{\mathbf{W}_k,\beta} \end{pmatrix} = \begin{pmatrix} V_{ref,\alpha} - \mathbf{W}_{k,\alpha} \\ V_{ref,\beta} - \mathbf{W}_{k,\beta} \end{pmatrix} \tag{1.37}$$

Thanks to these definitions, it is possible to compute two parameters. the parameter Dt and $D_{\mathbf{W}_k}$ for all the eights vectors.

$$Dt = \frac{1}{||\mathbf{\Delta}_{\mathbf{W}_k}||^2} \left(\langle \mathbf{\Delta}_{\mathbf{W}_k}, \mathbf{\Sigma} \rangle + \sqrt{D_{\mathbf{W}_k}} \right) \tag{1.38}$$

Where

$$D_{\mathbf{W}_k} = S^2 \left(\delta^2_{\mathbf{W}_k,\alpha} + \delta^2_{\mathbf{W}_k,\beta} \right) - \left(\sigma_{n,\alpha} \delta_{\mathbf{W}_k,\beta} - \sigma_{n,\beta} \delta_{\mathbf{W}_k,\alpha} \right)^2 \tag{1.39}$$

Dt is defined as the time, the vector $\mathbf{W}_k$ will be used until Σ is greater than S. On the other hand $D_{\mathbf{W}_k}$ specify if the use of the vector $\mathbf{W}_k$, will allow Σ to integer the feasible domain represented as a circle of radius S. Finally the scalar product between a specific voltage vector and Σ ($\langle \mathbf{\Delta}_{\mathbf{W}_k}, \mathbf{\Sigma} \rangle$), when greater than 0, means that the corresponding

vector will not allow to integer the feasible circle.

Then, thanks to this description, it is possible write the $\Delta\Sigma$ algorithm:

— If $||\Sigma|| > S$

  — For all the vectors $\mathbf{W}_k$ select the ones verifying $\langle \mathbf{\Delta}_{\mathbf{W}_k}, \mathbf{\Sigma} \rangle < 0$

  — Among the previous valid vectors, for all of them verifying $D_{\mathbf{W}_k} > 0$ select the one maximizing Dt

  — If there is no vector verifying $D_{\mathbf{W}_k} > 0$ select the one minimizing $||\mathbf{\Sigma} + \mathbf{\Delta}_{\mathbf{W}_k}||$

This way the voltage at the output can be controlled and be kept inside the tolerance error desired called S. Furthermore, this procedure increase the voltage quality applied to the load, and so, have a relatively good WTHD. Other advantages are intrinsic of the strategy as it was imagined to reduce the switching frequency imposed to the VSI's switches. Furthermore, the $\Delta\Sigma$ strategy never face to narrow pulses thanks to the S parameter setting.

The $\Delta\Sigma$ modulation is one of the rare model free voltage control. Indeed it exist other strategies based on a closed loop as the Hysteresis one or the Model Predictive Control (MPC) but are based on the current control. These strategies will be studied in the next subsection.

1.4.2 Model predictive control

The MPC for a PWM application, is, in a way, the extension of $\Delta\Sigma$ modulation. Indeed, the previous strategy was to control the voltage from its reference to the voltage output and by ignoring the load.

The purpose is then to take into account the load in order to drive the output current directly. The current reference properties are supposed to be provided by a black box.

The main difference with $\Delta\Sigma$ modulator, is that thanks to the current behavior anticipation, a more accurate current control can be applied by taking into account the connected load.

The objective of a predictive algorithm is to select the most suited switching state from the set of all discrete switching states of a power converter. As there is only 8 possible states, the predictive algorithm will select the one affording the less error variation $\frac{d\ e_k}{dt}$. Furthermore, thanks to its structure and the model reliability the MPC can be tuned to follow any objective function [63], [73], [92]. It is important to mention, that other structures than three phases two level inverter can benefits of MPC structure [93].

A scheme principle is proposed Fig. 1.24.

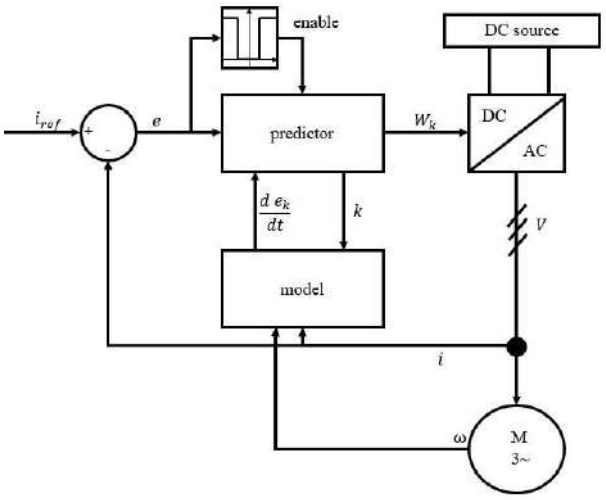

Figure 1.24 – A proposition of PWM MPC

The objective, on Fig. 1.24 is, thanks to the knowledge of the model and the possible switching states, to determine the one which will have a derivative of the error near to 0. Furthermore, by selecting the vector which is predicted to be stable for the maximum amount of time, a choice can be done on the vector to use. Indeed, at a specific time, it is highly probable that many vectors allow to get closer to the reference. Nevertheless, among those strategies, it is interesting to select the one which is preferable. This "preferable" selection is done regarding the amount of time each vector will be the "right one". The one which can be use the most of time is selected [16].

This time based consideration of switch is, as said previously, near the $\Delta\Sigma$ algorithm.

Next strategy is not based on a vector consideration and does not need a lot of considerations to be operational. Indeed, the hysteresis control presented here after is one of the simplest closed loop PWM control.

1.4.3 Hysteresis control

The principle of hysteresis control is to set, thanks to an hysteresis to keep the current variations inside a fixed bandwidth [32]. The control scheme of an Hysteresis is presented on Fig. 1.25.

Where a H parameter of the Hysteresis is introduced (see Fig. 1.26).

The principle is then easy to describe. Indeed, when the current error will be higher than an $\frac{H}{2}$ value the commutation cell will switch. In the opposite, when the error is

16. This principle is exactly the same than for $\Delta\Sigma$ control

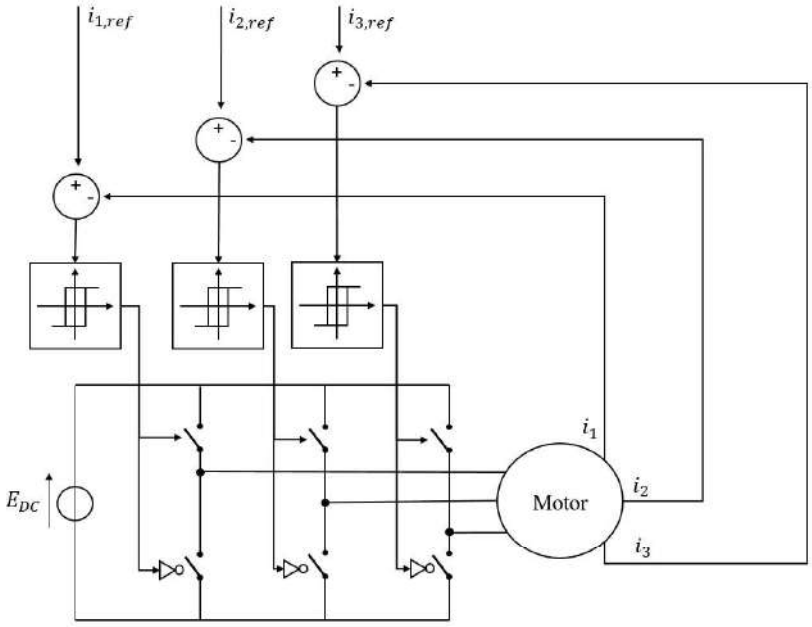

Figure 1.25 – abc Hysteresis PWM command

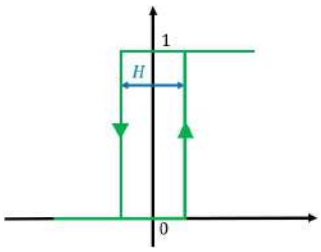

Figure 1.26 – Hysteresis principle

lower than $\frac{H}{2}$, the commutation cell will also change its value.

The Hysteresis control method is simple to implement, and its dynamic performance are excellent. Nevertheless there are some inherent drawbacks [94], as:

— The algorithm can produce as many switches as it desires. Especially at low modulation index, because there is no obligation to use zero space vector. Then for the number of switches per period is strongly linked with the modulation index.
— The current error is not strictly limited, as it is possible to have overshoot of $2\Delta i$.
— The generation of sub-harmonics components. Then because of their poor harmonic quality, they should be use in an high switching frequency context.

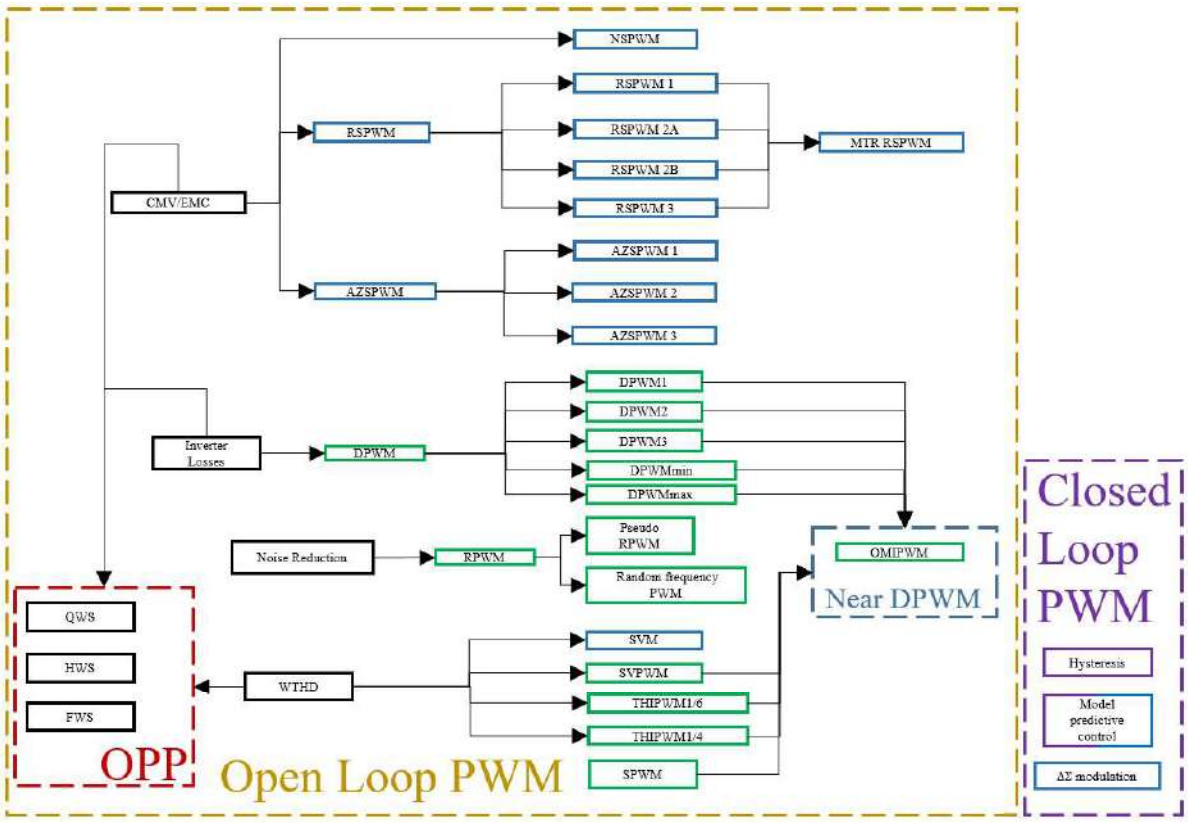

Figure 1.27 – Map of existing PWMs. blue: vector based strategies, green carrier based strategies, purple, closed loop strategies

1.5 Conclusion and thesis bias

1.5.1 Conclusion

1.5.1.1 Global overview

In this first chapter many strategies were presented and their pros and cons were underline. In order to understand the positioning of this research work a short summary is proposed.

As it was showed, it exists many strategies to control a two levels inverter. Even if this converter topology is now considered as a basic one, research continues to always find better PWM strategies for many applications. The quantity of strategies is so huge that it seems impossible to don't forget at least a paper (around 20 papers only for the OPP resolution techniques). Nevertheless an attempt to summarize all of them was done with Fig. 1.27.

This figure is a map, where the link between the different strategies is highlighted. Only three objectives was kept [17] as all of the objective depend principally to these behavior. Indeed, torque ripple is linked with noise improvement and harmonics reduction. CMV is directly linked with EMC...

It was identified two great families of strategies: The open loop strategies and the closed Loop PWM. Among the first one, three categories were identified, the OPP, the vector based and the carrier based.

1.5.1.2 Space vector strategies

Space vector strategies seems to have two main purposes, the following of the reference and the CMV reduction. About the first one, SVM seems to be the "gold standard" of strategies especially in a motor control context. But, because of its use of the null vectors, they generate high CMV, directly linked with EMC, which have to be limited. Many strategies exists to limit the CMV, but not all of them can be applied and they have all some voltage reference vectors they cannot reach.

Then , the perfect space vector strategy does not exist leading to optimal space vector modulation strategies in the recent years.

1.5.1.3 CBPWM

Some space vector strategies can be linked with CBPWM. As an example, SVM is equivalent to SVPWM and NSPWM to DPWM1. Then, they obviously suffer from the same problems then their space vector centered cousins.

Nevertheless, it also exists unique CBPWM not linked with space vector logic as the THIPWM, increasing in the same way than SVM the linear zone. Its advantage is to increase even more the harmonic quality.

On the opposite, it exists DPWM, they also allow to increase the linear zone but their purpose is to decrease the switching losses by allowing periodically each phase to avoid switching.

The RPWM is singular as it reduces the noise or torque ripple. Nevertheless the losses inside the VSI are significant and cannot be ignored.

Finally, in the same way than for space vector strategies, some middle strategies between those two objectives (losses, and harmonics) exist as the OMIPWM an example.

17. WTHD, CMV and Noise

In this manuscript we decided to call these middle strategies the "near DPWM" (see Fig. 1.27).

1.5.1.4 OPP

Space vector modulation and CBPWM have the same purpose: finding a technique to know the switching instants. The OPP principle, is then, under the synchronicity hypothesis, to compute directly the switching instants to impose to the VSI. Then the OPP principle is a generalization of synchronous SVM and synchronous CBPWM. This way, the OPP strategies offers better results in comparison to the two previous strategies. Nevertheless, their paradigms are not the same than the previous one and need high speed controllers to work properly.

In addition the imposed synchronicity avoid low frequencies to appear and then offer a better harmonic quality.

1.5.1.5 Closed loop PWM

Closed loop PWM change completely the paradigm of the previous strategies, and then, it is difficult to compare those strategies with the space vector based or the carrier based ones. Nevertheless, their advantages are to do not rely on any switching scheme allowing them to be really adaptative to the asked reference, and objective optimization. Nevertheless, these strategies are difficult to implement as a real time algorithm have to be implemented in the MPC case and $\Delta\Sigma$ one.

1.5.1.6 Other PWM purposes

Finally, in this first chapter, no other purpose was considered than following the voltage reference with the objective to minimize the perturbations. Nevertheless, communication protocols set aside, PWM can be also used to observe the angle of the motor [95], [96], or to do self diagnosis of the converter for example [97]–[99].

1.5.2 Thesis bias

As seen before, many control strategies exists to control the VSI voltage. More precisely, it appears to be three method classes to control the output voltage without adding any feedback.

Then the developing choice for the research work we envisaged were multiple and are depicted in the following.

— The first possibility is to work with OPP, indeed they are the strategies allowing the most possibilities as all the voltage sequences of a commutation cell is possible to be performed. Furthermore OPP are always synchronous. Nevertheless there is a need to do an optimization before implementation and to store the solutions inside the micro-controller/FPGA to be efficient. Their great flexibility allows to follow, in the best way all the objective functions.

— The second possibility is to rely on in the carrier based strategies. They afford the certitude to follow the reference thanks to the mean value theorem. Nevertheless, this mean value necessities a great switching frequency value to be really efficient. Furthermore, as the VSI is three phased, any third harmonic signal injected in the voltage reference would lead to a reference following. In addition because they are well known in the literature finding a new signal to inject inside would be a significant advantage as it would be easily implementable.

— The last possibility in our paradigm, is to work on space vector based techniques. For these strategies, when the vectors chosen to follow the reference are known, there is not that much flexibility in the command computation. Furthermore, some existing vector sequences often leads to an impossibility to follow some references [18]. Some works, improves the SVM, by adding some freedom degrees, as the possibility to change the strategy, depending on the modulation index value and sector. In addition, the greatest interest of these techniques is to be easily related to a motor control.

With the Highlight of this three main identified research axes, our research interest was first focused on OPP. Indeed, as they generalize the PWM command, this paradigm would lead to the best strategies.

As the objective is to provide the most pure sine wave at the input of the motor, the choice was done to mainly work with the WTHD. Indeed, as this objective rely on the hypothesis that the global control loop provides a control to overcome to other objectives [19]. It tries to generate a voltage near a pure sine wave and will then avoid motor issues.

Nevertheless, as OPP strategies need to change the hardware and the philosophy of

18. As a reminder, NSPWM, cannot be used for low modulation indexes
19. Torque ripple or the robustness of the control for example

the inverter control, OPP are not privileged to be used in a real motor application and especially in an industrial context.

Then, an attempt to transform the OPP to a ZSC injection was investigated. This transformation from the command control to the ZSC is quite complex and, because to the harmonics generated and Gibbs effect this transformation is not trivial at all. Then an injection of an optimized off-line ZSC seems to be the better option to have the best waveform with the easiest implementation. As the ZSC cannot be as good as OPP results, the idea was to also work with some losses simulations to evaluate the potential advantages on inverter losses.

In regard of all these elements, next chapter will be concerned on OPP investigations first and next one on synchronous carrier based strategies with a ZSC injection.

Chapter 2

A new off-line PWM: The Phase symmetry relaxation

The control of inverters has degrees of freedom that opens the way to improve the output harmonic spectrum. Numerous works dealing with this objective have been proposed in the literature particularly within the definition of switching angles [27], [66], [67]. Among them, the well known Pulse Width Modulation (PWM) techniques such as Quarter Wave Symmetry (QWS), Half Wave Symmetry (HWS) and Full Wave Symmetry (FWS) are based on Optimal Pulse Patterns (OPP) computation using symmetries angles constraints. In order to improve the harmonic quality, the symmetries angles constraints were relaxed leading to a new OPP method called the Phases Symmetry Relaxation (PSR). To highlight the interest of the PSR method, an evaluation in terms of Weighted Total Harmonic Distortion (WTHD) is performed. Simulation and experimental tests are conducted in comparison with the well known FWS, highlighting the interest of the proposed PSR strategy.

In this chapter, a p-phases inverter is considered, with either a voltage source or a current one. Indeed, the relaxation phases presented can be applied to any number of phases and independently of the source type. The choice have been done to present the strategies with a p-phases considerations and the results with a three phases VSI.

2.1 Classic OPP problem modeling

Because OPP already exists [27], [66]–[68], in order to compare the new strategy presented after with classical ones, it is necessary to set an optimization problem in order to find the best angle solutions. This optimization have to be performed for all the classical symmetries, and then, an optimization problem description is needed. As all optimization, its purpose is to minimize an objective function f.

symmetries	N_d	l_b	u_b
QWS	N_{qp}	$\delta\theta_{min}(\omega)$	$\frac{\pi}{2} - \frac{\delta\theta_{min}(\omega)}{2}$
HWS	$2N_{qp}$	$\delta\theta_{min}(\omega)$	$\pi - \delta\theta_{min}(\omega)$
FWS	$4N_{qp}+1$	$\delta\theta_{min}(\omega)$	$2\pi - \delta\theta_{min}(\omega)$

Table 2.1 – Optimization problem parameters

[1] representation. Nevertheless, an infinity of objective function can be selected. The advantage of the following description is, it does not depend on the f function selected.

$$\begin{cases} ObF & \min(f(\mathbf{x})) \\ U.C. & \alpha_k \leq \alpha_{k+1} + \delta\theta_{min}(\omega) \quad \forall k \in [\![1; N_d]\!] \\ & \alpha_{N_d} \leq u_b \\ & \alpha_1 \geq l_b \\ & a_{1,V} = 0 \\ & b_{1,V} = m \end{cases} \tag{2.1}$$

In the optimization problem eq. (2.1), there are two nonlinear constraints, because they depend of the Fourier decomposition, where a lot of trigonometric functions appear. Here, m designates the modulation index, defined as the percentage of use of the DC bus. In the case of a VSI modulation index is equal to $m = \frac{V_1}{E_{DC}}$, with V_1 the desired voltage amplitude and E_{DC} the bus voltage.

In Table 2.1 let's remark that the lower bound (l_b) and the upper bound (u_b) are not equal to the theoretical ones. The reason is technological, as the switches gap, $\delta\theta_{min}(\omega)$, must be taking into account in the bounds. Another remark, is with problem defined in (2.1), it is only necessary to focus on the first phase, because all the $p-1$ other phases will be deduced from this one. It is also the reason why the fundamental real part of the Fourier decomposition ($a_{1,V}$) is equal to zero. This leads to the main assumption of classical strategies (QWS, HWS and FWS), that is, angles of each phase are phase shifted symmetrically according to the first phase angles [2].

As demonstrated in Appendix G, this angle phase shift affords the advantage to eliminate harmonics multiple of p. On the other hand, this limits the number of solutions. Consequently solutions could be sub-optimal with respect to the set of possible solutions. Next section will focus on this problem consideration.

1. In this chapter the WTHD is chosen for its good motor behavior
2. It is very important to distinguish the angle symmetry and the phase symmetry, the first one is concerned on the switching angle and the second one about voltage symmetry

2.2 Phases Symmetry Relaxation method

The purpose of PSR method is to relax the angle phase shift constraint. As Birth [66] showed that an angle symmetry relaxation in a single phase improves the harmonic quality. The decision has been done to also do not consider the angle symmetry between phases. As an illustration of the proposed hypothesis relaxation, Fig. 2.1 highlights a particular case of the angle phase shift relaxation for three phases only. Doing so, the solution set is expanded. Nevertheless the symmetry between voltage (or current) phases will be imposed by constraints on the optimization problem, with respect to a specific precision.

Without the symmetric assumption, the optimization problem is now written like eq. (2.3). The idea, here, is to find an optimal solution for the angles, according to a chosen objective function f (in this chapter, the WTHD). This relaxation of the constraints increases the WTHD quality of the solutions as it will be shown in the sections 2.5 and 2.6.

2.2.1 Problem modeling

From the relaxations way of thinking, a new optimization setting is proposed, generating new freedom degrees and also extra constraints. Then three types of conditions must be met. First, the angle between two switches cannot be lower than a minimal angle $\delta\theta_{min}(\omega)$. This constraint will prevent narrow pulses and allows switches to commute properly with respect to the dead-time ($\delta\theta_{min}(\omega) > 2\omega\Delta t$).

[3]

Secondly, angles are bounded on a period, theoretically it would be 0 to 2π and practically see Table 2.2. Those two conditions together correspond to $4\,(N_{qp}+1)$ linear constraints.

Finally, all the optimized output signals must respect the correct amplitude and phase for the fundamental. Explaining why the $3p$ nonlinear equalities constraints eq. (2.2) and eq. (2.3) must be verified.

3. A narrow pulse is a pulse lower than the minimal angle, $\delta t_{min} < 2\Delta t$

$$\begin{aligned} \sqrt{a_{1,V}^2 + b_{1,V}^2} &= m \pm \epsilon_V \\ \tan\left(-\frac{2(Z-1)\pi}{p} \pm \epsilon_\theta\right) &= \frac{b_{1,Z,V}}{a_{1,Z,V}}, \forall Z \in \{1, 2, \cdots, p\} \end{aligned} \tag{2.2}$$

These equations are not necessary in the case of a single phase problem (QWS, HWS or FWS), as these constraints are automatically verified as all the switching angles of each phases are symmetric.

Remark: For the particular case presented in section 2.5 and 2.6, the equality constraint equations of the optimization problem are imposed to be precise at 2% on the amplitude and at $\frac{\pi}{25}$ on phases.

The optimization problem, is now the following one with the same objective function as 2.1:

$$\begin{cases} ObF & \min(f(\mathbf{x})) \\ U.C. & \mathbf{x} = [\mathbf{x_1}, \mathbf{x_2}, \cdots, \mathbf{x_p}] \\ & x_{1,k} \leq x_{1,k+1} + \delta\theta_{min}(\omega) \\ & x_{2,k} \leq x_{2,k+1} + \delta\theta_{min}(\omega) \\ & \cdots \\ & x_{p,k} \leq x_{p,k+1} + \delta\theta_{min}(\omega) \\ & x_{1,4N_{qp}+2} \leq u_b, \\ & x_{2,4N_{qp}+2} \leq u_b, \cdots \\ & x_{p,4N_{qp}+2} \leq u_b \\ & x_{1,1} \geq l_b, \quad x_{2,1} \geq l_b, \cdots, \quad x_{p,1} \geq l_b \\ & a_{0,1,V} = 0, \quad a_{0,2,V} = 0, \cdots, \quad a_{0,p,V} = 0 \\ & a_{1,1,V} = 0 \\ & a_{1,2,V} = m\sin(-\frac{2\pi}{p}), \cdots \\ & a_{1,p,V} = m\sin(-2\pi\frac{p-1}{p}) \\ & b_{1,1,V} = m, \\ & b_{1,2,V} = m\cos(-\frac{2\pi}{p}), \cdots \\ & b_{1,p,V} = m\cos(-2\pi\frac{p-1}{p}) \end{cases} \tag{2.3}$$

To analyze the command performances of the PSR, same equations than for the FWS are used. Precisely, eq. (1.31), eq. (1.32) and eq. (1.33) are the same for PSR, except that j vary between 1 and $4N_{qp}+2$. Here the symmetry between the angles is not deduced

	N_d	l_b	u_b
PSR	$3(4N_{qp}+2)$	$\delta\theta_{min}$	$2\pi-\delta\theta_{min}$

Table 2.2 – PSR Optimization problem parameters

from a single phase. Then no harmonics will be systematically equal to zero, which is the main difference with FWS. Remark that in the problem eq. (2.3), $k \in [\![1, 4N_{qp}+2]\!]$. It appears there is one more switching in comparison with FWS and two more switching in comparison with QWS and HWS. The first additional switching is due to the symmetry which requires to have a switching in π (see Fig. 1.20 and Fig. 1.21). The second additional switching is due to the 2π symmetry, this commutation is present in every classical symmetry (see Fig. 1.20, Fig. 1.21 and Fig. 1.22). This 2π periodicity is the reason why an extra switching seems to appears in the PSR problem constraints.

Concerning the dead-time (Δt), it is naturally implemented during the experiments presented in section 2.6 to avoid short circuits. Nevertheless it is neglected on (2.3) to simplify the WTHD computation. Indeed precise knowledge on dead-time influence is quite complex as presented in [100]. This claim is confirmed under the hypothesis of $f_1\Delta t << 1$, which verifies the first order development of the S_Z Fourier decomposition and gives (2.4) and (2.5).

$$\widetilde{a}_{c,n,FWS} = a_{c,n,FWS} - \frac{\omega\Delta t}{\pi}(-1)^{S_i}\left(\sum_{j=1}^{4N_{qp}+1}\cos(n\alpha_j)\right) + o(\Delta t^2) \tag{2.4}$$

$$\widetilde{b}_{c,n,FWS} = b_{c,n,FWS} - \frac{\omega\Delta t}{\pi}(-1)^{S_i}\left(\sum_{j=1}^{4N_{qp}+1}\sin(n\alpha_j)\right) + o(\Delta t^2) \tag{2.5}$$

Where $\widetilde{a}_{c,n,FWS}$ and $\widetilde{b}_{c,n,FWS}$ are the Fourier coefficient with dead-time effect. Their computation can be found in Appendix K. So under the assumption $f_1\Delta t << 1$, equations (2.4) and (2.5) gives $\widetilde{a}_{c,n,FWS} \approx a_{c,n,FWS}$ and $\widetilde{b}_{c,n,FWS} \approx b_{c,n,FWS}$. Consequently as to take in consideration the dead time on the FWS's WTHD equation and on PSR, this increases the complexity of the computation. It is why the dead-time Δt is neglected in this chapter. Nevertheless, if dead-time consideration is necessary to take in account in future works, it would be done by modifying (2.3) and δt_{min}.

Figure 2.1 – Three phases inverter example of PSR strategy

2.3 Computation Method

In order to compute an optimization solution, *fmincon* from the optimization toolbox of MatLab (MathWorks®) is used. Because the workspace has many local minimums, it is necessary to correctly select some starting points of *fmincon*.

Many techniques can be considered to generate a starting point allowing to find a good solution. A first basic idea consists to select a large amount of solutions and to evaluate which one is the better one. Then performing a local search with *fmincon* thanks to this point.

2.3.1 Random starting point generation

To compute a good starting point, the first step, before optimization, begins with the creation of some random initial points. After that an evaluation of the quality of each point is performed with eq. (2.6). This equation considers the actual value of the objective function, f, which is modified to f_v, in order to respects the constraints.

The initial decision matrix $\boldsymbol{x}_0$ is considered as an appropriate starting point, with respect to f_v, if the solutions has a good fitness (a low $f(\boldsymbol{x}_0)$) and which violate a minimum of nonlinear constraints (K_2 term) and not deeply (K_1 term). Linear constraints are not considered in eq. (2.6) because they are forced to be verified in the initial matrix. Indeed

it is easy to generate a random sorted and bounded matrix.

$$f_v = f(\boldsymbol{x}_0) + K_1 \sum_{i=1}^{3p} (\max(c_i, 0)) + K_2 \sum_{i=1}^{3p} g(c_i) \tag{2.6}$$

Where $\boldsymbol{x}_0 = [\mathbf{x_{10}}, \mathbf{x_{20}}, \cdots, \mathbf{x_{p0}}]$ is the initial decision matrix, K_1 and K_2 are two penalty coefficients [4]. Furthermore, g is defined as follow eq. (2.7):

$$g(c_i) = \begin{cases} 1 & \text{if } c_i > \epsilon \\ 0 & \text{otherwise} \end{cases} \tag{2.7}$$

Moreover $\boldsymbol{c} = (c_1, c_2 \cdots, c_{3p})$ is the vector of nonlinear constraints, these constraints are the same than for the problem eq. (2.3). Equation (2.6) is inspired by the work of Sierra et al. [101].

The first penalty (K_1 term) of eq. (2.6) indicates how far away the solutions are from the acceptable domain [5] and the second penalty (K_2 term) indicates how many constraints are outside the acceptable domain.

2.3.2 Solution search algorithm

After computing eq. (2.6), to a large quantity of initial matrices, a selection of the initial matrix with the minimal f_v is done. Then, this matrix is considered as a starting matrix for the optimization problem defined by eq. (2.3). Furthermore, in order to refine the solution quality, other starting matrices are considered. Three of these starting matrices are found by doing an extension of the previous symmetries. So QWS is extended to HWS eq. (2.8), the HWS to compute FWS eq. (2.9) and FWS to PSR eq. (2.10). This leads to the following symmetries extension.

$$\boldsymbol{\alpha}_{HWS} = [\alpha_{QWS,1}, \cdots, \alpha_{QWS,N}, \pi - \alpha_{QWS,N}, \cdots, \pi - \alpha_{QWS,1}] \tag{2.8}$$

$$\boldsymbol{\alpha}_{FWS} = [\alpha_{HWS,1}, \cdots, \alpha_{HWS,2N}, \pi, \pi + \alpha_{HWS,1}, \cdots, \pi + \alpha_{HWS,2N}] \tag{2.9}$$

$$\boldsymbol{\alpha}_{PSR} = \left[\boldsymbol{\alpha}_{FWS}; \text{sort}((\boldsymbol{\alpha}_{FWS} - \frac{2\pi}{3}) \bmod 2\pi); \text{sort}((\boldsymbol{\alpha}_{FWS} - \frac{4\pi}{3}) \bmod 2\pi)\right] \tag{2.10}$$

4. In sections 2.5 and 2.6, K_1 and K_2 are chosen equal to 10^6. This value is set really high to privilege feasible solutions against unfeasible but with a bad fitness value

5. The acceptable domain is the domain where the constraints are respected according to prefixed tolerance

A scheme of the proposed algorithm is given in Fig. 2.2. This algorithm computes the optimal switching angles of the PSR method from the N_m desired signals depending on the modulation index. If the index of the initial step j is lower than N_m the algorithm stops. Otherwise, as explained previously, an initial matrix $\mathbf{x_0}$ is selected (eq. (2.6)) and stored in $L_{x_0,j}$, from a random set of matrices $\mathbf{x}$. Then for each element i among the $n_{L,j}$ matrices of $L_{x_0,j}$, an optimization is performed from $L_{x_0,j,i}$. Next, the best solution found among all the starting matrices is selected and stored in Σ_{fin} (the set of final solutions for each modulation indexes). The solution is also stored in $L_{x_0,j+1}$, the next step is to set of starting matrices and $i = i + 1$. This part of the algorithm stops when i is greater than $n_{L,j}$ and then $j = j + 1$, and the algorithm go to the $j \leq N_m$ test. In order to preserve at least the local minimum found from the previous step of the algorithm. The solution from the previous modulation index is also chosen as a starting matrix. It can be seen on Fig. 2.2 where the j$^{\text{th}}$ solution is stored in the starting matrix list for the next modulation index $L_{x_{0,j+1}}$ [6].

2.4 Evaluation criteria

As mentioned in the first chapter, the WTHD is one of the most used objective concerning the OPP with the selective harmonic elimination. Then the WTHD was selected to perform the following evaluation (see Appendix F). Nevertheless, a risk was identified, it is about the risk of brutal variations inside a set of solutions, which risk to generate unexpected behavior. It was then decided to study the smoothness of the solutions found.

Indeed, because we are relaxing symmetries, it can exist a risk that the intrinsic brutal changes of the solutions is getting worse. Then the following smoothness criterion is introduced in order to verify that the solutions found do not introduce more brutal changes inside the set of solutions than classical OPPs as QWS, HWS and FWS.

2.4.1 Smoothness

This section is concerned to present a load independent criteria in order to decide if the smoothness of the angle set can be considered as good or poor. In other terms: What influence will have a tiny mistake on angles on the voltage or current load behavior? To

6. All the results are obtained with a modulation index discretization step of 0.001 and then, the solution found for $m = 0.5$, will be one of the starting matrix of the computation for the next discretization step $m = 0.501$

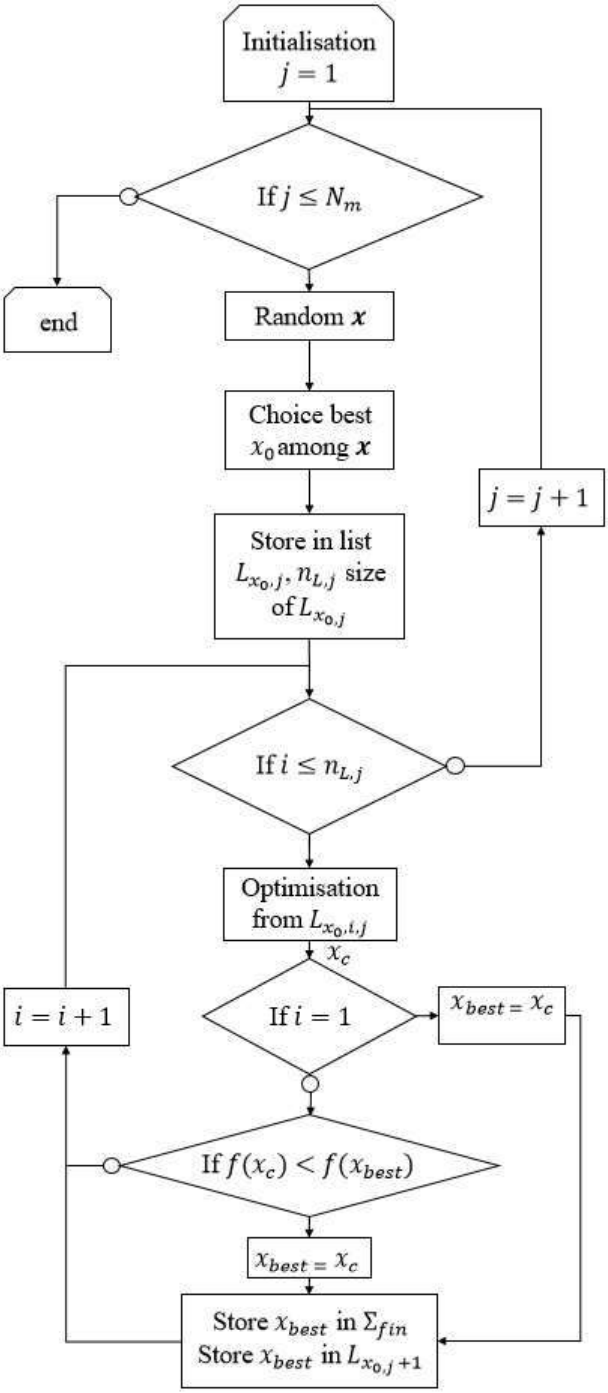

Figure 2.2 – Schematic view of the computation algorithm, N_m is the number of modulation index considered and Σ_{fin} is the final set of solutions found by the algorithm.

evaluate this influence, a polynomial regression is done on the switching angles, the idea behind is, if the variation for a specific angle is polynomial than its smoothness is considered as a good one.

In the following a precise methodology to evaluate this smoothness is presented. This methodology provides a number based on all the solutions found for a single symmetry. For OPP, decision variable in the algorithm is a vector or a matrix for PSR. Considering all the operating points a matrix could be establish where each line is a set of angle for a specific modulation index. Then a search for a polynomial equation eq. (2.11) of a specific order n is performed which fit a maximum with the evolution of an angle. Finally the correlation factor between estimated angles with a polynomial function and the real angles set is computed eq. (2.14). This number will be called the smoothness factor.

If the smoothness factor is close to 1 (a good smoothness) that mean that the two curves (the one described by eq. (2.11) and the solution set) are similar. The angle evolution can be then approximated by a polynomial equation of the specific order n. Otherwise correlation factor near 0, means there is no correlation between the computed curve and the real one. Then a degradation of the selected objective function must be considered in order to increase smoothness factor.

$$\mathcal{P}(m) = c_n m^n + c_{n-1} m^{n-1} + \cdots + c_0 \tag{2.11}$$

Where $c_i \ \forall i \in [\![0; n]\!]$ are computed with eq. (2.12). Note that in this equation the multiplication is a usual one of matrix by a vector. Consequently the Hankel matrix composed of H_j have to be inverted thanks to the pseudo-inverse matrix of Moore-Penrose because the H_j matrix is not regular. Then the chosen estimated angles minimize the euclidean norm to the angles computed with the algorithm (2.3) [7].

$$\begin{bmatrix} H_0 & \cdots & H_n \\ H_1 & \cdots & H_{n+1} \\ \vdots & \ddots & \vdots \\ H_n & \cdots & H_{2n} \end{bmatrix} \cdot \begin{bmatrix} c_0 \\ c_1 \\ \vdots \\ c_n \end{bmatrix} = \begin{bmatrix} T_0 \\ T_1 \\ \vdots \\ T_n \end{bmatrix} \tag{2.12}$$

7. The norm 2 have been chosen as it is similar to a distance estimation, then norm 2, in our context seemed to be the best choice

Parameter	value
ϵ_θ	$\pm\pi/25$rad
ϵ_V	$\pm 2mE_{DC}/100$V
K_1, K_2	10^6
δt_{min}	$1\mu s$
n_m	300
E_{DC}	400V
f_1	50Hz

Table 2.3 – Values of the parameters in order to find the presented results

Where T_j and H_j are defined in eq. (2.13)

$$\begin{cases} T_j = \sum_{i=1}^{n} m_i^j \alpha_{j,m_i} \\ H_j = \sum_{i=1}^{n} m_i^j \end{cases} \tag{2.13}$$

As $\mathbf{\Psi}_k = [\alpha_{k,m_1}, \cdots, \alpha_{k,m_{imax}}]^t$ a vector of m_{imax} dimensions of the angle number k computed with the problem defined with eq. (2.3). On the other hand $\widehat{\mathbf{\Psi}}_k$ is a vector of estimated values of $\mathbf{\Psi}_k$, according to the solution found by eq. (2.11), $\widehat{\mathbf{\Psi}}_k = \left[\mathcal{P}(m_1), \ \mathcal{P}(m_2), \ \cdots, \ \mathcal{P}(m_{max})\right]^t = \left[\hat{\alpha}_{k,m_1}, \ \hat{\alpha}_{k,m_2}, \ \cdots, \ \hat{\alpha}_{k,m_{max}}\right]^t$.

$$r_k = 100 \frac{\left(\mathbf{E}(\mathbf{\Psi_k}\widehat{\mathbf{\Psi}}_\mathbf{k}) - \mathbf{E}(\mathbf{\Psi_k})\mathbf{E}(\widehat{\mathbf{\Psi}}_\mathbf{k})\right)^2}{\left(\mathbf{E}(\mathbf{\Psi_k^2}) - \mathbf{E}(\mathbf{\Psi_k})^2)(\mathbf{E}(\widehat{\mathbf{\Psi}}_\mathbf{k}^\mathbf{2}) - \mathbf{E}(\widehat{\mathbf{\Psi}}_\mathbf{k})^2\right)} \tag{2.14}$$

Where r_k is the smoothness factor.

In order to highlight the well founded of the proposed method (i.e. optimization problems and criteria) an example of computation is proposed in the next section on a three phases voltage inverter.

2.5 Simulation results

2.5.1 WTHD comparison

The WTHD comparison, in simulation, is done with respect to the parameters given by Table 2.3. In this section, only FWS and PSR are presented because Birth's paper [66] showed the superiority of FWS over the QWS and HWS. Note that this superiority has been also found while investigations but are not presented here.

Because the more N_{qp} is great, the more a QWS consideration is enough to obtain good

results, the decision have been done to limit the computation to $N_{qp} = 5$. Furthermore, the choice have been done to consider only a three phases voltage inverter in order to highlight the well founded of the proposed method.

In the Fig. 2.3 and Fig. 2.4 WTHD comparison are shown respectively for $N_{qp} = 2$ and $N_{qp} = 5$.

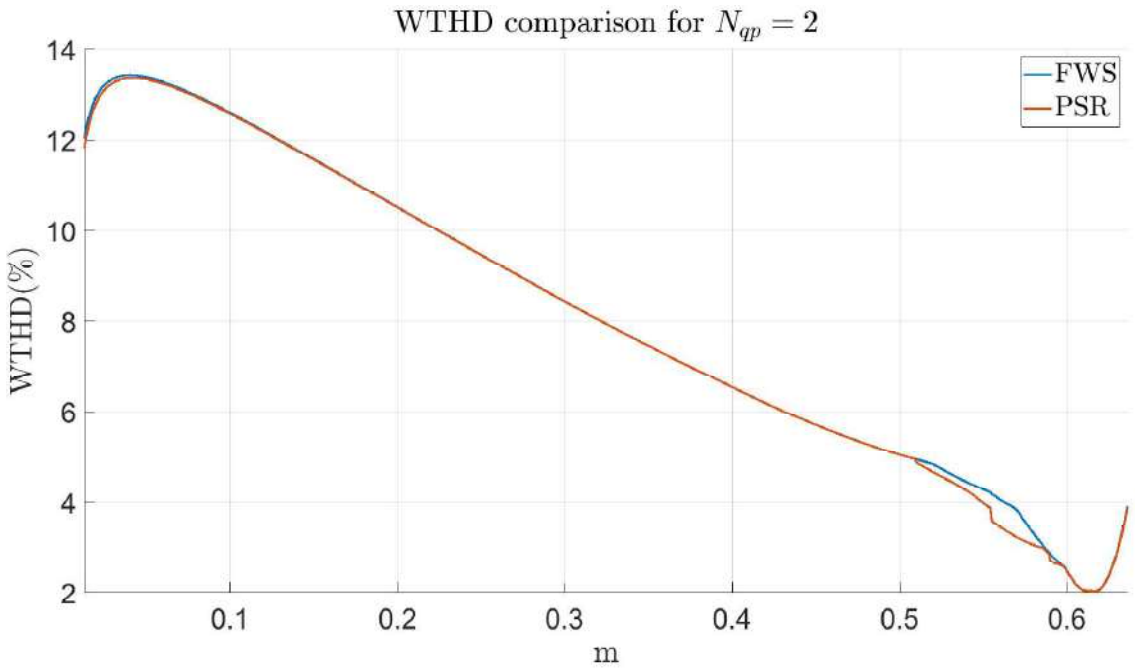

Figure 2.3 – Comparison between FWS and PSR method according to WTHD for $N_{qp} = 2$ when minimizing WTHD

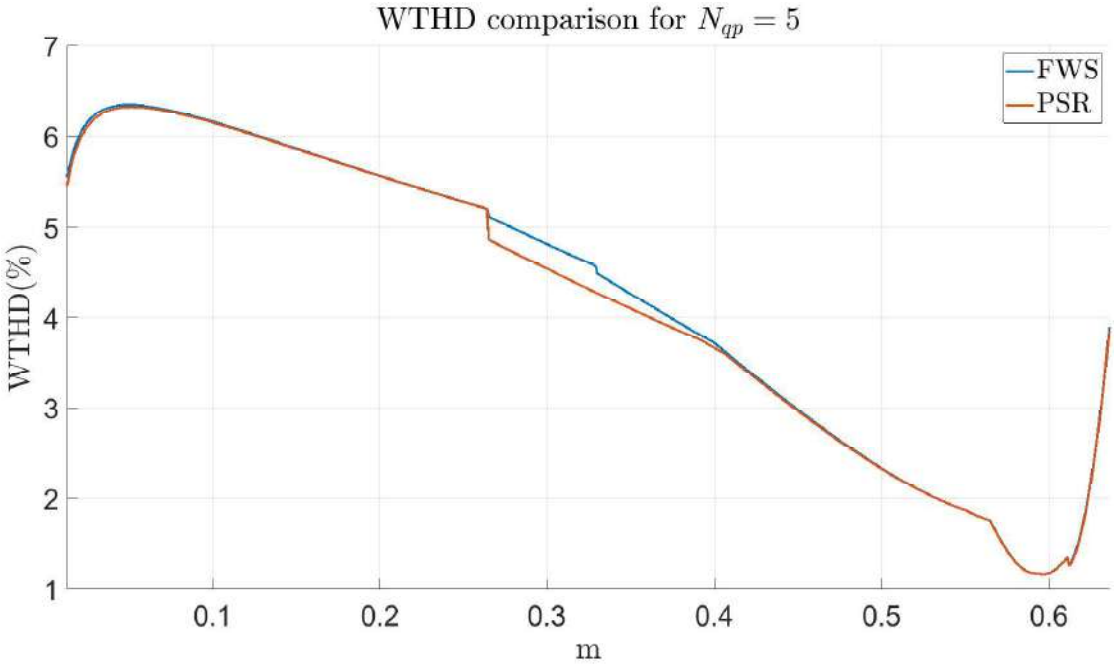

Figure 2.4 – Comparison between FWS and PSR method according to WTHD for $N_{qp} = 5$ when minimizing WTHD

The curves show that the PSR method provides best solutions than the other ones. For the WTHD objective function, the advantage of PSR method is for m around $\frac{1}{\pi}$ for $N_{qp} = 5$ and around $\frac{1}{\sqrt{3}}$ for $N_{qp} = 2$. Furthermore tables 2.4 and 2.5 show an improvement in comparison to other strategies.

Strategy	$N_{qp} = 2$	$N_{qp} = 5$
QWS	8.16%	4.30%
HWS	8.16%	4.26%
FWS	8.11%	4.21%
PSR	8.06%	4.16%

Table 2.4 – Simulation mean value of WTHD for different solutions in percentage according to (F.13)

N_{qp}	$m = \frac{V_1}{E_{DC}}$	ε
$N_{qp} = 2$	0.53	3.52%
	0.55	7.11%
	0.57	15.85%
$N_{qp} = 5$	0.27	5.02%
	0.3	5.67%
	0.33	4.84%

Table 2.5 – Simulation comparison between FWS and PSR for six specific operating points inside the improvement zone. Percentage of improvement have been computed thanks to (F.13) and (2.15).

It is interesting to note that all the symmetries relaxation allow to improve the results. Finally PSR strategy improve FWS with a mean value $V_{WTHD,\%} = 8.06\%$ for $N_{qp} = 2$ and $V_{WTHD,\%} = 4.16\%$ for $N_{qp} = 5$ according to (F.13). It could seem negligible because all the solutions give the same WTHD, on a wide range of modulation indexes. Nevertheless as it can be seen in Figs. 2.3 and 2.4 but also in Table 2.5, the maximum improvement of PSR in terms of WTHD in comparison with FWS is $\varepsilon = 16.15\%$ for $N_{qp} = 2$ and $\varepsilon = 6.37\%$ for $N_{qp} = 5$ according to (2.15). Then, even if the global mean value affords a small improvement, some operating points improve the WTHD of 16%. Furthermore the improvement zone is not negligible as it covers more than 30% of the feasible operating points.

$$\varepsilon = 100\frac{WTHD_{FWS} - WTHD_{PSR}}{WTHD_{FWS}} \tag{2.15}$$

2.5.2 Smoothness

Another criterion identified is the smoothness. To illustrate this criterion Fig. 2.5 and Fig. 2.6 show the regularity of the solutions.

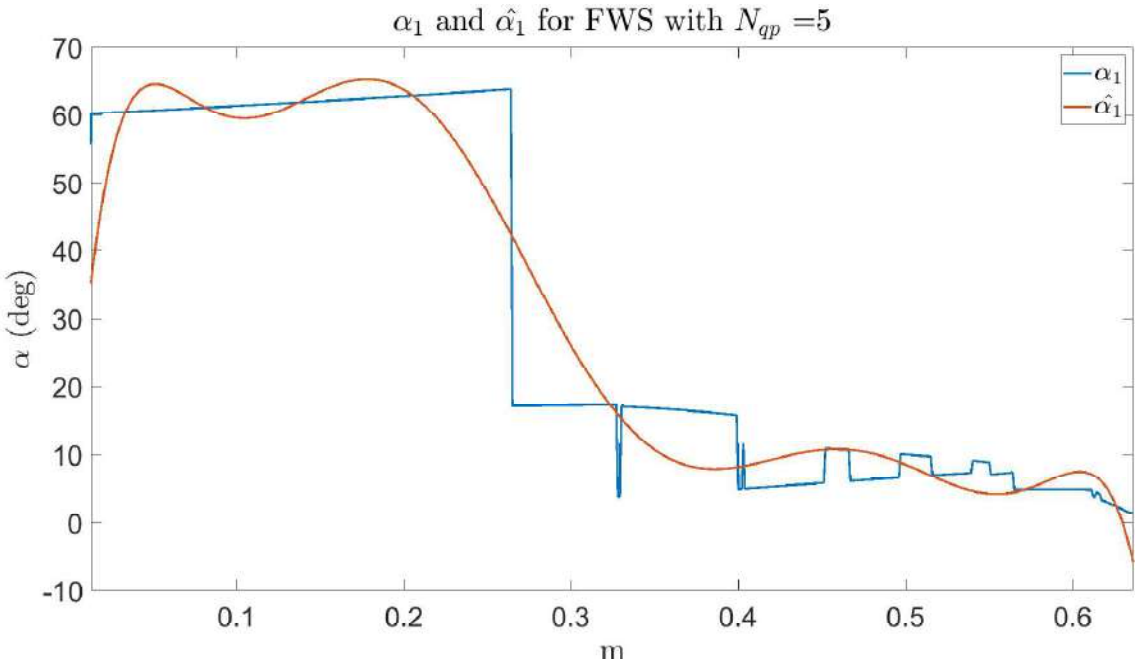

Figure 2.5 – Example of smoothness for the first angle of the WTHD, for the FWS solution with $N_{qp} = 5$

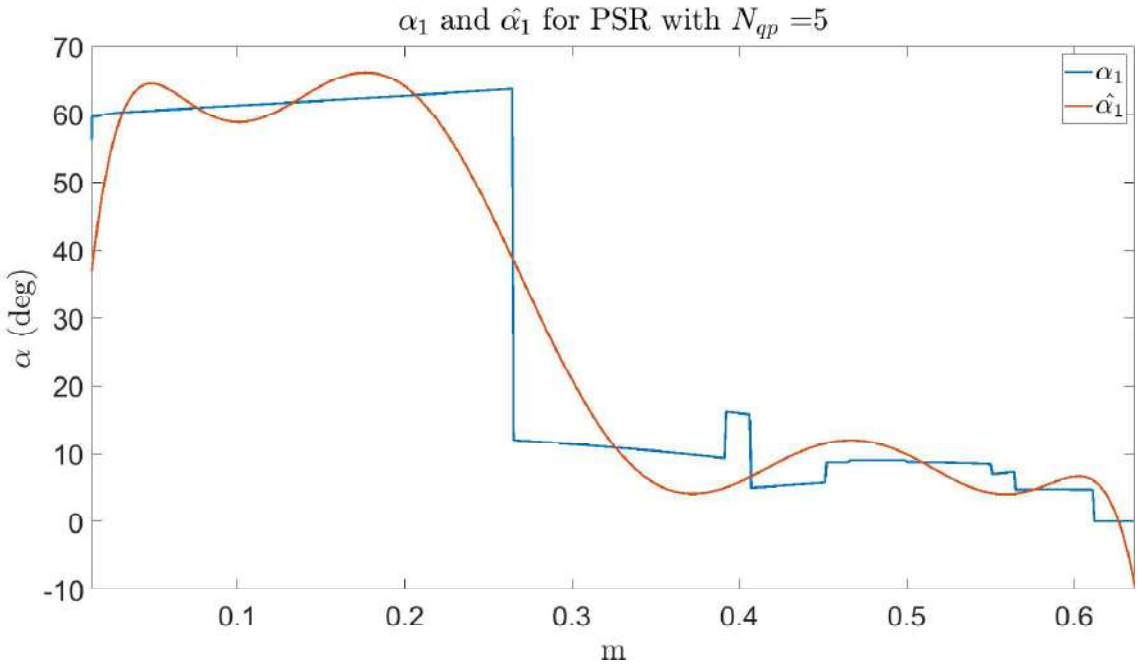

Figure 2.6 – Example of smoothness for the first angle of the WTHD, for the PSR solution with $N_{qp} = 5$

Strategy	$N_{qp} = 2$	$N_{qp} = 5$
QWS	85.6%	84.5%
HWS	85.6%	83.7%
FWS	67.7%	76.1%
PSR	63.8%	86.1%

Table 2.6 – Value of smoothness for different solutions in percentage (computed with WTHD) according to (2.14)

The smoothness computation has been done with a 8 order polynomial approximation [8]. In this case the smoothness is considered good enough, verified by the smoothness factor given in Table 2.6). In this table QWS affords the best smoothness and PSR the worst one for $N_{qp} = 2$ but for $N_{qp} = 5$ the PSR is the best one.

For QWS and HWS, the smoothness is better than FWS, this is due to the imposed symmetries inside the solutions which reduces the gaps between angles solutions.

Fig. 2.5 and Fig. 2.6 illustrate how works the smoothness factor. Indeed those curves are examples for the first angle of the first phase solution set, which is respectively equal to $r_k = 75.2\%$ and $r_k = 89.6\%$ according to (2.14).

2.5.3 Switching losses influence

About the influence of PSR on switching losses, it was decided to compute the efficiency of FWS and PSR in simulation for a particular case and compare both of them. The comparison is performed by computing the relative gap between the two efficiencies (2.19). In the following example the number of phases is also set to $p = 3$.

First, the efficiency η is defined thanks to eq. (2.16) and eqs.(2.17)-(2.18)

$$\eta = \frac{\mathcal{P}_u}{\mathcal{P}_{tot}} \tag{2.16}$$

P_u designates the useful power and P_{tot} the total one. As the three phases could be different because of the lack of symmetry, it is mandatory to compute their power independently

8. This order number is arbitrary, nevertheless, this order have to be chosen high enough to be precise and not too much high to avoid computational problems with badly scaled matrix. Then, different tests led us to consider the number 8.

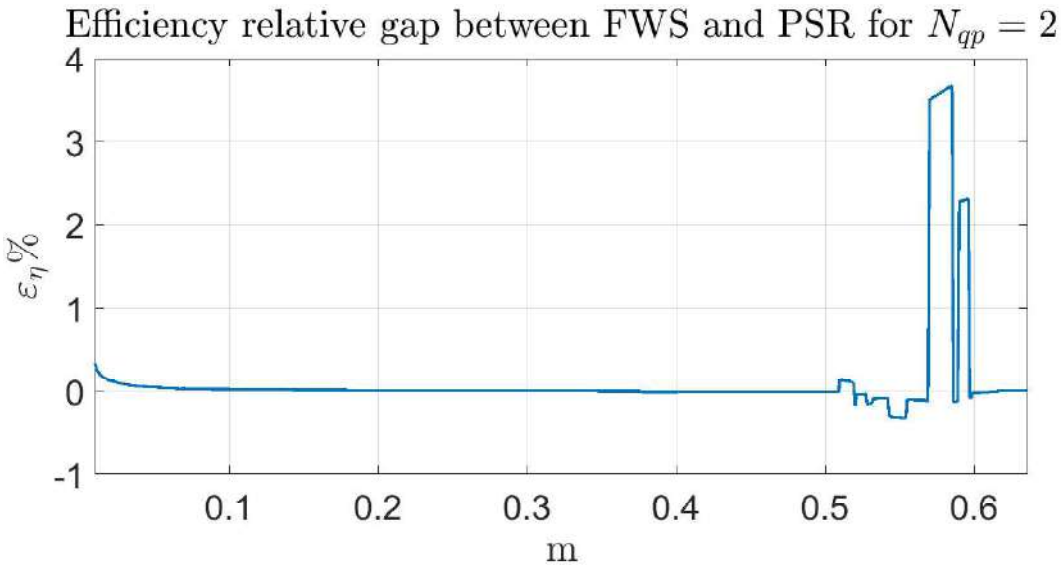

Figure 2.7 – Efficiency relative gap for (ε_η) for $N_{qp} = 2$

and not to use the usual $P_u = 3VI\cos(\varphi)$ formula.

$$\mathcal{P}_u = \sum_{k=1}^{p} V_{k,1} I_{k,1} \cos(\varphi_{k,1}) \tag{2.17}$$

$$\mathcal{P}_{tot} = \mathcal{P}_{sw} + \mathcal{P}_{con} + \sum_{k=1}^{p} \sum_{h=1}^{\infty} V_{k,h} I_{k,h} \tag{2.18}$$

With $\mathcal{P}_{sw}$ the power lost when the switches state change and $\mathcal{P}_{con}$ the power lost while the current go through the switch (see Appendix I for more details.)

Thanks to previous equations and arbitrary parameters of R, L, IGBT and diode components [9], it is possible to compare the FWS efficiency η_{FWS} and the PSR efficiency η_{PSR} with eq. (2.19).

$$\varepsilon_\eta = 100 \frac{\eta_{FWS} - \eta_{PSR}}{\eta_{FWS}} \tag{2.19}$$

As shown in figures 2.7 and 2.8 the influence of angle symmetry relaxation is positive on efficiency for highest operating points when $N_{qp} = 2$. For $N_{qp} = 5$ losses impact is almost negligible, because the impact is lower than 1%. Even if for this last configuration PSR decrease a little the efficiency value in comparison of FWS. These conclusions

9. The parameters are $R = 10\text{m}\Omega$; $L = 170\mu\text{H}$; similar but not equal to the ones provided by Renault. The arbitrary chosen switches are: https://www.onsemi.com/pdf/datasheet/ngtb40n60ihlw-d.pdf

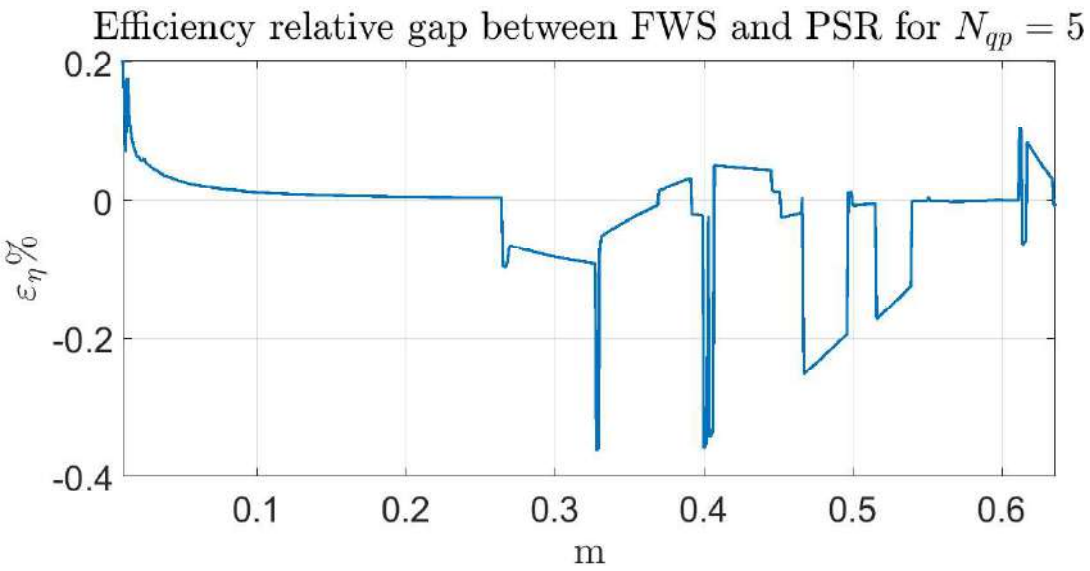

Figure 2.8 – Efficiency relative gap for (ε_η) for $N_{qp} = 5$

are not surprising as it is well known that the main influence on the switching losses is the switching frequency f_s. Furthermore a reader who would specifically reduce switching losses or increase efficiency can easily change the objective function in eq.(2.3) from WTHD to efficiency one or whatever he desires.

In this paper it is shown that the PSR strategy provides best results than FWS one. The superiority of PSR, in simulation, is then established for two purposes, increasing the solution quality and increasing the smoothness quality (as defined in section 2.4.1) without increasing drastically the switching losses.

2.6 Experimental results

In order to confirm experimentally the well funded of the proposed strategy, an experimental setting has been set up. It is composed of a DSpace© system (RTI 1103 with MatLab© 2010) that is generating the PWM signals sent to a three legs two levels inverter via I/O ports. Each switch is composed of a MOSFET with two freewheeling diodes. The power of the inverter is provided by a stabilized DC generator of 25V for safety reasons. Then the inverter is connected to a balanced three-phases inductive load composed with $R \approx 12.9\Omega$, $L \approx 1.2$H.

Remark that the angular precision in simulation section is equal to $100\pi \cdot 10^{-6}$ rad for an electrical frequency of 50Hz. Then in order to at least respect this angular precision

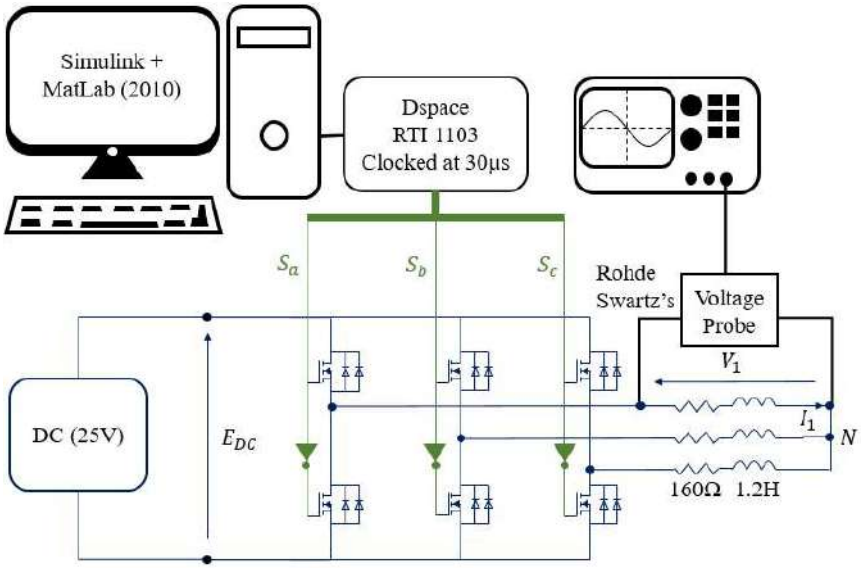

Figure 2.9 – Schematic representation of the experimental bench.

Parameter	Value
f_1	1Hz
δt_{min}	30µs
Δt	60µs
E_{DC}	25V
R	12.9Ω
L	1.2H

Table 2.7 – Experimental parameters

and the experimental device limitations, the experimental electrical frequency is set to 1Hz. Indeed a technical limitation of the micro-controller sampling period equal to 30µs. By doing so the angular precision is equal to $60\pi \cdot 10^{-6}$ rad, which is lower than the simulation one. Since the simulink scheme is real time the dead-time is equal to one step of controller computation and then is equal to 30µs$\equiv 60\pi$µrad

Concerning the voltage measurement, a Rohde Swartz's© probe is used and connected between the input of the RL load and the neutral point. The voltage is sent to the DSpace, by saving datas for ten periods (i.e. 10s). Then the harmonic spectrum of the voltage is extracted and finally the WTHD is computed by using eq. (F.12). A video of the experimental bench can be found in [102] and on figure 2.9, the parameters are sum up in Table 2.7.

In the Table 2.9, three specific points where selected for $N_{qp} = 2$ and $N_{qp} = 5$, with respect to the improvement zone visible on Figs. 2.3 and 2.4. The table results are computed with (2.15), and show a WTHD improvement of the PSR against the FWS.

In order to verify the behavior of the PSR against the FWS in all the validity domain. Other operating points are evaluated and are represented on Figs. 2.10 and 2.11. The shape of the curves is very similar to the simulation ones (Figs. 2.3 and 2.4). Thanks to these experiments a mean value of improvement was also computed and the results have been compiled in the Table 2.8. As for simulation results the mean increase is not that much impressive, but, by considering a local improvement with Table 2.9, the value of the PSR strategy is then much more visible.

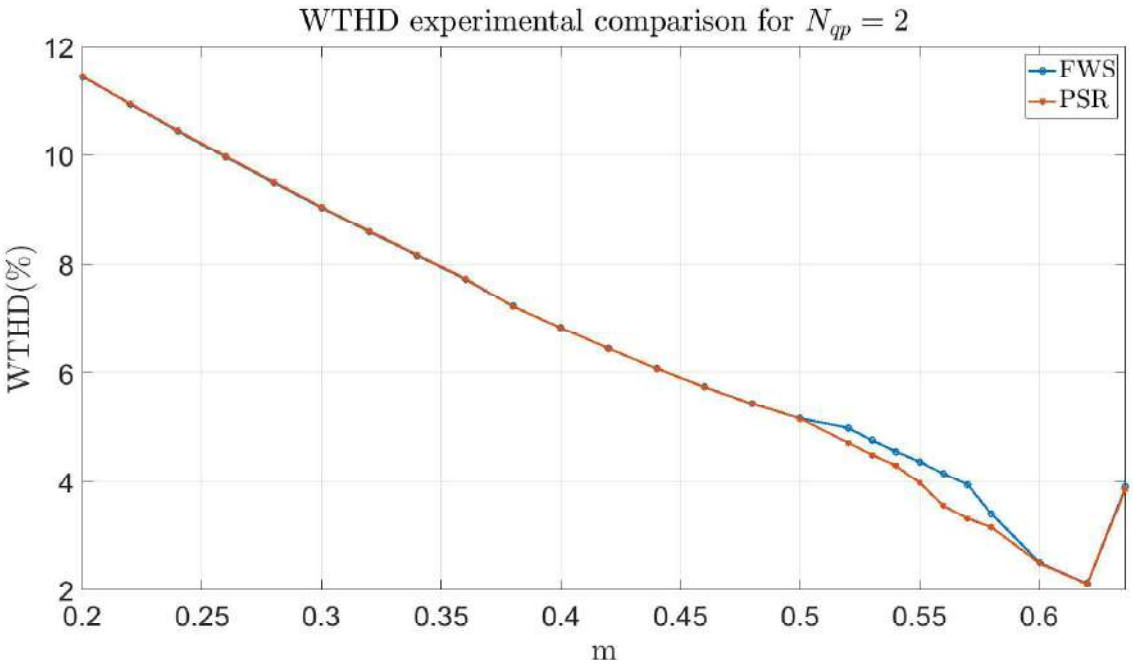

Figure 2.10 – WTHD value for $N_{qp} = 2$, the points have been computed with a step of 0.02

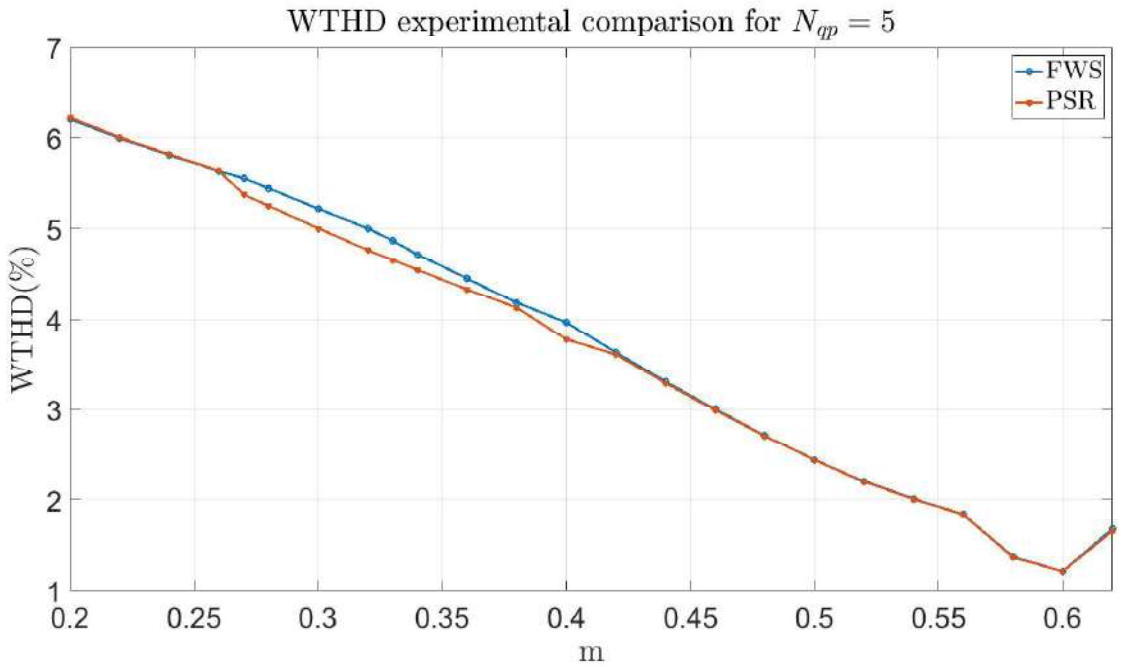

Figure 2.11 – WTHD value for $N_{qp} = 5$, the points have been computed with a step of 0.02

Strategy	$N_{qp} = 2$	$N_{qp} = 5$
FWS	6.44%	3.85%
PSR	6.34%	3.79%

Table 2.8 – Experimental mean value of WTHD for FWS and PSR in percentage. This percentage was computed with the same points than Figs. 2.10 and 2.11.

N_{qp}	$m = \frac{V_1}{E_{DC}}$	ε
$N_{qp} = 2$	0.53	5.53%
	0.55	9.03%
	0.57	16.02%
$N_{qp} = 5$	0.27	3.28%
	0.3	4.12%
	0.33	4.39%

Table 2.9 – Experimental comparison between FWS and PSR

for six specific operating points inside the improvement zone. Percentage of improvement have been computed thanks to (F.13) and (2.15).

Experimental results confirm the superiority of the PSR method against QWS, HWS or a FWS for low N_{qp}. For higher N_{qp} the results are similar for all the considered methods

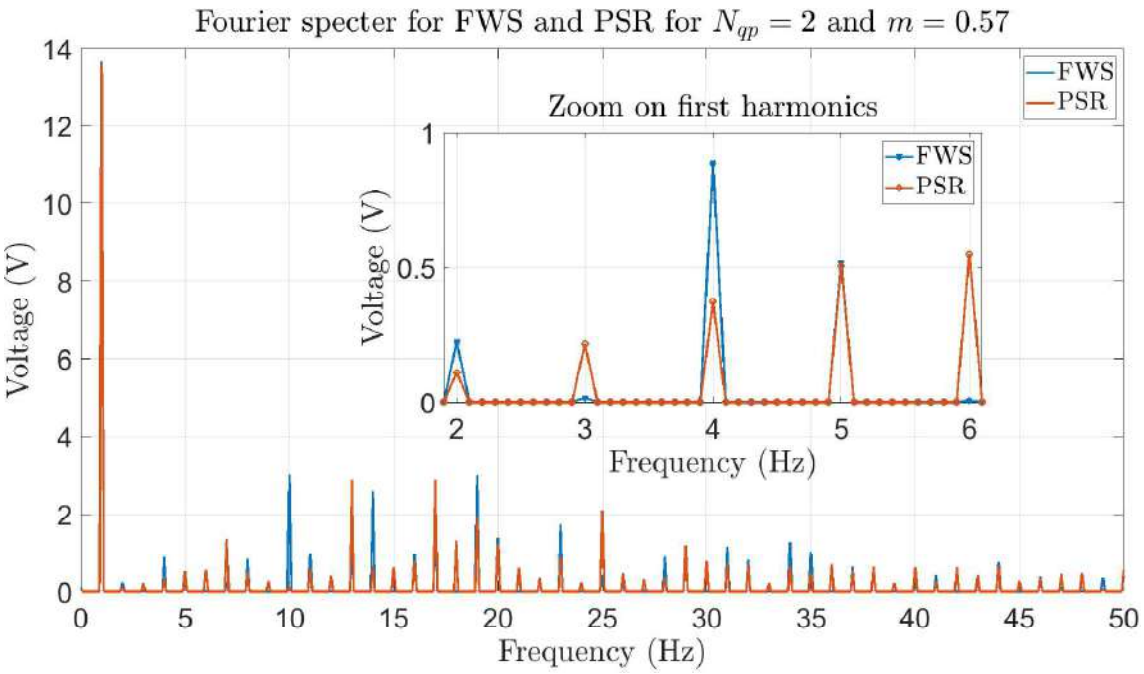

Figure 2.12 – Fourier spectrum for the FWS and PSR for $N_{qp} = 2$ and $m = 0.57$.

because significant voltage harmonics of eq. (F.13) would be in high enough frequency to be negligible.

Experimental results are also validated thanks the simulation ones as Table 2.4 corroborates with Table 2.8, but also Table 2.5 is similar in terms of improvement to 2.9.

As the experimental results depends on dead-time, it is shown there is no significant influence of Δt on experimental results. Nevertheless for higher electrical frequencies, it would be necessary to start again an optimization in order to ensure this kind of solutions quality (see Fig. 2.14). Indeed an increase of electrical frequency will also decrease the angular precision as δt_{min} is set to 1µs.

Fig. 2.12 is the Fourier transform of the phase voltage of Fig. 2.13 obtained with $N_{qp} = 2$ and $m = 0.57$. It can be seen from Fig. 2.12 in red color (PSR) the harmonics multiple of three are not removed (see zoom on first harmonics), which confirms the relaxations constraint of angle symmetry between phases (see eq. (G.5)) for PSR strategy.

About general implementation issues of classical methods and PSR method, the computed angles have to be stored inside a micro controller [66], [103]. The controller always reads the tables and send an interruption when the internal clock value (converted in angles) corresponds to the table one (Fig. 2.14). As the precision is function of the sampling time and electrical frequency, it is necessary for the same precision to increase the speed

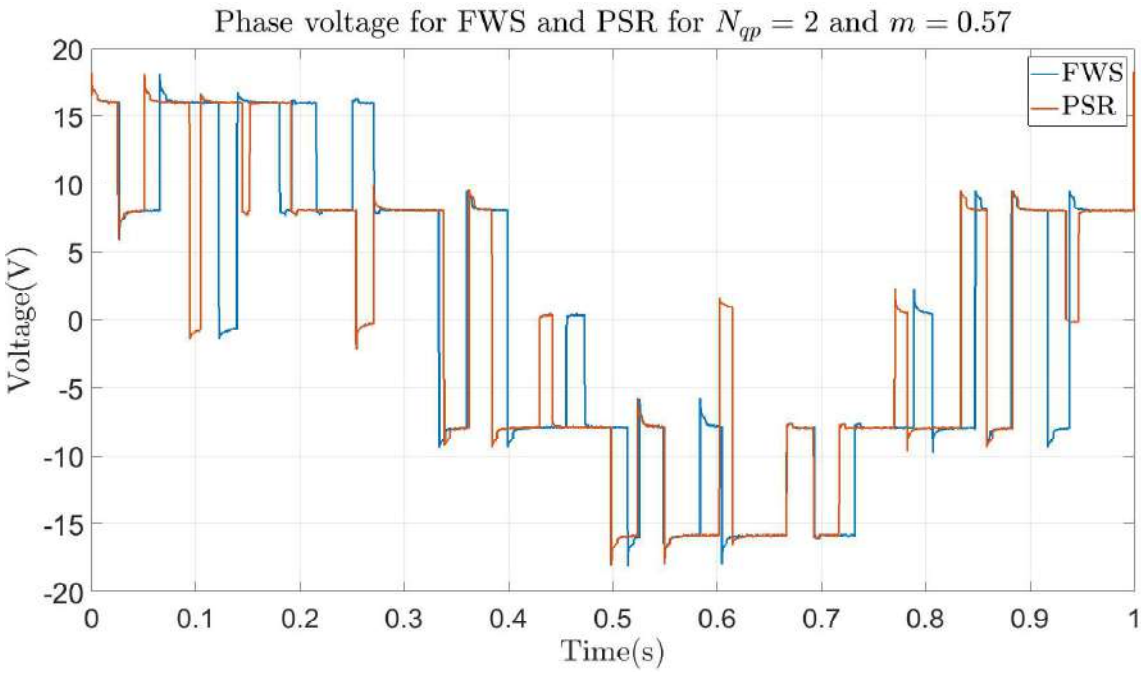

Figure 2.13 – Voltage waveform for the FWS and PSR for $N_{qp} = 2$ and $m = 0.57$.

of a micro controller if the electrical frequency increases. In the same way of thinking for a fixed controller speed the precision can be increased by lowering the electrical frequency, which is done in this section. It is important to remark that the storage of PSR is three times greater than the FWS one and twelve times greater than the QWS one. Nevertheless, the size of the tables is still technologically and economically acceptable.

Even if the previous example is dedicated to three phases RL load, the proposed strategy can be used for p-phases and any inductive or capacitive load.

2.7 PSR and Space vector modulation

The PSR, due to its intrinsic structure, select the switching angles for each phase independently. This selection, is rigorously equivalent to a space vector modulation. Indeed, every solution found will always belongs to the set of feasible vectors. Then an OPP, is always a vector method with extra freedom degrees.

The difference between classic space vector methods and OPP resides in the fact that the voltage reference following is not observed locally (see Appendix C) but on a whole

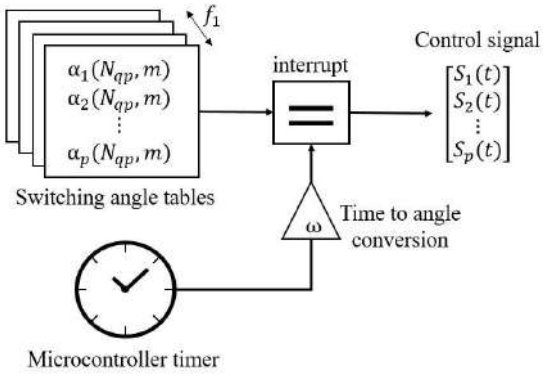

Figure 2.14 – Off-line PWM control in the particular case of a three phase inverter. Solutions depends also on fundamental frequency for the angular precision. For this third dimension, each table should be understood as a frequency interval and not as a specific frequency.

period [10]. This non-local condition is necessary to perform a low frequency vector method. Indeed, in a SVM paradigm, thanks to a high frequency ratio, the PWM voltage mean value is for every switching period equivalent to the desired voltage. This mean value hypothesis cannot be done when the frequency ratio is low.

Then the previous exposed constraint in a vector based idea force to release the classic vector hypothesis, i.e. to use two [11] adjacent vectors to generate the desired voltage, and for example use only one of them in addition with the zero voltage one and with a varying time value (Fig. 2.15). This technique allow to follow the reference even if the switching frequency is very low, which is impossible with classic techniques.

2.7.1 The zero sequence component extraction

For the same reason than for the vector consideration, the mean value computation of the duty cycle is not evident, due to the impossibility to use the mean value theorem (see Appendix D). Then, the more a low switching frequency is used, the more the duty cycle as an injection of Zero Sequence Component (ZSC) in the modulating signal is hard to extract.

Furthermore, it is well known that CBPWM have regular switches due to the carrier. This property is not shared with OPP. Then, this clue could mean that a link from OPP to CBPWM does not exist. Nevertheless, this impossibility have not been proved yet.

10. A quarter period for QWS, half period for HWS and full period for FWS and PSR
11. or three for other space vector modulation techniques

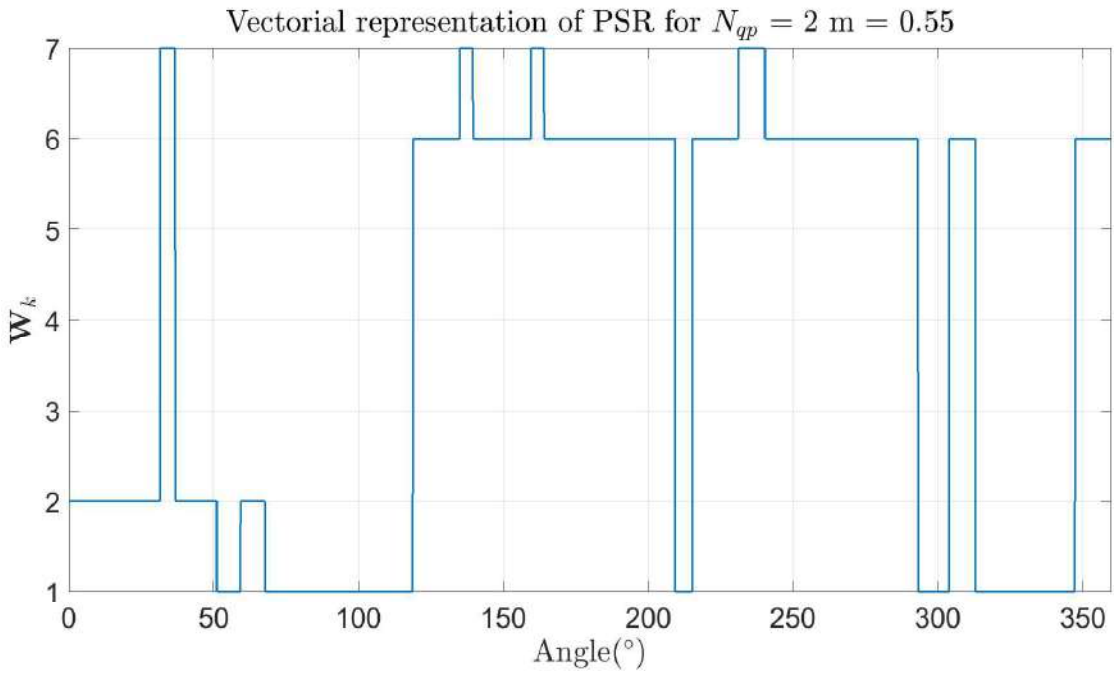

Figure 2.15 – PSR command as a space vector point of view

This probable incompatibility led us to consider the ZSC optimization as an entire work, as we faced to this physical barrier to extrapolate the PSR [12] to a ZSC injection one.

This is even more interesting as a carrier based PWM is way more easy to implement than an OPP which necessities to completely change the software structure.

2.8 Conclusion

In this chapter a new PWM method with a relaxation of symmetry for low switching frequency is exposed, called Phases Symmetry Relaxation (PSR). A simulation evaluation of this strategy was performed according to WTHD compared with classical PWM symmetry strategies for the specific case of a three phases voltage inverter. Furthermore experimental results corroborates the first results obtained in simulation for the same conditions.

For all the studied operating points, PSR strategy affords the best results in comparison with the classical OPP solutions as FWS, described in [66]. Indeed computation and

12. More generally, all the other low frequencies OPP, QWS, HWS and FWS

experiments performed shows an improvement of WTHD for some specific modulation index and for low switching frequency.

As a generic optimization problem was defined without specific load, it was highlighted that PSR method can be applied to a p-phases inverter to feed either an inductive (voltage WTHD) or a capacitive load (current WTHD). Furthermore a new smoothness criterion (Evaluates the smoothness of the switching angles when the modulation index changes) was presented and simulation results shown that PSR is competitive with other OPP.

In future works experimental validation of the proposed strategy will be done on a synchronous electric motor, which implies a variation of the electrical frequency and modulation index dynamically. Furthermore even if WTHD and smoothness are the most important criteria, some other criteria could be interesting to study in future works. In addition, the WTHD optimization related to PSR probably underestimate the benefits of the technique. Indeed on a motor with a non sinusoidal electromotive force, the interest is intuitively better for PSR as it plays with the phases symmetry. Nevertheless showing the PSR improve the WTHD is an important step as it is easy to understand and classic for OPP considerations especially thanks with the generic optimization proposed.

Future works would be interested to some sort of generic space vector equivalence or carrier based PWM equivalence in order to increase the feasibility of the solutions on a embedded device. Nevertheless, this generalization is presupposed hard due to the low switching frequency as explained in this chapter.

About a concrete real time implementation, it is not easy to perform as it needs a hardware configuration change (FPGA for example). In addition an attention to dead-time consideration would have be done. Indeed, for high electrical frequencies, the dead-time hypothesis we did (Appendix K), will be not feasible anymore.

Next chapter will be concerned on the zero sequence component and especially to its optimization. As exposed, in this chapter, the main problem is the implementation, then, finding a structure which keep the previous software architecture is appreciable for an easier and quicker implementation.

Chapter 3

Synchronous Carrier Based PWM

Because of the Optimal Pulse Pattern (OPP) problems presented in the previous chapter, vector based strategies and the carrier based ones seems to be easier to implement. Then, a sub-optimal strategy would be preferable if its implementation is easier to be done and rely on well known techniques. In addition, OPP strategies cannot be overpass in terms of results, explaining why the presented researches was focused on finding new easy implementable synchronous carrier based strategies. Following chapter will present two synchronous Carrier Based PWM (CBPWM), the Zero Sequence Component Modulation (ZSCM), which is an extension of Third Harmonic Injection PWM (THIPWM). But also the Saw-Tooth Injection PWM (STIPWM) which generalizes ZSCM for some operating points.

These two strategies will be explained and their improvement will be phased with the classic synchronous strategies knowledge.

In order to have a better understanding of these strategies, a short carrier based PWM context description is proposed in the next section.

3.1 The carrier based PWM context

CBPWM exists since almost one century [14] to control power electronic devices such as inverters. Many works tried to improve the PWM by injecting harmonics in the modulated signal [24], [27], [32], [51], [63], [64], [104].

More recently it also appeared OPPs strategies as [23], [47], [66], [69]–[72], [88], [105]. Most of the papers are concerned about the improvement of the harmonic quality thanks the WTHD. Indeed as it was explained, it is a good way to evaluate current behavior in an electric motor. As the motors behaves as a low pass filter, WTHD allows to take into account this dynamic without considering a specific electrical motor.

Even if OPPs offers better results, their main problem, is that for many power conversion structures, it necessities to change the whole command structure. Which cost a

lot of money [1], and is more difficult to ensure the security and the safety of the device [2]. These difficulties explain why OPP are not popular in the industry, despite their better results [23], [66], [67], [105].

To avoid OPP problems more recent researches was concerned about synchronous CBPWM optimization [86], [106], [107]. Furthermore, at the end of the 80's Boost suggested in a state of the art the apparition of a strategy which would generalize the THIPWM by injecting more than one harmonic [37]. Nevertheless, because of the technical limitations, it was not feasible to implement efficiently the suggested idea in 1988, because of the heavy optimization problem and technical limitations to implement such idea.

The present chapter, show investigations on the injection of a lot of third harmonics in order to reduce WTHD or losses, we will show that the harmonic quality of the output voltage of a three phases two-level inverter can be improved by this strategy we decided to call ZSCM. More precisely, we will highlight the benefits of ZSCM to reduce the WTHD and losses against the most classical CBPWM as THIPWM and SVPWM [24]. The idea of this strategy is basically to generalize CBPWM and by extension the THIPWM by injecting an infinity of harmonics multiple of three, in the same idea as Boost one [37].

Furthermore with ZSCM strategy, only the modulation component software is changed without modifying the existing hardware. Then, the well known robustness of classical CBPWM and the phase symmetry is also preserved.

Nevertheless ZSCM limits will be also highlighted as the Gibbs effect due to potential discontinuities inside the zero sequence component. In addition, it appears that for some specific operating points and objectives the ZSCM strategy looks like to converge to a saw-tooth shape. This convergence is the second subject of this chapter, and more precisely the mathematical understanding of this saw-tooth convergence and its benefits in terms of WTHD and losses.

As for the previous chapter, the control loop is considered as a black box, providing information about sinusoidal signal reference (f_1, V_1). These information are necessary to perform a correct synchronous CBPWM.

Thanks the context highlighting of this section, next, a description of the ZSCM is performed with the highlighting of its benefits and generalization to the other strategy proposed, the STIPWM.

1. Due to architecture and philosophy changes
2. Dead-time management and narrow pulses avoidance

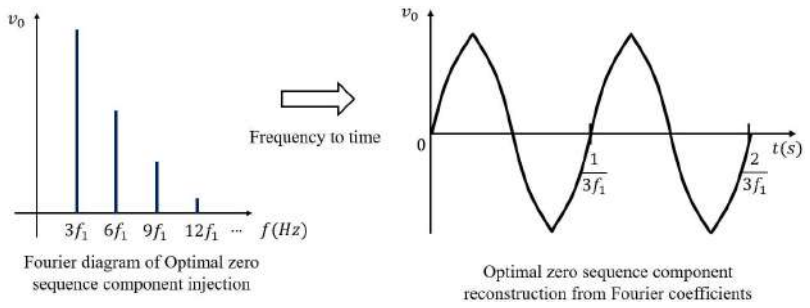

Figure 3.1 – Principle of ZSCM, a zero sequence component is generated from the computed optimal Fourier specter (here is represented as an example the SVM equivalent one).

3.2 A THIPWM generalization: The Zero Sequence Component Modulation

3.2.1 ZSCM description

The ZSCM consists to find the optimal harmonics to inject in the modulating signal [24]. The principle is not new regarding THIPWM strategies [37], but its generalization was not tested before.

The THIPWM principle is to inject inside the normalized reference signal a part of the third harmonic. This third harmonic have the advantage to be removed when provided to a three phased balanced load.

Nevertheless, this removing property is not only a specificity of the third harmonic. it is also true for every harmonic multiple of three, i.e. harmonics 3, 6, 9... Then injecting one or more of these harmonics inside the modulating signal would not impact the signal output.

The general idea of the ZSCM is then to generate a Zero Sequence Component (ZSC) signal, from the knowledge of n_h harmonics multiple of three. This principle, is deduced directly from the Fourier description of periodic signals. This principle is described more precisely thanks to Fig. 3.1.

On this figure, on the left is the Fourier specter of v_0, and thanks to the eq. (3.1), the temporal signal can be found. This signal would be injected inside the normalized reference one in order to generate the modulating signal. This procedure is shown on Fig 3.2.

In an analog representation than for THIPWM Fig. 1.6, Fig. 3.3, show a replacement

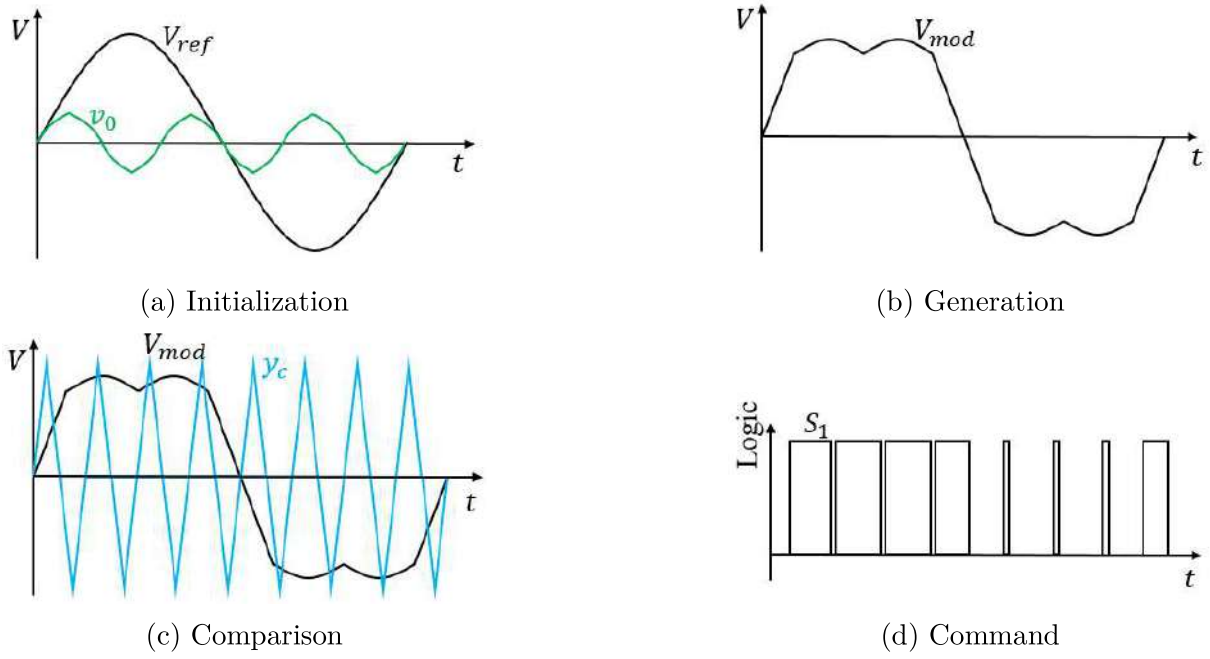

(a) Initialization

(b) Generation

(c) Comparison

(d) Command

Figure 3.2 – First, Fig. 3.2a represent the ZSC and the reference. On Fig. 3.2b it is the modulating signal (sum of the two last ones). Next Fig. 3.2c is the comparison between the modulated signal and the carrier signal. Finally Fig. 3.2d represent the generated switches.

of "Zero sequence component calculator", with a table, where are stored the real Fourier coefficients.

$$\begin{cases} v_0(t) = c_{0,v_0} + \sum_{n=1}^{n_h} 2ic_{n,v_0} e^{3in\omega t} \\ v_0(t) \in \left[-\frac{1}{2}; \frac{1}{2}\right] \end{cases} \tag{3.1}$$

It is also possible to write the eq. (3.1), thanks to real coefficients with eq. (3.2)

$$\begin{cases} v_0(t) = a_{0,v_0} + \sum_{n=1}^{n_h} a_{n,v_0} \cos(3n\omega t) + b_{n,v_0} \sin(3n\omega t) \\ v_0(t) \in \left[-\frac{1}{2}; \frac{1}{2}\right] \end{cases} \tag{3.2}$$

Once the ZSCM principle is exposed, it is necessary to find the correct complex coefficients of the ZSC [3], or equivalently, the real ones [4]. Next section is concerned about the concrete method helping to find these coefficients to inject in the reference signal.

3. c_{n,v_0}, in eq. (3.1)
4. a_{n,v_0}, b_{n,v_0}, in eq. (3.2)

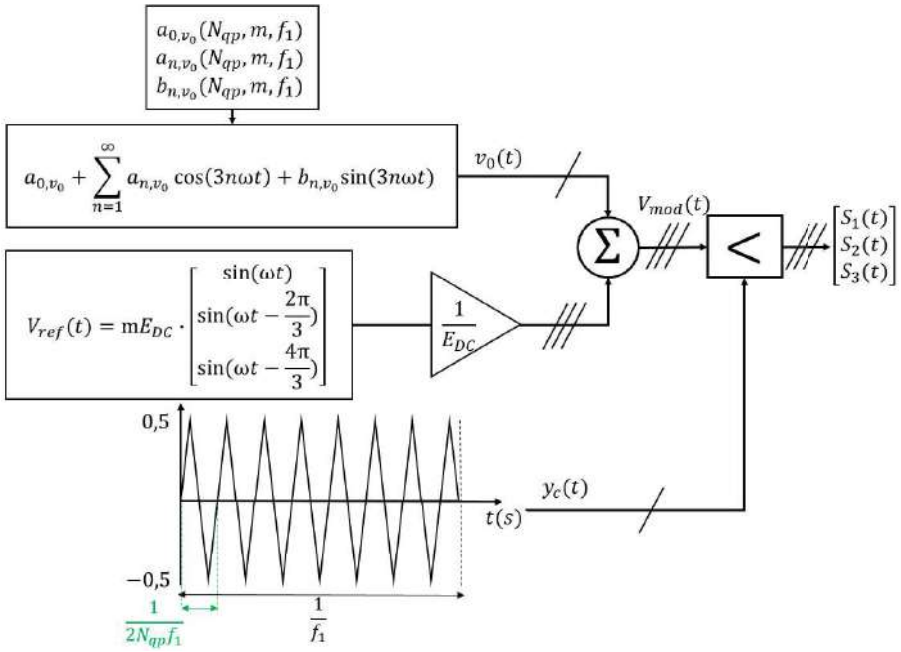

Figure 3.3 – Generation of ZSCM command

3.2.2 ZSCM optimization

It is well known that it is impossible to compute a complete Fourier decomposition, then, it is necessary to set the maximal harmonic we would consider to generate the ZSC, this number is called n_h. As an example it can be fixed arbitrary to $n_h = 20$, corresponding to 60 harmonics over the electrical frequency thanks to the third harmonic property of the ZSCM.

As this strategy, is based on a Fourier decomposition paradigm, this strategy can reproduce any periodic signal, under the hypothesis that n_h is large enough.

Consequently, this technique can reproduce SVPWM, THIPWM, Discontinuous PWM (DPWM), or any ZSC signal. Nevertheless this harmonic regeneration does not work properly with some strategies, due to discontinuities generating a strong Gibbs effect. This Gibbs effect generates unexpected extra switching discrediting some strategies to decomposed them as a ZSCM strategy, as the number of switching per period is fixed and equal to $4N_{qp}$ [5]. Furthermore, the principle of some DPWM is to forbid to switch a commutation cell for a defined amount of time. Doing so, it is impossible to set a fixed number of switching per period and then classic DPWM cannot be implemented under

5. The number of switching is different of the pulse number, indeed, for $4N_{qp}$ switches, the number of pulses is equal to $2N_{qp}$

the fixed number of switches.

As mentioned in the previous section, Fig. 3.1 shows the principle scheme of ZSCM. The idea is now to compute Fourier coefficients (c_{n,v_0}) with an optimization algorithm in order to generate the ideal ZSC according to a specified objective. This optimization problem is computed for a specific modulation index (m), frequency (f_1) and number of switches per period ($4N_{qp}$) with respect of the Fourier description of v_0 [6] found in eq. (3.1). In the next, the vector of Fourier coefficient is called $\mathbf{c}_{v_0} = [c_{0,v_0}, c_{1,v_0}, \cdots, c_{n_h,v_0}]^t$

$$\begin{aligned} y_c(\theta) &= (-1)^s \left(\frac{2N_{qp}}{\pi}\theta - s - \frac{1}{2} \right) \\ s &= \left\lfloor \frac{2N_{qp}}{\pi}\theta \right\rfloor \end{aligned} \tag{3.3}$$

With $\lfloor \cdot \rfloor$ the floor function which keep only the integer part of the number.

The intersection with a synchronous carrier signal (defined eq. (3.3)) with the ZSC (eq.(3.1)) added to the desired voltage normalized by E_{DC} leads to generate switching angles Fig. 3.2. The number of switching angles by period is equal to $4N_{qp}$. The switches found are then enumerated for the first leg as $0 < \alpha_1 < \alpha_2 \cdots < \alpha_{4N_{qp}} < 2\pi$. The first leg only have to be considered as all the legs are symmetric.

With these angles determination, eq. (3.4) and eq. (3.5) [66] allow to compute switching sequence ($\mathbf{S}(t)$), and then phase voltage of the inverter is accessible thanks to eq. (A.1).

Remark: Eq. (3.4) and eq. (3.5) are computed thanks the switching angles of only one phase, as the CBPWM generates symmetric switching angles.

$$c_{0,c} = \frac{1}{2\pi} \left(2\pi - \sum_{j=1}^{4N_{qp}} (-1)^j \alpha_j \right) \tag{3.4}$$

$$c_{n,c} = \frac{i}{2n\pi} \left(\sum_{j=1}^{4N_{qp}} (-1)^j e^{in\alpha_j} \right) \tag{3.5}$$

3.2.2.1 ZSCM algorithm

The algorithm used to solve the ZSCM problem, is very similar than for the PSR one, Nevertheless, it exist some particularities which have to be explained in the following.

6. Fourier coefficients are normalized over the DC voltage

First, as for the PSR optimization procedure, the **fmincon** function of the optimization toolbox of MatLab is used to perform the computation. As fmincon propose only local minimum solutions, a first good minimum search would be to select among a lot of solutions the best one. To do so, the same randomly evaluation start than PSR eq. (2.6) is used to evaluate the v_0 Fourier coefficients proposed. Nevertheless, the difference resides of the form of initial decision variable $\mathbf{x}_0 = [a_{0,v0}, a_{1,v0}, \cdots, a_{n_h,v0}, b_{1,v0}, \cdots, b_{n_h,v0}]$.

In addition, the choose of a specific objective function f is necessary. For this strategies, three objective functions are considered. The WTHD eq. (F.13), the losses inside the inverter only eq. (3.6) and the losses inside a RLE model with a sinusoidal EMF eq. (3.7) [7].

$$\mathcal{P}_K = \mathcal{P}_{cond} + \mathcal{P}_{sw} \tag{3.6}$$

$$\mathcal{P}_{tot} = \mathcal{P}_K + 3\sum_{n\geq 2} V_n I_n \tag{3.7}$$

$\mathcal{P}_{sw}$ is computed thanks to eq. (I.6) ,$\mathcal{P}_{cond}$ is computed thanks to eq. (I.12), and the currents used in eq. (3.7) are directly deduced from eq. (J.5).

It is interesting to underline that the second part of eq. (3.7), is similar to WTHD. We decided to consider it because the power in the harmonics do not produce work and have to be reduced. Furthermore, even if theoretically, this power go back to the battery, a very discontinuous current have to be avoided.

K_1 and K_2 are set to $K_1 = K_2 = 10^6$ in the same way than for the PSR strategy.

In the case of the ZSCM optimization, there are only three constraints leading to the constraint vector $\boldsymbol{c} = (c_1, c_2, c_3)$. These constraints are the same then the ones defined for the problem eq. (3.8) . In eq. (2.6), g is also defined thanks to eq. (2.7).

After selection of the best first v_0 (starting point) according to eq. (2.6). Fmincon find a local minimum around the starting point with respect to the problem defined by (3.8). This problem try to minimise objective function (eq. (F.13), eq. (3.6) or eq. (3.7)), which means decreasing WTHD and increasing efficiency. Those objectives are constrained by three constraints, to force the solutions to respect the desired voltage.

7. These three objective functions are always evaluated separately in the optimization

$$\begin{cases} ObF & \min(f(\mathbf{x})) \\ U.C. & a_{0,V_1} = 0 \\ & a_{1,V_1} = 0 \\ & b_{1,V_1} = mE_{DC} \end{cases} \tag{3.8}$$

In the same way than for PSR the algorithm presented on Fig. 2.2, is also used, in order to preserve local minimums found for previous modulation indexes.

In addition, and to ensure that harmonic injection increase the solution quality, the solutions obtained (v_0) from Fourier decomposition of SVM, DPWMMin, DPWMMax, THIPWM1/6, Opposite Median Injection PWM (OMIPWM) and THIPWM1/4 are also considered as starting points for (3.8) to be computed with Fig. 2.2. Nevertheless, even all these strategies are realisables, the algorithm will not retain them if, after the optimization procedure, more or less than $4N_{qp}$ switches are observed.

Thanks to this optimization method, some results were found and their description is the objective of the next section.

3.2.3 ZSCM results

As mentioned before, the procedure was computed for three specific objective functions, and for some number of pulses inside a period. More precisely the computation were performed from $N_{qp} = 2$ to $N_{qp} = 5$. Which correspond to very low switching frequencies. [8]

In the next, results found for $N_{qp} = 5$ and $N_{qp} = 3$ are presented. The first one, as its results are typical of what we found for other N_{qp}, and the second one ($N_{qp} = 3$) because its results are singular.

3.2.3.1 Five switches per quarter period

Improvements of the strategy First, Fig. 3.4, represent a WTHD comparison between SVPWM, THIPWM$\frac{1}{6}$ and optimal harmonic injection. The idea here is to represent the relative margin eq. (3.9) between ZSCM and two classical PWM methods.

$$\varepsilon_r = 100\frac{y_c - y_o}{y_c} \tag{3.9}$$

8. Switching frequency belongs to $f_s = 4f_1$Hz to $f_s = 10f_1$Hz

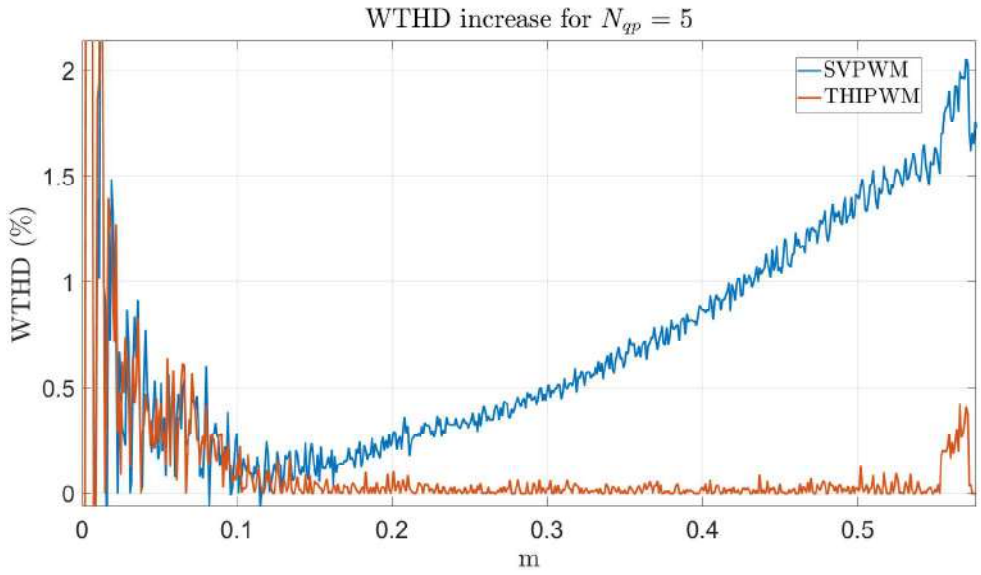

Figure 3.4 – Relative margin, (ε_r eq.(3.9)) for optimal harmonic injection compared with SVPWM and THIPWM $\frac{1}{6}$ applied to WTHD (eq.(F.12)) for $N_{qp} = 5$

In eq. (3.9) y_c represent the objective function cost of one of the classical symmetries (SVPWM or THIPWM$\frac{1}{6}$ in this chapter) and y_o the proposed objective function value of harmonic injection one. [9]

In addition to the WTHD, Fig. 3.5 provides the improvements for the switching losses only (i.e. eq. (3.6)) and Fig. 3.6 does the same comparison for the RLE load total losses (i.e. eq. (3.7)).

As we can see, for the proposed ZSCM the WTHD is improved in front of SVPWM for any modulation index and reach almost 2% for high modulation index (Fig. 3.4). On another hand, our optimal computation affords a small gain in comparison to THIPWM$\frac{1}{6}$ (according to WTHD objective function), the improvement never overcome 0.5% of improvement. Furthermore, for THIPWM$\frac{1}{6}$ the WTHD improvement is only for low and high modulation index. This observation is a confirmation of the literature, where THIPWM$\frac{1}{6}$ is considered as the best manner to reduce current harmonics. It is also important to notice very strong variations for very low modulation indexes, this instability can be explained to the switches precision that have a huge importance for these voltages.

About the losses in the converter, for switching losses only, the improvement is visible for a the SVPWM strategy and for the THIPWM$\frac{1}{6}$ one (Fig. 3.5). On the other hand, the total losses (Fig. 3.6) are not improved on high modulation indexes considering

9. The "c" indice in y_c stand for "classic" and "o" in y_o stand for "optimal"

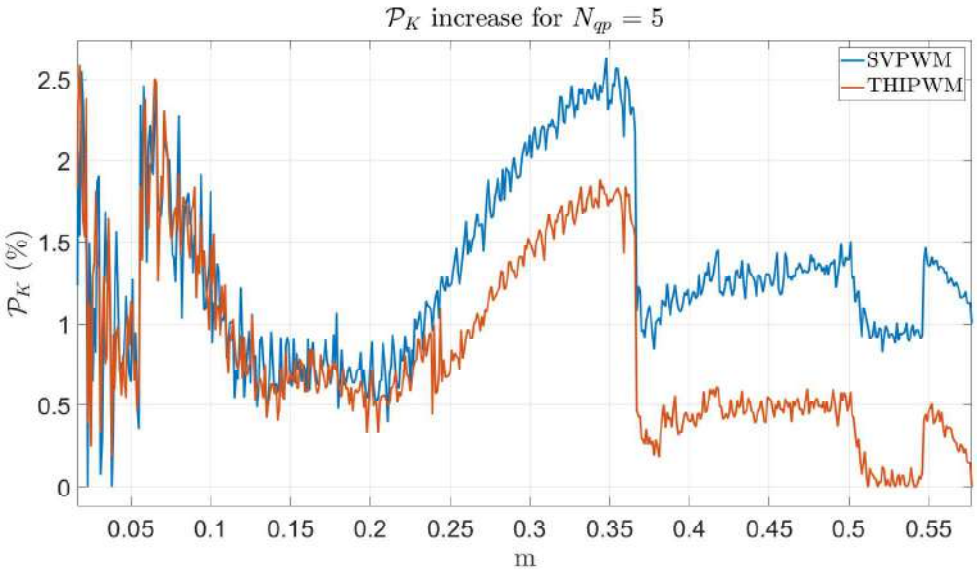

Figure 3.5 – Relative margin, (ε_r eq.(3.9)) for optimal harmonic injection compared with SVPWM and THIPWM $\frac{1}{6}$ applied to switches losses only ($\mathcal{P}_K$ eq.(3.6)) for $N_{qp} = 5$

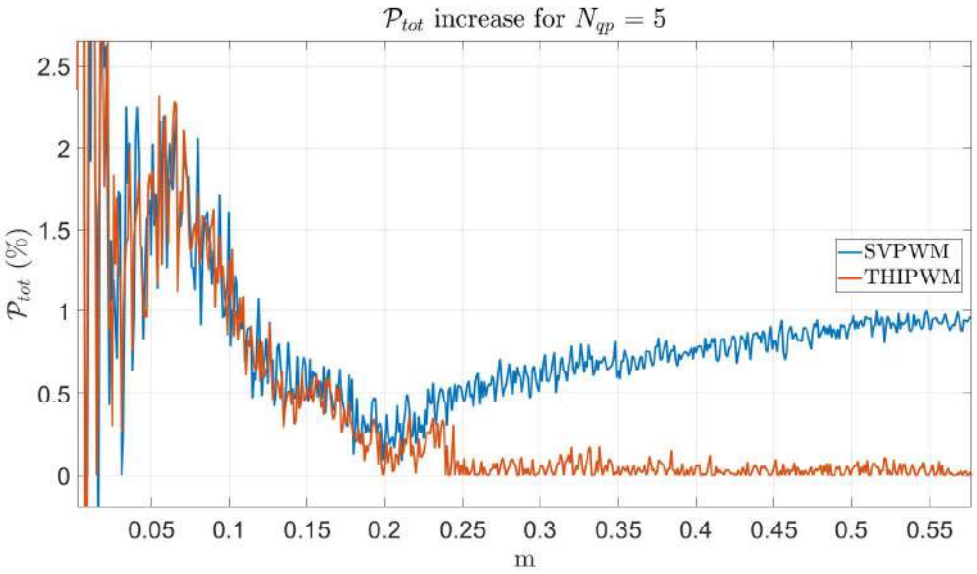

Figure 3.6 – Relative margin, (ε_r eq.(3.9)) for optimal harmonic injection compared with SVPWM and THIPWM $\frac{1}{6}$ applied to total losses ($\mathcal{P}_{tot}$ eq.(3.7)) for $N_{qp} = 5$

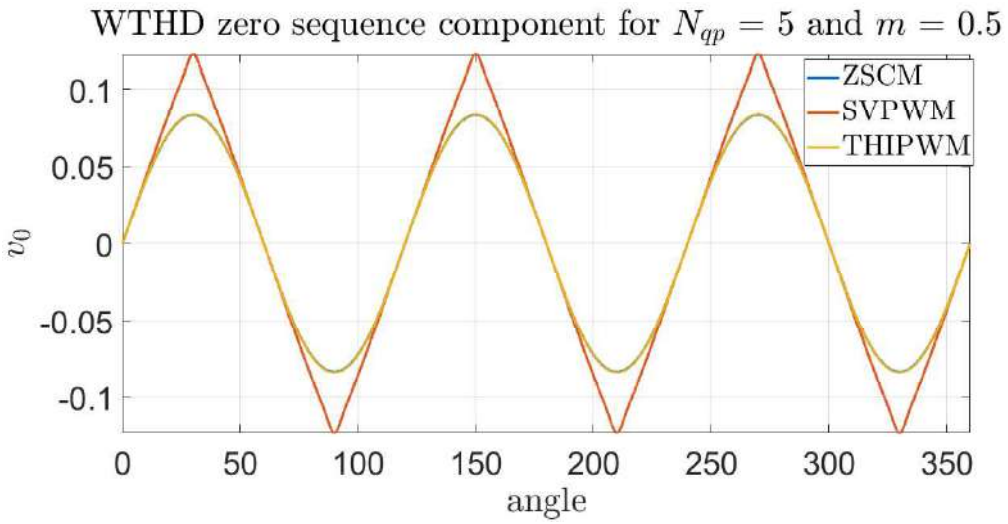

Figure 3.7 – Normalized and centered v_0 comparison between harmonic injection and SVPWM for WTHD (eq.(F.12)) considering $N_{qp} = 5$ and $m = 0.5$

the THIPWM in the same way the WTHD did. On another hand, for low modulation indexes the improvement can be seen and correspond to the kind of amplitude we saw on the inverter switching losses Fig. 3.5. This way, we can understand total losses as a mix between WTHD and switching losses. Indeed the results form is near the one found for WTHD in high modulation, and for low modulation indexes it looks like the switching losses one.

Let's notice on Figs. 3.4, 3.5 and 3.6, SVPWM and THIPWM$\frac{1}{6}$ solutions has a negative relative margins. This implies that classical solutions are better than optimal zero sequence component. Nevertheless, for these modulation index, SVPWM and THIPWM$\frac{1}{6}$ do not respect the specified constraints. So, both classical strategies are unfeasible according to constraints definition (see eq. (3.8)) and especially inside tolerance.

Zero sequence component shape Another interesting study besides the improvement is to observe the zero sequence component shape of the ZSCM results.

In Fig. 3.7 and Fig. 3.8 is represented respectively the zero sequence component for WTHD objective function and losses. For the WTHD (Fig. 3.7 corresponding to Fig. 3.4), as expected the optimal harmonic signal is near THIPWM$\frac{1}{6}$ wave form for the particular case of $m = 0.5$, which is not surprising according to the corresponding improvement of harmonic injection seen on Fig. 3.4.

About total losses and switching losses (Figs. 3.5, 3.6 and 3.8), the optimal curve for

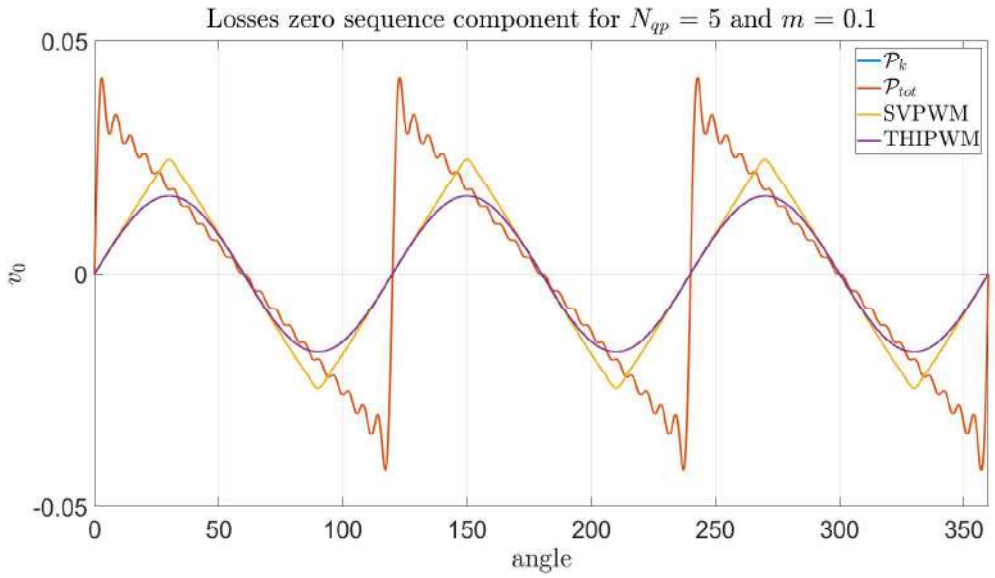

Figure 3.8 – Normalized and centered v_0 comparison between harmonic injection and SVPWM according to $\mathcal{P}_k$ and $\mathcal{P}_{tot}$ losses for $N_{qp} = 5$ and $m = 0.1$

low modulation index ($m = 0.1$) is quite surprising because it does not looks like any classical carrier based strategy. The curve looks like a saw-tooth function, and a small Gibbs effect appears near the discontinuities.

Furthermore the optimal injection for total losses and for switching losses only, seems to be the same.

As mentioned previously, the results are singular among the others when $N_{qp} = 3$, next subsection is concerned on the study of this specific operating point.

3.2.3.2 Three switches per quarter period

The previous result are presented for $N_{qp} = 5$, this choice has been done as its results are typical for all the other N_{qp} value computed. Nevertheless, the more N_{qp} will increase and the less the percentages performances will be great. However, there is a singularity among the results found for the specific case of $N_{qp} = 3$. Indeed, for this particular case, the improvement is way more visible and seems to largely improve the classic strategies.

On this specific case the improvement reach high values such as 25% of improvement for some high modulation indexes (see Fig. 3.9). Furthermore, for the losses the improvement can reach 6% in the case of $\mathcal{P}_{tot}$ (see Fig. 3.11) considerations and almost 4.5% for the $\mathcal{P}_K$ objective function (see Fig. 3.10). These results have a relative margin way more

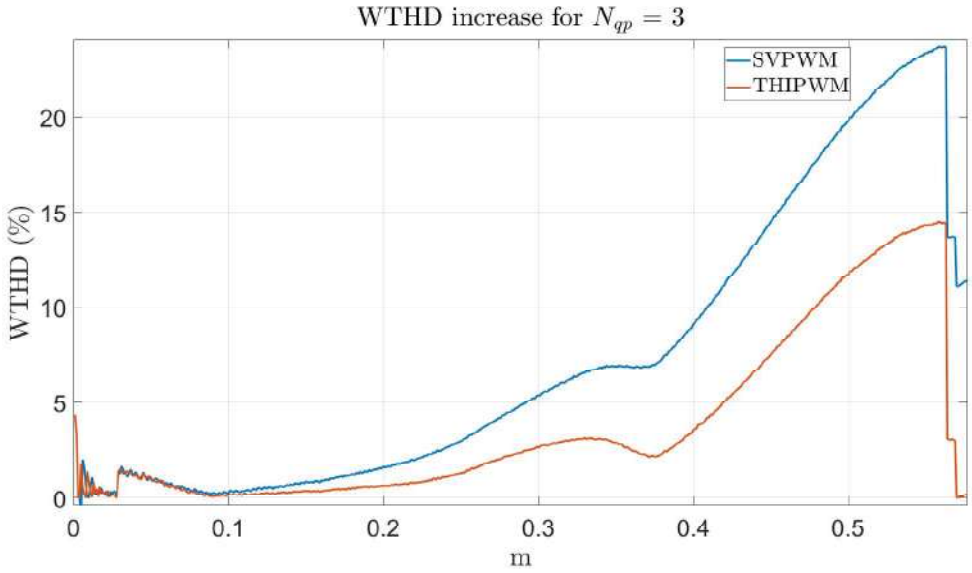

Figure 3.9 – Relative margin, (ε_r eq.(3.9)) for optimal harmonic injection compared with SVPWM and THIPWM $\frac{1}{6}$ applied to WTHD (eq.(F.13)) for $N_{qp} = 3$

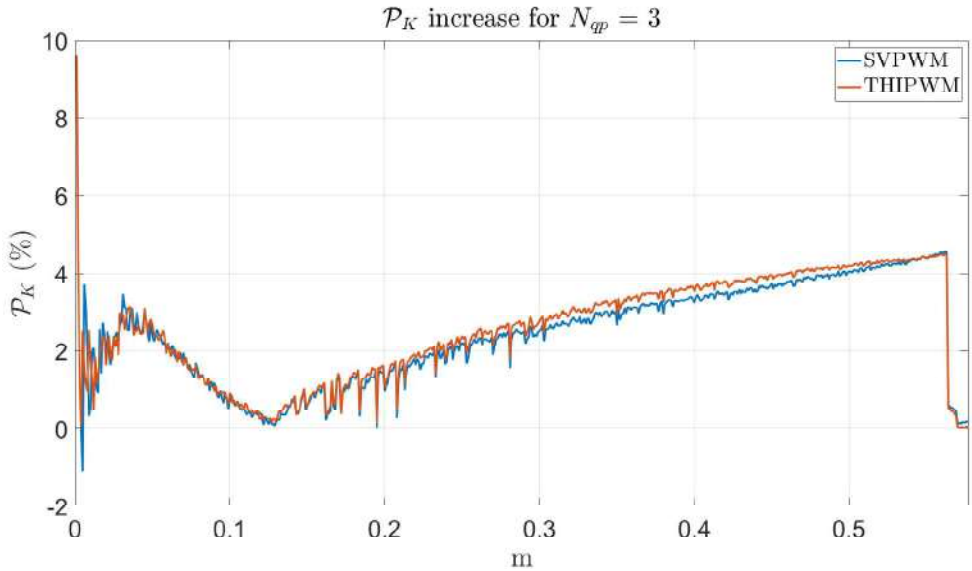

Figure 3.10 – Relative margin, (ε_r eq.(3.9)) for optimal harmonic injection compared with SVPWM and THIPWM $\frac{1}{6}$ applied to switches losses only ($\mathcal{P}_K$ eq.(3.6)) for $N_{qp} = 3$

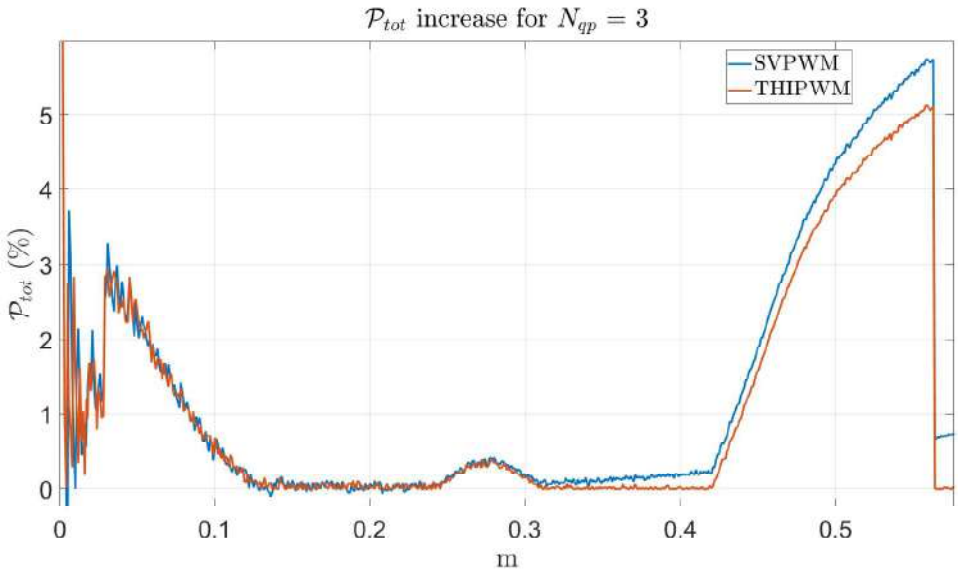

Figure 3.11 – Relative margin, (ε_r eq.(3.9)) for optimal harmonic injection compared with SVPWM and THIPWM $\frac{1}{6}$ applied to total losses ($\mathcal{P}_{tot}$ eq.(3.7)) for $N_{qp} = 3$

impressive than for $N_{qp} = 5$. Furthermore, the saw-tooth shape in the zero sequence component is also found here and visible on Figs. 3.12 for the WTHD objective function and Fig. 3.13, for the losses objectives.

All those result, are interesting since they improve classical strategies. Next, a study of the saw-tooth shape is necessary as it seems to be found for a large amount of operating points.

Conclusion on ZSCM results In order to do a synthesis of the ZSCM strategy, two tables have been done Table 3.1, is a table on the WTHD improvement and Table 3.2 on the losses one. For the computation of the previous results we decided to select only the modulation index greater than 0.03, as below the results are not relevant with the global curve obtained and would bias the following table.

N_{qp}	WTHD mean	WTHD max
2	-8.31%	7.85%
3	3.91%	14.49%
4	0.06%	0.14%
5	0.07%	0.42%

Table 3.1 – WTHD improvement againt THIPWM$\frac{1}{6}$ for different N_{qp}, maximum and mean value

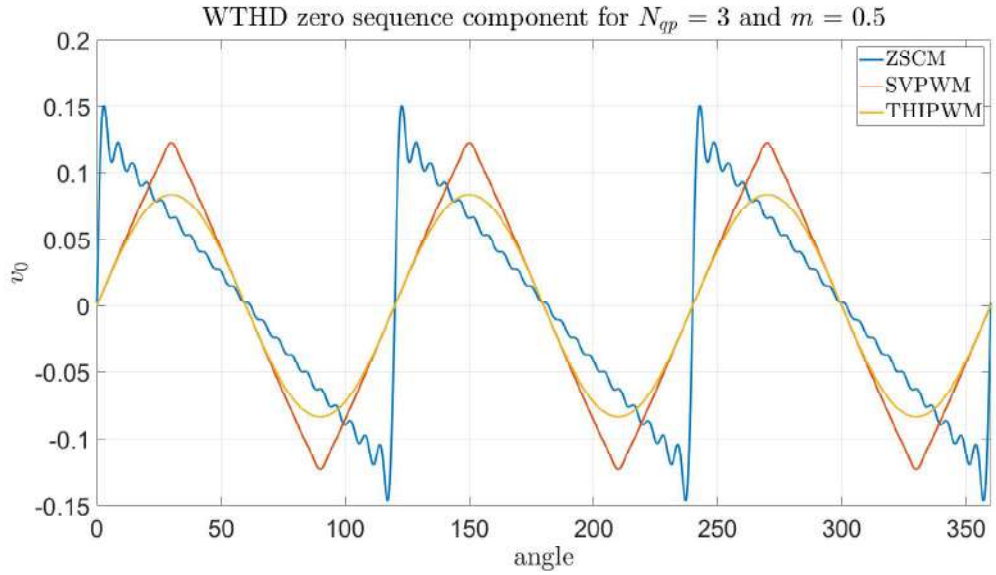

Figure 3.12 – Normalised and centred v_0 comparison between harmonic injection and SVPWM for WTHD considering $N_{qp} = 3$ and $m = 0.5$

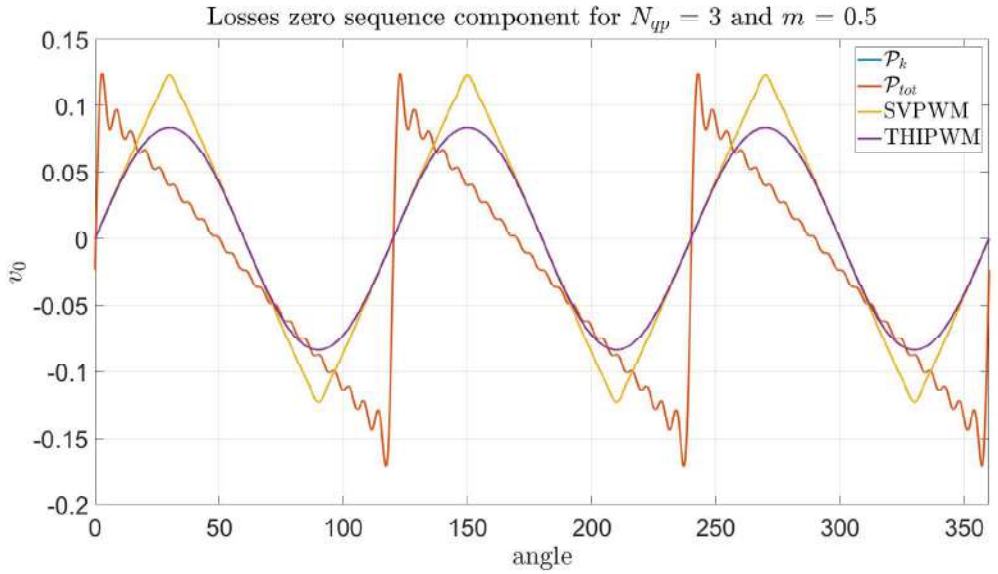

Figure 3.13 – Normalised and centred v_0 comparison between harmonic injection and SVPWM according to $\mathcal{P}_k$ and $\mathcal{P}_{tot}$ losses for $N_{qp} = 3$ and $m = 0.5$

N_{qp}	$\mathcal{P}_K$ mean	$\mathcal{P}_K$ max	$\mathcal{P}_{tot}$ mean	$\mathcal{P}_{tot}$ max
2	7.66%	31.02%	6.10%	26.14%
3	2.60%	4.49%	1.11%	5.12%
4	0.82%	2.53%	0.31%	1.32%
5	0.82%	2.50%	0.32%	2.37%

Table 3.2 – Losses improvement againt THIPWM$\frac{1}{6}$ for different N_{qp}, maximum and mean value

Thanks to these tables we can globally observe that a minimization of the number of switches will provide better relative results in comparison to classical one. An exception is done for the WTHD when $N_{qp} = 2$. Indeed, for this specific case, the SVPWM and the THIPWM$\frac{1}{6}$ are not feasible, and there is no feasible solutions succeeding to improve the WTHD. Nevertheless, the advantage of our strategy is to provide a strategy which is feasible even if the WTHD seems less good than for SVPWM and THIPWM strategy.

Furthermore, sometimes, the mean WTHD improvement is below 1% of improvement, nevertheless, the maximum improvement show, it exist, very interesting operating points to use the proposed ZSCM strategy.

After those results, and due to the carrier based property of the proposed strategy, a fast enough computation will ensure a relevant implementation. Nevertheless, the main problem of this strategy seems to be the synchronism, because one of our main assumption is to set invariant the number of commutations per period and per phase.

In this previous section, the idea beyond the so called ZSCM method is really simple, because it is just a particular case of harmonic injection. Because of the method carrier based property, this strategy will be easier to implement in comparison to the OPPs presented in the previous chapter. Off-lines solutions affording better solutions but are way more complicated to implement on a real engine.

Furthermore, electromagnetic compatibility (EMC) [108], or noise and harshness [22], [109], [110] problems are ignored but should be considered in future works as they will limit or not the easy implementation.

Previously it was shown that for some specific operating points and especially on losses, a saw-tooth like shape for the zero sequence component was found. The following section, will investigate on this specific observation.

3.2.4 ZSCM convergence to a saw-tooth waveform

In previous section, no certitude was afforded to confirm that the saw-tooth like waveform is really a saw-tooth and not some sort of approximation [24]. Then, to verify this conjecture, a least squared method was set up eq. (3.10).

$$\begin{aligned} \min \quad & || \mathbf{c}_{saw} - \mathbf{c}_{v_0} ||_2^2 \\ \text{where} & \\ \mathbf{c}_{saw} &= [c_{0,saw}, c_{1,saw}, c_{2,saw}, \cdots, c_{n_h,saw}]^t \\ c_{0,saw} &= \frac{h_{max} + h_{min}}{2} \\ c_{3k,saw} &= \frac{i}{2k\pi} (h_{min} - h_{max}), \ \forall k \in \left[\!\left[1, \left\lfloor \frac{n_h}{3} \right\rfloor \right]\!\right] \end{aligned} \tag{3.10}$$

Thanks to the least square problem eq. (3.10), it was possible to obtain the corresponding exact saw-tooth waveform. On Fig. 3.14 it is impossible to distinguish the ZSCM and the saw-tooth approximated with the first harmonics. Doing a Zoom on specific angles allow to distinguish the two signals on Fig. 3.15. As a complement, by computing the mean value for $N_{qp} = 3$ for modulation indexes below 0.5. The obtained mean value is approximately equal to $7.8 \cdot 10^{-7}$, as this value is below the least square algorithm precision (10^{-6}), it is possible to conjecture that the ZSCM effectively converged to a saw-tooth waveform.

Now, as the correlation between saw-tooth and ZSCM is highlighted. It is interesting to confirm the saw-tooth performances against classic strategies to justify the presented researches and investigations.

3.3 STIPWM interest for power electronics

As for the ZSCM and for PSR an optimization problem was set on eq. (3.11) with the objective to find the optimal saw-tooth waveform.

$$\begin{cases} ObF & \min(\xi([h_{min}; h_{max}])) \\ U.C. & mE_{DC} - \varepsilon_V \leq |c_{n,V}| \leq mE_{DC} + \varepsilon_V \end{cases} \tag{3.11}$$

In eq. (3.11) ξ is the objective function defined for the STIPWM problem, for example

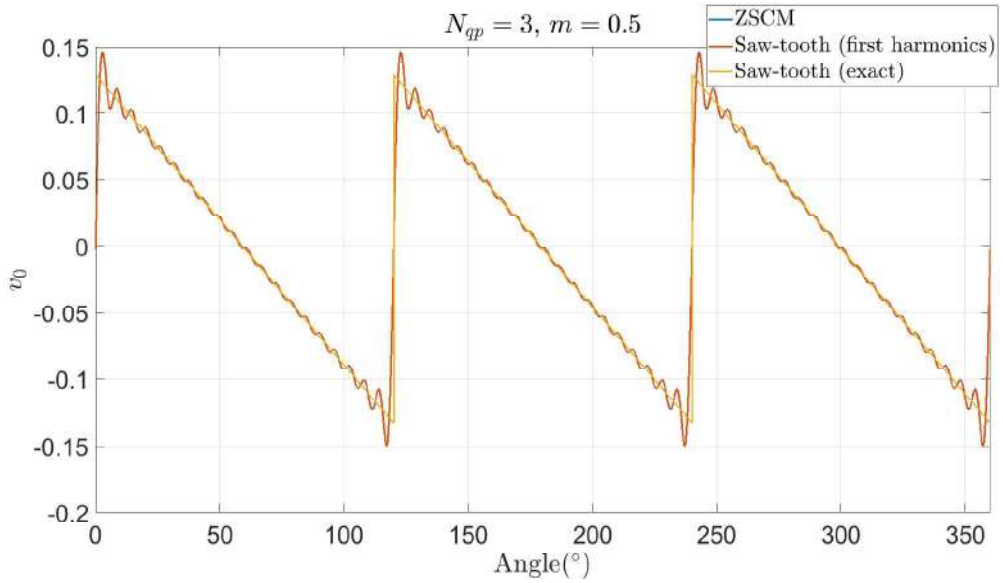

Figure 3.14 – Here are represented the ZSCM initial computation (blue) for $N_{qp} = 3$ and $m = 0.5$, the equivalent saw-tooth wave form with $n_h = 20$ harmonics considered (red) and the exact saw-tooth waveform (yellow). As shown, the ZSCM converged to a perfect saw-tooth as it is impossible to distinguish the ZSCM and the 20^{th} firsts harmonics saw-tooth.

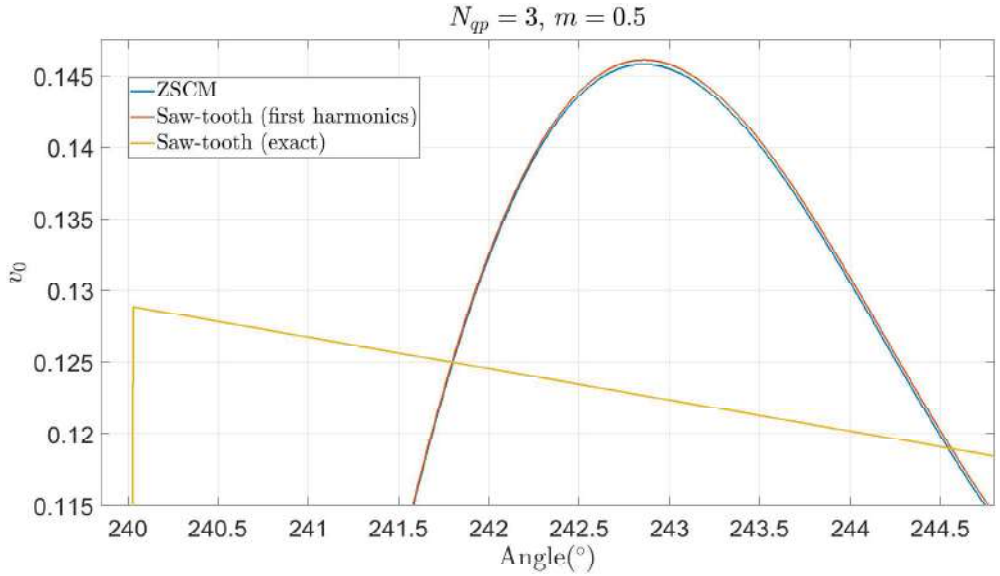

Figure 3.15 – Zoom on a saw-tooth edge to explicitly see the saw-tooth convergence of ZSCM.

for the WTHD ξ is defined thanks to eq. (3.12).

$$\xi([h_{min}; h_{max}]) := V_{\text{WTHD},\%} = \frac{100}{V_{1,1}} \sqrt{\sum_{n \geq 2} \left(\frac{V_{1,n}}{n} \right)^2} \tag{3.12}$$

In eq. (3.12) $V_{1,1}$ is the desired fundamental voltage of the first phase (expressed as mE_{DC}), and $V_{1,n}$ is the n$^{\text{th}}$ voltage harmonic amplitude of the first phase [23], [27], [67].

Remark: Eq. (F.13) is directly linked with h_{min} and h_{max}, as the voltage is deduced with eq. (A.1). Depending on the switching angle determination found by the comparison between the carrier signal and the modulating signal. Modulating signal depending on h_{min} and h_{max}. This same reasoning is possible to be done for every objective function, since the saw-tooth amplitude can be linked with the switching angles.

Thanks to the optimization problem eq. (3.11) optimised with the WTHD, $\mathcal{P}_K$ and $\mathcal{P}_{tot}$ with ε_V is the desired voltage precision. In this paper, ε_V is equal to 2% of the desired voltage.

The next following subsection are first concerned on WTHD and then on the losses analysis.

3.3.1 WTHD reduction

Thanks to the optimization problem (3.11), optimal h_{max} and h_{min} values were found for different N_{qp} values. For the WTHD optimization, only the $N_{qp} = 3$ affords significant results, and, then, we will be focused on this specific N_{qp} in the following.

The values describing the saw-tooth zero sequence component allow to draw WTHD values showed on Figure 3.16.

Figs 3.16 and 3.17 are the most interesting curve in terms of improvement, indeed on these curve ZSCM and STIPWM clearly improve classical THIPWM$\frac{1}{6}$ and SVPWM. Furthermore these curves confirm the presumptions of the previous section. Indeed, the STIPWM is not feasible after a modulation index of approximately 0.52, and the shape of the WTHD after $m = 0.4$ is not the same than for Fig. 3.17 meaning, that some STIPWM extrapolation operating points are not feasible. Still on Fig. 3.16, the presence of an impossibility for the ZSCM to converge to the best saw-tooth because of its technical limitations is visible between 0.3 and 0.4 modulation index.

In order to do an overview on all the operating points, Table 3.3, sum up the results found when the objective function is the WTHD. Thanks to this table, only the N_{qp} value equal 3 improve the WTHD on all the modulation indexes. Nevertheless, for some

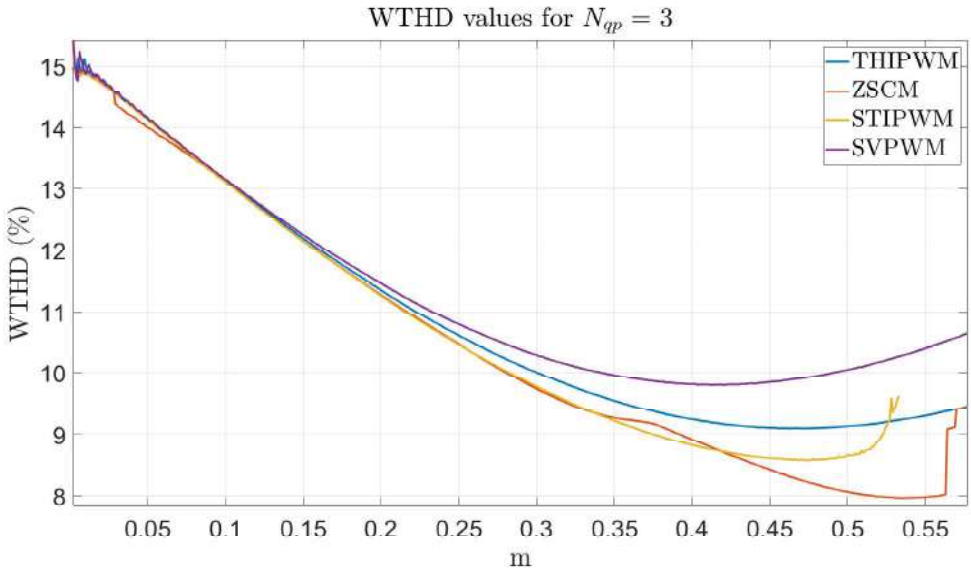

Figure 3.16 – Theoretical WTHD values for $N_{qp} = 3$

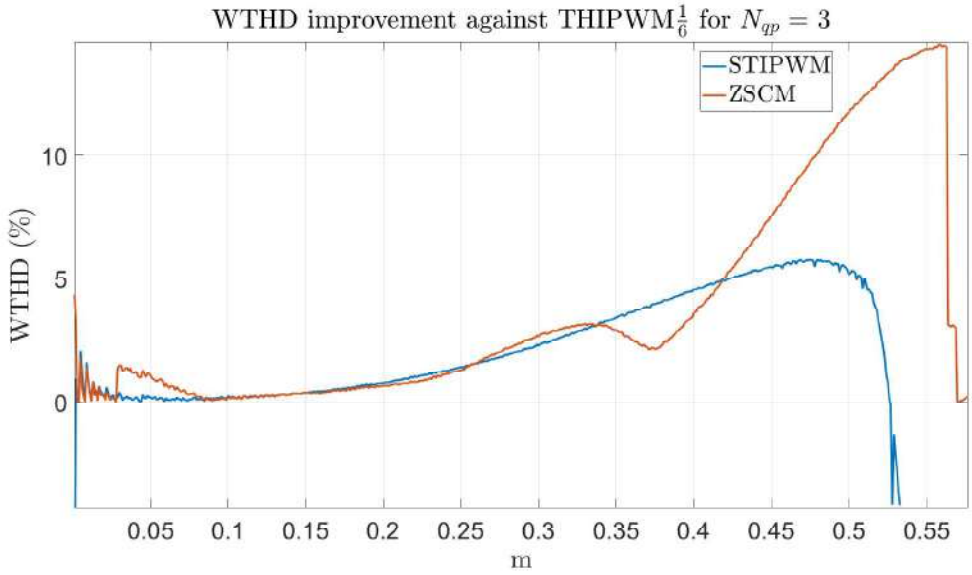

Figure 3.17 – Theoritical WTHD improvement against THIPWM for $N_{qp} = 3$

N_{qp}	STIPWM mean	STIPWM max
2	-10.42%	0.5%
3	2.29%	5.76%
4	-2.171%	0.83%
5	-3.27%	0.95%

Table 3.3 – Theoretical improvement mean and max value of WTHD against THIPWM for different N_{qp} values

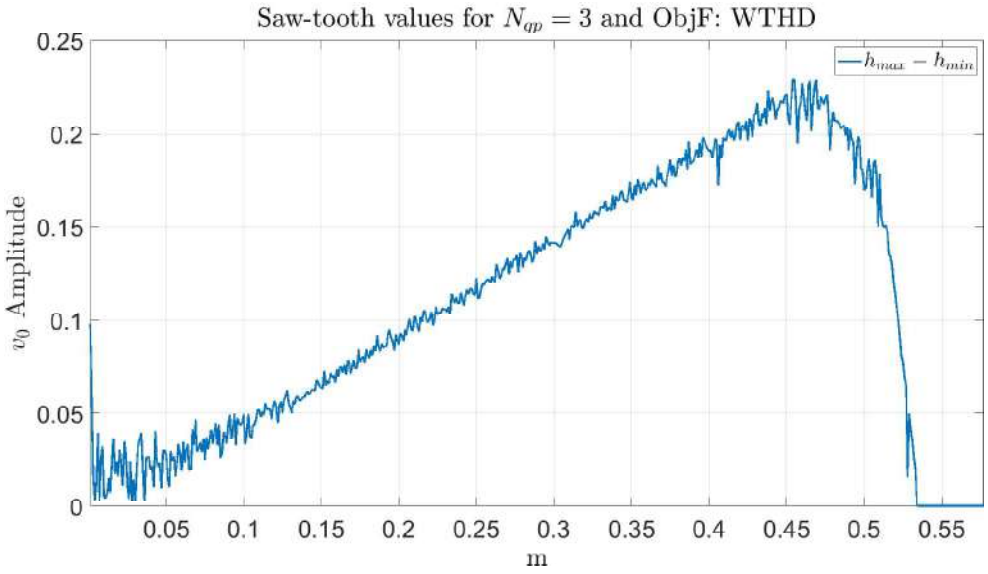

Figure 3.18 – Saw-tooth amplitude for $N_{qp} = 3$

operating points the STIPWM is the best strategy against the THIPWM even if, with the mean value, its global interest seems limited. Finally, for $N_{qp} = 2$, it is important to keep in mind that SVPWM and THIPWM are not feasible inside the considered bounds and then, even if the results seems poor, at least the STIPWM succeed to reach the reference.

As we showed it, the WTHD can be improved either with a ZSCM consideration or a STIPWM one for some operating points. Nevertheless, this section does not mention the possibilities of improvement of the STIPWM on losses, then, in the same way than for ZSCM, a theoretical study on losses is presented in the following subsection.

3.3.2 Losses reduction

About the losses reduction, improvement values are way different than for WTHD one, indeed, for the P_K losses, the improvement is visible for all the modulation index except when m is greater than 0.5 for $N_{qp} = 3$, Fig. 3.19. About the total losses, even if the STIPWM suceed to improve the SVPWM, for every N_{qp} computed except $N_{qp} = 2$, the losses are poorer for the STIPWM.

Thanks to Fig. 3.19, we can conclude the losses in the inverter are improved thanks to a saw-tooth shape, even if, this objective does not suceed to reduce efficiently the power lost inside the harmonics as we can see with Fig. 3.20.

In addition Table 3.4 sum up the results found for all the N_{qp} computed. This table

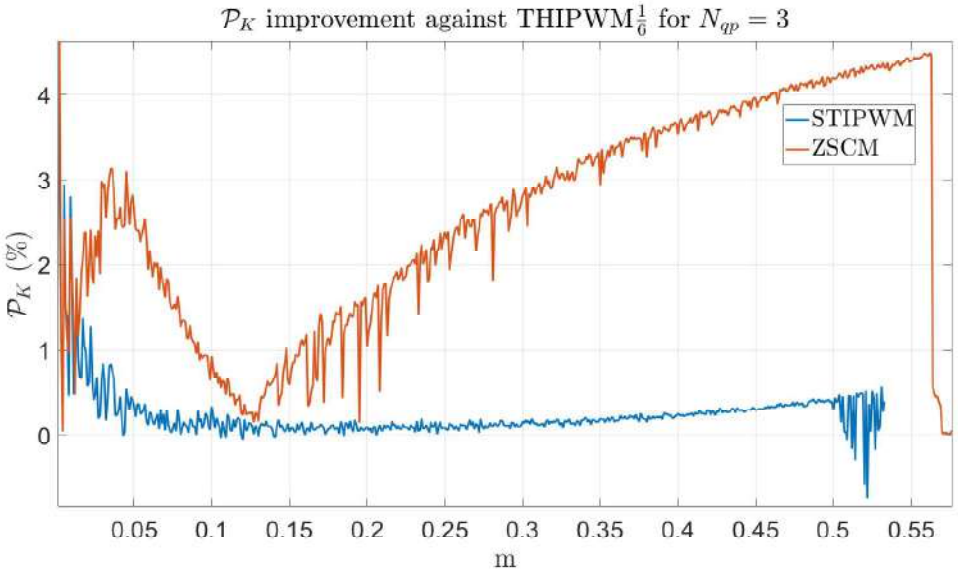

Figure 3.19 – Theoritical $\mathcal{P}_K$ improvement against THIPWM for $N_{qp} = 3$

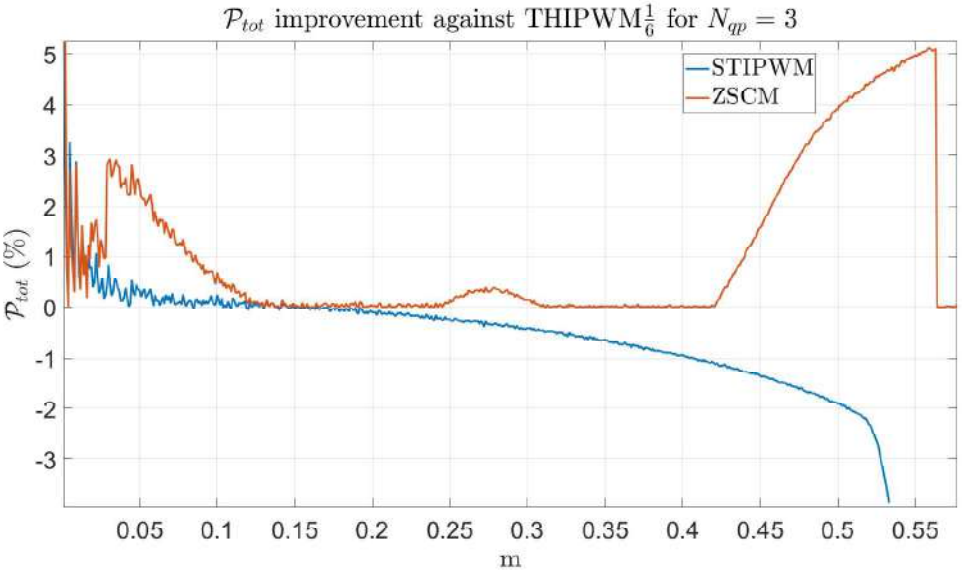

Figure 3.20 – Theoritical $\mathcal{P}_{tot}$ improvement against THIPWM for $N_{qp} = 3$

N_{qp}	$\mathcal{P}_K$ mean	$\mathcal{P}_K$ max	$\mathcal{P}_{tot}$ mean	$\mathcal{P}_{tot}$ max
2	10.05%	31.12%	8.32%	26.19%
3	0.18%	0.84%	-0.59%	0.84%
4	0.34%	1.56%	-0.32%	1.50%
5	0.47%	2.06%	-0.13%	1.95%

Table 3.4 – Theoretical improvement mean and max value of Losses against THIPWM for different N_{qp} values

show a large improvement for $N_{qp} = 2$ for $\mathcal{P}_K$ and $\mathcal{P}_{tot}$ this improvement is even more interesting as the SVPWM and THIPWM are not feasible for these operating points.

Nevertheless, it is important to be cautious with the theoretical losses found as they depend on the inductance the resistance and the power switches taken in account for the simulations and the experiments. The benefits to use a relative margin is that it makes a difference against two strategies, reducing the biais without removing it completely.

This way, even if WTHD is less precise than a specific loss, it have the advantage to always provide the same results independently to the load.

Then, as for some operating the WTHD but also the inverter losses can be improved, it is then interesting to understand deeply the STIPWM strategy. To do so, a presentation of some experiments on WTHD are provided to confirm the well funded of STIPWM found in simulation.

3.4 Results and discussion

3.4.1 Experimental Results

In order to confirm experimentally the well funded of the saw-tooth strategy, the same experimental setting than for PSR (Fig. 2.9 and Table 2.7)has been set up to evaluate the WTHD. Indeed, due to the platform limitations, a concrete study on losses was not possible to be done under the same assumptions than the simulation ones.

3.4.2 Discussion

Figs. 3.21 and 3.22 show the results found on the experimental platform. The first one are the WTHD found for 4 different strategies including the ZSCM, in order to do a comparison. The second figure Fig. 3.22 shows the improvement of ZSCM and STIPWM against the THIPWM$\frac{1}{6}$. For the three last points of the experimental STIPWM, the curve is exactly the same than for THIPWM, indeed, as the STIPWM cannot reach modulation index greater than 0.52, the decision was done to replace the saw-tooth injection by the THIPWM one when the point is not reachable.

As we can see on the improvement Fig. 3.22, the STIPWM improve the ZSCM for modulation indexes below than 0.52. Nevertheless, after this point the ZSCM becomes the best strategy. It is also important to notice a quality fall visible on both Figs. 3.17 and 3.22 around $m = 0.45$, probably due that the saw-tooth have less amplitude possibilities

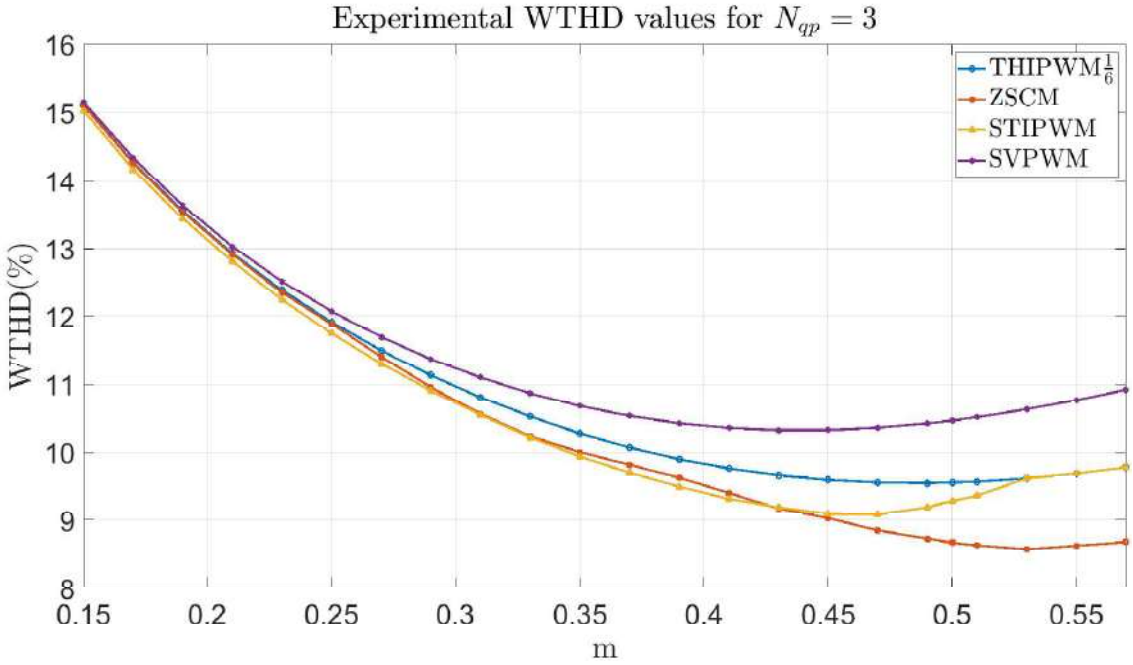

Figure 3.21 – Experimental results of WTHD for different strategies when $N_{qp} = 3$

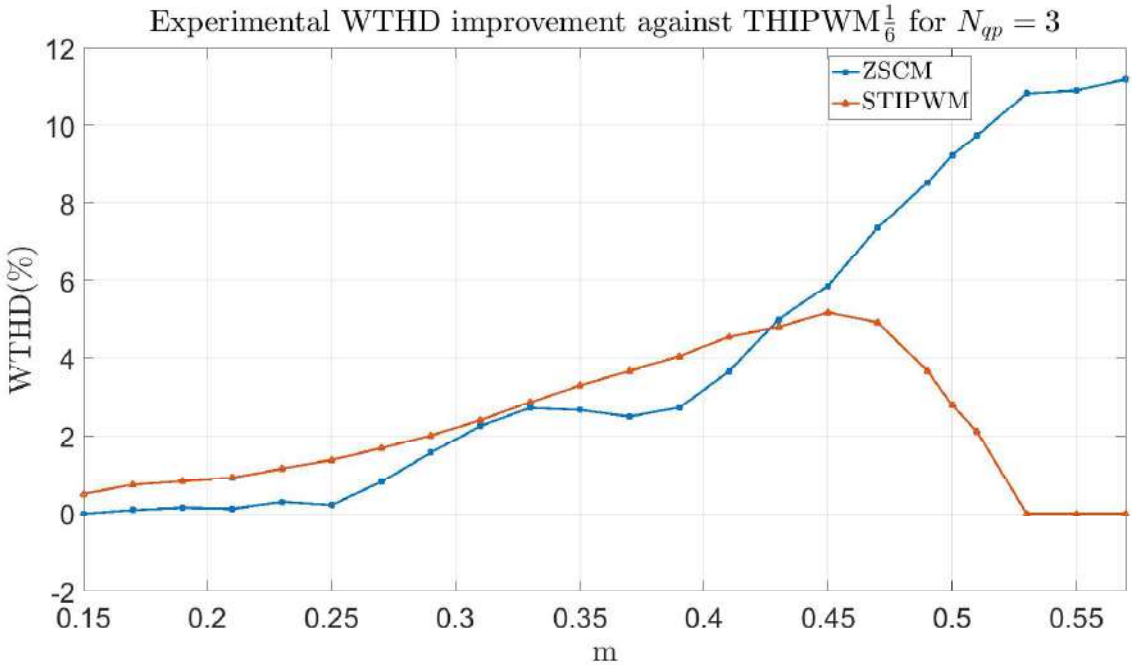

Figure 3.22 – Experimental relative gap for different strategies against THIPWM$\frac{1}{6}$ when $N_{qp} = 3$

due to the saturation and then cannot succeed to meet both reference criteria and WTHD minimization.

The main advantage of STIPWM is its fast implementation, even if, for now, this strategy is better only for some specific operating points.

Indeed, the carrier based property with the simple shape of the STIPWM will ensure a fast implementation. Nevertheless, the main problem remains that no generalization of the STIPWM exist yet and an optimization have to be done to use the STIPWM properly.

This generalization, does not seems impossible as the saw-tooth amplitude is regular for all the N_{qp}. For example, for $N_{qp} = 3$ the shape looks like a ramp Fig. 3.18.

Then finding a method to compute simply the saw-tooth would lead to many advantages, the first one, would be an easy implementation without any solution storage. The second one, is to deeply understand the properties of STIPWM which allow such improvement. Understanding these properties could lead to new strategies even more interesting than the actual saw-tooth injection. Due to all these motivations, an understanding attempt based on mathematics is presented in the following section.

To simplify the problem, next section will not be concerned on efficiency as it depends on the considered load. Then, only WTHD reduction will be studied, for $N_{qp} = 3$.

3.5 Mathematical description and presentation of the incomplete demonstration

First of all, some additional details and demonstrations can be found at the web address in the foot note [10]. This document will help the reader with the understanding of the equations. These equation development are not in appendix of the thesis as this document due to the number of equations is up to 40 pages.

3.5.1 Problem description and hypothesis

In this section, in order to simplify the WTHD reduction problem, it is considered that $h_{max} = -h_{min} = h$. This hypothesis was done because the mean value of saw-tooth waveform is equal to zero leading to consider a single parameter h. This hypothesis simplify eq. (3.13).

10. https://box.ec-nantes.fr/index.php/s/kG9mJfgZjYjTmNm

$$\begin{aligned} v_{0,STIPWM}(\theta) &= (h_{max} - h_{min})\left(\gamma - \frac{3}{2\pi}\theta\right) - \gamma h_{min} \\ &\forall \gamma \in \mathbb{Z}, \forall \theta \in \frac{2\pi}{3}\,]\gamma; \gamma + 1] \end{aligned} \tag{3.13}$$

On the other side, ZSC of THIPWM is described thanks eq. (3.14), and its computation is developed in [27] page 249.

$$v_{0,THIPWM}(\theta) = \frac{m}{6}\sin(3\theta) \tag{3.14}$$

Then, in the following, $v_0(\theta) = v_{0,STIPWM}(\theta)$

Conjecture 1

$$\begin{aligned} &\exists h \in \mathbb{R}^* \backslash, \\ &\sum_{n\geq 2}\left(\frac{V_{1,n,STIPWM}}{n}\right)^2 \leq \sum_{n\geq 2}\left(\frac{V_{1,n,THIPWM}}{n}\right)^2, \\ &\forall m \in \left]0; \frac{1}{2}\right], \\ &N_{qp} = 3, V_{1,1,STIPWM} = V_{1,1,THIPWM} = V_1. \end{aligned}$$

With natural language, conjecture 1 says that it exist a saw-tooth with an amplitude h which can reduce the WTHD of the THIPWM when $N_{qp} = 3$ with the respect of the desired amplitude. Indeed reducing the WTHD must not be done at the expense of the reference following.

It is also possible to formulate a "low" conjecture by replacing THIPWM by SPWM. Where SPWM ($h = 0$) is the natural PWM [27].

3.5.2 An incomplete demonstration

As the conjecture 1 is strongly linked with Fourier decomposition, the idea is to study them. To do it, a good start seems to develop the Fourier coefficients in the same idea than

in Holmes's book [27] page 99, thanks to double Fourier description. To do the proposed comparison, here is only presented the Fourier coefficient computation of STIPWM as the THIPWM coefficients are accessible in Holmes book[27] page 249.

Thanks to the double Fourier description method and in the same way than Holmes, a description of the command $S_1(\theta)$ eqs. (3.15) and (3.16) can be done. In this thesis, a short reminder on double Fourier equations is presented in appendix H.

$$\begin{aligned} S_1(\theta) &= \frac{A_{0,0}}{2} + \sum_{n=1}^{\infty} \left[A_{0,n}\cos(n\theta) + B_{0,n}\sin(n\theta)\right] \\ &+ \sum_{k=1}^{\infty} \left[A_{k,0}\cos(2kN_{qp}\theta) + B_{k,0}\sin(2kN_{qp}\theta)\right] \\ &+ \sum_{k=1}^{\infty}\sum_{\substack{n=-\infty \\ n\neq 0}}^{\infty} \left[A_{k,n}\cos((2kN_{qp}+n)\theta)\right. \\ &+ \left. B_{k,n}\sin((2kN_{qp}+n)\theta)\right] \end{aligned} \tag{3.15}$$

Fourier coefficients of eq. (3.15), are deduced thanks to eq.(3.16)

$$\begin{aligned} C_{k,n} &= -\frac{i^{k+1}}{2k\pi^2}\int_{-\pi}^{\pi}\left(e^{ik\pi(m\sin(\theta)+v_0(\theta))}\right) \\ &\cdot \left(e^{in\theta} + (-1)^{k+1}e^{-in\theta}\right)d\theta, \forall n \in \mathbb{Z}, \forall k \in \mathbb{N}^* \end{aligned} \tag{3.16}$$

Previous Fourier coefficient description could be described thanks to integer Bessel's function when v_0 is equal to 0 (SPWM) [27].

Nevertheless, by considering eq. (3.13) with $h_{max} = -h_{min} = h$, it behaves exactly as if n^{th} coefficient is modified by a factor $\beta = 3kh$ (eq.(3.20)). Then h influence can be understood as an artificial move to the harmonics with a upper frequency (harmonic n are moved to $3kh \pm n$). This fact is interesting because harmonics are reduced the more they are high frequency in a WTHD purpose. Then an intuitive understanding about the WTHD reduction for some h parameters can be done even if no mathematical proof of this intuition can be afforded yet.

In the next, $f_\nu(w,z)$ is introduced to simplify the writing eq. (3.17).

$$f_\nu(w,z) = e^{i(w\sin(z)-\nu z)} \tag{3.17}$$

Remark: If ν an integer in eq. (3.17), its integration on a period is a Bessel's function.

$$C_{0,0} = 1 \tag{3.18}$$

$$\begin{aligned} C_{0,1} &= i\,m \\ C_{0,n} &= i\frac{2h}{n\pi}\left(1 + 2\cos\left(\frac{2n\pi}{3}\right)\right) \ \forall n \geq 2 \end{aligned} \tag{3.19}$$

The previous equation, eq. (3.19) gives the Fourier decomposition of the saw-tooth function.

$$\begin{aligned} C_{k,n} &= -\frac{i^{k+1}}{2k\pi^2}\cdot \\ &\quad \left\{\overline{e^{3ikh\pi}}\int_{\frac{2\pi}{3}}^{\pi}\overline{f_{3kh-n}(km\pi,\theta)}d\theta\right. \\ &+ \overline{e^{ikh\pi}}\int_{0}^{\frac{2\pi}{3}}\overline{f_{3kh-n}(km\pi,\theta)}d\theta \\ &+ e^{ikh\pi}\int_{0}^{\frac{2\pi}{3}} f_{3kh-n}(km\pi,\theta)d\theta \\ &+ e^{3ikh\pi}\int_{\frac{2\pi}{3}}^{\pi} f_{3kh-n}(km\pi,\theta)d\theta \\ &- (-1)^k\overline{e^{3ikh\pi}}\int_{\frac{2\pi}{3}}^{\pi}\overline{f_{n+3kh}(km\pi,\theta)}d\theta \\ &- (-1)^k\overline{e^{ikh\pi}}\int_{0}^{\frac{2\pi}{3}}\overline{f_{n+3kh}(km\pi,\theta)}d\theta \\ &- (-1)^k e^{ikh\pi}\int_{0}^{\frac{2\pi}{3}} f_{n+3kh}(km\pi,\theta)d\theta \\ &- \left.(-1)^k e^{3ikh\pi}\int_{\frac{2\pi}{3}}^{\pi} f_{n+3kh}(km\pi,\theta)d\theta\right\} \\ &\quad \forall k \in \mathbb{N}^*, \forall n \in \mathbb{Z}, \forall h \in \mathbb{R}, \forall m \in \left]0;\frac{1}{2}\right] \end{aligned} \tag{3.20}$$

To find interesting values for eq. (3.20), an evaluation of the antiderivate of $f_{\beta\pm n} = f_\nu$ can be considered.

$$\frac{\partial f_\nu(w,z)}{\partial z} = i\left(w\cos(z) - \nu\right) f_\nu(w,z) \tag{3.21}$$

This eq.(3.21) implies:

$$\begin{aligned} F_\nu(w,z) &:= \int f_\nu(w,z)dz = \frac{i}{\nu} f_\nu(w,z) \\ + \quad & \frac{w}{2\nu}\int \left(f_{\nu+1}(w,z) + f_{\nu-1}(w,z)\right) dz + C(w,\nu) \end{aligned} \tag{3.22}$$

Eq. (3.22) leads to the following sequence:

$$\begin{aligned} F_{\nu+1}(w,z) &= \frac{2\nu}{w} F_\nu(w,z) - F_{\nu-1}(w,z) \\ &- \frac{2i}{w} f_\nu(w,z) + C(w,\nu) \ \forall \nu, w \in \mathbb{R}^{*^2} \end{aligned} \tag{3.23}$$

let's set:
$\mathbf{X}_{\nu+1}(w,z) = \begin{pmatrix} F_{\nu+1}(w,z) \\ F_\nu(w,z) \end{pmatrix}$

$$\begin{aligned} \mathbf{X}_{\nu+1}(w,z) &= \begin{pmatrix} \frac{2\nu}{w} & -1 \\ 1 & 0 \end{pmatrix} \mathbf{X}_\nu(w,z) \\ &- \begin{pmatrix} \frac{2i}{w} f_\nu(w,z) - C(w,\nu) \\ 0 \end{pmatrix} \\ &= \mathbf{A}_\nu(w,z)\mathbf{X}_\nu(w,z) - \mathbf{B}_\nu(w,z) \end{aligned} \tag{3.24}$$

This sequence eq. (3.24) is interesting as it is possible to describe each harmonics thanks to the knowledge of the previous one. Doing so, it is possible, from a recursion demonstration, to demonstrate eq. (3.25) for every $n \geq 1$. This demonstration is accessible at the web address provided as a footnote at the beginning of section 3.5.

$$\begin{aligned}\mathbf{X}_{\nu+1}(w,z) &= \left(\prod_{k=0}^{n-1}\mathbf{A}_{\nu-k}(w,z)\right)\mathbf{X}_{\beta+1}(w,z)\\ &- \sum_{k=1}^{n-1}\left[\left(\prod_{j=0}^{k-1}\mathbf{A}_{\nu-j}(w,z)\right)\mathbf{B}_{\nu-k}(w,z)\right]\\ &- \mathbf{B}_{\nu}(w,z)\end{aligned} \tag{3.25}$$

Eq. (3.25), can be used inside eq. (3.20). Indeed, $\int_a^b f_\nu(w,z)dz = F_\nu(w,b) - F_\nu(w,a)$. Because the link between $\mathbf{X}_\nu$ and $\mathbf{X}_{\beta+1}$ was found, the voltage reference constraint allows to select some precise possible values for $\mathbf{X}_{\beta+1}$ and then each harmonic of the STIPWM should be computed as they all depend on $\mathbf{X}_{\beta+1}$ (eq. (3.25)). To archive the demonstration of the conjecture, the previous computation must be linked with the THIPWM computation. Indeed the proposed conjecture propose a comparison between THIPWM and STIPWM. Fourier description of THIPWM is classic in the literature and can be found in Holmes's book[27] and more precisely in page 249. The Holmes's description provides a Fourier decomposition thanks to Bessel functions, such a same description is not possible in the proposed paper. Indeed, as it is shown in eq.(3.20), it is not possible to do the same Bessel dependency as the ν part of eq.(3.17) is not an integer and then, cannot be described by a Bessel's functions. Doing so, it was decided to find a similar link thanks to eq. (3.22) and eq. (3.23), leading finally to eq. (3.25). Nevertheless, even with an analytical Fourier decomposition of STIPWM and THIPWM, the demonstration would not be over, as the conjecture is concerned on the WTHD and not on specific harmonics.

Based on the conjecture 1, it is possible to develop perspectives in addition with the WTHD reduction (Fig. 3.16), as for example:

— Reduction of electrical noises due to the specter spreading[22]
— Real time diagnostic or detection [111] of the connected device is possible thanks to the rich harmonic injection.
— Existence of a space vector modulation equivalent to the STIPWM in a motor control context.
— ...

The remaining open problem is to demonstrate the STIPWM conjecture 1.

3.5.3 A Mathematical intuition on STIPWM

Even if the previous demonstration is incomplete, some interesting path of understanding can be presented. Indeed, eq. (3.20), is particularly interesting, in fact, this description is almost a Bessel's function. Furthermore the modifications afforded to the integer Bessel's definition are the complex coefficient of each integral an the second one is the $3kh$ coefficient which appears in the $f_\nu(x, y)$ definition. This second term is particularly interesting as it seems to behave as an harmonic offset. Then, for the harmonic n, it move to the harmonic $n + 3kh$, then as the WTHD filter the high harmonics we can intuitively understand the addition of a saw-tooth will reduce the WTHD. Nevertheless, there is of course a side effect of this reduction otherwise the saw-tooth would be always the minimum and h would be maximum. In fact this side effect is probably due to the necessity to follow the reference, and then possible h value are limited. Furthermore, for now, we ignore the effects of the complex coefficient of each integral, which can also limit the improvements of the STIPWM on the WTHD.

All these reasoning have to be explored, thanks to the sequence eq. (3.25), or any other mathematics tool, to still improve low switching frequencies synchronous carrier based PWM. This particular intuition led us to another unsuccessful idea. Indeed, considering the harmonics shift, it is possible to try to find a $C_{k,n}$ function that would be written as eq. (3.26).

$$C_{k,n} = \mathcal{C}(h) \int_{-\pi}^{\pi} f_{n+\mathcal{K}(h)}(\mathcal{X}(h), \theta) d\theta \tag{3.26}$$

With $\mathcal{C}$, $\mathcal{K}$ and $\mathcal{X}$ functions to determine depending on the v_0 shape and amplitude.

Indeed, finding a v_0 function leading to eq. (3.26) would be very efficient on WTHD. Nevertheless, its results would not be miraculous as the reference have to be followed.

For us, actually, such v_0 equation satisfying eq. (3.26) remains unsuccessful.

3.6 Conclusion

In this chapter two new modulation strategy (ZSCM and STIPWM) are exposed. The first method have been obtained by doing a generalization of THIPWM by injecting a large amount of harmonics.

The second one was obtained thanks to the previous one, by an observation wich gave the intuition of a saw-tooth injectin.

The new solutions turns out to have interesting characteristics which opens the way to other proposals of this type that are interesting to the power electronics community.

For the STIPWM, we are convinced that a better mathematical understanding would allow to find new simple PWM strategies in the future. It is why an incomplete demonstration is presented here.

We would finish this chapter with highlighting some interesting future works we could imagine to be done.

In this research work, the STIPWM demonstration is under the assumption $h_{max} = -h_{min}$ and $N_{qp} = 3$ for a synchronous PWM but can be generalized to asynchronous PWM or other N_{qp}. It is also possible to imagine a phase shift inside the saw-tooth, which could lead to different solutions.

As the saw-tooth seems to be an intermediate form between continuous PWM and DPWM one, it could be also interesting to allow the saturation of the saw-tooth and then study how it behaves in a DPWM consideration.

General Conclusion

This thesis on the PWM command control optimization, led us to consider two kind of strategies. The OPP ones and the carrier based ones, these two classes belongs to a triptych with the closed loop strategies and a choice has been done to only be concerned on the two first ones. These researches was done under some assumptions as, the synchronicity and a low number of switching per period. These constraints have shown many advantages.

— The first one is to reduce the switching losses as it directly depends on the switching frequency.
— The second one is more practical than theoretical, indeed, for a high speed motor, the ratio between the switching frequency and the fundamental will be small.
— The third one is due to the synchronicity itself which removes harmonics below the fundamental.

On the other hand, a three phases two level inverter was considered for further advantages

— It is a well known and robust device.
— The cost of a three phases two level inverter is reduced in comparison to multilevel ones.
— The industrial production of multilevel converter is difficult and necessities a lot of changes
— The size of this inverter is reduced
— It necessities no hardware changes in the vehicle.

In the light of the previous assumptions advantages, it was first possible to study the OPP strategies.

Conclusion on optimal pulse patterns

The first researches was on the OPPs, indeed, theoretically, they will always afford the best results as the switching angles are selected precisely and then finding a better OPP is comparable to approach the global minimum of PWM strategies. Furthermore it

appears in the literature that the idea is always to relax the symmetry constraints inside each phases. Then, first the QWS was found, next the HWS, and the FWS. In the same line, the idea was to relax the angle symmetry between phases and to keep the feasibility of the output voltage.

This idea led to improve the WTHD for low switching and synchronous frequencies. Furthermore, even if the results was found for a three phases inverter, it is possible to generalize the problem to any number of phases. Then the main idea behind this strategy is to afford a methodology to generate optimal OPP with a phase symmetry relaxation.

The WTHD reduction can be understood as a better spreading of the harmonics. In fact, the harmonics multiples of two or three are often systematically removed. By relaxing the phases symmetry the harmonics can have a better distribution and then improve the WTHD. The last advantage is that it can reproduce any other OPP as the QW, HWS or the FWS and then will never decrease the results found.

On the opposite the main problem of OPPs are their implementation, which need a fast micro-controller or FPGA with large tables computed off-line to perform a correct output voltage or current.

Conclusion on carrier based PWM

On the opposite, the carrier based PWM, does not generate the most perfect output waveform but benefits of the simplicity. In fact, carrier based PWM, with the space vector based PWM are the gold standard of PWM. All those strategies have pros and cons, DPWM reduce losses, NSPWM the EMC, SVM and THIPWM increase the maximum modulation index, RPWM reduce noise and harshness ...

The first idea developed in this thesis was to do a generalization of THIPWM, by injecting not a single third harmonic but an infinity. In fact, an infinity of harmonics is not feasible, and we decided to be limited to the 20 firsts harmonics [11].

This method, called the zero sequence component modulation (ZSCM), succeed to improve the losses and the WTHD against classic strategies. Nevertheless, it was highlighted a difficult implementation as the zero sequence component have to be computed with a high precision. Furthermore some Gibbs effect appears for some operating points which means the algorithm modulate precisely the angle by adding extra harmonics. Nevertheless, for some operating points and N_{qp} the ZSCM solutions seems to converge to a

11. i.e. 60 harmonics for the fundamental electrical frequency

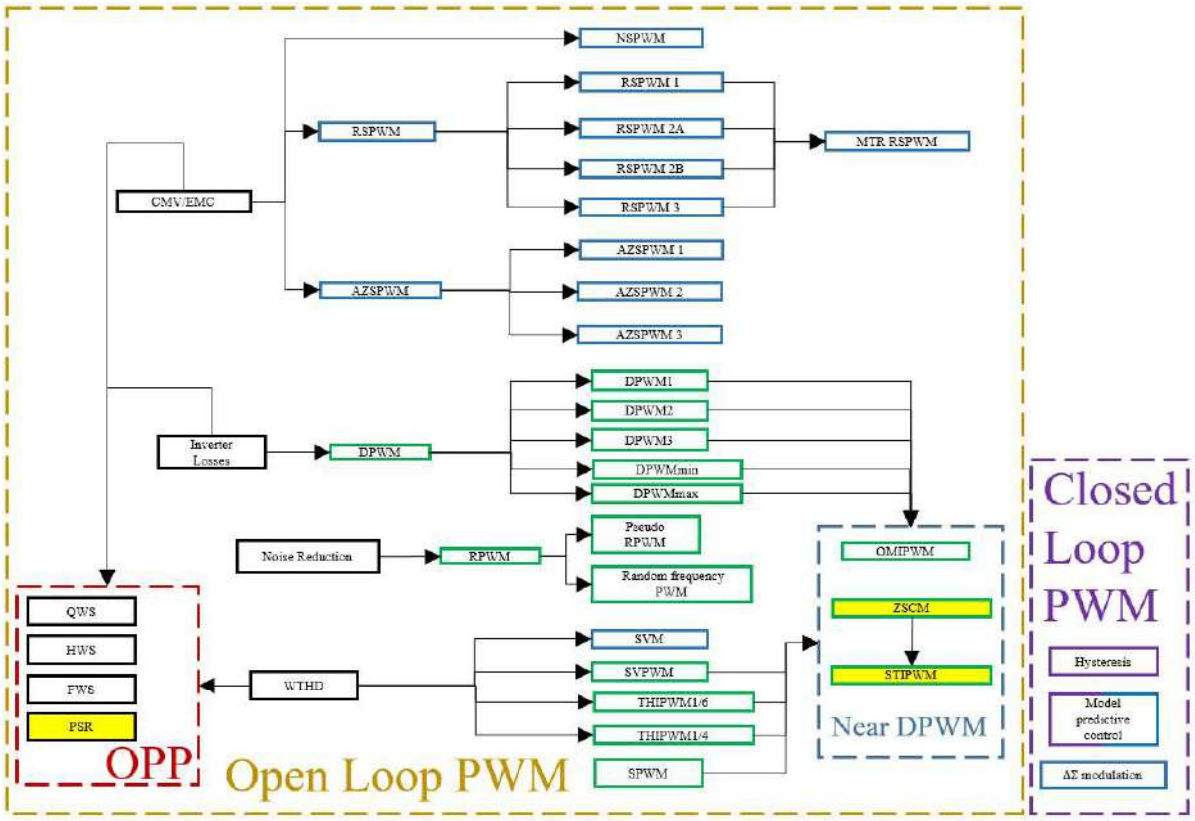

Figure 3.23 – Map of existing PWMs after the PhD thesis. blue: vector based strategies, green carrier based strategies, purple, closed loop strategies

saw-tooth.

The saw-tooth injection convergence was confirmed and was then optimized. It is the so called saw-tooth injection PWM. This strategy showed very interesting results especially for WTHD and $N_{qp} = 3$. This observation led us to consider a mathematical understanding, which is for now not conclusive even if some interesting preliminary results were found.

After the presentation of the strategies, we can draw again the map of existing PWM presented in the first chapter Fig. 1.27, but, in addition the strategies developed during this thesis work are also presented in yellow Fig. 3.23

However, despite all the presented results and strategies, many researches are still possibles to be done on carrier based PWM and OPP. Next section is concerned about the description of interesting ideas but also about ideas that does not succeed during the PhD works. Since a method that has not worked does not mean a method that will never work, we decided to mention them in the following perspective section of the conclusion.

Nevertheless, a separation is done between the attempted ideas and the brand new ones.

Perspectives

Not conclusive ideas

Among all the ideas that did not provide enough interesting results, we can mention:

From PSR to ZSC One of the first idea was to convert the PSR into a ZSC to inject in a carrier based strategy. The first thing that appeared is, if the modulating signal is exactly the switching pattern, then, the output will be the switching pattern. Then we supposed that it exist a ZSC v_0, which could lead to a similar switching pattern than an OPP (QWS, HWS, FWS or PSR). This idea was proposed as an OPP is not easy to implement on a real embedded system in comparison to carrier based ones.

This idea led to first extract the v_0 signal from well known strategies in order to study its feasibility, this step was blocking as due to the low switching frequencies considered, the information is completely melted with noise. This impossibility to extract the v_0 from a simple strategy, led us to ignore this strategy and to do the opposite, i.e. optimize the v_0 to inject in the normalized desired signal which led to the ZSCM strategy.

Fifty shades of ZSCM The idea to inject a generalization of a THIPWM, was not the first idea, an attempt was done to perform the ZSCM with polynomial equations, but also with not periodic functions, or with harmonics multiples of 1. All these strategies was unsuccessful as they provided results poorer than classical ones.

Once the idea to generalize the THIPWM was found, we decided to do a computation similar to Appendix B. In order to find what kind of amplitude should be considered to perform the best output signal, and perhaps increase the maximum modulation index. Indeed, the THIPWM proof, show that it is impossible to overcome $m_{max} = \frac{1}{\sqrt{3}}$, but no paper was found about an injection of an infinity of harmonics. This demonstration, leading to a positive or a negative result, was not successful.

STIPWM demonstration wanderings The incomplete demonstration presented in this thesis, was not the first idea we had, many attempt was done, the first one was to compute theoretically the switching angles for any v_0 and to determine the switching angles for the saw-tooth case.

Another attempt was done by trying to start from the $C_{k,n}$ shape and then to determine the corresponding v_0, but here again the attempt was not successful.

As a PhD cannot be exhaustive on all the strategies it remains many ideas to explore for future works. The following subsection is concerned about providing some of them.

Short an middle term perspectives

Here are some ideas completely unexplored in this thesis work but which would be interesting to investigate to go further in the specific topic of synchronous PWM optimisation.

— In the same idea than a RPWM, but with a regular pattern, how would behave the output if the carrier is optimized and no more the modulating signal? What happen if both are optimized? What would be the behavior if a classical strategy is used with an optimized carrier?

— Thanks to the PSR, it is possible to choice the amplitude of many harmonics, then is it possible to use this effect in order to observe the angular position of the motor? Meaning the PWM will generate itself the angular knowledge to control itself.

— The PSR improves the WTHD for a balanced load, does it still work for an unbalanced load? Is there is advantages? What would happen with non sinusoidal EMF? As the PSR can be unbalanced the benefits of this strategy can be supposed way better.

— The STIPWM is a carrier based strategy, nevertheless, is it possible to find a vector equivalence of the STIPWM? would it help the understanding of the STIPWM benefits? In the same way, is there is an equivalence between PSR and vector based methods?

— Is it possible to find an optimal STIPWM where there is no need of optimization or to store parameters?

— About the ZSCM, what would happen if the ZSC is different for each phase? What would happen is the carrier is optimized for each phase? Is it possible to find some regularities? Is it possible to generalize it?

— How would behave a ZSCM, a STIPWM or the PSR on a real electrical motor? Will we found unexpected behavior? What would be their effect on EMC?

— How would behave closed loop strategies (Delta-Sigma, Hysteresis, Model predictive control) with a low switching frequency? Is it possible to improve them for this specific case?

— What would happen if we allow the STIPWM to saturate, i.e. to behave as a DPWM?
— All the strategies presented relies on local minimum search algorithms, nevertheless it is almost sure we can increase the speed and reliability of these local minimum search.

Long term perspectives

Researches on a specific field, can have unexpected applications on other fields. In the following are presented, some applications we can develop without being exhaustive.

— In cryptography domain, it is possible to imagine a communication protocol through the electricity wires. In fact, as we are able to select the harmonics amplitude, and especially of harmonics which are usually removed, then, we can still provide power, but, in the same time provide information.
— In cyber-security, it is possible to imagine to inject deleterious harmonics to an enemy plant, almost invisible, in order to destroy slowly their infrastructure, or to damage their process.
— In the electrical grid management domain, the injection of some specific harmonics, could be used as a signature of an electricity provided by fossil power plant, or of a zero emission one. In fact, the energy transformation inside the grids through an inverter could be used to add a signal inside the power to discriminate if the energy comes from a polluting source or not. This idea could be used to provide a solution of the so called "green electrons" detection.
— In electrical engineering, we can use the harmonics generated to perform self diagnosis of rotary machines, gears or any device sensible to specific harmonics.
— Still in electrical engineering, All those strategies and methods can be modified to fit to other power conversion devices as multilevel converters, DC/DC, AC/DC or AC/AC ones.

Thus, in the light of this PhD work, the well known two-level inverter has not given all its secrets. Additionally, for all his advantages, the two-level inverter topology would remains the most used device thanks to its robustness and easy topology. As mentioned, the results found, could have unexpected applications in many surprising fields, and future applications of the present work could surprise us in a short or long term future.

Appendix A

The Inverter structure

A.1 The Voltage source Inverter

An inverter is a static converter able to transform the electrical energy from a continuous form (DC) to an alternative one (AC). More precisely, in this thesis, a three legs, two-level inverter is considered (see Fig. A.1). This topology, with a DC voltage as an input, transforms the continuous voltage to three phases voltages phased of $\frac{2\pi}{3}$rad two by two.

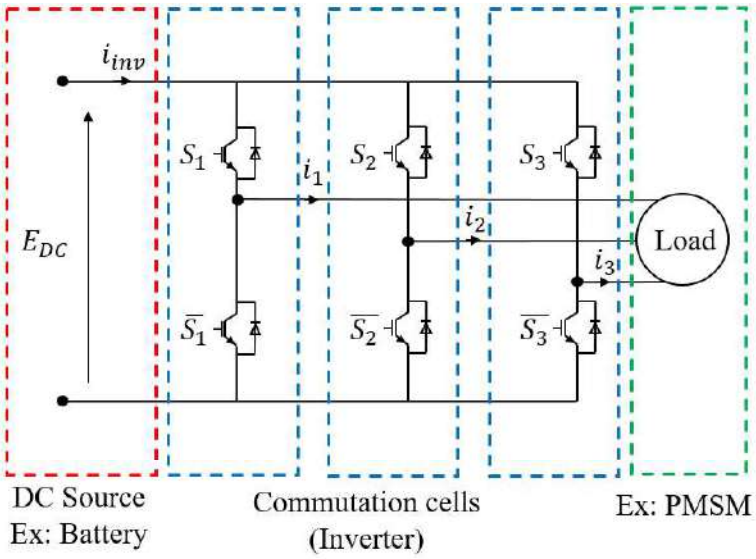

Figure A.1 – Scheme of a three phase two levels VSI

As all the static power converters are made of commutation cells, a short reminder is proposed to settle some definitions ans constraints .

A.2 Commutation cells

A commutation cell is a model of a power electronics circuit providing the controlled connection between a voltage source and a current load and vice versa [26]. This structure is the most basic one in power electronics.

To illustrate a commutation cell, Fig. A.2 represent a generic voltage (respectively current) source connected to a generic current (respectively voltage) load. In this Figure, K_1 represent the upper switch and V_{K_1} its voltage. On the opposite, K_2 represent the lower switch and V_{K_2} its voltage. V is a voltage source (DC or AC) and J is a current source (DC or AC).

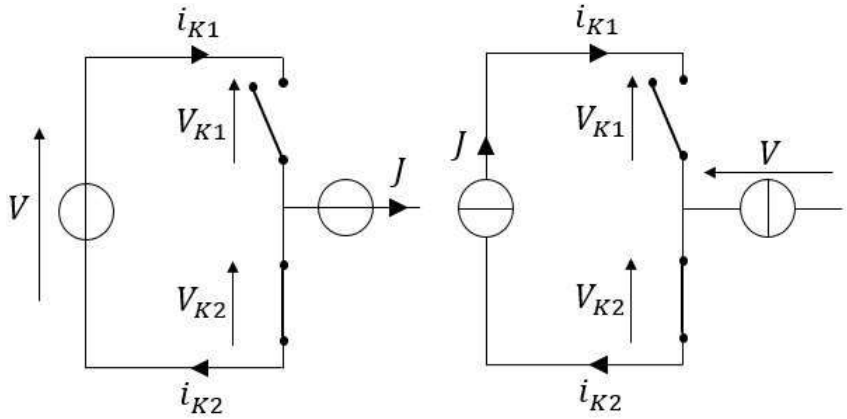

Figure A.2 – Two examples of commutation cell. Voltage source to a current load (on the left). Current source to a voltage load (on the right).

Remark: In the case of a voltage to current commutation cell, the two switches K_1 and K_2 are allowed to be open together. But must be not closed together (short circuit) destroying the entire circuit.In the opposite, a current source is not allowed to be open, then K_1 and K_2 are allowed to be closed together but not open together.These strong constraint explain why dead-times have to be considered in a real application.

A.3 VSI structure

As seen on Fig. A.1, a VSI is composed of three commutation cells, one per phase. As an inverter is a DC/AC converter, it is usually composed IGBT with anti-parallel diode to behave as a bidirectional switch.

Abusively, the state of the commutation cell is summarized by the state of the upper

switch of the commutation cell as the second one will have a complementary state with the first one. Usually, to simplify the equations, switching time [1] is considered as null.

Thanks the previous VSI description, only eight (2^3) different inverter states are possibles as every commutation cell have two different states.

These possible states are summarized thanks to Fig. A.3

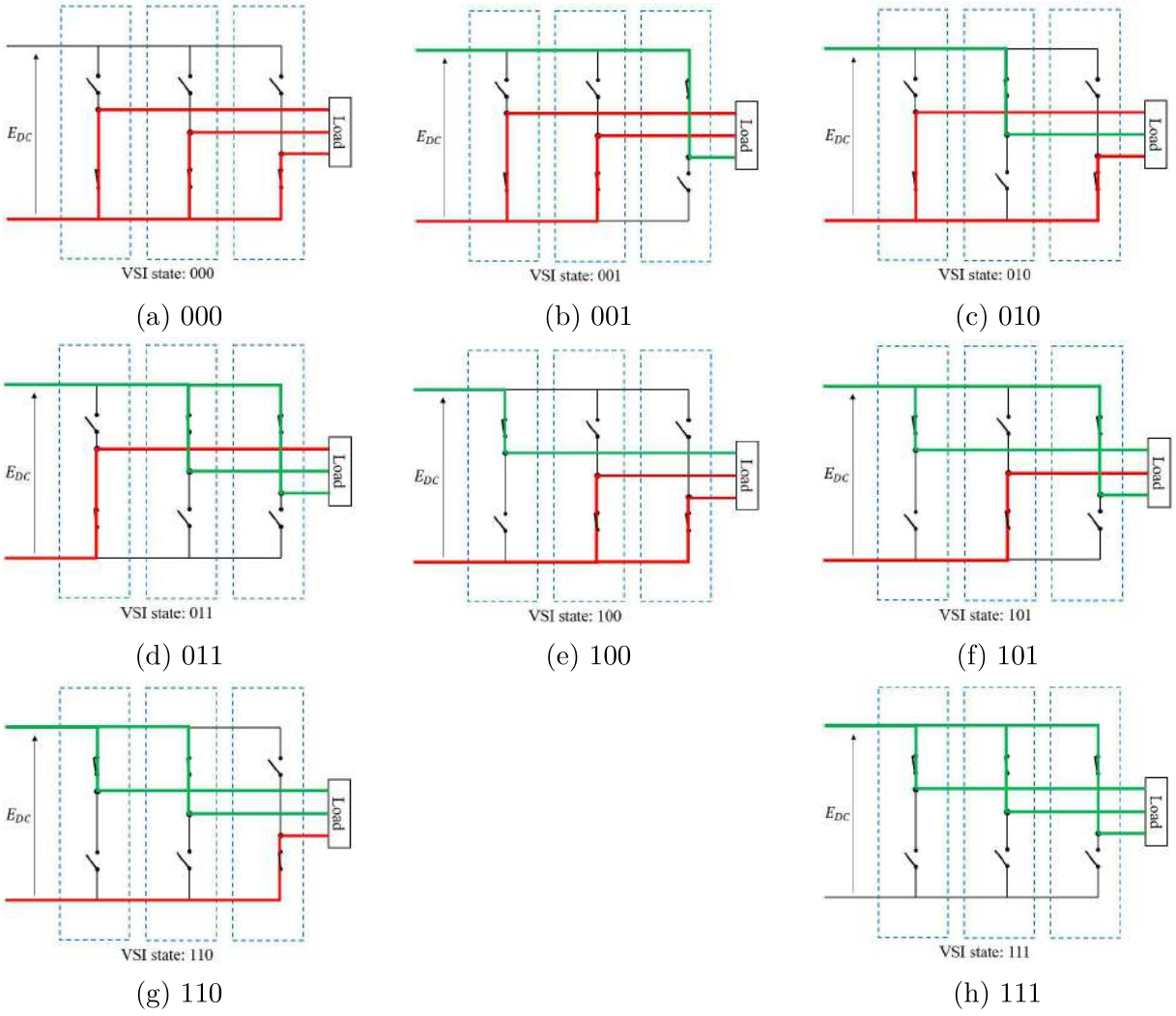

(a) 000 (b) 001 (c) 010

(d) 011 (e) 100 (f) 101

(g) 110 (h) 111

Figure A.3 – Possible switch positions for a three level inverter

1. Time required to turn on the switch or to turn off

A.4 VSI fundamental principle and equations

The basic principle of an inverter is to distribute the electrons from the DC source to the legs of the AC output thanks power switches, doing so, it is possible to deduce the output voltage thanks the switching sequence driving the commutation cells eq. (A.1).

$V_x(t)$ is the single voltage output for the phase x and $S_x(t)$ the upper switch command of the leg x.

$$\begin{pmatrix} V_1(t) \\ V_2(t) \\ V_3(t) \end{pmatrix} = \frac{E_{DC}}{3} \begin{pmatrix} 2 & -1 & -1 \\ -1 & 2 & -1 \\ -1 & -1 & 2 \end{pmatrix} \begin{pmatrix} S_1(t) \\ S_2(t) \\ S_3(t) \end{pmatrix} \tag{A.1}$$

Let's remark that the matrix eq. (A.1) has a determinant equal to zero. Meaning there is an infinity of solutions in order to impose the desired voltage output value thanks to switches states. This very simple equation is an element to explain why so many control strategies exists to control VSI in the literature. Indeed the existence of this infinity of solutions show the presence of an additional freedom degree to control a three phases two-level VSI.

eq. (A.1) is fundamental as it allow to understand that all the purpose of a DC/AC converter command is to choose properly the $S_j(t)$ (command of each leg of a VSI), in order to realize the best voltage output according to a specific objective.

Nevertheless, besides this specific objective, it is imperative to keep in mind the necessity to follow the desired voltage. Doing so, decompose a period into many parts and compute the mean voltage inside each part, is historically the way considered to compute the PWM signal. Indeed, this mean value computation can be archived with a comparison between the desired signal (also called the modulating signal) and a carrier. These two signals have to be normalized, then, the voltage reference is divided by the DC bus voltage and the carrier will be between -0.5 and 0.5 (see Fig. A.4).

This is the so called natural PWM, also called Sinusoidal PWM [27]. The comparison between the sine wave and the carrier one will drive the switches.

Indeed, if the sine wave is greater than the carrier one, then the corresponding commutation cell value will be set to 1. In the opposite, if the carrier is greater, a 0 value will be obtained. A logical representation of this command generation is represented with eq. (A.2).

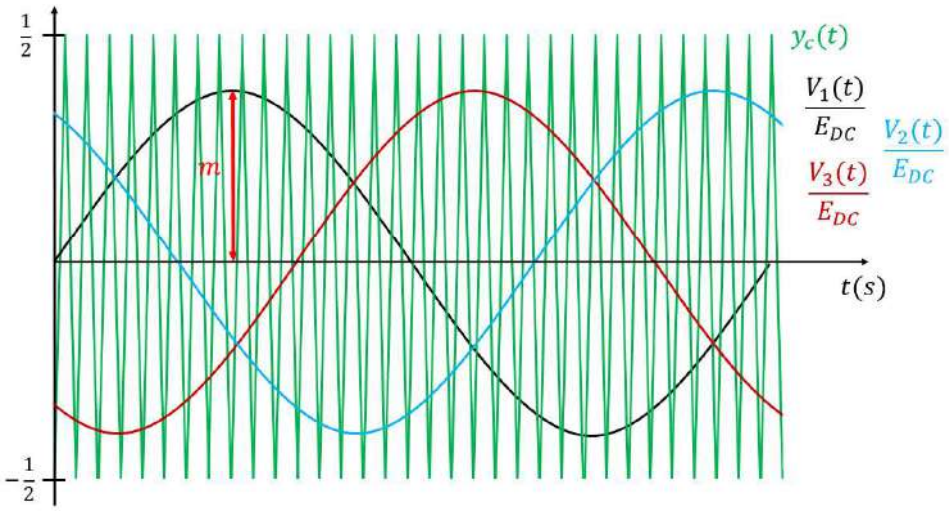

Figure A.4 – Modulating signal and carrier based signal in order to select the switches

$$\mathbf{S}(t) = (y_c(t) > \mathbf{V}_{ref}(t)) \tag{A.2}$$

Nevertheless a carrier signal as presented here, is not the only way to generate the correct output signal. Saw-tooth PWM and synchronous carrier based PWM are also existing methods to generate PWM. On another hand a vectorial representation is also possible and will be presented in chapter 1 (see section 1.2).

Appendix B

THIPWM PROOF

The objective of this appendix, is to prove the original idea of THIPWM as defined by Buja et al. [16], [38].

To find the amplitude of the third harmonic injection, it is necessary to find which amplitude of a in eq. (1.5) will minimise the amplitude of V_{mod}. Indeed, as the third harmonic injected in the desired signal will be invisible in the voltage due to its third harmonic component (see Appendix G), a minimization of the amplitude of V_{mod} will increase the maximum feasible modulation index.

To find a minimum, it is usual to use derivations and check whenever it is equal to zero.

Then derivation of eq. (1.5) leads to eq. (B.1).

$$\frac{dV_{mod}}{d\theta} = \cos(\theta) + 3a\cos(3\theta) = 0 \tag{B.1}$$

This last derivation eq. (B.1) can be simplified as follow:

$$\begin{aligned}
0 &= \cos(\theta) + 3a\cos(3\theta) \\
&= \cos(\theta)\left(1 + 3a\left(2\cos(2\theta) - 1\right)\right) \\
&= \cos(\theta)\left(1 + 3a\left(2\cos(\theta)^2 - 2\sin(\theta)^2 - 1\right)\right) \\
&= \cos(\theta)\left(1 + 3a\left(2\cos(\theta)^2 - 2\left[1 - \cos(\theta)^2\right] - 1\right)\right) \\
&= \cos(\theta)\left(12a\cos(\theta)^2 - 9a + 1\right)
\end{aligned}$$

Then the minimums and maximum of $\widehat{V}_{mod}$ are reached when:

$$\cos(\theta) = 0 \tag{B.2}$$

$$\cos(\theta) = \pm\sqrt{\frac{9a-1}{12a}} \tag{B.3}$$

From eq. (B.2), (B.4) is obtained.

$$\sin(\theta) = 1 \tag{B.4}$$

And from eq. (B.3), eq. (B.5) is found.

$$\begin{aligned} \sin(\theta) &= \pm\sqrt{1-\cos(\theta)^2} \\ &= \pm\sqrt{1-\frac{9a-1}{12a}} \\ &= \pm\sqrt{\frac{3a+1}{12a}} \end{aligned} \tag{B.5}$$

Remarking that:

$$\sin(3\theta) = 3\sin(\theta) - 4\sin(\theta)^3 \tag{B.6}$$

Then thanks Eq. (B.6), Eq. (1.5) becomes:

$$V_{mod} = (1+3a)\sin(\theta) - 4\sin(\theta)^3 \tag{B.7}$$

Then, thanks to eqs.(B.4) and (B.5), the maximums and minimums of V_{mod} are called $\widehat{V}_{mod}$. Then, $\widehat{V}_{mod}$ becomes:

$$\widehat{V}_{mod} = 1-a \tag{B.8}$$

$$\widehat{V}_{mod} = \pm 2\sqrt{\frac{3a+1}{12a}}\left(a+\frac{1}{3}\right) \tag{B.9}$$

The optimum values of a are then obtain by derivation of maximums and minimums of V_{mod} (eqs. (B.8) and (B.9)).

$$\frac{d\widehat{V}_{mod}}{da} = -1 \tag{B.10}$$

$$= \pm\frac{1}{a\sqrt{a}}\sqrt{a+\frac{1}{3}}\left(a-\frac{1}{6}\right) \tag{B.11}$$

Then $\widehat{V}_{mod}$ is maximal/minimal when $a = \left\{-\frac{1}{3} \cup \frac{1}{6}\right\}$. As the desired result is to obtain the minimal amplitude to reach maximal possible modulation index, then the a considered is $a = \frac{1}{6}$[38].

Thanks to Eq. (B.3), we obtain $\cos(\theta) = \pm\frac{1}{2}$, corresponding to $\theta = k\frac{\pi}{3}$, with $k \in \mathbb{Z}^*$

and k not multiple of 3.

Then

$$\widehat{V}_{mod} = \frac{\sqrt{3}}{2} \tag{B.12}$$

leading finally to

$$\begin{aligned} 0.5 &= m_{max}\frac{\sqrt{3}}{2} \\ m_{max} &= \frac{1}{\sqrt{3}} \end{aligned} \tag{B.13}$$

Appendix C

Space Vector Modulation time computation

The objective is to find the times T_{W_0}, T_{W_k}, $T_{W_{k+1}}$ and T_{W_7}. Where k is the sector number as described on Fig.1.14. The idea here is to do a composition with the known vectors ($\mathbf{W}_0$ to $\mathbf{W}_7$ [1]) composing the vector representation in order to realize the desired voltage $\mathbf{V}_{ref}$. This output will be performed thanks to the Chasles's relation. Indeed every vector $\mathbf{V}_{ref}$ can be computed with the two nearest vectors. Then for the sector k, the feasible voltages $\mathbf{W}_k$ and $\mathbf{W}_{k+1}$ would be required. Next a short remind on this strategy computation will be performed.

Remark: An example of the switching instants for the first sector ($k = 1$) is represented on Fig. C.1. We would remark a symmetry on this figure. Thanks to this symmetry the time are the same on the right of the figure.

In complex, $\mathbf{V}_{ref}$ can be written as: $\mathbf{V}_{ref} = V_1 e^{i\,\theta}$. Thanks to the figure 1.14, we understand that $\mathbf{W}_0 = \mathbf{W}_7 = \mathbf{0}$, in other terms it exist two similar vectors in the SVM representation. These two vectors together are the zero sequence components.

As a choice, we will force $T_{W_0} = T_{W_7}$, we will force this equality for every sector.

In the following we will note: T_d the switching period, and T_{W_k} the time used of the vector $\mathbf{W}_k$.

As previously, the following equation have to be respected:

$$T_{W_0} + T_{W_k} + T_{W_{k+1}} + T_{W_7} = T_d \tag{C.1}$$

by writing it as a vector equation vector $\mathbf{W_0}$ and $\mathbf{W_7}$ disappear because they are null vectors.

$$\mathbf{V}_{ref} = \frac{T_{W_k}}{T_d}\mathbf{W}_k + \frac{T_{W_{k+1}}}{T_d}\mathbf{W}_{k+1} \tag{C.2}$$

1. $\mathbf{W}_0$ and $\mathbf{W}_7$ have an output voltage equal to zero and are so called the null vectors.

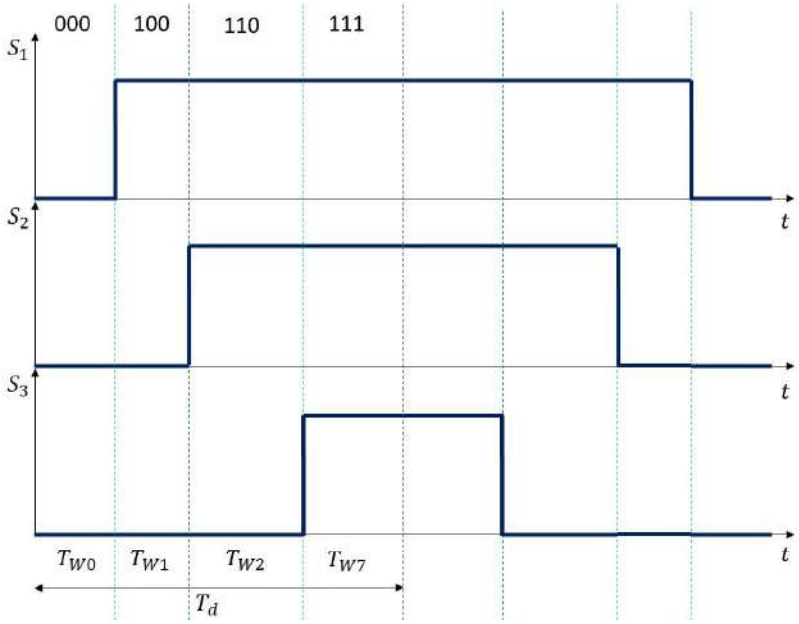

Figure C.1 – first sector symmetric switches

Then, Eq. (C.2) can be extended:

$$V_1 e^{i\theta} = \frac{2}{3}\frac{1}{T_d} E_{DC} e^{i\,k\frac{\pi}{3}} \left(T_{W_k} e^{-i\frac{\pi}{3}} + T_{W_{k+1}} \right) \tag{C.3}$$

Thanks to the consideration that: $e^{i\theta} = \cos(\theta) + i\sin(\theta)$. previous equation is also equal to:

$$\frac{3}{2} m T_d \cos(\theta) = \cos\left((k-1)\frac{\pi}{3}\right) T_{\mathbf{W}_k} + \cos\left(k\frac{\pi}{3}\right) T_{W_{k+1}} \tag{C.4}$$

$$\frac{3}{2} m T_d \sin(\theta) = \sin\left((k-1)\frac{\pi}{3}\right) T_{\mathbf{W}_k} + \sin\left(k\frac{\pi}{3}\right) T_{W_{k+1}} \tag{C.5}$$

leading to:

$$T_{W_k} = \sqrt{3} m T_d \cos\left(\theta + (3-2k)\frac{\pi}{6}\right) \tag{C.6}$$

$$T_{W_{k+1}} = \sqrt{3} m T_d \sin\left(\theta + (2-2k)\frac{\pi}{6}\right) \tag{C.7}$$

$$T_{W_0} = \frac{T_d}{2}\left[1 - \sqrt{3} m \cos\left(\theta - (2k-1)\frac{\pi}{6}\right)\right] \tag{C.8}$$

Then thanks to these three equations (eqs. (C.6), (C.7) and (C.8)), it is then possible

to reconstruct the SVM voltage. Nevertheless, in order to avoid extra switches it is necessary to respect the adjacency between the vectors. Then, for the an even sector k, the vector succession will be $\mathbf{W}_k\mathbf{W}_{k+1}$, in the opposite an odd sector k, the vector succession will be $\mathbf{W}_{k+1}\mathbf{W}_k$. This information is sum up with Table C.1.

Sector	Sequence
1	$\mathbf{W}_0\mathbf{W}_1\mathbf{W}_2\mathbf{W}_7\mathbf{W}_7\mathbf{W}_2\mathbf{W}_1\mathbf{W}_0$
2	$\mathbf{W}_0\mathbf{W}_3\mathbf{W}_2\mathbf{W}_7\mathbf{W}_7\mathbf{W}_2\mathbf{W}_3\mathbf{W}_0$
3	$\mathbf{W}_0\mathbf{W}_3\mathbf{W}_4\mathbf{W}_7\mathbf{W}_7\mathbf{W}_4\mathbf{W}_3\mathbf{W}_0$
4	$\mathbf{W}_0\mathbf{W}_5\mathbf{W}_4\mathbf{W}_7\mathbf{W}_7\mathbf{W}_4\mathbf{W}_5\mathbf{W}_0$
5	$\mathbf{W}_0\mathbf{W}_5\mathbf{W}_6\mathbf{W}_7\mathbf{W}_7\mathbf{W}_6\mathbf{W}_5\mathbf{W}_0$
6	$\mathbf{W}_0\mathbf{W}_1\mathbf{W}_6\mathbf{W}_7\mathbf{W}_7\mathbf{W}_6\mathbf{W}_1\mathbf{W}_0$

Table C.1 – SVM sequence with extra switching respect for a whole switching period T_d

Appendix D

SVM Equivalence with carrier based PWM

The following subsection will demonstrate that SVPWM is rigorously equivalent to SVM [55], [56], [104]. Nevertheless their philosophy is very different and must not be confused. Furthermore, in the following the different computations are depending on the section (and so on angle consideration) depending on time.

Here after, we will call: $d_k(t) = \frac{T_{W_k}(t)}{T_d}$, $d_{k+1}(t) = \frac{T_{W_{k+1}}(t)}{T_d}$ and $d_0(t) = d_7(t) = \frac{T_{W_0}(t)}{T_d}$

First, because of the vector representation, we will decompose the vector $\mathbf{W}_k$ as: $\mathbf{W}_k = W_{k,\alpha} + jW_{k,\beta}\ \forall k \in [\![1;6]\!]$. In the same way, the desired vector can be written as: $\mathbf{V}_{ref}(t) = V_{1,\alpha}(t) + jV_{1,\beta}(t)$. Then the '$\beta$' parameters are the complex ones and the 'α' ones are the real part.

$$\mathbf{V}_{ref}(t) = d_0(t)\mathbf{W}_0 + d_k(t)\mathbf{W}_k + d_{k+1}(t)\mathbf{W}_{k+1} + d_7(t)\mathbf{W}_7 \tag{D.1}$$

As Eq. (D.1) is vectorial it ispossible to rewrite it as a matrix form Eq.(D.2).

$$\begin{bmatrix} V_{1,\alpha}(t) \\ V_{1,\beta}(t) \end{bmatrix} = \begin{bmatrix} W_{k,\alpha} & W_{k+1,\alpha} \\ W_{k,\beta} & W_{k+1,\beta} \end{bmatrix} \cdot \begin{bmatrix} d_k(t) \\ d_{k+1}(t) \end{bmatrix} \tag{D.2}$$

As we know that $\mathbf{W}_k = \frac{2}{3}E_{DC}e^{i(k-1)\frac{\pi}{3}}$, we can write Eq. (D.2) as Eq. (D.3).

$$\begin{bmatrix} V_{1,\alpha}(t) \\ V_{1,\beta}(t) \end{bmatrix} = \frac{2}{3}E_{DC} \begin{bmatrix} \cos\left((k-1)\frac{\pi}{3}\right) & \cos\left(k\frac{\pi}{3}\right) \\ \sin\left((k-1)\frac{\pi}{3}\right) & \sin\left(k\frac{\pi}{3}\right) \end{bmatrix} \cdot \begin{bmatrix} d_k(t) \\ d_{k+1}(t) \end{bmatrix} \tag{D.3}$$

It is possible to prove (see C), that $d_0(t)$, $d_7(t)$, $d_k(t)$ and $d_{k+1}(t)$ can be computed for each sector as Eq. (D.4).

$$\begin{aligned} d_0(t) = d_7(t) &= \frac{1}{2}\left[1 - \sqrt{3}m\cos\left(\theta - (2k-1)\frac{\pi}{6}\right)\right] \\ d_k(t) &= \sqrt{3}m\cos\left(\theta + (3-2k)\frac{\pi}{6}\right) \\ d_{k+1}(t) &= \sqrt{3}m\sin\left(\theta + (2-2k)\frac{\pi}{6}\right) \end{aligned} \tag{D.4}$$

Furthermore as the duty cycle depends on the chosen sector. In the following, we decided to consider the first sector as an example to simplify the computation and for clarity. Thanks to the Fig.C.1, we deduce the following eqs. (D.5) depending on eqs. (D.4).

$$\begin{aligned} \Gamma_1(t) &= d_1(t) + d_2(t) + d_7(t) \\ \Gamma_2(t) &= d_2(t) + d_7(t) \\ \Gamma_3(t) &= d_7(t) \end{aligned} \tag{D.5}$$

We insist that those equations are not the same for each sector as the vector sequence changes.

Because $d_0(t)$ have to be equal to $d_7(t)$. We can write the duty cycle without $d_7(t)$ to obtain eqs. (D.6).

$$\begin{aligned} \Gamma_1(t) &= \frac{1}{2}(1 + d_1(t) + d_2(t)) \\ \Gamma_2(t) &= \frac{1}{2}(1 - d_1(t) + d_2(t)) \\ \Gamma_3(t) &= \frac{1}{2}(1 - d_1(t) - d_2(t)) \end{aligned} \tag{D.6}$$

As we considered for this example $k = 1$ (the first sector), eq. (D.2) becomes eq. (D.7).

$$\begin{bmatrix} V_{1,\alpha}(t) \\ V_{1,\beta}(t) \end{bmatrix} = \frac{2}{3}E_{DC}\begin{bmatrix} 1 & \frac{1}{2} \\ 0 & \frac{\sqrt{3}}{2} \end{bmatrix} \cdot \begin{bmatrix} d_1(t) \\ d_2(t) \end{bmatrix} \tag{D.7}$$

Then by inverting eq.(D.7), it becomes eq.(D.8).

$$\begin{bmatrix} d_1(t) \\ d_2(t) \end{bmatrix} = \frac{3}{2}\frac{1}{E_{DC}} \begin{bmatrix} 1 & -\frac{1}{\sqrt{3}} \\ 0 & \frac{2}{\sqrt{3}} \end{bmatrix} \cdot \begin{bmatrix} V_{1,\alpha}(t) \\ V_{1,\beta}(t) \end{bmatrix} \tag{D.8}$$

Now we can write all the duty cycles depending on $\mathbf{V}_{ref}$ and so on $V_{1,\alpha}(t)$ and $V_{1,\beta}(t)$ with eqs. (D.9).

$$\begin{aligned} \Gamma_1(t) &= \frac{1}{2} + \frac{\sqrt{3}}{4}\frac{1}{E_{DC}}\left(\sqrt{3}V_{1,\alpha}(t) + V_{1,\beta}(t)\right) \\ \Gamma_2(t) &= \frac{1}{2} + \frac{3}{4}\frac{1}{E_{DC}}\left(\sqrt{3}V_{1,\beta}(t) - V_{1,\alpha}(t)\right) \\ \Gamma_3(t) &= \frac{1}{2} - \frac{\sqrt{3}}{4}\frac{1}{E_{DC}}\left(\sqrt{3}V_{1,\alpha}(t) + V_{1,\beta}(t)\right) \end{aligned} \tag{D.9}$$

By the introduction of the equation known as "Amplitude Concordia" [112], we have a matrix equation linking the complex representation to the natural one.

$$\begin{bmatrix} V_{1,\alpha}(t) \\ V_{1,\beta}(t) \end{bmatrix} = \frac{2}{3} \cdot \begin{bmatrix} 1 & -\frac{1}{2} & -\frac{1}{2} \\ 0 & \frac{\sqrt{3}}{2} & -\frac{\sqrt{3}}{2} \end{bmatrix} \cdot \begin{bmatrix} V_1(t) \\ V_2(t) \\ V_3(t) \end{bmatrix} \tag{D.10}$$

As a reminder the sum of all the voltages is equal to zero:

$$V_1(t) + V_2(t) + V_3(t) = 0 \tag{D.11}$$

Thanks to the combination of eqs. (D.10) and (D.11). $V_{1,\alpha}(t)$ and $V_{1,\beta}(t)$ becomes eqs. (D.12).

$$\begin{aligned} V_{1,\alpha}(t) &= V_1(t) \\ V_{1,\beta} &= \frac{1}{\sqrt{3}}\left(V_2(t) - V_3(t)\right) \end{aligned} \tag{D.12}$$

Doing so, we write the duty cycles $\Gamma_1(t)$, $\Gamma_2(t)$ and $\Gamma_3(t)$ depending on $V_1(t)$, $V_2(t)$ and $V_3(t)$. Furthermore, as the first sector median voltage is $V_{med}(t) = V_2(t)$ [1] . The duty cycle

1. $V_{med}(t) = V_2(t)$ For the first and the fourth sectors only!

of the first sector is then written thanks to the simple voltage knowledge in eqs. (D.13). By the same reasoning it is also possible to find the equivalent equations for each sector.

As, those equations are the same than for SVPMW, the link between SVM and SVPWM is established.

$$\begin{aligned} \Gamma_1(t) &= \frac{1}{2} + \frac{1}{E_{DC}} \left(V_1(t) + \frac{V_{med}(t)}{2} \right) \\ \Gamma_2(t) &= \frac{1}{2} + \frac{1}{E_{DC}} \left(V_2(t) + \frac{V_{med}(t)}{2} \right) \\ \Gamma_3(t) &= \frac{1}{2} + \frac{1}{E_{DC}} \left(V_3(t) + \frac{V_{med}(t)}{2} \right) \end{aligned}$$

Appendix E

Fourier Decomposition

Fourier decomposition is a very useful tool in order to describe a periodic signal. Indeed, Fourier theory teach us that any periodic signal can be decomposed into an infinity sum of sine waves.

Let's suppose the existence of a periodic function f. This function can be written thanks to (E.1)

$$f(t) = a_0 + \sum_{n \geq 1} a_n \cos(n\omega t) + b_n \sin(n\omega t) \tag{E.1}$$

Where a_0 is the mean value of the signal and a_n and b_n are called the Fourier coefficients. Furthermore ω is the pulsation, defined by $\omega = 2\pi f_1$ and f_1 the fundamental frequency of the periodic function f

In the specific case of an inverter, if the switching angles are known, it is possible to describe the switches command thanks a Fourier decomposition. Indeed for a specific desired signal, the switching command is periodic with a frequency f_1. (See Figs. 1.20, 1.21 and 1.22)

In the following sections, we will suppose the existence of exactly N_{qp} switching angles per quarter period.

$$\begin{aligned} c_n &= \frac{1}{2\pi} \int_0^{2\pi} S(\alpha) e^{-in\alpha} d\alpha \\ c_n &= \frac{1}{2\pi} \left(\int_0^{\frac{\pi}{2}} S(\alpha) e^{-in\alpha} d\alpha + \int_{\frac{\pi}{2}}^{\pi} S(\alpha) e^{-in\alpha} d\alpha + \int_{\pi}^{\frac{3\pi}{2}} S(\alpha) e^{-in\alpha} d\alpha + \int_{\frac{3\pi}{2}}^{2\pi} S(\alpha) e^{-in\alpha} d\alpha \right) \end{aligned}$$

E.1 QWS

$$c_n = \frac{i}{2n\pi}\left((-1)^n - 1\right)\left(1 + 2\sum_{j=1}^{N_{qp}}(-1)^j \cos(n\alpha_j)\right)$$

Because this computation was done when $S_i = 1$, it is possible to deduce a generic equation when $S_i = 0$ or 1.

$$c_n = \frac{i}{2n\pi}(-1)^{S_i+1}\left((-1)^n - 1\right)\left(1 + 2\sum_{j=1}^{N_{qp}}(-1)^j \cos(n\alpha_j)\right) \tag{E.2}$$

E.2 HWS

The next natural idea is to consider switching angles on the half of the period, then, using the same computation philosophy as for QWS, Fourier coefficients can be computed thanks eq. (E.3).

$$c_n = \frac{i}{2n\pi}(-1)^{S_i+1}\left((-1)^n - 1\right)\left(1 + \sum_{j=1}^{2N_{qp}}(-1)^j e^{-in\alpha_j}\right) \tag{E.3}$$

E.3 FWS

For the FWS the number of switching per period is an odd number, giving equation (E.4)

$$c_n = \frac{i}{2n\pi}(-1)^{S_i+1}\left(\sum_{j=1}^{4N_{qp}+1}(-1)^{j+1} e^{-in\alpha_j} - 1\right) \tag{E.4}$$

E.4 PSR

For the PSR strategy, the number of switching is even as the last switch ($\alpha = 2\pi$) must be considered, giving (E.5)

$$c_n = \frac{i}{2n\pi}(-1)^{S_i+1}\left(\sum_{j=1}^{4N_{qp}+2}(-1)^{j+1} e^{-in\alpha_j}\right) \tag{E.5}$$

Finally, the real and complex part of the Fourier decomposition can be obtained thanks

$$\begin{aligned} a_n &= c_n + c_{-n} \\ b_n &= i\,(c_n - c_{-n}) \end{aligned} \tag{E.6}$$

Appendix F

Weighted Total Harmonic Distortion

To evaluate the predicted losses inside the converter and the load. A current, respectively voltage computation is needed, indeed current respectively voltage value is responsible of switches losses, losses inside the load, torque, etc..

F.1 Inductive load

A lot of studies are based on WTHD, because it does not depends on a load and allows to evaluate the solution quality quite fast and easily. WTHD is an approximation of all the currents norm inside the inductive load. This load is composed with an inductance L with a resisting part R, subject to a voltage signal of pulsation ω. Note that, through out the thesis $L\omega$ and R are constant.

WTHD is the norm of all the harmonics currents in a case of purely inductive load ($R = 0$). In the case of only inductive load, WTHD is an approximation of the current norm. The approximation depends on the value of $\frac{R}{L\omega} << 1$. This condition is justified by the demonstration below [67].

Current can be expressed as the first order differential equation eq. (F.1). $\mathbf{I}(t) = [i_1(t), i_2(t), \cdots, i_p(t)]^t$ is the vector of the current in the load p phases.

$\mathbf{V}(t) = [v_1(t), v_2(t), \cdots, v_p(t)]^t$ is the simple voltage vector (output of the inverter to neutral point voltage) in the p phases.

It is important to notify that in the next demonstration, square roots, multiplication and divisions of vectors are assumed to be term to term. The following demonstration is similar to the Hartgenbusch one [67].

$$\frac{d\mathbf{I}(t)}{dt} = \frac{\mathbf{V}(t)}{L} - \frac{R}{L}\mathbf{I}(t) \tag{F.1}$$

Thanks to the periodic property of the voltage and current, and without considering the dead-time influence for the voltage computation, it is possible to decompose the signal with Fourier series.

$$\mathbf{V}(t) = \mathbf{a}_{0,V} + \sum_{n\geq 1} \mathbf{a}_{n,V}\cos(n\omega t) + \mathbf{b}_{n,V}\sin(n\omega t) \tag{F.2}$$

$$\mathbf{I}(t) = \mathbf{a}_{0,I} + \sum_{n\geq 1} \mathbf{a}_{n,I}\cos(n\omega t) + \mathbf{b}_{n,I}\sin(n\omega t) \tag{F.3}$$

$$\frac{d\mathbf{I}(t)}{dt} = \sum_{n\geq 1} n\omega\mathbf{b}_{n,I}\cos(n\omega t) - n\omega\mathbf{a}_{n,I}\sin(n\omega t) \tag{F.4}$$

On the equation below, Fourier coefficient are p components vectors, each for one phase.

Equations (F.1) to (F.4) lead to eq. (F.5)

$$\begin{cases} \mathbf{0} &= \frac{1}{L}\mathbf{a}_{0,V} - \frac{R}{L}\mathbf{a}_{0,I} \\ n\omega\mathbf{b}_{n,I} &= \frac{1}{L}\mathbf{a}_{n,V} - \frac{R}{L}\mathbf{a}_{n,I} \\ n\omega\mathbf{a}_{n,I} &= \frac{R}{L}\mathbf{b}_{n,I} - \frac{1}{L}\mathbf{b}_{n,V} \end{cases} \tag{F.5}$$

and then:

$$\begin{cases} \mathbf{a}_{0,I} &= \frac{1}{R}\mathbf{a}_{0,V} \\ \mathbf{a}_{n,I} &= \frac{1}{R^2+(nL\omega)^2}\left(R\mathbf{a}_{n,V} - nL\omega\mathbf{b}_{n,V}\right) \\ \mathbf{b}_{n,I} &= \frac{1}{R^2+(nL\omega)^2}\left(nL\omega\mathbf{a}_{n,V} + R\mathbf{b}_{n,V}\right) \end{cases} \tag{F.6}$$

Finally, considering $nL\omega >> R \quad \forall n \in \mathbb{N}^*$, current Fourier decomposition can be approximated with eq. (F.7).

$$\begin{cases} \mathbf{a}_{0,I} &= \frac{1}{R}\mathbf{a}_{0,V} \\ \mathbf{a}_{n,I} &\simeq -\frac{\mathbf{b}_{n,V}}{nL\omega} \\ \mathbf{b}_{n,I} &\simeq \frac{\mathbf{a}_{n,V}}{nL\omega} \end{cases} \tag{F.7}$$

With this approximation amplitude of each current harmonic ($\mathbf{I}_n$) is given by eq. (F.8). As $L\omega$ is a constant, let's define $\mathbf{I}'_n = L\omega\mathbf{I}_n$. Indeed a constant do not influence direction of variation of the current.
Remembering that the harmonics must be eliminated or at least reduced, computation will be then performed thanks to $\mathbf{I}'_n$ instead of $\mathbf{I}_n$, both equations are described below.

$$\mathbf{I}_n = \sqrt{\mathbf{a}_{n,I}^2 + \mathbf{b}_{n,I}^2} \quad \forall n \in \mathbb{N}^* \tag{F.8}$$

$$\mathbf{I}'_n = \frac{1}{n}\sqrt{\mathbf{a}^2_{n,V} + \mathbf{b}^2_{n,V}} \quad \forall n \in \mathbb{N}^* \tag{F.9}$$

Remark that in eq. (F.9) the Fourier coefficients are with respect to voltage instead of current as eq. (F.8).

Moreover $\mathbf{I}'_n$, can be described with respect to voltage amplitude:

$$\mathbf{I}'_n = \sqrt{\frac{\mathbf{V}^2_n}{n^2}} \quad \forall n \in [\![2; \infty[\![\tag{F.10}$$

Finally, in order to have a scalar criteria, norm of all the $\mathbf{I}'_n$ for each phase is performed with eq. (F.11).

$$||\mathbf{I}'_n|| = \sqrt{\sum_{n>1} \mathbf{I}'^2_n} = \sqrt{\sum_{n>1} \frac{\mathbf{V}^2_n}{n^2}} \tag{F.11}$$

From eq. (F.11) the WTHD equation is written for each phase as following:

$$\mathbf{V}_{\text{WTHD},\%} = \frac{100}{\mathbf{V}_1}||\mathbf{I}'_n|| = \frac{100}{\mathbf{V}_1}\sqrt{\sum_{n>1} \frac{\mathbf{V}^2_n}{n^2}} \tag{F.12}$$

Under the assumption that angles from each phase are independent eq. (F.12) and to reduce to a scalar, mean value of the WTHD is computed below.

$$V_{\text{WTHD},\%} = \frac{100}{pV_1}\sum_{i=1}^{p}\sqrt{\sum_{n>1} \frac{\mathbf{V}^2_{n,i}}{n^2}} \tag{F.13}$$

In previous equation, $\mathbf{V}_1$ becomes V_1, because all the terms of the vector are equals and the vector division is done term to term. Finally, eq. (F.13) provides the WTHD function.

F.2 Capacitive load

According to a capacitive load, and then a current source, eq. (F.1) will be transformed to equation (F.14).

$$\frac{d\mathbf{V}(t)}{dt} = \frac{\mathbf{I}(t)}{C} - \frac{1}{RC}\mathbf{V}(t) \tag{F.14}$$

With the same way of thinking, WTHD of eq. (F.12) becomes eq. (F.15)

$$\mathbf{I}_{\mathrm{WTHD},\%} = \frac{100}{\mathbf{I}_1}\sqrt{\sum_{n\geq 2}\frac{\mathbf{I}_n^2}{n^2}} \tag{F.15}$$

As for its voltage counterpart, the considered current WTHD is finally written as:

$$I_{\mathrm{WTHD},\%} = \frac{100}{pI_1}\sum_{i=1}^{p}\sqrt{\sum_{n\geq 2}\frac{\mathbf{I}_{n,i}^2}{n^2}} \tag{F.16}$$

Consequently for capacitive load, eq. (F.16) provides the WTHD function.

Appendix G

Symmetry harmonics removing

It is well known that the phases symmetry remove some harmonics, and specially the harmonics multiple of the number of legs p of the considered converter. Thanks the computation of Fourier coefficients (eqs. (E.2)-(E.4)), we will show that some harmonics are systematically removed when a phases symmetry is considered. Indeed, for a p-phases inverter, harmonics multiple of p will be removed [27]. A short demonstration is shown here after.

Let's assume the leg command number k ($k \in [\![0, p-1]\!]$) is described by:

$$S_k(\theta) = a_{0,k} + \sum_{n\geq 1} a_{n,k} \cos\left(n\left(\theta - \frac{2k\pi}{p}\right)\right) + b_{n,k} \sin\left(n\left(\theta - \frac{2k\pi}{p}\right)\right) \tag{G.1}$$

The voltage of the first leg of a p-phases load can then be described by eq. (G.4) thanks to matrix defined by eq. (G.2) multiplied by vector of components eq. (G.1).

Remark: as the $a_{0,k}$ are equals, the resulting mean voltage is equal to 0, $\frac{p-1}{p} a_{0,1} - \frac{1}{p}\sum_{i=1}^{p-1} a_{0,i} = 0$.

$$M = \frac{1}{p}\begin{pmatrix} p-1 & -1 & \cdots & -1 \\ -1 & p-1 & \cdots & -1 \\ \vdots & & \ddots & \vdots \\ -1 & \cdots & -1 & p-1 \end{pmatrix} \tag{G.2}$$

Voltage of all the phases can be deduced from the command thanks to (G.1) and (G.2) and is written as follow eq. (G.3).

$$\begin{pmatrix} V_1(\theta) \\ V_2(\theta) \\ \vdots \\ V_p(\theta) \end{pmatrix} = E_{DC} \cdot M \cdot \begin{pmatrix} S_1(\theta) \\ S_2(\theta) \\ \vdots \\ S_p(\theta) \end{pmatrix} \tag{G.3}$$

With the previous eq. (G.3), voltage of the first phase is written as (G.4).

$$\begin{aligned} V_1(\theta) &= E_{DC}\frac{p-1}{p}\sum_{n\geq 1} a_{n,1}\cos(n\theta) + b_{n,1}\sin(n\theta) \\ &- \frac{E_{DC}}{p}\sum_{n\geq 1} a_{n,2}\cos\left(n\theta - n\frac{2\pi}{p}\right) + b_{n,2}\sin\left(n\theta - n\frac{2\pi}{p}\right) \\ &\cdots \\ &- \frac{E_{DC}}{p}\sum_{n\geq 1} a_{n,p}\cos\left(n\theta - n(p-1)\frac{2\pi}{p}\right) \\ &+ b_{n,p}\sin\left(n\theta - n(p-1)\frac{2\pi}{p}\right) \end{aligned} \tag{G.4}$$

$$\begin{aligned} V_1(\theta) &= E_{DC}\frac{p-1}{p}\sum_{n\geq 1} a_{n,1}\cos(n\theta) + b_{n,1}\sin(n\theta) \\ &- \frac{E_{DC}}{p}\sum_{n\geq 1} a_{n,2}\cos(n\theta)\cos\left(n\frac{2\pi}{p}\right) + a_{n,2}\sin(n\theta)\sin\left(n\frac{2\pi}{p}\right) \\ &- b_{n,2}\sin(n\theta)\cos\left(n\frac{2\pi}{p}\right) + b_{n,2}\cos(n\theta)\sin\left(n\frac{2\pi}{p}\right) \\ &\cdots \\ &- \frac{E_{DC}}{p}\sum_{n\geq 1} a_{n,p}\cos(n\theta)\cos\left(n(p-1)\frac{2\pi}{p}\right) + a_{n,p}\sin(n\theta)\sin\left(n(p-1)\frac{2\pi}{p}\right) \\ &+ b_{n,p}\sin(n\theta)\cos\left(n(p-1)\frac{2\pi}{p}\right) - b_{n,p}\cos(n\theta)\sin\left(n(p-1)\frac{2\pi}{p}\right) \end{aligned} \tag{G.5}$$

For $n = p$, $\cos\left(n\frac{2\pi}{p}\right) = 1$ and $\sin\left(n\frac{2\pi}{p}\right) = 0$, then the harmonics of rank $n = p$ of the voltage are systematically removed because the norm $\sqrt{a_{n,k}^2 + b_{n,k}^2}$ is constant for every phase k. This demonstration can be done for each phase voltage from 1 to p.

Appendix H

Double Fourier Decomposition

When a signal contains some dependents signals, it is interesting to decompose the signals thanks multiple Fourier decomposition. Inside a Carrier based PWM generation, there are two signals, the modulating one and the carrier one (in some cases, it can be a saw-tooth one). In the following, the carrier will be supposed to be synchronous. Meaning the fundamental frequency and the switching one are linked by an integer. In this thesis $f_s = 2N_{qp}f_1$.

To link the carrier signal with the modulating one, we introduced for this section two variables.

Let's note $x = 2N_{qp}\theta$ the carrier corresponding angle and $y = \theta$ the voltage reference angle. As we said it, the carrier signal and the modulating one are linked due to the intrinsic structure of a PWM control. Then, in the same way than [27] a relationship between x and y can be done. This relationship can be visualized for the natural PWM thanks to Fig. H.1.

Remark: The carrier is equal to $-\frac{1}{2}$ when $\theta = 0$, furthermore the carrier evolves between $-\frac{1}{2}$ and $\frac{1}{2}$.

The x,y relationship can be established thanks eq.(H.1).

$$\begin{cases} x = -\frac{\pi}{2}\left(2m\sin(y) + 2v_0(y) + 1\right) \\ x = \frac{\pi}{2}\left(2m\sin(y) + 2v_0(y) + 1\right) \end{cases} \tag{H.1}$$

As for the simple Fourier transform, the original periodic signal can be found again with the generic equation (H.2).

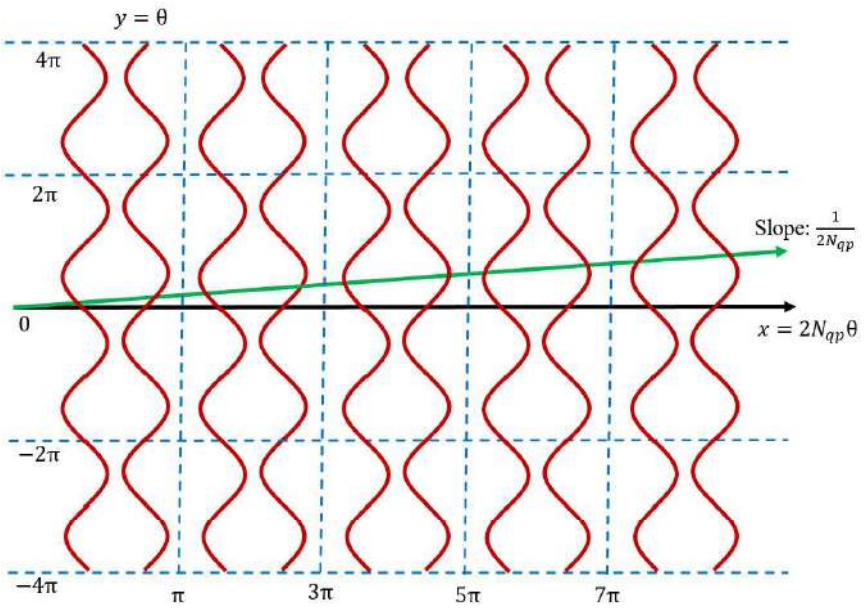

Figure H.1 – A plane representation of the switches angles generated by the comparison between a triangular carrier (slope) and a SPWM (sines)

$$\begin{aligned} f(x,y) &= \frac{A_{0,0}}{2} + \sum_{n=1}^{\infty} \left[A_{0,n}\cos(ny) + B_{0,n}\sin(ny)\right] \\ &+ \sum_{k=1}^{\infty} \left[A_{k,0}\cos(kx) + B_{k,0}\sin(kx)\right] \\ &+ \sum_{k=1}^{\infty} \sum_{\substack{n=-\infty \\ n\neq 0}}^{\infty} \left[A_{k,n}\cos(kx+ny) + B_{k,n}\sin(kx+ny)\right] \end{aligned} \tag{H.2}$$

In our specific case, as x and y are linked with the angular position θ. Generic equation (H.2), becomes eq.(H.3).

$$
\begin{aligned}
f(\theta) &= \frac{A_{0,0}}{2} + \sum_{n=1}^{\infty} \left[A_{0,n} \cos(n\theta) + B_{0,n} \sin(n\theta) \right] \\
&+ \sum_{k=1}^{\infty} \left[A_{k,0} \cos(2kN\theta) + B_{k,0} \sin(2kN\theta) \right] \\
&+ \sum_{k=1}^{\infty} \sum_{\substack{n=-\infty \\ n\neq 0}}^{\infty} \left[A_{k,n} \cos((2kN+n)\theta) + B_{k,n} \sin((2kN+n)\theta) \right]
\end{aligned}
\tag{H.3}
$$

$A_{k,n}$ and $B_{k,n}$ are the Fourier coefficients defined thanks equation (H.4).

$$
C_{k,n} = \frac{A_{k,n} - iB_{k,n}}{2} = \frac{1}{2\pi^2} \int_{-\pi}^{\pi} \int_{-\pi}^{\pi} f(x,y) e^{i(kx+ny)} dxdy \tag{H.4}
$$

Computation of the previous equation (H.4), for different values of k and n leads to eqs.(H.5), (H.6), (H.7) and (H.8)

$$
C_{0,0} = 1 \tag{H.5}
$$

$$
C_{0,1} = im + \frac{1}{\pi} \int_{-\pi}^{\pi} e^{iy} v_0(y) dy \tag{H.6}
$$

$$
C_{0,n} = \frac{1}{\pi} \int_{-\pi}^{\pi} e^{iny} v_0(y) dy \ \forall n \geq 2 \tag{H.7}
$$

$$
C_{k,n} = \begin{cases} \frac{-i^{k+1}}{k\pi^2} \int_{-\pi}^{\pi} \left(e^{ik\pi m \sin(y) + ik\pi v_0(y)} \right) \cos(ny) dy & \forall n \in \mathbb{Z} \ \& \ \forall k \in \mathbb{N}^* \text{ odd} \\ \frac{i^k}{k\pi^2} \int_{-\pi}^{\pi} \left(e^{ik\pi m \sin(y) + ik\pi v_0(y)} \right) \sin(ny) dy & \forall n \in \mathbb{Z} \ \& \ \forall k \in \mathbb{N}^* \text{ even} \end{cases} \tag{H.8}
$$

Appendix I

Switches losses

This appendix is concerned on the computation of the VSI losses, and more precisely, about the switching and conduction losses of the power switches.

As mentioned the losses can be decomposed in two categories, the switching ones, corresponding to the losses when the switch is opened or closed and another one, corresponding to the losses when the current go through the switch [113].

Next section is concerned about the characterization of the switching losses.

I.1 Switching losses

Switching losses are defined as the power lost when the switch is turning on or off, then the energy lost by every commutation can be written thanks to eqs. (I.1).

$$\begin{aligned} E_{on} &= \int_{t_1}^{t_2+dt_{on}} V_{CE} I_C dt \\ E_{off} &= \int_{t_1}^{t_2+dt_{off}} V_{CE} I_C dt \end{aligned} \tag{I.1}$$

With V_{CE} the voltage between the collector and the emitter, I_C the current throw the collector(see Fig. I.1), t_1 is the time when the switch is asked to change state, t_2 is the time when the state transition is over. dt_{on} and dt_{off} are times provided by the builder to compute properly the switching losses.

Nevertheless, eqs. (I.1) are not used this way, as the switches builder often provide the E_{on} and E_{off} losses depending only on the current for some T_j parameters and V_{GE} ones too. Then, we can consider for a steady state consideration that E_{on} and E_{off} only depends on the current of the considered phase x, $i_x(t_1)$.

Then the energy lost for a single switch on a whole period can be written thanks to

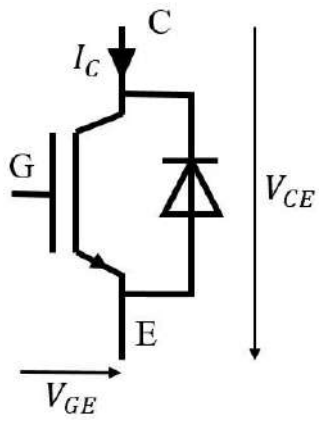

Figure I.1 – Switches nomenclature of current and voltage. "C" means Collector, "E" Emitter and "G" Grid

eq. (I.2).

$$\mathcal{E}_{sw,1} = \frac{1}{2} \sum_{j=1}^{4N_{qp}+2} \left(1 + (-1)^j\right) E_{on} \left(i_1 \left(\frac{\alpha_{j,1}}{\omega}\right)\right) + \left(1 - (-1)^j\right) E_{off} \left(i_1 \left(\frac{\alpha_{j,1}}{\omega}\right)\right) \tag{I.2}$$

As the lower switch have an opposite state than the upper one, the energy lost by the second switch can be described by eq. (I.3). [1]

$$\overline{\mathcal{E}}_{sw,1} = \frac{1}{2} \sum_{j=1}^{4N_{qp}+2} \left(1 + (-1)^j\right) E_{off} \left(i_1 \left(\frac{\alpha_{j,1}}{\omega}\right)\right) + \left(1 - (-1)^j\right) E_{on} \left(i_1 \left(\frac{\alpha_{j,1}}{\omega}\right)\right) \tag{I.3}$$

Then thanks to eqs. (I.2) and (I.3), the switching losses of any commutation cell x can be deduced by doing the same reasoning on each phase and lead to eq. (I.4).

$$\begin{aligned} E_{sw,x} &= \mathcal{E}_{sw,x} + \overline{\mathcal{E}}_{sw,x} \\ &= \sum_{j=1}^{4N_{qp}+2} E_{on} \left(i_x \left(\frac{\alpha_{j,x}}{\omega}\right)\right) + E_{off} \left(i_x \left(\frac{\alpha_{j,x}}{\omega}\right)\right) \end{aligned} \tag{I.4}$$

In this thesis context, by doing the sum of the three phases energy lost, we obtain the energy lost by the VSI for a single period, eq. (I.5)

1. Under the hypothesis the dead-time is negligible or null.

$$E_{sw} = E_{sw,1} + E_{sw,2} + E_{sw,3} \tag{I.5}$$

leading to a power loss $\mathcal{P}_{sw}$ defined by eq.(I.6)

$$\mathcal{P}_{sw} = f_1 E_{sw} \tag{I.6}$$

Thanks to eqs. (I.4) and (I.6), the switching losses can be computed. As we can see, the more the switching angles $\alpha_{j,x}$ will cut small currents, the less the inverter will dissipate energy.

I.2 Conduction losses

As the switches are not perfect components, the current flow through the switches will generate a power loss. The equivalent equations of an IGBT and a diode are composed of a resistance, and of a voltage dead-band. These two characteristics leads to consider eqs. (I.8) for the conduction losses.

$$\mathcal{P}_T(i(t)) = V_{ce,0}\,|i(t)| + r_{ce} i(t)^2 \tag{I.7}$$
$$\mathcal{P}_D(i(t)) = V_{F,0}\,|i(t)| + r_F i(t)^2 \tag{I.8}$$

Thanks to this previous description, it is important to notice that the conduction losses will be the ones produced by the IGBT when the current $i(t)$ is positive and the diode one when the current is negative. Then, the conduction losses for the upper switch of the commutation cell can be expressed thanks to eq. (I.9).

$$\mathcal{P}_{cond,1} = \frac{f_1}{2} \int_0^{\frac{1}{f_1}} S_1(t) \left[(1 + \text{sign}\,(i_1(t)))\, \mathcal{P}_T(i_1(t)) + (1 - \text{sign}\,(i_1(t)))\, \mathcal{P}_D(i_1(t)) \right] dt \tag{I.9}$$

Following an equivalent reasoning, the lower switch conduction losses can be expressed thanks to eq. (I.10).

$$\overline{\mathcal{P}}_{cond,1} = \frac{f_1}{2} \int_0^{\frac{1}{f_1}} \overline{S}_1(t) \left[(1 - \text{sign}\,(i_1(t)))\, \mathcal{P}_T(i_1(t)) + (1 + \text{sign}\,(i_1(t)))\, \mathcal{P}_D(i_1(t)) \right] dt \tag{I.10}$$

Then, thanks the same considerations on all the commutation cells, it is possible to obtain the total power lost for any commutation cell x, eq. (I.11).

$$\begin{aligned} P_{cond,x} &= \mathcal{P}_{cond,x} + \overline{\mathcal{P}}_{cond,x} \\ &= f_1 \int_0^{\frac{1}{f_1}} \frac{\mathcal{P}_T(i_x(t)) + \mathcal{P}_D(i_x(t))}{2} \\ &+ \left[\mathcal{P}_T(i_x(t)) - \mathcal{P}_D(i_x(t))\right] \text{sign}\left(i_x(t)\right) \left[S_x(t) - \frac{1}{2}\right] dt \end{aligned} \tag{I.11}$$

As there are three phases and two commutation cells in the inverter, the conduction power lost by a VSI can be expressed thanks to eq. (I.12)

$$\mathcal{P}_{cond} = P_{cond,1} + P_{cond,2} + P_{cond,3} \tag{I.12}$$

Finally, thanks to the knowledge of conduction and switching power losses, it is possible to determine the inverter losses and then the efficiency.

Appendix J

Motor model

The losses inside the inverter are linked to the current (respectively the voltage) generated by the load. To do so, a current description have to be done in order to evaluate the effects of some strategies on the losses.

Then, all the following models and descriptions will be supposed to be in the the established zone. So no transient period is considered for the seek of simplicity and also the possibility to write the voltage and current as a Fourier decomposition because of the periodicity of the signals.

Then, in the following eqs. (J.1), (J.2) and (J.3) are considered as true.

$$\mathbf{V}(t) = \mathbf{a}_{0,V} + \sum_{n\geq 1} \mathbf{a}_{n,V}\cos(n\omega t) + \mathbf{b}_{n,V}\sin(n\omega t) \tag{J.1}$$

$$\mathbf{I}(t) = \mathbf{a}_{0,I} + \sum_{n\geq 1} \mathbf{a}_{n,I}\cos(n\omega t) + \mathbf{b}_{n,I}\sin(n\omega t) \tag{J.2}$$

$$\frac{d\mathbf{I}(t)}{dt} = \sum_{n\geq 1} n\omega\mathbf{b}_{n,I}\cos(n\omega t) - n\omega\mathbf{a}_{n,I}\sin(n\omega t) \tag{J.3}$$

We remember to our reader that $\mathbf{V}$ and $\mathbf{I}$ are vectors composed of three lines.

J.1 RLE model

The easiest motor model is the RLE one. This motor is described thanks to Fig. J.1. This description lead to eq. (J.4).

$$\frac{d\mathbf{I}(t)}{dt} = \frac{\mathbf{V}(t) - \mathbf{E}(t)}{L} - \frac{R}{L}\mathbf{I}(t) \tag{J.4}$$

Previous equation lead by identification to a Fourier decomposition represented thanks to eqs. (J.5). Note that these obtained equations are still true, eve if the EMF is not

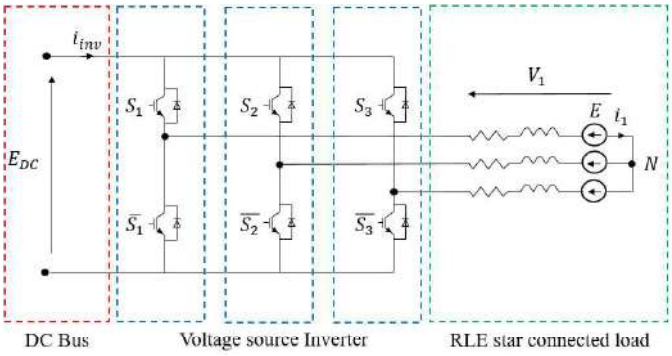

Figure J.1 – Description of the RLE model

considered as perfectly sinusoidal.

$$\begin{cases} \mathbf{a}_{0,I} = \frac{1}{R}\mathbf{a}_{0,V} \\ \mathbf{a}_{n,I} = \frac{1}{R^2+(nL\omega)^2}\left(R\left(\mathbf{a}_{n,V} - \mathbf{a}_{n,E}\right) - nL\omega\left(\mathbf{b}_{n,V} - \mathbf{b}_{n,E}\right)\right) \\ \mathbf{b}_{n,I} = \frac{1}{R^2+(nL\omega)^2}\left(nL\omega\left(\mathbf{a}_{n,V} - \mathbf{a}_{n,E}\right) + R\left(\mathbf{b}_{n,V} - \mathbf{b}_{n,E}\right)\right) \end{cases} \tag{J.5}$$

Then thanks to these equations, a link between the current and the voltage provided is done. Furthermore, as this voltage is directly linked with the command (and the switching angles). The PWM effect on current, and then on losses can be found immediately.

Appendix K

Dead time consideration

Dead-time effect is a very complex parameter to consider depending on the current value [114], [115]. Nevertheless as a first simple approximation, it is possible to consider it as a fixed time preventing short circuits (Fig.K.1). The equation eq. (K.1) corresponds to this fixed time strong hypothesis.

$$\overline{\alpha_j} = \alpha_j + (-1)^{j+1}\omega\Delta t \ \forall j \in [\![1, N_d]\!] \tag{K.1}$$

The objective of the next development is to quantify the dead-time influence on harmonics when $\omega\Delta t << 1$. By replacing α_j by $\overline{\alpha_j}$, new Fourier coefficients can be described. Giving equations (K.2),(K.3) and (K.4) instead of eqs. (1.31),(1.32) and (1.33).

$$\lambda_{c,0,FWS} = \frac{1}{\pi}(-1)^{S_i+1}\left(\sum_{j=1}^{4N_{qp}+1}(-1)^{j+1}\left(\alpha_j + (-1)^{j+1}\omega\Delta t\right) + 2\pi\right) \tag{K.2}$$

$$\lambda_{c,n,FWS} = \frac{1}{n\pi}(-1)^{S_i+1}\left(\sum_{j=1}^{4N_{qp}+1}(-1)^{j+1}\sin\left(n\left(\alpha_j + (-1)^{j+1}\omega\Delta t\right)\right)\right) \tag{K.3}$$

$$\xi_{c,n,FWS} = \frac{1}{n\pi}(-1)^{S_i}\left(\sum_{j=1}^{4N_{qp}+1}(-1)^{j+1}\cos\left(n\left(\alpha_j + (-1)^{j+1}\omega\Delta t\right)\right) - 1\right) \tag{K.4}$$

Thanks to eq.(K.2), the new mean value of the first phase command becomes eq.(K.5)

$$\lambda_{c,0,FWS} = a_{c,0,FWS} + \frac{1}{\pi}(-1)^{S_i+1}\left(4N_{qp}+1\right)\omega\Delta t \tag{K.5}$$

Then, for the harmonics, by considering trigonometric properties equations (K.3) and (K.4) becomes respectively, (K.6) and (K.7)

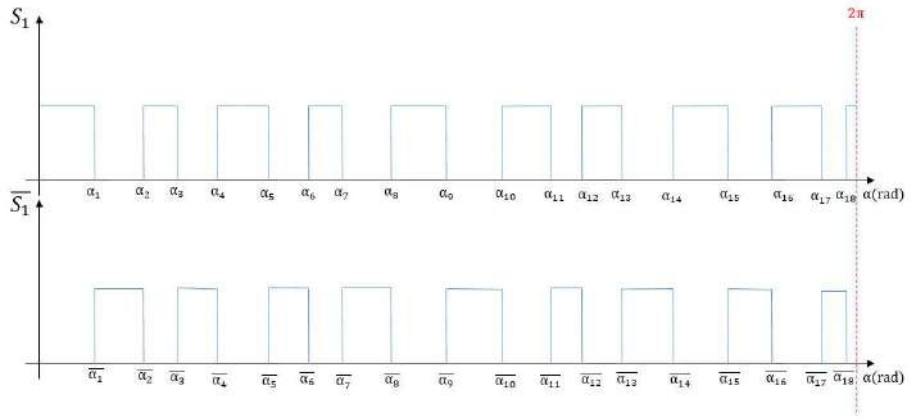

Figure K.1 – Dead-time representation

$$\lambda_{c,n,FWS} = \frac{1}{n\pi}(-1)^{S_i+1}\left(\sum_{j=1}^{4N_{qp}+1}\left[(-1)^{j+1}\cos(n\omega\Delta t)\sin(n\alpha_j) + \sin(n\omega\Delta t)\cos(n\alpha_j)\right]\right) \tag{K.6}$$

$$\xi_{c,n,FWS} = \frac{1}{n\pi}(-1)^{S_i}\left(\sum_{j=1}^{4N_{qp}+1}\left[(-1)^{j+1}\cos(n\omega\Delta t)\cos(n\alpha_j) - \sin(n\omega\Delta t)\sin(n\alpha_j)\right] - 1\right) \tag{K.7}$$

As we supposed $\omega\Delta t << 1$, it is possible to do the following approximation:

$$\begin{aligned}\cos(n\omega\Delta t) &= 1 - \left(n - \frac{1}{2}\right)(\omega\Delta t)^2 + o\left(\Delta t^2\right)\\ \sin(n\omega\Delta t) &= n\omega\Delta t + o\left(\Delta t^2\right)\end{aligned} \tag{K.8}$$

Thanks equations (K.8), (K.6) and (K.7) it is easy to simplify the equations to obtain eq.(K.9) and eq.(K.10), the modified Fourier coefficients replacing eqs. (1.31),(1.32) and (1.33).

$$\lambda_{c,n,FWS} = a_{c,n,FWS} + \frac{\omega \Delta t}{\pi}(-1)^{S_i+1}\left(\sum_{j=1}^{4N_{qp}+1}\cos(n\alpha_j)\right) + o\left(\Delta t^2\right) \quad \text{(K.9)}$$

$$\xi_{c,n,FWS} = b_{c,n,FWS} + \frac{\omega \Delta t}{\pi}(-1)^{S_i+1}\left(\sum_{j=1}^{4N_{qp}+1}\sin(n\alpha_j)\right) + o\left(\Delta t^2\right) \quad \text{(K.10)}$$

BIBLIOGRAPHY

[1] A. Juton, X. Rain, V. Sauvant-Moynot, *et al.*, *Technologies des voitures électriques, Motorisation, batteries, hydrogène, recharge et interactions réseau* (Collection technique ingénierie, Electrotechnique). Dunod, 2021, ISBN: 978-2-10-081806-8. DOI: 10.1002/978111936729 (cit. on pp. 25–28).

[2] B. Walton, J. Hamilton, G. Alberts, S. Fullerton-Smith, E. Day, and J. Ringrow, « Electric vehicles setting a course for 2030 », *Deloitte*, 2020 (cit. on p. 25).

[3] French governement, « Certificat air », French governement, France, Jul. 21, 2022 (cit. on p. 25).

[4] A. Feitz, « Royaume-uni: l interdiction dès 2030 des voitures thermiques accroit la pression sur les industriels », *Les Echos*, 2020 (cit. on p. 25).

[5] European Commission, « Co2 emission performance standards for cars and vans », European Commission, Europe, 2022 (cit. on p. 25).

[6] V. Masson-Delmotte, P. Zhai, A. Pirani, *et al.*, « Ipcc, 2021: climate change 2021: the physical science basis. contribution of working group i to the sixth assessment report of the intergovernmental panel on climate change », *Cambridge University Press*, (cit. on p. 25).

[7] IFP Energies Nouvelles, « Bilan transversal de l'impact de l'électrification par segment : projet e4t », ADEME, France, 2018 (cit. on pp. 25–28).

[8] Y. Dahmane, M. Ghanes, R. Chenouard, and M. Alvarado-Ruiz, « Decentralized control of electric vehicle smart charging for cost minimization considering temperature and battery health », in *2019 IEEE International Conference on Communications, Control, and Computing Technologies for Smart Grids (SmartGridComm)*, 2019, pp. 1–6. DOI: 10.1109/SmartGridComm.2019.8909796 (cit. on p. 27).

[9] S. Rouquet, M. Ghanes, J.-P. Barbot, Y. B. Shtessel, and L. Merienne, « Energy management in a mechatronics system with delay: a series hybrid electric vehicle case », in *2020 IEEE Conference on Control Technology and Applications (CCTA)*, 2020, pp. 679–684. DOI: 10.1109/CCTA41146.2020.9206269 (cit. on p. 27).

[10] A. Messali, M. A. Hamida, M. Ghanes, and M. Koteich, « Estimation procedure based on less filtering and robust tracking for a self-sensing control of ipmsm », *IEEE Transactions on Industrial Electronics*, vol. 68, no. 4, pp. 2865–2875, 2021. DOI: 10.1109/TIE.2020.2978702 (cit. on p. 27).

[11] R. Parrot, M. Briday, and O. H. Roux, « Pipeline optimization using a cost extension of timed petri nets », in *2021 IEEE 28th Symposium on Computer Arithmetic (ARITH)*, 2021, pp. 37–44. DOI: 10.1109/ARITH51176.2021.00018 (cit. on p. 27).

[12] H. Al Attar, M. A. Hamida, M. Ghanes, and M. Taleb, « Llc dc-dc converter performances improvement for bidirectional electric vehicle charger application », *World Electric Vehicle Journal*, vol. 13, no. 1, 2022, ISSN: 2032-6653. DOI: 10.3390/wevj13010002 (cit. on p. 27).

[13] B. Thomas, *History: early ac-to-dc power conversion (https: //magazine.ieee-pes.org /septemberoctober-2013 /history-9 /)*, IEEE, 2013 (cit. on p. 28).

[14] D. Prince, « The inverter », *GE Review*, vol. 28, no. 10, pp. 676–681, 1925 (cit. on pp. 28, 105).

[15] E. Owen, « History [origin of the inverter] », *IEEE Industry Applications Magazine*, vol. 2, no. 1, pp. 64–66, 1996. DOI: 10.1109/2943.476602 (cit. on p. 29).

[16] G. Buja and G. Indri, « Improvement of pulse width modulation techniques », *Archiv für Elektrotechnik*, vol. 57, no. 5, pp. 281–289, 1975 (cit. on pp. 29, 43, 148).

[17] M. Depenbrock, « Pulse width control of a 3-phase inverter with non-sinusoidal phase voltages », in *Conf. Record of IEEE/IAS Annu. Meeting*, 1977, pp. 399–403 (cit. on pp. 29, 44).

[18] H. van der Broeck, H.-C. Skudelny, and G. Stanke, « Analysis and realization of a pulsewidth modulator based on voltage space vectors », *IEEE Transactions on Industry Applications*, vol. 24, no. 1, pp. 142–150, 1988. DOI: 10.1109/28.87265 (cit. on pp. 29, 50, 55).

[19] S. Du, A. Dekka, B. Wu, and N. Zargari, *Modular multilevel converters: analysis, control, and applications*. John Wiley & Sons, 2017 (cit. on p. 29).

[20] H.-J. Kim, H.-D. Lee, and S.-K. Sul, « A new pwm strategy for common-mode voltage reduction in neutral-point-clamped inverter-fed ac motor drives », *IEEE Transactions on Industry Applications*, vol. 37, no. 6, pp. 1840–1845, 2001. DOI: 10.1109/28.968199 (cit. on p. 29).

[21] L. G. Franquelo, J. Rodriguez, J. I. Leon, S. Kouro, R. Portillo, and M. A. Prats, « The age of multilevel converters arrives », *IEEE Industrial Electronics Magazine*, vol. 2, no. 2, pp. 28–39, 2008. DOI: 10.1109/MIE.2008.923519 (cit. on pp. 30, 35).

[22] C. Gieras J.F. Wang and J. Lai, *Noise of Polyphase Electric Motors*. CRC Press, 2006, ISBN: 9781315220987. DOI: https://doi.org/10.1201/9781420027730 (cit. on pp. 30, 47, 120, 134).

[23] A. Bourgeade, M. Ghanes, M. Fadel, A. Bouarfa, and J.-P. Barbot, « Off-line pwm control with a three phases relaxed symmetry applied to a two-level inverter », in *2021 IEEE Conference on Control Technology and Applications (CCTA)*, 2021, pp. 595–600. DOI: 10.1109/CCTA48906.2021.9659137 (cit. on pp. 32, 105, 106, 123).

[24] A. Bourgeade, M. Ghanes, M. Fadel, A. Bouarfa, and J.-P. Barbot, « A new pwm control based on an optimized zero sequence component injection: application in a two-level inverter », in *IECON 2021 – 47th Annual Conference of the IEEE Industrial Electronics Society*, 2021, pp. 1–6. DOI: 10.1109/IECON48115.2021.9589469 (cit. on pp. 32, 105–107, 121).

[25] H. Foch, P. Ladoux, and H. Piquet, *Association de cellules de commutation: éléments de synthèse des convertisseurs statiques*, 2011 (cit. on p. 35).

[26] H. Foch, M. Metz, T. Meynard, H. Piquet, and F. Richardeau, « Des dipôles à la cellule de commutation », *Techniques de l'ingénieur*, vol. 0, no. d3075, 2006 (cit. on pp. 35, 144).

[27] D. Holmes and T. Lipo, *Pulse Width Modulation for Power Converters: Principles and Practice*. Wiley-IEEE Press, 2003, ISBN: 9780470546284 (cit. on pp. 35, 37, 41, 44, 50, 52, 63, 65, 79, 105, 123, 130, 131, 134, 146, 165, 167).

[28] L.-C. Thevenin, « Comptes rendus de l'académie des sciences », *Académie des sciences*, p. 159, 1883 (cit. on p. 35).

[29] C. Suchet, « Léon charles thévenin: (1857–1926) », *Electrical Engineering*, vol. 68, no. 10, pp. 843–844, 1949. DOI: 10.1109/EE.1949.6432503 (cit. on p. 35).

[30] D. Holmes, « The significance of zero space vector placement for carrier-based pwm schemes », *IEEE Transactions on Industry Applications*, vol. 32, no. 5, pp. 1122–1129, 1996. DOI: 10.1109/28.536874 (cit. on pp. 35, 50).

[31] J. Holtz, G. da Cunha, N. Petry, and P. J. Torri, « Control of large salient-pole synchronous machines using synchronous optimal pulsewidth modulation », *IEEE Transactions on Industrial Electronics*, vol. 62, no. 6, pp. 3372–3379, 2014 (cit. on pp. 35, 68).

[32] J. Holtz, « Pulsewidth modulation for electronic power conversion », *Proceedings of the IEEE*, vol. 82, no. 8, pp. 1194–1214, 1994 (cit. on pp. 36, 48, 63, 71, 105).

[33] B. Castillo-Toledo, S. Di Gennaro, A. G. Loukianov, and J. Rivera, « Hybrid control of induction motors via sampled closed representations », *IEEE Transactions on Industrial Electronics*, vol. 55, no. 10, pp. 3758–3771, 2008. DOI: 10.1109/TIE.2008.928117 (cit. on p. 37).

[34] S. K. Pandey, S. L. Patil, D. Ginoya, U. M. Chaskar, and S. B. Phadke, « Robust control of mismatched buck dc–dc converters by pwm-based sliding mode control schemes », *Control Engineering Practice*, vol. 84, pp. 183–193, 2019 (cit. on p. 37).

[35] R. Madonski, K. Łakomy, M. Stankovic, S. Shao, J. Yang, and S. Li, « Robust converter-fed motor control based on active rejection of multiple disturbances », *Control Engineering Practice*, vol. 107, p. 104 696, 2021 (cit. on p. 37).

[36] U. Drofenik and J. Kolar, « Comparison of not synchronized sawtooth carrier and synchronized triangular carrier phase current control for the vienna rectifier i », in *ISIE '99. Proceedings of the IEEE International Symposium on Industrial Electronics (Cat. No.99TH8465)*, vol. 1, 1999, 13–19 vol.1. DOI: 10.1109/ISIE.1999.801749 (cit. on p. 39).

[37] M. Boost and P. Ziogas, « State-of-the-art carrier pwm techniques: a critical evaluation », *IEEE Transactions on Industry Applications*, vol. 24, no. 2, pp. 271–280, 1988. DOI: 10.1109/28.2867 (cit. on pp. 43, 106, 107).

[38] J. A. Houldsworth and D. A. Grant, « The use of harmonic distortion to increase the output voltage of a three-phase pwm inverter », *IEEE Transactions on Industry Applications*, vol. IA-20, no. 5, pp. 1224–1228, 1984. DOI: 10.1109/TIA.1984.4504587 (cit. on pp. 43, 148, 149).

[39] A. Alesina and M. Venturini, « Solid-state power conversion: a fourier analysis approach to generalized transformer synthesis », *IEEE Transactions on Circuits and Systems*, vol. 28, no. 4, pp. 319–330, 1981. DOI: 10.1109/TCS.1981.1084993 (cit. on p. 44).

[40] A. Hava, R. Kerkman, and T. Lipo, « A high-performance generalized discontinuous pwm algorithm », *IEEE Transactions on Industry Applications*, vol. 34, no. 5, pp. 1059–1071, 1998. DOI: 10.1109/28.720446 (cit. on pp. 44, 45).

[41] O. Ojo, « The generalized discontinuous pwm scheme for three-phase voltage source inverters », *IEEE Transactions on Industrial Electronics*, vol. 51, no. 6, pp. 1280–1289, 2004. DOI: 10.1109/TIE.2004.837919 (cit. on p. 44).

[42] F. Zaamouche, S. Saad, and L. Hamiche, « A discontinuous pwm techniques evaluation by analysis of voltage and current waveforms », *Internationnal Journal of Scientific Research & Engineering Technology (IJSET)*, vol. 7, no. 2, pp. 8–13, 2019 (cit. on p. 44).

[43] T. Habetler and D. Divan, « Acoustic noise reduction in sinusoidal pwm drives using a randomly modulated carrier », *IEEE Transactions on Power Electronics*, vol. 6, no. 3, pp. 356–363, 1991. DOI: 10.1109/63.85902 (cit. on p. 47).

[44] A. Trzynadlowski, F. Blaabjerg, J. Pedersen, R. Kirlin, and S. Legowski, « Random pulse width modulation techniques for converter-fed drive systems-a review », *IEEE Transactions on Industry Applications*, vol. 30, no. 5, pp. 1166–1175, 1994. DOI: 10.1109/28.315226 (cit. on p. 47).

[45] G. Covic and J. Boys, « Noise quieting with random pwm ac drives », *IEE Proceedings-Electric Power Applications*, vol. 145, no. 1, pp. 1–10, 1998 (cit. on p. 47).

[46] S. Gelfand, *Essentials of audiology*. New York: Thieme, 2016, ISBN: 9781604068610 (cit. on p. 47).

[47] K. Shi and H. Li, « Optimized random pwm strategy based on genetic algorithms », in *IECON'03. 29th Annual Conference of the IEEE Industrial Electronics Society (IEEE Cat. No.03CH37468)*, vol. 1, 2003, 7–11 vol.1. DOI: 10.1109/IECON.2003.1279946 (cit. on pp. 48, 63, 105).

[48] P. Sreeja, L. Padmasuresh, and P. Muthukumar, « Fpga based random pulse width modulation for three phase vsi », *IJRTE*, vol. 8, no. 2S6, 2019 (cit. on p. 48).

[49] A. Stankovic, G. Verghese, and D. Perreault, « Randomized modulation of power converters via markov chains », *IEEE Transactions on Control Systems Technology*, vol. 5, no. 1, pp. 61–73, 1997. DOI: 10.1109/87.553665 (cit. on p. 48).

[50] A. Bouarfa, M. Fadel, and M. Bodson, « A new pwm method for a 3-phase 4-leg inverter based on the injection of the opposite median reference voltage », in *2016 International Symposium on Power Electronics, Electrical Drives, Automation and Motion (SPEEDAM)*, 2016, pp. 791–796. DOI: 10.1109/SPEEDAM.2016.7525959 (cit. on p. 49).

[51] M. Bouarfa A. Bodson and M. Fadel, « An optimization formulation of converter control and its general solution for the four-leg two-level inverter », *IEEE Transactions on Control Systems Technology*, vol. 26, no. 5, pp. 1901–1908, 2018. DOI: 10.1109/TCST.2017.2738608 (cit. on pp. 49, 52, 63, 68, 105).

[52] J. Baik, S. Yun, D. Kim, C. Kwon, and J. Yoo, « Remote-state pwm with minimum rms torque ripple and reduced common-mode voltage for three-phase vsi-fed blac motor drives », *Electronics*, vol. 9, no. 4, p. 586, 2020 (cit. on pp. 54, 57, 62).

[53] A. M. Hava and E. Ün, « Performance analysis of reduced common-mode voltage pwm methods and comparison with standard pwm methods for three-phase voltage-source inverters », *IEEE Transactions on Power Electronics*, vol. 24, no. 1, pp. 241–252, 2009. DOI: 10.1109/TPEL.2008.2005719 (cit. on pp. 54, 56, 60).

[54] E. Un and A. M. Hava, « A near-state pwm method with reduced switching losses and reduced common-mode voltage for three-phase voltage source inverters », *IEEE Transactions on Industry Applications*, vol. 45, no. 2, pp. 782–793, 2009. DOI: 10.1109/TIA.2009.2013580 (cit. on p. 55).

[55] D. Holmes, « The general relationship between regular sampled pulse width modulation and space vector modulation for hard switched converters », in *Confer-*

ence Record of the 1992 IEEE Industry Applications Society Annual Meeting, 1992, 1002–1009 vol.1. DOI: 10.1109/IAS.1992.244437 (cit. on pp. 56, 154).

[56] K. Zhou and D. Wang, « Relationship between space-vector modulation and three-phase carrier-based pwm: a comprehensive analysis [three-phase inverters] », *IEEE Transactions on Industrial Electronics*, vol. 49, no. 1, pp. 186–196, 2002. DOI: 10.1109/41.982262 (cit. on pp. 56, 63, 154).

[57] Y.-C. Son and S.-K. Sul, « A new active common-mode emi filter for pwm inverter », *IEEE Transactions on Power Electronics*, vol. 18, no. 6, pp. 1309–1314, 2003. DOI: 10.1109/TPEL.2003.818829 (cit. on p. 57).

[58] G. Oriti, A. Julian, and T. Lipo, « A new space vector modulation strategy for common mode voltage reduction [in pwm invertors] », in *PESC97. Record 28th Annual IEEE Power Electronics Specialists Conference. Formerly Power Conditioning Specialists Conference 1970-71. Power Processing and Electronic Specialists Conference 1972*, vol. 2, 1997, 1541–1546 vol.2. DOI: 10.1109/PESC.1997.618066 (cit. on p. 60).

[59] M. Gendrin, J.-Y. Gauthier, and X. Lin-Shi, « A predictive hybrid pulse-width-modulation technique for active-front-end rectifiers », *IEEE Transactions on Power Electronics*, vol. 32, no. 7, pp. 5487–5496, 2017. DOI: 10.1109/TPEL.2016.2612832 (cit. on p. 62).

[60] Jian Sun and H. Grotstollen, « Optimized space vector modulation and regular-sampled pwm: a reexamination », in *IAS '96. Conference Record of the 1996 IEEE Industry Applications Conference Thirty-First IAS Annual Meeting*, vol. 2, 1996, 956–963 vol.2. DOI: 10.1109/IAS.1996.560198 (cit. on p. 62).

[61] B. McGrath, D. Holmes, and T. Lipo, « Optimized space vector switching sequences for multilevel inverters », *IEEE Transactions on Power Electronics*, vol. 18, no. 6, pp. 1293–1301, 2003. DOI: 10.1109/TPEL.2003.818827 (cit. on p. 62).

[62] A. Kernick, J. L. Roof, and T. M. Heinrich, « Static inverter with neutralization of harmonics », *Transactions of the American Institute of Electrical Engineers, Part II: Applications and Industry*, vol. 81, no. 2, pp. 59–68, 1962. DOI: 10.1109/TAI.1962.6371793 (cit. on p. 63).

[63] J. Holtz, « Advanced pwm and predictive control—an overview », *IEEE Transactions on Industrial Electronics*, vol. 63, no. 6, pp. 3837–3844, 2015 (cit. on pp. 63, 65, 70, 105).

[64] S. Capitaneanu, B. de Fornel, M. Fadel, J. Faucher, and A. Almeida, « Graphical and algebraic synthesis for pwm methods », *EPE Journal*, vol. 11, no. 3, pp. 16–28, 2001. DOI: 10.1080/09398368.2001.11463485 (cit. on pp. 63, 105).

[65] A. M. Bozorgi, M. Monfared, and H. R. Mashhadi, « Optimum switching pattern of matrix converter space vector modulation », in *2012 2nd International eConference on Computer and Knowledge Engineering (ICCKE)*, 2012, pp. 89–93. DOI: 10.1109/ICCKE.2012.6395358 (cit. on p. 63).

[66] A. Birth, T. Geyer, H. du Toit Mouton, and M. Dorfling, « Generalized three-level optimal pulse patterns with lower harmonic distortion », *IEEE Transactions on Power Electronics*, vol. 35, no. 6, pp. 5741–5752, 2019 (cit. on pp. 63–65, 68, 79, 81, 89, 100, 103, 105, 106, 110).

[67] N. Hartgenbusch, R. W. De Doncker, and A. Thünen, « Optimized pulse patterns for salient synchronous machines », in *2020 23rd International Conference on Electrical Machines and Systems (ICEMS)*, 2020, pp. 359–364. DOI: 10.23919/ICEMS50442.2020.9290786 (cit. on pp. 63, 68, 79, 106, 123, 161).

[68] E. Sournac, « Variateur de vitesse pour machine asynchrone commande numérique et stratégies mli, optimisation des modulations », Ph.D. dissertation, ENSEEIHT, Laboratoire d'Electrotechnique et d'Electronique Industrielle, 1990 (cit. on pp. 63, 67, 68, 79).

[69] K. Shi and H. Li, « Optimized pwm strategy based on genetic algorithms », *IEEE Transactions on industrial electronics*, vol. 52, no. 05, pp. 1458–1461, 2005 (cit. on pp. 63, 68, 105).

[70] X. Fei W. Ruan and B. Wu, « A generalized formulation of quarter-wave symmetry she-pwm problems for multilevel inverters », *IEEE Transactions on Power Electronics*, vol. 24, no. 7, pp. 1758–1766, 2009 (cit. on pp. 63, 67, 68, 105).

[71] J. Birda A.D. Reuss and C. Hackl, « Synchronous optimal pulse-width modulation with differently modulated waveform symmetry properties for feeding synchronous motor with high magnetic anisotropy », *ReseachGate, Working Copy*, 2017 (cit. on pp. 63, 68, 105).

[72] H. Hosseinnia and D. Nazarpour, « Utilization of a novel meta heuristic algorithm to minimize total harmonic distortion », *Majlesi Journal of Electrical Engineering*, vol. 12, no. 3, pp. 77–84, 2018 (cit. on pp. 63, 68, 105).

[73] J. Holtz and N. Oikonomou, « Synchronous optimal pulsewidth modulation and stator flux trajectory control for medium voltage drives », in *Fourtieth IAS Annual Meeting. Conference Record of the 2005 Industry Applications Conference, 2005.*, IEEE, vol. 3, 2005, pp. 1748–1791 (cit. on pp. 63, 70).

[74] F. Turnbull, « Selected harmonic reduction in static dc—ac inverters », *IEEE Transactions on communication and Electronics*, vol. 83, no. 73, pp. 374–378, 1964 (cit. on pp. 63, 67).

[75] H. S. Patel and R. G. Hoft, « Generalized techniques of harmonic elimination and voltage control in thyristor inverters: part i–harmonic elimination », *IEEE Transactions on Industry Applications*, vol. IA-9, no. 3, pp. 310–317, 1973. DOI: 10.1109/TIA.1973.349908 (cit. on pp. 63, 67).

[76] H. S. Patel and R. G. Hoft, « Generalized techniques of harmonic elimination and voltage control in thyristor inverters: part ii — voltage control techniques », *IEEE Transactions on Industry Applications*, vol. IA-10, no. 5, pp. 666–673, 1974. DOI: 10.1109/TIA.1974.349239 (cit. on pp. 63, 67).

[77] J. Sun, S. Beineke, and H. Grotstollen, « Optimal pwm based on real-time solution of harmonic elimination equations », *IEEE Transactions on Power Electronics*, vol. 11, no. 4, pp. 612–621, 1996. DOI: 10.1109/63.506127 (cit. on pp. 63, 67).

[78] Y. Sahali and M. Fellah, « Selective harmonic elimination pulse-width modulation technique (she pwm) applied to three-level inverter / converter », *IEEE*, pp. 1112–1117, 2003 (cit. on pp. 63, 67, 68).

[79] M. S. A. Dahidah and V. G. Agelidis, « Selective harmonic elimination pwm control for cascaded multilevel voltage source converters: a generalized formula », *IEEE Transactions on Power Electronics*, vol. 23, no. 4, pp. 1620–1630, 2008. DOI: 10.1109/TPEL.2008.925179 (cit. on pp. 63, 67, 68).

[80] C. Buccella, M. Cimoroni, C. Cecati, A. Di Tommaso, C. Nevoloso, and G. Schettino, « Mathematical formulation of pulse amplitude modulation selective harmonic elimination in multilevel three phase inverters », in *SPEEDAM 2022 – 2022*

International Symposium on Power Electronics, Electrical Drives, Automation and Motion, 2022 (cit. on p. 63).

[81] R. Fotouhi, L. Leitner, R. Kennel, and H. du Toit Mouton, « An efficient method to calculate optimal pulse patterns for medium voltage converters », in *IECON 2014-40th Annual Conference of the IEEE Industrial Electronics Society*, IEEE, 2014, pp. 1221–1226 (cit. on p. 68).

[82] R. Fotouhi, A. Sorokin, R. Kennel, and H. du Toit Mouton, « An efficient method to calculate optimal pulse patterns for multi-level converters », in *2015 9th International Conference on Power Electronics and ECCE Asia (ICPE-ECCE Asia)*, IEEE, 2015, pp. 533–539 (cit. on p. 68).

[83] A. Trzynadlowski and S. Legowski, « Application of neural networks to the optimal control of three-phase voltage-controlled inverters », *IEEE Transactions on Power electronics*, vol. 9, no. 4, pp. 397–404, 1994 (cit. on p. 68).

[84] N. O. Cherchali, A. Tlemçani, M. Boucherit, and A. Morsli, « Elimination of low order harmonics in multilevel inverter using nature-inspired metaheuristic algorithm », *International Journal of Energy and Power Engineering*, vol. 13, no. 9, pp. 638–644, 2019 (cit. on p. 68).

[85] A. L. Kouzou, A. Krama, S. S. Refaat, and H. Abu-Rub, « Selective harmonic elimination pwm for a cascaded multi-level inverter », in *2020 IEEE International Conference on Industrial Technology (ICIT)*, 2020, pp. 1145–1150. DOI: 10.1109/ICIT45562.2020.9067207 (cit. on p. 68).

[86] J. Rathore A.K. Holtz and T. Boller, « Synchronous optimal pulsewidth modulation for low-switching-frequency control of medium-voltage multilevel inverters », *IEEE Transacions on industrial electronics*, vol. 57, no. 7, pp. 2374–2381, 2010 (cit. on pp. 68, 106).

[87] A. Tripathi and G. Narayanan, « Optimal pulse width modulation of voltage-source inverter fed motor drives with relaxation of quarter wave symmetry condition », *IEEE Conecct2014*, 2014 (cit. on p. 68).

[88] M. S. A. Dahidah, G. Konstantinou, and V. G. Agelidis, « A review of multilevel selective harmonic elimination pwm: formulations, solving algorithms, implementation and applications », *IEEE Transactions on Power Electronics*, vol. 30, no. 8, pp. 4091–4106, 2015. DOI: 10.1109/TPEL.2014.2355226 (cit. on pp. 68, 105).

[89] A. Tripathi and G. Narayanan, « Investigations on optimal pulse width modulation to minimize total harmonic distortion in the line current », *IEEE Transactions on industry applications*, vol. 53, no. 1, pp. 212–221, 2017 (cit. on p. 68).

[90] G. Friedrich and J. Vilan, « A comparison between two pwm strategics: natural sampling and instantaneous feedback », in *EPE 1986 Rec.*, 1987, pp. 281–285 (cit. on p. 69).

[91] J. Vilain and C. Lesbroussart, « Une nouvelle stratégie de modulation du vecteur d'espace pour un onduleur de tension triphasé: la modulation delta sigma vectorielle », *Journal de Physique III*, vol. 5, no. 7, pp. 1075–1088, 1995 (cit. on p. 69).

[92] M. Li, X. Wu, S. Huang, and G. Liang, « Model predictive direct power control using optimal section selection for pwm rectifier with reduced calculation burden », *International Journal of Electrical Power & Energy Systems*, vol. 116, p. 105 552, 2020 (cit. on p. 70).

[93] D. Patino, M. Bâja, P. Riedinger, H. Cormerais, J. Buisson, and C. Iung, « Alternative control methods for dc–dc converters: an application to a four-level three-cell dc–dc converter », *International Journal of Robust and Nonlinear Control*, vol. 21, no. 10, pp. 1112–1133, 2011 (cit. on p. 70).

[94] D. M. Brod and D. W. Novotny, « Current control of vsi-pwm inverters », *IEEE transactions on Industry Applications*, no. 3, pp. 562–570, 1985 (cit. on p. 72).

[95] G. Wang, M. Valla, and J. Solsona, « Position sensorless permanent magnet synchronous machine drives—a review », *IEEE Transactions on Industrial Electronics*, vol. 67, no. 7, pp. 5830–5842, 2020. DOI: 10.1109/TIE.2019.2955409 (cit. on p. 75).

[96] D. Surroop, P. Combes, and P. Martin, « Towards an industrially implementable pwm-injection scheme », in *2021 IEEE International Electric Machines Drives Conference (IEMDC)*, 2021, pp. 1–6. DOI: 10.1109/IEMDC47953.2021.9449593 (cit. on p. 75).

[97] F. Zidani, D. Diallo, M. E. H. Benbouzid, and R. Nait-Said, « A fuzzy-based approach for the diagnosis of fault modes in a voltage-fed pwm inverter induction motor drive », *IEEE Transactions on Industrial Electronics*, vol. 55, no. 2, pp. 586–593, 2008. DOI: 10.1109/TIE.2007.911951 (cit. on p. 75).

[98] M. Trabelsi, M. Boussak, and M. Gossa, « Pwm-switching pattern-based diagnosis scheme for single and multiple open-switch damages in vsi-fed induction motor drives », *ISA transactions*, vol. 51, no. 2, pp. 333–344, 2012 (cit. on p. 75).

[99] H. Yan, Y. Xu, F. Cai, H. Zhang, W. Zhao, and C. Gerada, « Pwm-vsi fault diagnosis for a pmsm drive based on the fuzzy logic approach », *IEEE Transactions on Power Electronics*, vol. 34, no. 1, pp. 759–768, 2019. DOI: 10.1109/TPEL.2018.2814615 (cit. on p. 75).

[100] T. Itkonen, J. Luukko, A. Sankala, T. Laakkonen, and R. PÖllÄnen, « Modeling and analysis of the dead-time effects in parallel pwm two-level three-phase voltage-source inverters », *IEEE Transactions on Power Electronics*, vol. 24, no. 11, pp. 2446–2455, 2009. DOI: 10.1109/TPEL.2009.2033064 (cit. on p. 83).

[101] M. Sierra and C. Coello, « Improving pso-based multi-objective optimization using crowding, mutation and ϵ-dominance », *Evolutionary Multi-Criterion Optimization, Third international Conference EMO*, pp. 505–519, 2005 (cit. on p. 85).

[102] B. Adrien, M. Ghanes, F. Maurice, B. Abdelkader, B. Jean-Pierre, and B. Robert, *Phases symmetry relaxation (PSR) experimental plateform (https://youtu.be /995fgSWSobk)*, Youtube, 2021 (cit. on p. 97).

[103] D. O. Neacşu, Y. Zheng, and B. Lehman, « An sd card flash-memory-based implementation of a multioptimal three-phase pwm generator », *IEEE Transactions on Power Electronics*, vol. 31, no. 1, pp. 39–51, 2016. DOI: 10.1109/TPEL.2015.2424200 (cit. on p. 100).

[104] S. Bowes and Y.-S. Lai, « The relationship between space-vector modulation and regular-sampled pwm », *IEEE Transactions on Industrial Electronics*, vol. 44, no. 5, pp. 670–679, 1997. DOI: 10.1109/41.633469 (cit. on pp. 105, 154).

[105] E. Sournac, J. Hapiot, P. Maussion, and C. Sabourin, « Implementation of optimised modulation in an industrial speed drive for asynchronous machines », *EPE, Aachen*, 1989 (cit. on pp. 105, 106).

[106] S. Bowes and D. Holliday, « Optimal regular-sampled pwm inverter control techniques », *IEEE Transacions on industrial electronics*, vol. 54, no. 3, pp. 1547–1559, 2007 (cit. on p. 106).

[107] S. K. Sahoo and T. Bhattacharya, « Phase-shifted carrier-based synchronized sinusoidal pwm techniques for a cascaded h-bridge multilevel inverter », *IEEE Transactions on Power Electronics*, vol. 33, no. 1, pp. 513–524, 2018. DOI: 10.1109/TPEL.2017.2669084 (cit. on p. 106).

[108] P. Lezynski, « Random modulation in inverters with respect to electromagnetic compatibility and power quality », *IEEE Journal of Emerging and Selected Topics in Power Electronics*, vol. 6, no. 2, pp. 782–790, 2018. DOI: 10.1109/JESTPE.2017.2787599 (cit. on p. 120).

[109] I. Takahashi and H. Mochikawa, « Optimum pwm waveforms of an inverter for decreasing acoustic noise of an induction motor », *IEEE Transactions on Industry Applications*, vol. IA-22, no. 5, pp. 828–834, 1986. DOI: 10.1109/TIA.1986.4504800 (cit. on p. 120).

[110] A. Ruiz-Gonzalez, M. J. Meco-Gutierrez, F. Perez-Hidalgo, F. Vargas-Merino, and J. R. Heredia-Larrubia, « Reducing acoustic noise radiated by inverter-fed induction motors controlled by a new pwm strategy », *IEEE Transactions on Industrial Electronics*, vol. 57, no. 1, pp. 228–236, 2010. DOI: 10.1109/TIE.2009.2031185 (cit. on p. 120).

[111] J. Zhang, J. Zhao, D. Zhou, and C. Huang, « High-performance fault diagnosis in pwm voltage-source inverters for vector-controlled induction motor drives », *IEEE Transactions on Power Electronics*, vol. 29, no. 11, pp. 6087–6099, 2014. DOI: 10.1109/TPEL.2014.2301167 (cit. on p. 134).

[112] E. Clarke, C. N. Weygandt, and C. Concordia, « Overvoltages caused by unbalanced short circuits: effect of amortisseur windings », *Electrical Engineering*, vol. 57, no. 8, pp. 453–468, 1938. DOI: 10.1109/EE.1938.6430868 (cit. on p. 156).

[113] P. Bastiani, « Stratégies de commande minimisant les pertes d'un ensemble convertisseur-machine alternative: application à la traction électrique », Ph.D. dissertation, Lyon, INSA, 2001 (cit. on p. 170).

[114] Y.-S. Lai and F.-S. Shyu, « Optimal common-mode voltage reduction pwm technique for inverter control with consideration of the dead-time effects-part i: basic development », *IEEE Transactions on Industry Applications*, vol. 40, no. 6, pp. 1605–1612, 2004. DOI: 10.1109/TIA.2004.836149 (cit. on p. 176).

[115] Y.-S. Lai, P.-S. Chen, H.-K. Lee, and J. Chou, « Optimal common-mode voltage reduction pwm technique for inverter control with consideration of the dead-time effects-part ii: applications to im drives with diode front end », *IEEE Transactions on Industry Applications*, vol. 40, no. 6, pp. 1613–1620, 2004. DOI: 10.1109/TIA.2004.836151 (cit. on p. 176).

Titre : Optimisation de la commande par MLI d'un onduleur à deux niveaux

Mot clés : MLI synchrone, Onduleur, Optimisation, Hors-ligne, Injection de séquence nulle

Résumé : Malgré les améliorations de topologies des convertisseurs DC/AC, l'onduleur à deux niveaux reste le "gold standard" dans l'industrie ceci pour de multiples raisons : simplicité, fiabilité, etc. Dans le cadre de cette thèse entre Centrale Nantes et Renault, de nouvelles commandes d'onduleur ont été développées afin d'améliorer les performances sans modifier la topologie du convertisseur. Pour cela, deux approches basées sur des commandes hors-ligne synchrones ont été proposées. Premièrement, celles qui relaxent la contrainte de symétrie angulaire entre phases, usuellement imposée au convertisseur. Deuxièmement, celles qui sont à porteuse triangulaire consistant à injecter une séquence homopolaire de fréquence triple dans la modulante. La conséquence de cette approche est une généralisation de l'injection d'harmonique classique de rang trois. Un calcul aux limites a permis de montrer l'existence d'une méthodologie facilement implantable, qui prend la forme d'une injection d'une dent de scie. Les deux approches revisitent les stratégies de commande par modulation de largeur d'impulsion (MLI) de la littérature grâce à des considérations simples à base de relaxation et d'extension de propriétés existantes. L'ensemble de ces stratégies améliorent significativement le taux de distorsion harmonique des tensions ou courants fournis par l'onduleur pour des fréquences de commutations synchrones faibles. Ces observations ont été réalisées en simulation et validées sur un banc expérimental de faible puissance.

Title: PWM control optimization of a two-level inverter

Keywords: Synchronous PWM, Inverter, Optimization, Off-line, Signal injection

Abstract: Despite improvements in DC/AC converter topologies, the two-level inverter remains the "gold standard" in the industry for many reasons: simplicity, reliability, etc. In this thesis between Ecole Centrale and Renault, new inverter controls have been developed to improve the performance without modifying the converter topology. For this purpose, two approaches based on synchronous off-line controls have been proposed. Firstly, an angular symmetry relaxation between phases usually imposed on the converter. Secondly triangular carrier based strategies, meaning injecting a triple frequency homopolar sequence into the modulating signal. The consequence of this approach has given rise to a generalization of the classical third harmonic injection. A calculation extension has shown the existence of an easily implementable methodology, which takes the form of a sawtooth injection. Both approaches revisit the pulse width modulation (PWM) control strategies of the literature with simple considerations based on relaxation and extension of existing properties. The advantage of all these strategies is that they improve significantly the harmonic distortion rate of the voltages or currents supplied by the inverter for low synchronous switching frequencies. These observations have been done in simulation and validated on a low power experimental bench.